TAMPEREEN TEKNILLINEN YLIOPISTO
TAMPERE UNIVERSITY OF TECHNOLOGY

Samuli Kivistö

Short Pulse Lasers Using Advanced Fiber Technology and Saturable Absorbers

Julkaisu 889 • Publication 889

Tampere 2010

Tampereen teknillinen yliopisto. Julkaisu 889
Tampere University of Technology. Publication 889

Samuli Kivistö

Short Pulse Lasers Using Advanced Fiber Technology and Saturable Absorbers

Thesis for the degree of Doctor of Technology to be presented with due permission for public examination and criticism in Tietotalo Building, Auditorium TB104, at Tampere University of Technology, on the 11th of June 2010, at 12 noon.

Tampereen teknillinen yliopisto - Tampere University of Technology
Tampere 2010

ISBN 978-952-15-2362-5 (printed)
ISBN 978-952-15-2402-8 (PDF)
ISSN 1459-2045

Abstract

Ultrafast fiber lasers with superb pulse and beam quality are becoming important in various fields of applications including high-precision material processing, bio-medicine, fiber optical communications, and ranging. This thesis is concerned with the research and development of ultrafast fiber laser technology. Passively mode-locked and Q-switched fiber lasers operating at 1-2.2 μm IR-spectral range have been developed and studied.

Passively Q-switched Tm-Ho-doped fiber lasers operating at 2 μm were thoroughly investigated. A strong impact of a new effect - dynamic gain induced pulse shortening, on the duration, repetition rate and energy of a Q-switched fiber laser was studied. Using this effect in combination with a short-length fiber cavity and a highly nonlinear antimonide-based semiconductor saturable absorber mirror resulted in generation of record-short 20 ns energetic Q-switched pulses at 2 μm.

Well-controlled chirped fiber Bragg grating (CFBG) technology was developed and used for inscription of high-performance all-fiber dispersion compensators. All-fiber ytterbium (Yb) and bismuth (Bi) lasers generating picosecond soliton pulses at 1 μm and at 1.2 μm were demonstrated using CFBG-dispersion compensators. The powerful Yb-doped laser followed by an all-fiber amplifier was used to generate octave-spanning supercontinuum radiation in a nonlinear photonic crystal fiber.

Various wavelength tuning methods of ultrafast soliton fiber lasers, such as self-frequency shifting of Raman solitons and electronic tuning using an acousto-optic tunable filter, were also investigated. In addition, an environmentally stable 200 fs mode-locked Yb-doped fiber laser with dispersion compensation by an index guiding photonic crystal fiber was demonstrated.

Novel Bi-doped mode-locked fiber sources operating at a wavelength of ~1.2 μm using dilute nitride saturable absorbers were developed and studied. The first Bi-doped fiber laser delivering sub-picosecond soliton pulses was demonstrated. Harmonic mode-locking in a Bi-doped mode-locked fiber laser with dispersion compensation by a CFBG was used to increase significantly the initially low repetition rate of the Bi-fiber laser. Pulse dynamics of mode-locked Bi-lasers were also investigated in detail.

Ultrashort wavelength-tunable pulses beyond 2 μm with durations below 200 fs were generated through a soliton self-frequency shift in a Tm-Ho fiber amplifier seeded by a Tm-Ho master oscillator mode-locked by a GaSb-based saturable absorber. Finally, a novel ultra-broadband saturable absorber based on carbon nanotubes layered on top of an Ag-mirror was demonstrated. The same sample of polymer-free carbon nanotube absorber was used to reliably mode-lock ytterbium-, erbium-, and thulium-holmium-doped soliton fiber lasers producing sub-picosecond pulses at 1 μm, 1.56 μm, and 2 μm, respectively.

Acknowledgements

The work presented in this thesis has been carried out at the Optoelectronics Research Centre (ORC), Tampere University of Technology, during the years 2007-2010. The work has been supported in part by the graduate school of Tampere University of Technology, the Finnish Foundation for Economic and Technology Sciences, the Ulla Tuominen Foundation, the Jenny and Antti Wihuri Foundation, the Nokia Foundation, the Emil Aaltonen Foundation, the Elisa Foundation, the Walter Ahlström Foundation and the Väisälä Foundation.

I gratefully acknowledge my supervisor Prof. Oleg Okhotnikov for his support, guidance, and professional knowledge in the field. I would also like to thank Prof. Markus Pessa for giving me the opportunity to work at ORC, an internationally high-level scientific environment. I thank Dr. Pekka Savolainen for managing the ORC since 06/2009.

I gratefully thank my former 'tutors', supervisors Dr. Matei Rusu and Dr. Robert Herda. I have learned a lot from you! I thank Robert also for his contribution on various articles included in this thesis. In addition, I would like to thank Prof. Mircea Guina for various valuable discussions. This work has been a team work. I would like to thank my great current and former colleagues in fiber optics Tommi Hakulinen, Regina Gumenyuk, Dr. Antti Isomäki, Dionisio Pereira, and Chris Thür. I thank Dr. Antti Härkönen and Dr. Lasse Orsila for various valuable discussions related to practical issues during my stay at ORC. I also thank the whole UIO group, in particular Esa Saarinen, Juho Kerttula, and Jussi Rautiainen. It has been a pleasure to work in this group. I thank Dr. Soile Suomalainen, Jonna Paajaste, Riku Koskinen, Janne Puustinen and Ville-Markus Korpijärvi for their professional and valuable work with MBE-growth of the saturable absorbers used in this work. A special thanks for Dr. Charis Reith for improving the fluency of the English in the thesis and for Anne Viherkoski for handling the administrative issues. I also want to thank Ilkka Hirvonen and the team in the metallic workshop. I thank the whole ORC staff for the great and enjoyable research environment.

I thank Prof. Evgeny Dianov and Dr. Mikhail Melkumov from Fiber Optic Research Center (Moscow) and Dr. Stuart Jackson from Optical Fibre Technology Centre (Sydney) for providing special first-class doped fibers. I also thank the Nanomaterials group at HUT, particularly Dr. Albert Nasibulin, for co-operation with the carbon nanotube films. I thank Prof. K. Rößner and Prof. A. Forchel from the University of Würzburg. I thank my thesis pre-examiners Reto Häring (Toptica Photonics) and Vladimir Karpov (MPB Communications) for the review and comments.

I warmly thank my family for supporting my studies. Big thanks also to all my friends. Most of all, I would like to thank my dear wife Anu and son Joona for all the support and love.

Tampere, March 2010

Samuli Kivistö

Table of contents

List of publications

This thesis contains some unpublished material but is mainly based on the following publications that are included as appendices and referred to in the text as [P1]…[P10].

[P1] R. Herda, S. Kivistö, and O. G. Okhotnikov, "Dynamic gain induced pulse shortening in Q-switched lasers," *Optics Letters* **33**, 1011-1013, 2008.

[P2] S. Kivistö, R. Koskinen, J. Paajaste, S. D. Jackson, M. Guina, and O. G. Okhotnikov, "Passively Q-switched Tm^{3+}, Ho^{3+}-doped silica fiber laser using a highly nonlinear saturable absorber and dynamic gain pulse compression," *Optics Express* **16**, 22058–22063, 2008.

[P3] R. Herda, S. Kivistö, O. G. Okhotnikov, A. F. Kosolapov, A. E. Levchenko, S. L. Semjonov, and E. M. Dianov, "Environmentally stable mode-locked fiber laser with dispersion compensation by index-guided photonic crystal fiber," *IEEE Photonics Technology Letters* **20**, 217-219, 2008.

[P4] S. Kivistö, R. Herda, and O. G. Okhotnikov, "All-fiber supercontinuum source based on a mode-locked ytterbium laser with dispersion compensation by linearly chirped Bragg grating," *Optics Express* **16**, 265-270, 2008.

[P5] S. Kivistö, R Herda, and O. G. Okhotnikov, "Electronically tunable mode-locked Yb-doped fiber laser," *IEEE Photonics Technology Letters* **20**, 51-53, 2008.

[P6] S. Kivistö, J. Puustinen, M. Guina, O. G. Okhotnikov, and E. M. Dianov, "Tunable mode-locked bismuth-doped soliton fibre laser," *IEE Electronics Letters* **44**, 1456-1458, 2008.

[P7] S. Kivistö, R. Gumenyuk, J. Puustinen, M. Guina, E. M. Dianov, and O. G. Okhotnikov, "Mode-locked Bi-doped all-fiber laser with chirped fiber Bragg grating," *IEEE Photonics Technology Letters* **21**, 599-601, 2009.

[P8] S. Kivistö, J. Puustinen, M. Guina, S. Marcinkevicius, E. M. Dianov, and O. G. Okhotnikov, "Pulse dynamics of a passively mode-locked Bi-doped fiber laser," *Optics Express* **18**, 1041-1048, 2010.

[P9] S. Kivistö, T. Hakulinen, M. Guina, and O. G. Okhotnikov, "Tunable Raman soliton source using mode-locked Tm-Ho fiber laser," *IEEE Photonics Technology Letters* **19**, 934-936, 2007.

[P10] S. Kivistö, T. Hakulinen, B. Aitchison, D. Brown, A. Kaskela, A. Nasibulin, E. Kauppinen, A. Härkönen, and O. G. Okhotnikov, "Carbon nanotube films for ultrafast broadband technology," *Optics Express* **17**, 2358-2363, 2009.

List of supplemental publications

The following publications are mentioned but not included in the thesis. In the text, these publications are referred to as [S1]…[S4].

[S1] S. Kivistö, T. Hakulinen, M. Guina, O. G. Okhotnikov, K. Rößner, and A. Forchel, "2 Watt 2 μm Tm/Ho fiber laser system passively Q-switched by antimonide semiconductor saturable absorber," *SPIE Photonics Europe* Proc. Of SPIE 6998, 69980Q-1-69980Q-8 (2008), Strasbourg, France 7.-11.4.2008.

[S2] M. Rusu, S. Kivistö, C. Gawith, and O. G. Okhotnikov "Red-green-blue (RGB) light generator using tapered fiber pumped with a frequency-doubled Yb-fiber laser," *Optics Express* **13**, 8547-8554, 2005.

[S3] M. Rusu, R. Herda, S. Kivistö, and O. G. Okhotnikov, "Fiber tapers for dispersion management in a mode-locked ytterbium fiber laser," *Optics Letters* **31**, 2257-2259, 2006.

[S4] R. Gumenyuk, C. Thür, S. Kivistö, and O. G. Okhotnikov, "Tapered fiber Bragg gratings for dispersion compensation in mode-locked Yb-doped fiber laser," *IEEE Journal of Quantum Electronics* **46**, 769-773, 2010.

Author's contribution

This thesis includes 10 papers published in international peer-reviewed journals. It also contains material from supplementary publications and some new unpublished material.

For all work reported, the author designed and built the experimental setup and made most of the experimental measurements. The author was also directly involved in designing and manufacturing passive fiber components. In addition, the author participated in performing the fiber laser simulations. However, the achievements presented here are a part of team work. The author benefited from the work contribution of various co-authors, especially in the saturable absorber and doped-fiber manufacturing, and laser simulations. The author had a major role in writing the manuscripts [P2], [P4]…[P10] and publishing the results in peer-reviewed journals.

The author's contribution to the experimental work, writing and refining the manuscript is listed in the Table below.

Paper	Contribution to experimental work	Contribution to writing the paper
[P1]	40%	Co-author (20%)
[P2]	90%	First author (90%)
[P3]	50%	Co-author (40%)
[P4]	60%	First author (70%)
[P5]	80%	First author (90%)
[P6]	90%	First author (90%)
[P7]	70%	First author (90%)
[P8]	70%	First author (70%)
[P9]	90%	First author (90%)
[P10]	40%	First author (70%)

List of abbreviations

AOM	Acousto-optic modulator
AOTF	Acousto-optic tunable filter
ASB	Aluminosilicate Bi-glass
ASE	Amplified spontaneous emission
BC	Bismuth center
CFBG	Chirped fiber Bragg grating
CNT	Carbon nanotube
CPA	Chirped pulse amplification
CR	Cross-relaxation
cw	Continuous wave
DBR	Distributed Bragg reflector
DCF	Dispersion compensating fiber
DIRCM	Directed infrared countermeasure
DSF	Dispersion-shifted fiber
EOM	Electro-optic modulator
ESA	Excited state absorption
FBG	Fiber Bragg grating
FSF	Frequency shifted feedback
GSA	Ground-state absorption
GSB	Germanosilicate Bi-glass
GTI	Gires-Tournois interferometer
GVD	Group velocity dispersion
HOM	Higher order mode
IR	Infrared
LIDAR	Light detection and ranging
LMA	Large-mode area
MBE	Molecular beam epitaxy
MCVD	Modified chemical vapor deposition
NALM	Nonlinear amplifying loop mirror
NLPR	Nonlinear polarization rotation
NSE	Nonlinear Schrödinger equation
PBGF	Photonic bandgap fiber
PCF	Photonic crystal fiber
PGSB	Phosphogermanosilicate Bi-glass
QW	Quantum well
RF	Radio frequency
SAM	Saturable absorber mirror
SBS	Stimulated Brillouin scattering
SEM	Scanning electron microscope
SESAM	Semiconductor saturable absorber mirror
SMF	Single-mode fiber
SPM	Self-phase modulation

SSFS	Soliton self-frequency shift
SWCNT	Single-walled carbon nanotube
TBP	Time-bandwidth product
TEM	Transmission electron microscope
TOD	Third order dispersion
UV	Ultraviolet
WDM	Wavelength division multiplexing
XPM	Cross-phase modulation
ZBLAN	(ZrF, BaF, LaF, AlF and NaF) glass

1. Introduction

During the last decade world-wide laser markets have grown tremendously. Continuous-wave and pulsed laser sources have started to be employed in a broad range of completely new application fields. The requirements of industrial applications have routed the development towards compact, maintenance-free, efficient systems with clean Gaussian-shaped beam quality and moderate cost. The fiber laser is a good candidate to meet the above-mentioned criteria. Owing to the nature of the fiber laser cavity, which in the ideal case is constituted only of fiber components and does not have any free-space optics or other bulk elements, the fiber laser offers unprecedented reliability and turn-key operation. Additionally, the output light with nearly ideal beam quality is delivered initially in an optical fiber and is thus easily routed towards specific targets.

The engine of the fiber laser cavity is the active medium; doped fiber. Doped fibers employed in lasers are typically able to provide broad gain spectra with relatively high gain. This allows building of efficient lasers with great potential for wide wavelength tuning and ultrashort pulse generation. Figure 1.1 shows the wavelength regions covered by doped fibers and fiber lasers. Neodymium- (Nd), ytterbium- (Yb) and erbium (Er)-doped fibers and lasers have been intensively researched during the last two decades and the results have already been successfully commercialized. However, the gain bandwidth of Er-doped fiber is limited to the wavelength range from 1.53 μm to ~1.62 μm, whereas Yb- and Nd-doped fiber lasers typically operate close to 1 μm. In order to cover the whole spectral region from 1 μm to 2 μm, new active fibers doped with bismuth (Bi)- and thulium (Tm)-ions have recently started to be investigated. Bi-doped fibers provide broad gain situated around the loss minimum of silica fibers at ~1.3 μm and the Tm-doped fibers around 1.9 μm (see Fig. 1.1).

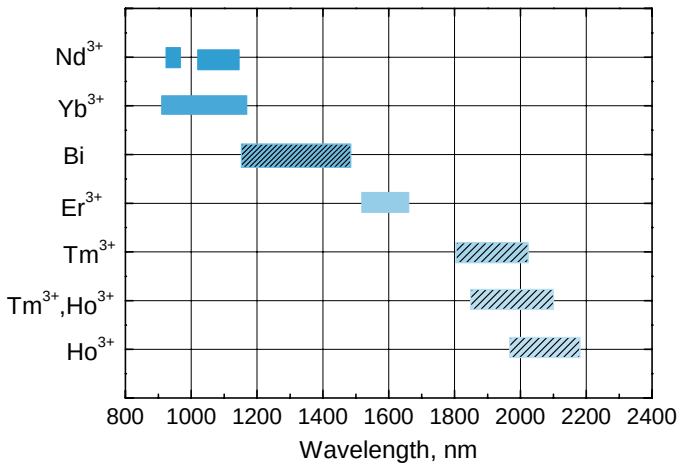

Fig. 1.1. Wavelengths covered by doped fiber materials and fiber lasers. The dashed areas show the relatively unexplored wavelengths and materials important for this work.

Continuous wave and pulsed fiber lasers have various industrial and scientific applications in the fields of material processing, bio-medicine, optical communications, spectroscopy, imaging, and ranging. In particular, ultrafast mode-locked and energetic Q-switched fiber lasers delivering pulses with durations from several tens of femtoseconds to a few hundred nanoseconds are gaining more and more interest in micromachining [1-5], eye and dental surgeries [6,7], tissue welding [8], optical coherence tomography [9,10], and LIDAR [11-13]. Table 1.1 summarizes several applications of pulsed fiber lasers at different wavelength regimes.

Table 1.1. Applications of mode-locked and Q-switched fiber lasers.

Gain fiber	*Wavelength range (μm)*	*Application*	*Ref.*
Yb	0.98-1.11	High-precision cutting and drilling, micro patterning, cold ablation, surgeries, frequency doubling	[1]-[8]
Bi	1.15-1.5	Optical communication, frequency doubling, bio-medicine	[14], [15]
Er	1.53-1.62	Optical communication, Eye-safe LIDAR, bio-medicine	[10]-[12]
Tm, Tm-Ho, Ho	1.8-2.1	Eye-safe LIDAR, directed infrared countermeasures (DIRCM), minimally invasive surgery, CO_2-spectroscopy	[13], [16]-[19]

Development of fiber lasers operating at new wavelengths has also led to a need for saturable absorbers based on new materials and compositions able to initiate pulsed operation. Among the different options, semiconductor saturable absorber mirrors (SESAMs) are the most widespread and conventional method to initiate the passive mode-locking or Q-switching of a fiber laser. Nowadays, using high-precision molecular beam epitaxy (MBE) growth, SESAMs and their material compositions can be tailored to cover the wavelengths of fiber lasers within the 1-2 μm range. Another fascinating material with nonlinear absorption characteristics are carbon nanotubes, which have recently been demonstrated to work as a multifunctional material in various different fields such as nano-optoelectronics [20], electronics [21], optics [22], and material science [23]. As a saturable absorber, single-walled carbon nanotubes (SWCNTs) provide fast absorption recovery and broad absorption characteristics, which are by nature beneficial for mode-locking of lasers operating at different wavelengths.

1.1 Aims of this thesis

This thesis aims to design and develop mode-locked and Q-switched fiber lasers based on various doped fibers covering the whole near-shortwave infrared spectral region from 1 μm to 2.2 μm. The main focus is on the development of pulsed fiber lasers operating at

new wavelength regimes of 1.15-1.35 μm and 1.9-2.2 μm. Pulse generation and evolution in mode-locked and Q-switched fiber lasers employing saturable absorbers are studied. The thesis gives a broad inspection of state-of the-art ultrafast fiber laser technology including novel doped fibers, saturable absorbers, passive fiber components, wavelength tuning and intra-cavity dispersion compensation methods. The findings and technology of this work could be used in the future for the development of fiber-based sources targeting new applications.

The thesis consists of an introduction followed by four main chapters and conclusions. Chapter 2 introduces optical gain fibers with a focus on novel Bi-doped and relatively unexplored Tm-Ho-doped fibers. A short review of fiber lasers is also provided. Chapter 3 describes the basic principles of Q-switching and optimization of passively Q-switched fiber lasers. A new observation, dynamic gain induced pulse shortening is described and employed in Tm-Ho-doped fiber lasers. Chapter 4 describes the basic principles of mode-locked fiber lasers. Pulse dynamics, dispersion compensation and wavelength tuning methods are covered. Chapter 5 is devoted to the main achievements and findings of this thesis: the development of ultrafast mode-locked fiber lasers based on Bi- and Tm-Ho-doped fibers. Mode-locked Bi-doped fiber lasers operating at 1.17 μm and 1.33 μm are reported. Pulse dynamics and pulse evolution within a Bi-laser cavity are precisely studied. Wavelength-tunable few hundred femtosecond pulses are generated beyond 2 μm wavelengths using a Tm-Ho-doped master oscillator and a Tm-Ho-doped fiber amplifier/Raman shifter. Additionally, a broadband saturable absorber based on carbon nanotubes capable of mode-locking Yb-, Er-, and Tm-Ho-doped fiber lasers is demonstrated. Using the same saturable absorber, sub-picosecond mode-locked pulses are generated at the wavelengths of 1 μm, 1.56 μm and 2 μm.

2. Rare-earth- and bismuth (Bi)-doped gain fibers

This chapter concentrates on the rare-earth-ion doped fibers that are used as gain media in high power and ultra-short pulse fiber lasers. The main emphasis is on the relatively unexplored and novel gain fiber materials important for this work; bismuth and thulium -doped fibers. However, ytterbium, erbium, and holmium-doped fibers are also considered. A general review of fiber lasers is provided in the last section of this chapter.

2.1 Active fibers doped with ytterbium (Yb), erbium (Er), thulium (Tm), holmium (Ho), and Tm-Ho-ions

The three most important gain media are based on ytterbium (Yb), erbium (Er), and thulium (Tm) doped fibers. The emission band of Yb-doped fibers is centered around 1 μm, the emission band of the Er-doped fibers around 1.55 μm, and the emission band of thulium-doped fibers around 2 μm. In order to extend the emission band of the Tm-ions, new holmium (Ho), and thulium-holmium (Tm-Ho) doped fibers have also been manufactured and demonstrated.

Ytterbium (Yb)-doped fibers

Yb is an element that belongs to the group of rare earth metals. It provides optical amplification and gain around 1 μm wavelength [24]. As an optically active element, it is already well known and has been rather intensively studied during the last two decades. Initially, Yb-activated glass was proposed for laser material as early as 1962 [25]. However, the first Yb-based silica gain fiber was demonstrated 26 years later, in 1988 [26]. Since then, Yb-doped fibers have been extensively employed to create efficient, high-power, and pulsed fiber lasers. These lasers operating at 1 μm find various applications in the fields of laser welding [27], material processing [3], eye surgery [6,28] and other biomedical applications.

In the field of photonics Yb is used in the form of Yb^{3+}-ions. These ions create strong fluorescence bands at ~980 nm and at ~1050 nm. The absorption of Yb is broad (850 nm–1000 nm), therefore allowing the use of various commercially available high power semiconductor lasers for pumping. The main pumping wavelengths are ~920 nm and ~980 nm. The absorption and fluorescence spectra of Yb^{3+} are shown in Fig. 2.1(a), whereas the energy level diagram is shown in Fig. 2.1(b). Yb^{3+} is a quasi-three level laser medium, meaning that the lower laser level is so close to the ground state that significant thermal occupation occurs at that level at room temperature. It has been experimentally demonstrated that the change in the Yb-laser dynamics from a three-level transition to a four-level transition occurs approximately in the middle of the 1 μm emission band at ~1.06 μm [29]. The small quantum defect and feeble excited state absorption (ESA) reduce the thermal effects and allow high efficiencies for Yb-lasers and amplifiers. It is possible to use very high Yb-doping concentrations in the fiber fabrication process,

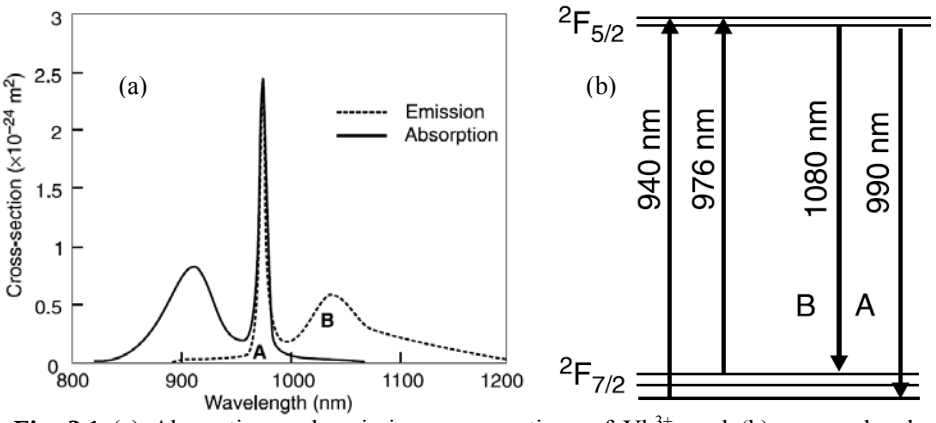

Fig. 2.1 (a) Absorption and emission cross-sections of Yb^{3+}, and (b) energy level diagram (adapted from [30]).

which leads to fibers with very high absorption and short length. This is typically favorable in short-pulse mode-locked and Q-switched fiber lasers. However, some Yb-doped fibers, especially those with high doping concentration, have recently been shown to suffer from photodarkening [31-34]. Photodarkening is an effect that results in a broadband loss centered at the visible wavelengths with a tail of the loss extending to near-infrared emission wavelengths under optical pumping of the fiber. This loss decreases the output power efficiency and long-term reliability of a high power or high-peak power laser. Photodarkening should therefore be avoided by careful fiber doping concentration and core structure design.

Erbium (Er)-doped fibers

Another commonly used rare earth metal element is erbium. Er^{3+} ions provide gain in a broad wavelength range around 1.55 μm, in the low-loss transmission window of optical fibers. This wavelength range is particularly interesting and important for optical communications. Therefore, Er-fibers were intensively studied during the end of the 20th century. The first Er-fibers were manufactured and reported in 1985 followed by demonstrations of Er-doped fiber amplifiers and lasers during 1987 [35-37].

The main absorption bands of Er^{3+}-ions from the aspect of optical pumping appear at ~980 nm and at 1480 nm (in-band pumping). These wavelengths are well-suited for commercial semiconductor laser diodes. The absorption and emission cross-sections of erbium are shown in Fig. 2.2. In lasers, the Er behaves as a quasi-three-level system as confirmed by experimental relaxation oscillation measurements [38]. Er-fibers are often co-doped with Yb-ions (sensitizer ions). Co-doping improves the pumping efficiency at 980 nm. In addition to telecommunication applications, Er-fibers are typically beneficial for ultrafast mode-locked fiber lasers because the fiber gain spectrum is broad and the fiber dispersion at 1.55 μm is anomalous. Anomalous dispersion supports the soliton pulse regime of mode-locked fiber lasers. In the soliton pulse regime, the anomalous dispersion and nonlinearity of the fiber are balanced, leading to very stable, self-adjusting soliton pulses that are resistant to noise and losses. High-quality soliton pulses are particularly beneficial in long-distance high-speed optical fiber communications.

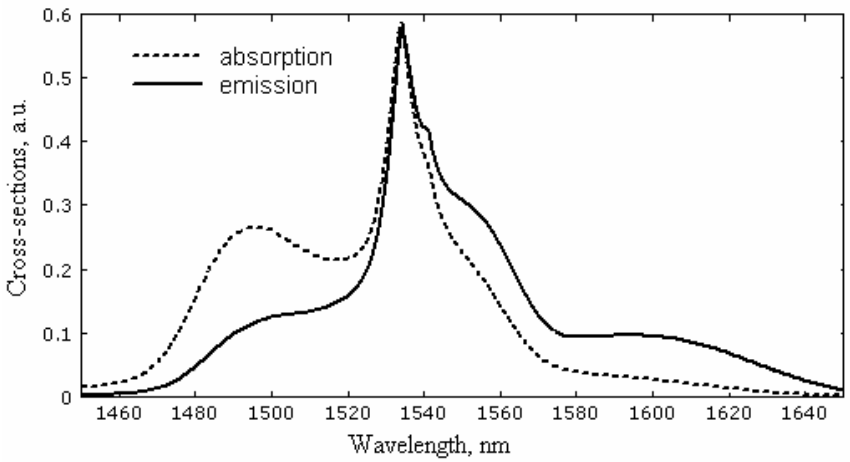

Fig. 2.2. Absorption and emission cross-sections of Er^{3+}-ions (adapted from [39]).

Thulium (Tm), thulium-holmium (Tm-Ho), and Ho-doped fibers

The long-wavelength amplification L-band of Er-doped fiber is limited to ~1.6 μm. Therefore, Tm-doped glass is an attractive material for extending the wavelength range of fiber amplifiers and lasers further into the short-wave - mid infrared region. Thulium-doped fibers provide optical gain for wavelengths situated close to 2 μm. The main applications for lasers operating in the short-wave - mid infrared range (1.8 - 3 μm) are spectroscopy, ranging, and biomedical and military applications [13,18,19] The first Tm-doped fiber laser operating at 1.9 μm was reported in 1988 [40]. The laser was pumped by a dye laser at ~0.8 μm. Since then, various high power and pulsed operation demonstrations have followed for Tm^{3+}-based glasses. Typical host materials for Tm^{3+} are silica and fluoride-based glasses. Fluoride-based glasses, often called ZBLAN (composition of ZrF, BaF, LaF, AlF and NaF) glass, benefit from the lower unsaturable absorption beyond 2 μm, but on the other hand are trickier to handle. Recently, tellurite-based (TeO_2) host glasses have also been demonstrated [41].

The main absorptions bands of thulium are located at ~0.8 μm, at ~1.15 μm, and at ~1.55 μm, as seen in Fig. 2.3(a) [40,42]. The main emission band is broad, ranging from ~1.7 μm to 2.15 μm (see Fig. 2.3(b)) [40]. According to relaxation oscillation experiments, change in transition dynamics of Tm^{3+} from the three-level transition to the four-level transition occurs at ~2025 nm meaning that Tm^{3+} is a quasi-three level medium [43]. The energy level diagram of thulium is shown in Fig. 2.4. The energy levels allow for several different pumping options. The most commonly used pump wavelength is 0.8 μm, with multimode semiconductor pump diodes widely available at this wavelength. However, when pumping with 0.8 μm, the quantum defect is large, leading to increase of temperature and cooling problems in Tm^{3+}-doped fibers. The absorption at ~1.15 μm also allows the use of commercial semiconductor-based laser bars. The main obstacle related to pumping at this wavelength is the relatively low powers of the 1.15 μm laser bars available. In terms of low quantum defect, a good option for pumping of Tm-doped fibers is an erbium fiber laser operating at 1.56 μm. This type of single mode lasers allow direct pumping into the core of the fiber and decrease the quantum defect significantly. Core-

pumping technique is useful for low- and medium power mode-locked and Q-switched fiber lasers.

Tm-doped fibers can also be used to generate visible blue and ultraviolet fluorescence emission via various upconversion processes [44-47]. Ground-state absorption (GSA), excited state absorption (ESA), and cross-relaxation (CR) processes can all be pronounced in Tm^{3+}-doped fibers [48,49]. Using ESA, upconversion lasers delivering several hundred mW output power have been demonstrated at the interesting wavelength of 480 nm using 1.15 μm pumping [44,46]. Weaker ESA can occur also with other pump wavelengths. When Tm^{3+}-doped fibers are used for ~2 μm laser emission these effects are detrimental and should be minimized by careful choice of fiber doping level.

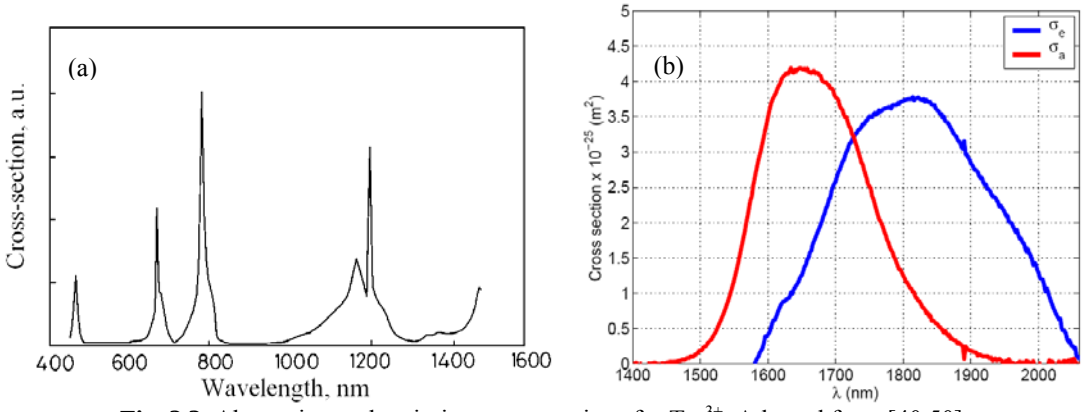

Fig. 2.3. Absorption and emission cross-sections for Tm^{3+}. Adapted from [40,50].

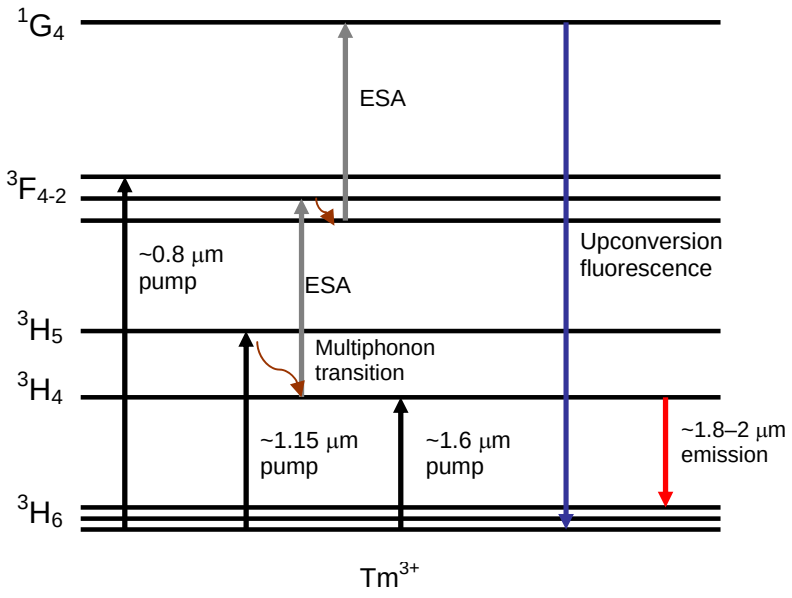

Fig. 2.4. Simplified energy level diagram of Tm^{3+} showing the most important transitions.

Although Tm^{3+}-doped fibers have a broad emission band ranging up to 2.15 μm, the long wavelength tail beyond 2 μm is generally weak, forcing the lasers to operate at wavelengths typically below 2 μm, or with significantly decreased efficiency. In order to enhance the fluorescence beyond 2 μm, Ho^{3+}-ions can be added as sensitizers. As a result it is possible to design lasers with high efficiency at 2.1 μm and even beyond [51]. Typically the doping ratio of Tm^{3+} and Ho^{3+} ions used is in the range of 10:1 [52]. The energy level diagram of a Tm^{3+},Ho^{3+} co-doped silica fiber, shown in Fig. 2.5, is very similar to the energy level diagram of a purely Tm-doped fiber. The excitation of the Tm^{3+},Ho^{3+} system to levels $^3H_4$, $^3H_5$ or $^3F_4$ can be made using the same pump wavelengths of ~1.6 μm, 1.15 μm, or 0.8 μm as with Tm-doped fibers. The energy is then transferred to the $^5I_7$ level of Ho^{3+} where the ~2 μm lasing transition takes place. However, if the Ho^{3+}-concentration, fiber length, or pumping power are too small it is conceivable that that laser radiation is only emitted from the $^3H_4$-level of Tm^{3+}, i.e. the Ho^{3+} does not affect the lasing at all. The Tm^{3+},Ho^{3+}-codoped fiber also changes its transition dynamics from a three-level transition to a four-level transition at the long wavelength tail, comparable to Tm^{3+} [53].

Fibers solely doped with Ho-ions have also been reported. Singly Ho-doped fiber lasers operate at 2.0-2.2 μm [54-57]. Another emission band of Ho is centered further in the mid-IR at ~2.9 μm, demonstrated for the first time as early as 1990 [58,59]. Ho-doped fibers can be pumped with 1.15 μm diodes, similarly to Tm, or using in-band pumping with Tm-doped fiber lasers operating at ~1.9 μm. In the first demonstration of a Ho fiber laser, the doped fiber was pumped at the visible absorption peak located at ~640 nm [58]. Typical host materials for Ho-doped fibers are fluoride and silica glasses for 2.9 μm and 2.1 μm operation wavelengths, respectively. A simplified energy level diagram for Ho is shown in Fig. 2.6.

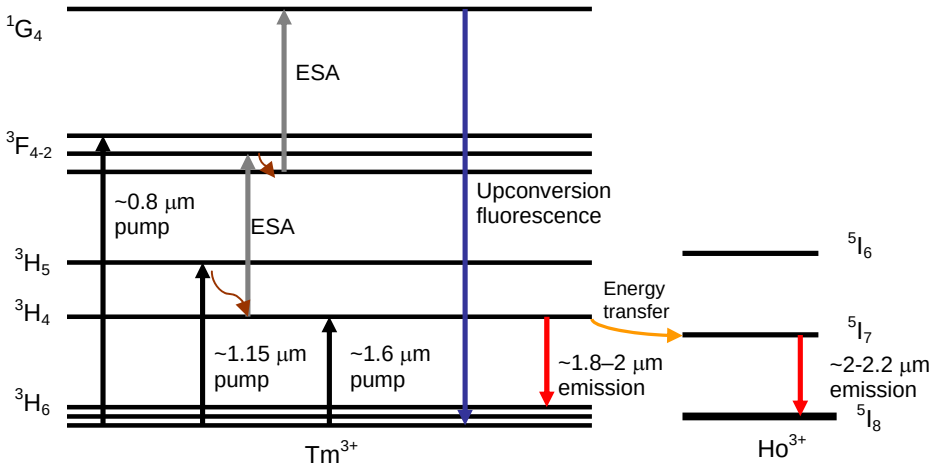

Fig. 2.5. Simplified energy level diagram of Tm^{3+}, Ho^{3+} - codoped fiber.

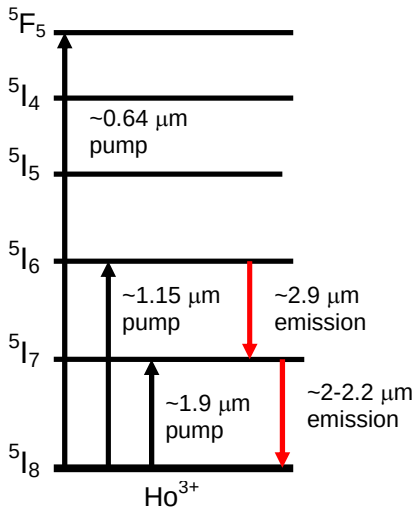

Fig. 2.6. Simplified energy level diagram of Ho^{3+}.

2.2 Active fibers doped with Bi-ions

Recently, a new type of fiber doped with Bi-ions has been demonstrated to provide optical gain and amplification over a broad wavelength range from 1100 nm to 1500 nm [60-63]. A driving force behind the development of these active fibers has been the lack of an appropriate fiber material between the gain bandwidths of Yb and Er-doped fiber lasers in the second telecommunication window situated at ~1.3 μm. At this wavelength range the loss of silica fiber is small, and therefore signals can be transmitted long distances in fiber optical links without amplification. In addition, the chromatic dispersion of optical fiber is close to zero around 1.3 μm, reducing the need for additional dispersion compensating fibers and other elements. Fiber amplifiers and lasers operating at this wavelength range could be ideal sources for optical communication. Lasers operating in the 1150-1300 nm wavelength range can also be frequency doubled employing nonlinear second harmonic generation to produce visible yellow-red emission. These sources could be used in various biomedical and astronomical applications.

The fabrication of bismuth-doped fibers with high gain and low unsaturable losses is very challenging. In recent years, considerable effort has been devoted to solving the main problems related to the concentration of Bi-ions and the chemical composition of the host material. In general, it has only been possible to use small concentrations of bismuth ions (~0.005 weight %) to initiate lasing in Bi-fibers. Higher doping levels, for reasons not precisely known, significantly increase the unsaturable 'grey' losses [64-66]. Further fundamental research on the properties of Bi in glasses is still required and is currently in progress.

Bismuth belongs to the group of metals. It also behaves differently as a laser gain medium compared to the rare earth metals used in doping of gain fibers. As already mentioned, the infrared luminescence centers in rare-earth atoms (Yb, Er, Tm, Ho) are typically due to the 3^+-ions. The characteristic of the valence state of bismuth that is responsible for IR-luminescence in Bi-fibers is different and still not completely understood. In 2001 Fujimoto and Nagatsuka reported an intense luminescence around

1.2 μm in bismuth-doped silica glasses co-doped with aluminum [67]. They proposed that Bi-centers emitting in the near-IR are Bi^{5+}-ions [67]. Since then, there have been various reports on broadband emission in Bi-doped bulk glasses and in silicate-hosted fibers fabricated by modified chemical vapor deposition (MCVD) or surface-plasma chemical vapor deposition (SPCVD) techniques [60-63,68-75]. Different luminescent centers, such as Bi^{+} [69], BiO [70], Bi-clusters [71], and interstitial negative-charged bismuth dimers Bi_2^{-}, Bi_2^{2-} [72] have been proposed to be responsible for the near-IR emission. In 2006, it was proposed, based on experimental observations, that luminescence takes place only for the simultaneous presence of Bi with Al in the glass network [73]. However, in 2008 a different glass composition in the fiber core, alumina-free Bi-doped phosphogermanosilicate glass (PGSB), was reported to provide near-IR luminescence in the wavelength region of 1300–1470 nm [62]. In general, it has been observed that aluminosilicate Bi-fibers (ASB) provide gain and can be employed in the 1140-1215 nm spectral range [76]. The spectral region from 1300 nm to ~1500 nm can be covered either with PGSB-fibers [62], germanosilicate fibers (GSB) [77], or ASB-fibers [63]. In the case of PGSB and GSB-fibers, it has been proposed that the emission in the short wavelength wing of the 1100-1500 nm band could be attributed to bismuth-associated active centers (bismuth center, BC) combined with a P atom. The long wavelength wing of the band can be attributed to BC combined with Ge and Si [76].

A typical amplified spontaneous emission (ASE) spectrum of a bismuth-doped aluminosilicate fiber is shown in Fig. 2.7(a). As can be seen, the spectrum is broad, ranging from ~1100 nm to 1400 nm, with the gain peaking at ~1200 nm. The broad amplification band potentially allows femtosecond pulse generation in mode-locked lasers. The absorption spectrum of the same fiber is shown in Fig. 2.7(b). The sharp peak in the absorption and rapid decrease in the gain at ~1400 nm are due to the presence of OH-group absorption in this particular bismuth-fiber [68,73]. It should be noted, that in general the shapes of the absorption and emission spectra in bismuth-fibers depend critically on the core glass composition [73]. Absorption spectra of various bulk glasses doped with Bi in combination with Al have been shown to have broad bands at ~300 (for silicate glass), 500, 700, 800, and 1000 nm [67,68,70,73]. The absorption edge at ~300 nm is attributed to Bi_2O_3, and the other bands are due to the specific optically active Bi center under study [73]. The absorption bands at 700, 800, and 1000 nm can also be seen in the absorption spectrum shown in Fig. 2.7(b).

Even though several absorption bands are clearly seen in the wavelength range from 700 nm to 1100 nm, the optical pumping wavelength of aluminosilicate bismuth fiber is still not a straightforward choice. Good options from the pump laser point of view could be 800 nm, 920 nm, 980 nm, and 1080 nm, as suitable pump lasers are readily available for these wavelengths. However, Bi-doped fiber lasers have so far only been demonstrated using pumping at ~1080 nm band [64-66]. The limiting factor for pumping below ~1040 nm seems to be the growing ESA towards shorter pump wavelengths [78-80]. It has been shown that strong ESA appears at 915 and 975 nm when pumping below 1047 nm, whereas no significant ESA is observed when pumping at the 1080 nm band, or in the primary emission band of Bi-doped silicate fiber lasers [78-80]. Moreover, it was observed that the spectral shape of the emission cross sections depended on the pump wavelength, and the emission cross-section peak was reduced under 915 and 975 nm pumping . Therefore, it seems that pump wavelengths below 1000 nm cannot be used for

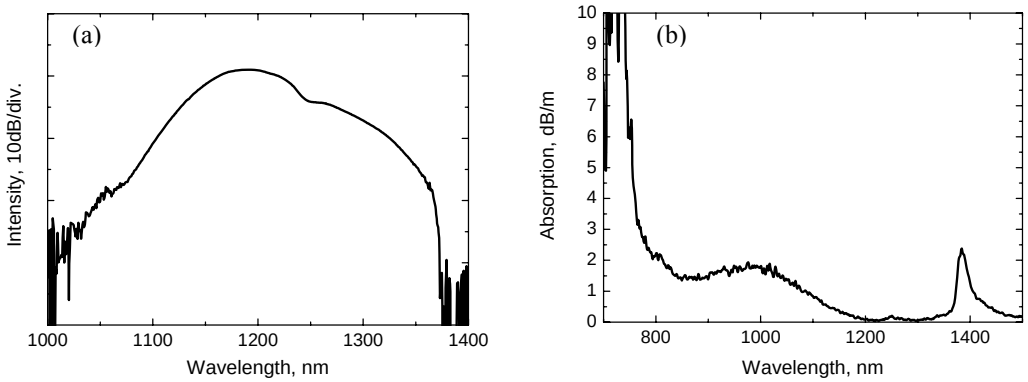

Fig. 2.7. (a) ASE-spectrum of a bismuth-doped aluminosilicate fiber under 980 nm pumping manufactured using SPCVD-technique. (b) Absorption spectrum of the same fiber.

core-pumping of efficient aluminosilicate bismuth lasers. Efficient cooling of the fiber has also been shown to reduce the temperature-induced unsaturable losses of the Bi-fibers and increase the laser efficiency [81]. Bi-doped fibers designed for 1.33 μm wavelength operation can also be efficiently in-band pumped with lasers emitting at ~1.23 μm, whereas Bi-lasers operating at ~1.48 μm can be pumped with 1.33 μm lasers [76].

2.3 Review of fiber lasers

In general, a fiber laser is a laser with a gain medium made of doped optical fiber. Sometimes this definition is further restricted to those lasers whose gain medium, and all or most of the intra-cavity components, are made of optical fibers. The first experiments and demonstrations with gain fibers were performed as early as at the beginning of 1960 century [82,83]. A flash lamp pumped Nd^{3+}-doped fiber with a core diameter of ~10 μm and length of 1 m was employed and substantial gain values were reported [83]. Since then, fiber lasers have developed greatly and become practical and compact systems with various advantages.

During 1970's fiber laser development was mainly targeted at different optical pumping methods and glass composition studies [84-86]. An important step was the manufacturing and using of low absorption loss silica (SiO_2) host glass fibers in 1973 [84]. The first single mode cw fiber lasers, however, were not developed until 1985 [87]. At that time a group in the University of Southampton in the UK developed an optical fiber manufacturing technology for rare-earth ion doped fibers based on the modified chemical vapor deposition (MCVD) method [35,88]. This was an essential step towards the practical rare-earth ion doped fiber lasers with very precisely known and controlled doping concentrations. After this demonstration, novel lasers and gain fibers doped with Er, Yb, and Tm were fabricated and used for optical amplification in silica based host glasses, with the main emphasis being on Er-doped fibers at the beginning.

Soon after the first demonstration of a single-mode cw fiber laser, the first Q-switched and mode-locked fiber lasers were reported [89,90]. The pulse initiating element was an acousto-optic modulator. The pulse widths in these demonstrations were 200 ns and ~1 ns, respectively, for Q-switching and mode-locking. The first mode-locked fiber laser

benefiting from soliton pulse shaping was reported in 1989 [91]. The Er-doped fiber laser delivered ~4 ps pulses. Sub-picosecond pulses were reported for the first time in 1990 from a Nd-doped fiber laser including dispersion compensation by a grating pair [92]. One year later, in 1991, the development of mode-locked Nd-doped fiber lasers was improved using a nonlinear amplifying loop mirror (NALM) for pulse generation and a grating pair for pulse compression [93]. This was the first passively mode-locked fiber laser with pulse durations as short as 125 fs. The development towards compact all-fiber lasers without additional bulk elements such as modulators, gratings and prisms was accelerated during the same year when Duling reported an all-fiber Er-laser mode-locked by a nonlinear loop mirror [94,95]. This laser, with a so-called figure-eight cavity configuration, was composed only of truly fiber components.

During the last two decades a countless number of development reports from ultrafast fiber oscillators has been published. The pulse widths have been significantly scaled down, to the fs-regime, and the pulse energies have been scaled up to nJ-levels [96,97]. The shortest pulses (sub-50 fs) are typically obtained from Yb-fiber lasers with very broad gain using passive mode-locking [97,98]. So far, the shortest pulse duration reported for a fiber laser is 28 fs [98]. The chirped pulse amplification (CPA) technology employed at the present time also enables amplification of the short pulses to high peak and average powers [99,100].

The output characteristics of Q-switched fiber lasers have also been drastically improved since 1986. A comparison of achievements related to Q-switched lasers is not as straightforward as with mode-locked short-pulse lasers, because the work has not only focused on the shortest possible pulses but also on high pulse energies and peak powers. I here content myself with mentioning only a few of the best results. In 1999, Paschotta *et al* reported a passively Q-switched Er-doped fiber laser delivering ~20 ns pulses with a pulse energy of ~15 μJ [101]. The master oscillator was further power-scaled up to 0.1 mJ energy using a power amplifier. The next year, an actively Q-switched Yb-doped fiber laser was demonstrated to deliver pulses with pulse energy up to 2.3 mJ [102]. In 2007, sub-10 ns pulses with pulse energies up to 2 mJ were reported from an actively Q-switched short-length rod type Yb-doped photonic crystal fiber laser [103]. Quite recently, at 2 μm wavelengths ~40 ns pulses with pulse energies of 0.27 mJ were demonstrated using an actively Q-switched Tm-doped fiber laser [104]. So far, the shortest pulses for a stable passively Q-switched fiber laser was reported for a highly-doped short-length Yb-doped fiber laser Q-switched by a high-contrast semiconductor saturable absorber mirror [105]. Pulses as short as 8 ns were demonstrated. Even shorter pulses can be obtained using the self-Q-switching regime based on the stimulated Brillouin scattering (SBS) mechanism [106-108].

Parallel to the development of ultrafast and Q-switched fiber oscillators, high power cw fiber lasers have been extensively studied and developed as fibers have a very high surface-to-volume ratio which avoids heat issues. The route for the rapid development of high power fiber lasers was already opened in 1989 with the invention and use of a double-clad fiber structure [109]. This nowadays commonly used structure has a core for signal propagation together with a larger second cladding for the multimode pump light. This geometry allows the use of low-brightness, fairly inexpensive multimode emitters for pumping while preserving the desired single-mode beam-quality for the signal. The

growth of the high power fiber laser market has also partly been enabled by the increasing power available from low-brightness semiconductor pump diodes.

Another important development step in the field of high power fiber lasers was the variation of the effective mode-field by changing the core diameter and numerical aperture of the fiber, i.e. invention and use of large-mode area (LMA) fibers [110]. LMA fibers allow single-mode or few-mode operation in a fiber with extended core size compared to standard single mode telecommunication fibers, therefore significantly reducing the effects of fiber nonlinearities and allowing higher powers.

During the last few years most of the efforts have been directed towards Yb-doped cw fiber lasers operating at 1 μm for the use in micromachining, and material processing applications in heavy industry. Just to mention a few of the milestones during the past few years, in 2003, 0.5 kW of cw power with very good beam quality was reported at the wavelength of 1 μm [111]. The next year the 1 kW borderline was exceeded for Yb-doped fiber lasers with high efficiency and only single delivery fiber [112]. Currently, nearly single mode and diffraction-limited high-power systems can deliver up to 10 kW of cw power in a one delivery fiber and multimode systems even up to 50 kW [113].

3. Q-switched fiber lasers for energetic nanosecond pulse generation

This chapter describes the basic principles of Q-switching. The most common Q-switching methods are reviewed with a focus on passively Q-switched fiber lasers. A new effect, gain induced pulse shortening, remarkably affecting the characteristics of a Q-switched fiber laser, is introduced using numerical simulations and experimental results [P1]. In the last section, a Tm^{3+},Ho^{3+}-doped fiber laser Q-switched by a highly nonlinear GaSb-based semiconductor saturable absorber mirror is studied and optimized in order to produce short, high-energy pulses in an important wavelength range around 2-μm [P2].

3.1 Basic principles of Q-switching

In general Q-switching is a method used to generate energetic pulses (giant pulses), with durations typically in the range of nanoseconds, by modulating intra-cavity losses of a laser. When the losses of a resonator are varied, the resonator Q-factor is also varied, resulting in a so-called Q-switched operation. The intra-cavity loss-modulation can be performed actively using, for example, modulators, or passively with saturable absorbers. Basically, the laser pumping builds up a large inversion producing large gain while the resonator losses are sustained at high levels. Suddenly, the resonator losses are minimized; the energy stored in the cavity is released in the form of an intense pulse. Usually, the growth of the pulse begins from the spontaneous emission. After the strong pulse, the high initial inversion drops back to the 'normal' low level until the next pulse starts to grow again. Typically, Q-switched lasers are employed in applications that require high pulse energies and peak powers with reasonably high average powers and short pulses. [114]

3.1.1 Active Q-switching

In active Q-switching the losses of the laser cavity are modulated actively by employing acousto- (AOM) or electro-optic modulators (EOM), or mechanically by inserting a quickly rotating mirror or a prism. The latter method, however, suffers from the limited speed, accuracy and reliability of the available rotating motors. Acousto- and electro-optic modulators are fast and do not have any movable parts, and therefore offer Q-switched pulses with relatively low timing jitter. Timing jitters lower than 0.5 ns have been reported for actively Q-switched microchip lasers [115]. This value can in principle be reduced by nearly two orders of magnitude using a modulator in combination with a saturable absorber [116].

Fig. 3.1 shows the temporal evolution of gain and loss inside an actively Q-switched laser cavity. The inversion, and hence the gain and energy, increases when the cavity losses are kept at high level when the modulator is in the off-state (low Q). When the modulator is switched to the on-state (high Q), meaning that the cavity losses are low, a short and intense pulse grows from the spontaneous emission and gathers the energy

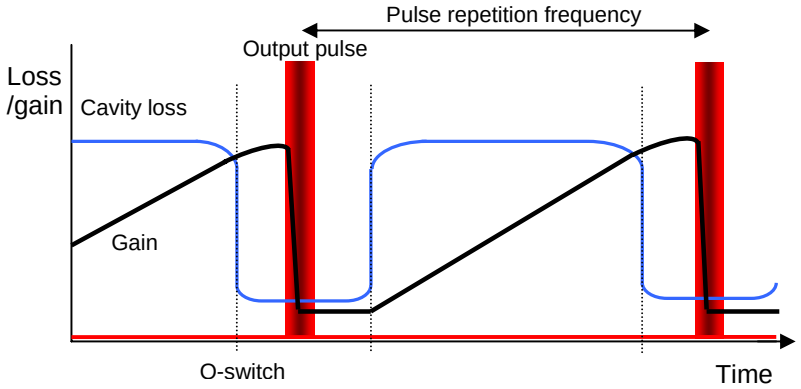

Fig. 3.1. Temporal evolution of laser cavity losses and gain in an actively Q-switched laser. The pulse is created after the cavity losses are switched off using a modulator.

stored in the cavity (the gain well exceeds the losses in the cavity). During the pulse, the initial inversion and gain in the cavity are depleted. The modulator goes back to the off-state and the cavity again starts to store the energy for the next consecutive pulse. It is worth noting that, it is beneficial to use a gain medium with a high upper-state life-time, so that the stored energy is not lost as fluorescence emission before the opening of the Q-switch [114].

The modulator frequency, and consequently, the laser repetition rate, can be varied by driving the modulator with different seed signals. Typically the repetition rates used are in the range of 1-100 kHz. The pulse duration and pulse energy of the laser depend on the stored pulse energy in the cavity, i.e. the modulator frequency and pump power. Usually the pulse duration decreases and pulse energy increases with increased pump power [104,114,117]. It has been shown that the pulse duration has the following relation to the laser gain and cavity round-trip time:

$$t_w = \frac{8.1 \cdot t_{rt}}{g_{rt}}, \tag{3.1}$$

where t_{rt} is the cavity round-trip time and $g_{rt} = \ln G_{rt}$ is the round-trip gain coefficient when the pulse begins to form [115,117]. As can be seen, the pulse width decreases by shortening the cavity length and by increasing the gain by stronger pumping. The reflectivity of the output coupler also affects the gain and hence the pulse duration. The pulse energy of an actively Q-switched laser can be increased by decreasing the repetition rate with certain restrictions; with low repetition rates the amplified spontaneous emission degrades the laser operation (the upper-state lifetime is shorter than the pulse period) and limits the higher pulse energies [114].

3.1.2 Passive Q-switching

Passive Q-switching typically employs a saturable absorber to modulate the cavity losses and gain. Saturable absorbers can be made of various materials such as different semiconductor compounds or crystals doped with ions like Cr^{2+}, Cr^{4+}, V^{3+}, or Co^{2+} [101,118-123]. Sometimes doped fibers can also be used as saturable absorbers to passively generate Q-switch pulses in all-fiber lasers [124,125]. However, the pulse trains

of these lasers are rather unstable. Compared to active Q-switching, passive Q-switching is typically a more cost-effective and simpler method to provide compact setups as there is no need for rather expensive and bulky AOMs or EOMs. However, the timing jitter, typically in the range of microseconds, is large compared to actively Q-switched lasers due to fluctuations in temperature, pump power, losses, etc. Especially in fiber lasers with relatively high level of intracavity spontaneous emission, the jitter may be significant, as the Q-switching starts from noise-like spontaneous emission with large timing fluctuation - a "first photon"-principle. Indeed, the jitter can be significantly reduced, from microsecond to nanosecond level, by optically modulating or triggering the saturable absorber [126-128].

In a passively Q-switched laser the cavity loss is modulated by the saturable absorber which transmission/reflection depends on the light intensity. Basically, the pulse is released when the cavity energy reaches a certain value determined by the absorber saturation fluence. The pulse repetition rate therefore depends on the stored energy, i.e. pump power. Relatively high repetition rates, up to few MHz-level, can be obtained with passively Q-switched lasers [129]. Pulse energy and pulse width are often nearly independent of the pumping [117,130]. However, this is not the case with all fiber lasers, as will be shown in section 3.3 [P1].

3.2 Main parameters of passively Q-switched lasers

Pulse energy

Let us now consider a laser cavity with a gain element having a length of L_g providing a time-dependent gain coefficient g(t); a saturable absorber with a saturable loss coefficient q(t) (unbleached value is q_0 and bleached value is 0) and a nonsaturable loss of l_p; an output coupler with transmission of T_{out} and output coupling coefficient l_{out} ($T_{out} = 1 - 10^{-l_{out}}$) (see Fig. 3.2.) [130]. The total nonsaturable loss of the cavity within a one cavity roundtrip is therefore $l = l_p + l_{out}$. The saturation energy of the absorber (E_a) is considered to be small compared to the saturation energy of the gain medium (E_l).

The stored energy in the gain medium under optical pumping can be described as follows:

$$E_{stored} = AL_g N_2 h\nu_l , \tag{3.2}$$

where N_2 is the excitation density, $h\nu_l$ is the photon energy at the pumping wavelength, and AL_g is the pumped gain volume. This can be modified to

$$E_{stored} = \frac{h\nu_l}{2\sigma_l} Ag = E_l g , \tag{3.3}$$

where $g = 2\sigma_l N_2 L_g$ is the gain coefficient per round trip, σ_l is the emission cross section of the laser material, and E_l the saturation energy of the gain medium given by

$$E_l = \frac{h\nu_l}{2\sigma_l} A. \tag{3.4}$$

The released energy can then be expressed using the stored energy and the difference of the initial and final gain coefficients (gain coefficient just before and after the pulse):

$$E_{released} = E_l (g_i - g_f) = E_l \Delta g \,. \tag{3.5}$$

The output pulse energy can then be obtained by multiplying the released energy with the output coupling efficiency:

$$E_p = E_l \Delta g \frac{l_{out}}{l_{out} + l_p} \,. \tag{3.6}$$

The maximum achievable energy can be expressed as $E_p=E_l g_i$, because Δg can naturally not exceed the value of g_i. The unknown parameter Δg can be derived for four different phases of a Q-switch pulse cycle.

In the first phase the saturable absorber is in its unbleached high-loss state. The pulse starts to grow when the gain reaches the value of the unsaturated losses:

$$g_i = l + q_0 \,. \tag{3.7}$$

The intra-cavity power grows slowly starting from spontaneous emission noise, until it is sufficient to bleach the absorber [130]. In the second phase when the absorber is fully bleached, the power grows quickly as the net gain is $g_i - l - q \approx q_0$. The pulse maximum is reached when the net gain is zero, i.e. g = l. After the pulse maximum, the gain starts to decrease. In phase three, the gain decreases. In phase four, the absorber recovers back to its unbleached state and the gain in the cavity starts to grow again with pumping. When the gain reaches the threshold level, phase one begins again. The cavity prepares to create the next pulse. A simplified evolution of gain, loss and power in a passively Q-switched laser cavity is shown in Fig. 3.2.

Obviously, the gain reduction Δg during phase three depends on the modulation depth of the absorber q_0 and the total nonsaturable losses of the cavity l. For large output coupling ratios ($l>>q_0$) the gain difference can be expressed as (see Fig. 3.2) [130]:

$$\Delta g \approx 2q_0 \,. \tag{3.8}$$

Inserting equation (3.8) into (3.6) we obtain an expression for the pulse energy:

$$E_p = \frac{h\nu_l}{2\sigma_l} A \cdot 2q_0 \frac{l_{out}}{l_{out} + l_p} \,, \; l>>q_0. \tag{3.9}$$

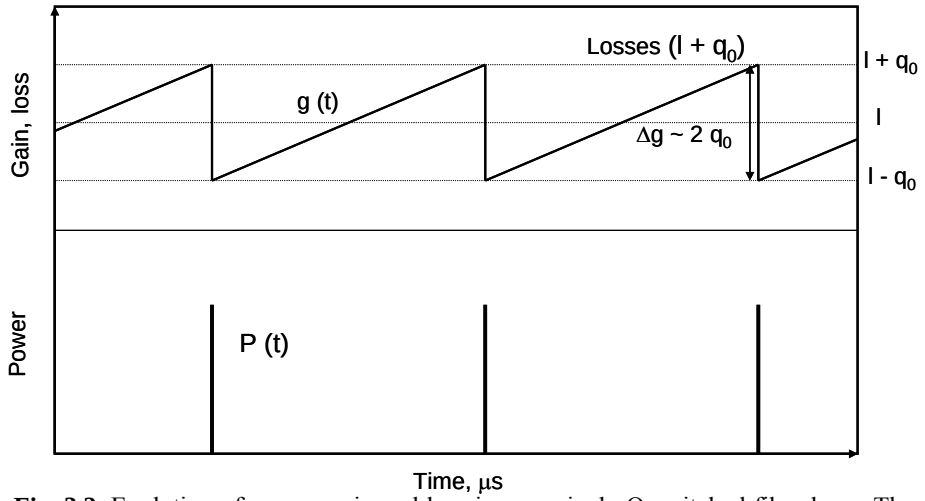

Fig. 3.2. Evolution of power, gain and loss in a passively Q-switched fiber laser. The time scale has units of μs. Typical Q-switch pulse duration is on the ns level.

The gain, and consequently the pulse energy, can be increased by increasing q_0 and l. However, the available gain limits the value of $g_i = l + q_0$ [130]. In addition, the absorber nonsaturable losses typically increase with the increase in the modulation depth. It has been shown that for absorbers with parasitic losses, an optimized pulse energy can be obtained with $l \approx q_0$ [130].

Pulse width

The pulse width of a passively Q-switched laser can be shown to be directly proportional to the cavity round-trip time and inversely proportional to the saturable losses of the laser cavity, i.e. modulation depth of the saturable absorber [117,130]. According to [131] the pulse width can be expressed as:

$$\tau_p = \frac{S_p T_r}{q_0}\left[\frac{\delta(1+\delta)\eta}{\delta - \ln(1+\delta)}\right], \tag{3.10}$$

where S_p ~0.88 is the pulse-shape factor, T_r is the cavity round-trip time, η is the energy extraction efficiency of a light pulse given by $\eta(1+\delta) = -\ln(1-\eta)$, and $\delta = q_0/(l_p+l_{out})$, is the ratio between the saturable and unsaturable cavity losses. With a given value of saturable loss (absorber modulation depth), the shortest attainable pulse width approaches the value of [117,131]:

$$\tau_p \approx \frac{3.52 T_r}{q_0}, \ (l_p + l_{out} >> q_{0)}. \tag{3.11}$$

This expression gives the shortest pulse width achievable from a passively Q-switched laser using classical methods. It is notable that the equation (3.11) is derived using an assumption that the duty cycle is low, which is not always the case with fiber lasers. The calculated dependence of the pulse width on the modulation depth of the absorber for two different cavity round-trip times, that correspond to typical highly doped fiber cavity lengths, is plotted in Fig. 3.3. As can be seen the modulation depth of the absorber and the cavity length have a significant effect on the pulse duration.

However, the optimization for short pulse widths decreases the laser efficiency and increases the threshold. Actually, the optimizations for a short pulse width, high

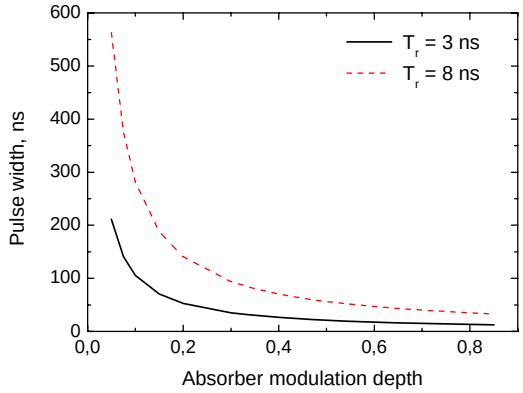

Fig. 3.3. Calculated dependence of pulse width on modulation depth of the saturable absorber with cavities having round-trip times of 3 ns and 8 ns.

efficiency, and low threshold are a trade-off and finally determined by the requirements of the application. In the limit of low saturable losses, expression (3.10) reaches a value of [131]:

$$\tau_p \approx \frac{0.88T_r}{l_p + l_{out}}, (l_p + l_{out} << q_0). \tag{3.12}$$

As can be seen, the extraction efficiency is high, but at the expense of the pulse width.

Repetition rate

An equation for the repetition rate can be derived using the expressions for pulse energy and average output power. The average output power can be expressed as follows:

$$P_{ave} = \eta_s (P_p - P_{th}), \tag{3.13}$$

where η_s is the laser slope efficiency, P_p the pump power, and P_{th} the threshold pump power. Therefore, the pulse repetition rate f can be expressed as:

$$f = \frac{\eta_s (P_p - P_{th})}{E_p} \propto r - 1. \tag{3.14}$$

The repetition rate is dependent on the pump parameter r that is defined as the ratio of the pump power to the threshold pump power. The pump power and the threshold power can be further expressed in more useful forms [130]:

$$P_p = \frac{h\nu_p A}{2\sigma_l \tau_l \eta_p} g_0, \qquad P_{th} = \frac{h\nu_p A}{2\sigma_l \tau_l \eta_p} (l + q_0). \tag{3.15}$$

Here $h\nu_p$ is the pump photon energy, η_p is the pumping efficiency, and τ_l is the upper state life-time of the gain medium. The expression for repetition rate can now be derived using equations (3.6) and (3.15):

$$f = \frac{g_0 - (l + q_0)}{\Delta g \tau_l} \approx \frac{g_0 - (l + q_0)}{2q_0 \tau_l}. \tag{3.16}$$

When operating far above the threshold, the expression assumes the simpler form of [132]

$$f \approx \frac{g_0}{2q_0 \tau_l}. \tag{3.17}$$

The repetition rate can also be estimated (at pump powers well above the threshold) by relating it to the ratio of absorbed pump power and absorbed threshold pump power [131]:

$$f \approx \frac{P_{p,abs}}{P_{th,abs} \tau_l}. \tag{3.18}$$

The repetition rate depends linearly on pump power assuming traditional theory. This has also been confirmed by various experiments using short pulse microchip and fiber lasers [126,130,104].

3.3 Dynamic gain induced pulse shortening in passively Q-switched fiber lasers

In the previous section the main parameters of passively Q-switched lasers were considered using well-established theory made for microchip lasers described in [117,130,131]. The main assumptions in the formalism are low duty cycle and constant inversion within the short laser cavity. In fiber lasers with larger gain and longer cavity-length, the duty cycle attains much higher values and the pulse evolution within the cavity is more complicated than in microchip lasers. In this section we introduce and describe an effect, "gain induced pulse shortening", which affects the Q-switching parameters in fiber lasers with large gain volume [P1]. We derive new equations for pulse width, pulse energy and repetition rate and compare them to experimental results. The analysis tends to extend the well-known theory of passively Q-switched microchip lasers to fiber lasers that have longer cavity length, and larger gain and duty cycle. The driving force for this analysis was the unexpected behavior of a passively Q-switched Tm^{3+},Ho^{3+}-doped fiber laser that will also be described here.

The Tm^{3+},Ho^{3+}-doped fiber laser was Q-switched using a GaSb-based semiconductor saturable absorber mirror consisting of 15 GaInSb quantum wells placed within a 3-λ GaSb cavity grown on top of an 18-pair AlAsSb–GaSb Bragg reflector. The modulation depth of the absorber was 8% at the laser wavelength of 1970 nm. The absorber was used as grown without post irradiation in order to maintain the absorption recovery time at the level of hundreds of picoseconds beneficial to Q-switching. The schematic of the passively Q-switched Tm^{3+},Ho^{3+}-doped fiber laser used in the experiments is shown in Fig. 3.4.

The cavity round-trip time is 20 ns. According to equation 3.11 the expected pulse width is ~800 ns (low duty cycle limit). However, the shortest obtained pulse width during the measurements was 160 ns (see inset to Fig. 3.5(a)) corresponding to a pump power exceeding 15 times the threshold pump power. Fig. 3.5(a) illustrates the dependence of pulse duration on the ratio of pump power to threshold pump power. As can be seen, the pulse width essentially depends on the pump power which is contrary to the traditional theory.

In order to resolve the inconsistency, rate equation analysis was applied [130]. Saturation of the gain g, the saturable absorption q, and the evolution of the intracavity power P can be respectively expressed as:

$$\frac{dg(t)}{dt} = -\frac{g(t)-g_0}{\tau_g} - \frac{gP(t)}{E_{sat,q}}. \tag{3.19}$$

$$\frac{dq(t)}{dt} = -\frac{q(t)-q_0}{\tau_a} - \frac{qP(t)}{E_{sat,a}}. \tag{3.20}$$

$$\frac{dP}{dt} = (g-l-q)\frac{P}{T_r}. \tag{3.21}$$

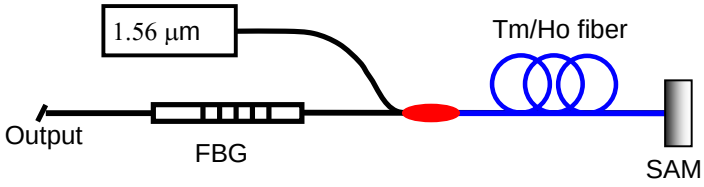

Fig. 3.4. The schematic of the passively Q-switched fiber laser.

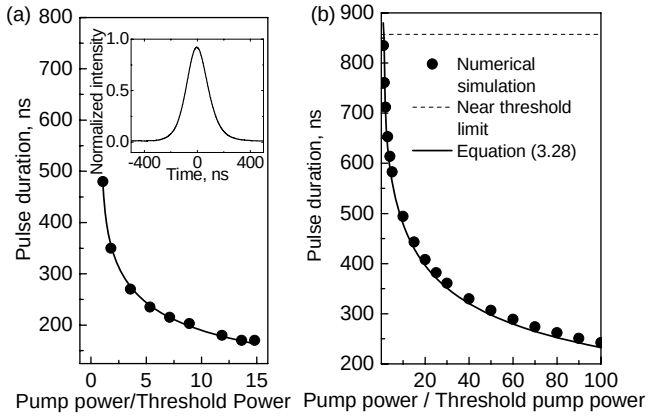

Fig. 3.5. (a) Measured Q-switched pulse durations for different pump powers fitted according to equation (3.28) and oscilloscope trace of a ~160 ns Q-switched pulse for the laser pumped highly above the threshold, 15× (inset), (b) Q-switched pulse width obtained from numerical simulation using the rate equations (3.19-3.21) (scatter plot), in the near threshold limit (dashed line) assuming $\Delta g=2q_0$, and estimated with equation (3.28) (solid line).

In (3.19) and (3.20), $E_{sat,g}$ and $E_{sat,a}$ are the saturation energies and τ_g and τ_a the recovery times for the saturable gain and saturable loss, respectively. In (3.21) l is the cavity loss and T_r is the roundtrip time. Figures 3.5 and 3.6 show the results of the numerical simulations based on the above equations made with the following laser parameters: $E_{sat,g}$=10 μJ, $E_{sat,a}$=10 pJ, τ_g=1 ms, τ_a=1 ns, q_0=0.083, l=0.693, T_r=20 ns, P_0=1 nW. Two different operation regimes were considered in the calculations: operation near the threshold (see Fig. 3.6(a)) with $g_0=1.1(q_0+l)$ and operation far above the threshold (Fig 3.6(b)) with $g_0=25(q_0+l)$. The situation in Fig. 3.6(a) basically matches the low-duty cycle pulse evolution shown in Fig. 3.2. On the other hand, it can be seen that for strong pumping, the gain recovers to a value far above the level $l+q_0$ and drops to a value much lower than $l-q_0$, in contrast to the assumption that gain variation ranges from $l+q_0$ to $l-q_0$, typically used in Q-switched laser calculations. The increased range of gain variation under strong pumping found in the above analysis is an observation that provides a basis for explaining the pulse narrowing mechanism.

During the gain recovery phase and pulse build-up, the gain recovery can be expressed as:

$$g(t) = \left[l + q_0 - g_0\right]\exp(-t/\tau_g) + g_0, \tag{3.22}$$

assuming an unbleached saturable absorber. The gain reaches the level of the losses $l+q_0$ at the time t = 0 (dashed line in Fig. 3.6(b)). At the time t = 0 the pulse power starts to develop from the noise level $P(t = 0) = P_0$. Assuming far above threshold pumping, the gain increases until the power level reaches the value of $g_0E_{sat,g}/\tau_g$. When the gain

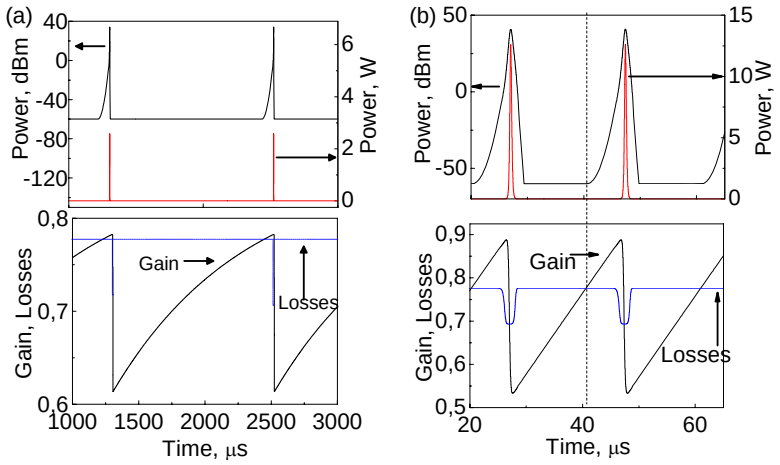

Fig. 3.6. Simulation of Q-switching illustrated with temporal evolution of cavity gain/loss and output power during Q-switched pulse formation. Pumping condition corresponds to operation (a) close to lasing threshold (low duty cycle) (b) far above the lasing threshold. The intracavity power is shown both in linear and dBm scale.

parameter g_0 is close to the threshold gain, the gain recovers to a value close to the threshold value $g = l+q_0$. In contrast, when the gain is much higher than the threshold gain, the gain recovers to a much higher value. The intracavity power during the gain recovery can be expressed in the form:

$$P(t) = P_0 \exp\left[\frac{t^2(g_0 - l - q_0)}{2\tau_g T_r}\right]. \tag{3.23}$$

From this equation it is possible to obtain an expression for the time needed for to recover from the threshold value to the onset of the gain depletion when $P(t) = g_0 E_{sat,g}/\tau_g$:

$$t = \sqrt{\frac{2\tau_g T_r}{g_0 - l - q_0} \log\left(\frac{g_0 E_{sat,g}}{\tau_g P_0}\right)}. \tag{3.24}$$

At this time the gain has recovered to the value

$$g_i = l + q_0 + \sqrt{2}\sqrt{\frac{T_r}{\tau_g}}\sqrt{g_0 - l - q_0}\sqrt{\log\left(\frac{g_0 E_{sat,g}}{\tau_g P_0}\right)}. \tag{3.25}$$

The gain reduction/compression during the Q-switching process can be expressed as [130]:

$$\Delta g + l\log(1 - \Delta g / g_i) = 0\,.$$

Therefore, it can be shown that the gain variation can be written in the following form:

$$\Delta g = 2q_0 + 2\sqrt{2}\sqrt{\frac{T_r}{\tau_g}}\sqrt{g_0 - l - q_0}\sqrt{\log\left(\frac{E_{sat,g}}{\tau_g P_0}\right)} = 2\left(q_0 + A\sqrt{P / P_{threshold} - 1}\right), \tag{3.26}$$

with

$$A = \sqrt{2}\sqrt{\frac{T_r}{\tau_g}}\sqrt{\log\left(\frac{E_{sat,g}}{\tau_g P_0}\right)}\sqrt{l + q_0}, \frac{P}{P_{threshold}} = \frac{g_0}{l + q_0}. \tag{3.27}$$

By using the large output coupling estimation ($l \gg q_0$), a new expression for pulse duration that takes into account the gain-induced shortening in fiber lasers is obtained:

$$\tau = 7.04T_r / \Delta g = \frac{3.52T_r}{q_0 + A\sqrt{P / P_{threshold} - 1}}. \quad (3.28).$$

Fig. 3.5(b) shows the numerically simulated (rate equation analysis) and calculated [equation (3.28)] dependence of pulse width on pump power. As can be seen, simulation and calculation are in very good agreement. With pump powers far above the threshold (the duty cycle increases with pumping), the pulse width is well below the expected pulse width value of ~800 ns obtained using the near threshold, low-duty cycle analysis. In addition, the experimental data shown in Fig. 3.5(a) is fitted using the equation (3.28). The solid curve fits very well with the experimental measurement points.

Similar expressions for pulse energy and repetition rate can be derived by replacing the value of the gain variation $\Delta g=2q_0$ used in the near-threshold, low duty cycle analysis by expression (3.26). The pulse energy is then given by $E_{released}= E_{sat,g}\Delta g$ and the repetition rate by $f = (g-l-q_0)/(\tau_g \Delta g)$. Fig. 3.7 illustrates the simulated (rate-equations), calculated [equation (3.27)], and near threshold low duty cycle values of pulse energy and repetition rate for the passively Q-switched Tm^{3+},Ho^{3+}-doped fiber laser with parameters described above. As can be seen, the pulse energy actually depends significantly on the pump power in contrast to the nearly constant pulse energy obtained using the near-threshold (low duty cycle) analysis. The repetition rate of the laser does not depend linearly on the pump power with pump powers exceeding ~15 times the threshold, but rather starts to slightly level off (sub-linear behavior).

In conclusion, we have extended the traditional low duty cycle theory of passively Q-switched lasers to be better suitable for fiber lasers with typically relatively long-length cavity and large gain. We show that far above threshold pumping in passively Q-switched fiber lasers might lead to large gain variations (larger than $l+q_0-(l-q_0) = 2q_0$). The unsaturated gain value can substantially exceed the cavity losses and on the other hand, the saturable gain can achieve much lower values than expected. This leads to a large gain excursion Δg during pulse build-up. This feature can primarily be obtained and enhanced in fiber lasers, which typically have a much larger gain volume than, for example semiconductor based microchip lasers often used for generation of passively Q-switched pulses.

At low pumping powers when the duty cycle is relatively low also in fiber lasers, the values obtained using the dynamic gain induced pulse shortening analysis agree well with the traditional theory. However, when the pump power is increased, the duty cycle increases in Q-switched fiber lasers leading to large differences in the behavior of pulse width, pulse energy and repetition rate compared to the traditional low duty cycle theory derived mainly for microchip lasers. The deviations between the experiments and the numerical simulations seen in Figs. 3.5 and 3.7 can be attributed to the complicated pulse evolution in Q-switched fiber lasers. Additionally, it is notable and against the assumptions made in the numerical simulations that the inversion during a cavity round-trip in fiber lasers is not constant.

In the current experiments with the Tm^{3+},Ho^{3+}-doped fiber laser, we observed pulse shortening from ~800 ns to 160 ns when the pump power was increased from the threshold (low duty cycle limit) to 15 times the threshold. The strong shortening was related to the fairly long (1.2 m) gain fiber, which was used due to relatively low fiber doping concentration and low modulation depth of the used SESAM.

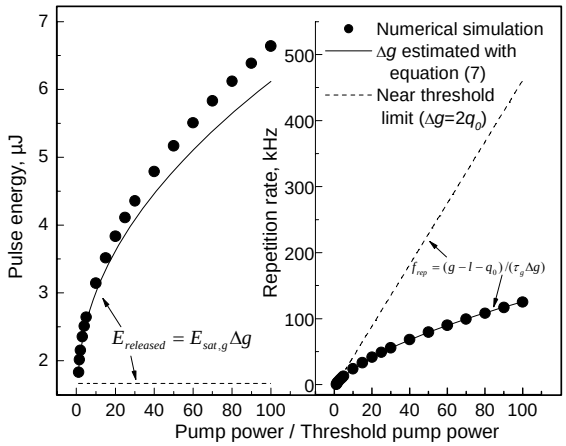

Fig. 3.7. Q-switched pulse energy (left side) and repetition rate (right side) obtained from numerical simulation (scatter) for near-threshold, low duty cycle limit (dotted line) and calculated with equation (3.27) (solid line).

3.4 Towards short pulse Q-switched lasers: optimization of passively Q-switched fiber lasers

As shown in the previous section, the main parameters affecting the pulse width in passively Q-switched fiber lasers are the cavity round-trip time, the absorber modulation depth and the gain-induced pulse shortening. Since the pulse width is directly proportional to the cavity round-trip time and inversely proportional to the modulation depth of the saturable absorber, the shortest pulse width achievable from fiber lasers is typically set by the cavity length, which can not be made as short as the value used, for example, in microchip lasers. Therefore, large modulation depth saturable absorbers together with short-length highly doped fibers should be used in order to attain short pulse widths. In addition, the gain induced pulse shortening gives an additional impact for shortening the pulse. Despite that, the shortest attainable pulse widths remain on the nanosecond level compared to the sub-ns pulses obtained from microchip lasers. The single-mode fiber lasers deliver typically pulses having duration of ~100 ns and good beam quality.

3.4.1 Passively Q-switched Tm-Ho-fiber laser using a highly resonant semiconductor saturable absorber mirror and dynamic gain induced pulse shortening

In this work we demonstrate and optimize the operation of a compact passively Q-switched 2 μm fiber laser [P2]. The aim is to provide pulses as short as possible while still maintaining fairly high average output power and pulse energy with good pulse quality. Passively and actively Q-switched Tm^{3+}-based fiber lasers demonstrated so far have exhibited pulse durations in the range from ~40 ns to 1 μs [104,124,133,134]. Among them, the most advanced 2 μm Q-switched fiber laser sources have relied on active switching techniques delivering, however, rather unstable pulses with fairly broad

spectra [104,134]. Pulsed and energetic laser sources operating at 2 μm wavelength can be used for eye-safe LIDAR, gas sensing (CO_2), and as counter measures in military applications.

The built all-fiber laser is shown schematically in Fig. 3.8. The oscillator comprises a short piece (~20 cm) of very highly doped Tm^{3+} (2.5 wt.%), Ho^{3+} (0.25 wt.%) aluminosilicate fiber, a dichroic pump coupler, a narrow bandwidth fiber Bragg grating (FBG) and InGaSb-based highly resonant semiconductor saturable absorber mirror. The exceptionally short doped fiber length is enabled by the use of core-pumping. A single mode cw Er-doped fiber laser operating at 1.56 μm acts as a pump source. The cavity round-trip time is ~4 ns. The resonant-SESAM comprises 20 InGaSb quantum-wells placed within a GaSb cavity with a Fabry-Pérot resonance at 1970 nm, and 18 AlAsSb/GaSb pairs for the distributed Bragg reflector (DBR) [see Fig. 3.9(a)]. To enhance the cavity induced effect and to increase the nonlinear response, the structure is capped with a 4-pair AlAsSb/GaSb DBR which increases the finesse of the Fabry-Pérot structure. The low intensity reflectivity of the SESAM is shown in Fig. 3.9(b). At the resonant wavelength of 1970 nm, the modulation depth of the absorber approaches ~70%. A ~300 μm-diameter collimated beam is directed onto the SESAM; the fluence for the Q-switched pulses at the resonant wavelength is ~70 mJ/cm^2, which corresponds to fully bleached absorption.

Fig. 3.10(a) shows the effect of the modulation depth on the pulse width; at the highest absorbed pump power of 5 W, the pulse width decreases from 67 ns to 19.6 ns for ΔR_{SAM} = 10% and 70%, respectively. When the SESAM is operated off-resonance at 1942 nm, 1948 nm or 1957 nm, the laser produces a pump dependent pulse width which approaches, at high pump powers, values that are shorter than those expected from classical low duty cycle passive Q-switching theory [dashed lines in Fig. 3.10(a)]. The dynamic gain induced pulse shortening obviously shortens the pulse to values below the near-threshold (low duty cycle) limit value. Fig. 3.10(b) illustrates further the effect of the modulation depth on pulse compression which we define as $(\tau_{P,threshold}-\tau_P)/\tau_{P,threshold}$, where $\tau_{P,threshold}$ is the pulse width at the lasing threshold and τ_P is the pulse width at a given pump power. The experimental results for pulse shortening, shown in Fig. 3.10(a), are also plotted against the SESAM modulation depth in Fig. 3.10(b) for two values of the pump power. The solid lines represent the numerical results obtained using equation (3.28) and are in a good agreement with the experimental data. As can be seen, the pulse shortening is more pronounced when an absorber with a small modulation depth is employed. This also explains the observed strong pulse shortening in [P1,S1].

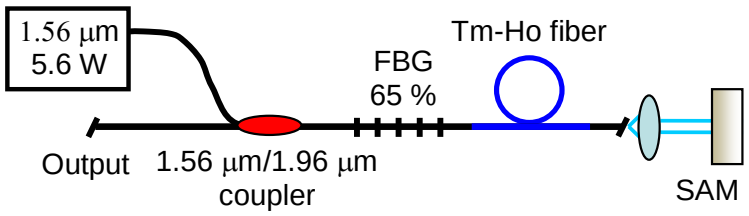

Fig. 3.8. Schematic of the passively Q-switched Tm^{3+},Ho^{3+}-doped aluminosilicate fiber laser.

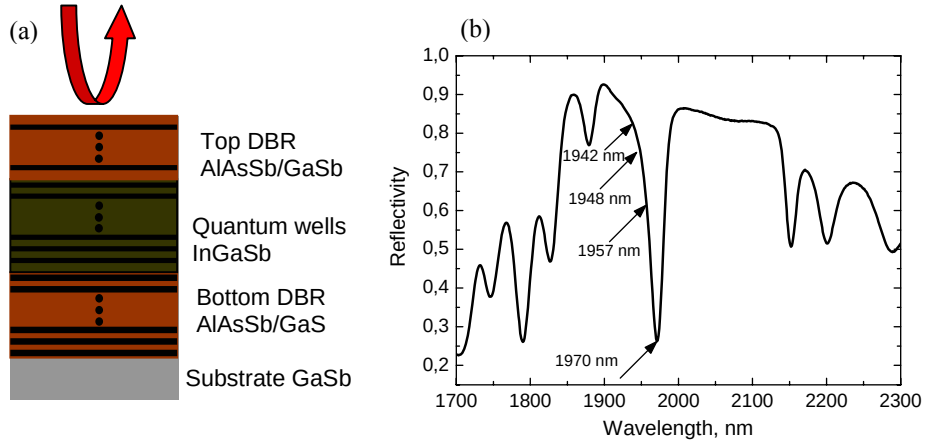

Fig. 3.9. (a) Structure and (b) low intensity reflectivity of the SESAM. The arrows show the operation wavelengths of the laser. The resonant wavelength is 1970 nm.

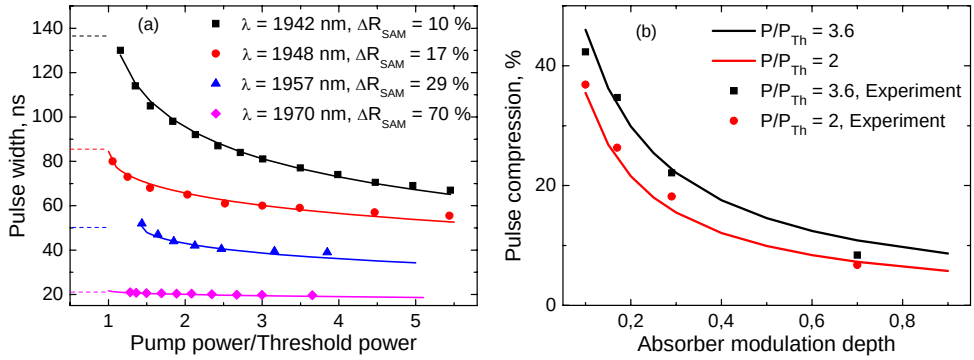

Fig. 3.10. (a) The effect of the pump power and operation wavelength (hence ΔR_{SAM}) on the pulse width. The dashed lines show the pulse width calculated from theory without taking into account the gain induced pulse shortening. (b) The effect of the modulation depth on pulse shortening at different power levels exceeding the threshold power. Solid lines are the fittings according to egn. (3.28).

The repetition rate and pulse energy of the laser for the absorber modulation depths of 10% and 70% are plotted in Fig. 3.11. For off-resonance operation the repetition rate does not depend linearly on pump power but rather begins to level off with higher pump powers, as also expected from the section introducing the dynamic gain shortening (see Fig. 3.7). The pulse energy also increases with the pump power. For operation at the resonance, the repetition rate increases nearly linearly and the pulse energy is fairly constant, ~15 μJ. The solid curves in the Fig. 3.11 represent numerical calculations based on $E_{released} = E_{sat,g}\Delta g$, where Δg is the gain variation which takes into account pulse shortening for operation well above threshold by replacing the value for the gain variation $\Delta g=2q_0$ used in the near-threshold (low duty cycly) analysis (dashed lines). The difference in the laser characteristics (i.e. the pulse width, repetition rate, and pulse energy) between the off-resonant and resonant operation of the absorber is therefore due to pulse shortening effect that is strong for small modulation depths but is minimal at resonant operation, where ΔR_{SAM} attains large values.

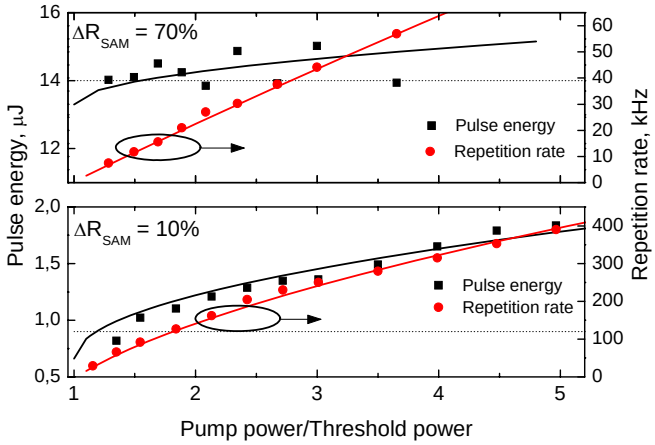

Fig. 3.11. The effect of the pump power and operation wavelength (hence ΔR_{SAM}) on the Q-switched pulse energy and repetition rate. Solid lines are the numerical fittings, and the dashed lines the near-threshold limit values for the pulse energy.

A typical oscilloscope trace reveals a nearly Gaussian-shaped pulse without any substructure, as shown in 3.12. The small asymmetry in the pulse shape is due to the large initial inversion leading to a fast rise time and a slightly slower decay time of the pulse [114]. Optical spectra at the four operating wavelengths are shown in the inset of Fig. 6. The spectral width was <0.6 nm, which was limited by instrument resolution. The pulse jitter ranged from ~20 μs to 5 μs as the repetition rate increased, as seen from the inset to Fig. 3.12. The large jitter, which is typical for passively Q-switched lasers, is caused by amplified spontaneous emission, fluctuations in the pump power, loss and temperature effects [127].

In conclusion, we built and studied a passively Q-switched, short-length ~2-μm Tm^{3+}, Ho^{3+}-doped fiber laser using a high contrast InGaSb resonant semiconductor saturable absorber mirror. The compact core-pumped all-fiber laser incorporating an optimized absorber mirror and pumped far above the threshold delivered nearly Gaussian-shaped

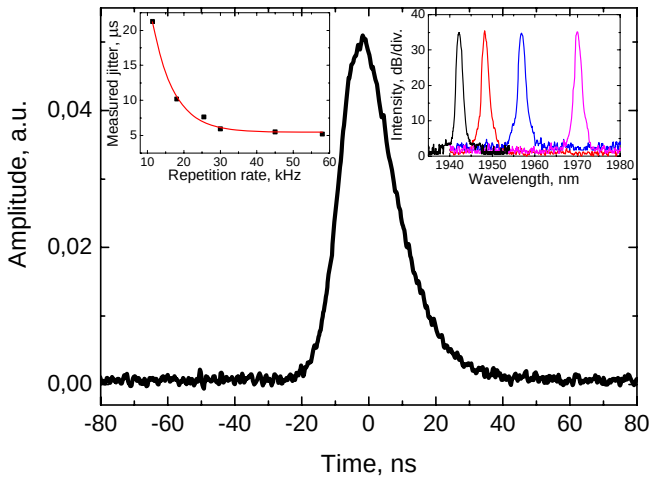

Fig. 3.12. Oscilloscope trace of a 19.6 ns Q-switched pulse observed at the resonant wavelength of the SAM. The insets show the narrow optical spectra at the four operating wavelengths (right) and the jitter vs. repetition rate of the laser (left).

20 ns pulses with a narrow spectrum, a repetition rate of 57 kHz, and a pulse energy of 15 μJ. The absorber modulation depth was shown to have a significant influence on the contribution of dynamic gain-induced pulse shortening and the Q-switched pulse characteristics. Further power and pulse energy scaling could be enabled by using a master oscillator-power amplifier configuration as demonstrated in another passively Q-switched Tm^{3+}, Ho^{3+} laser [S1].

4. Mode-locked fiber lasers for pico- and femtosecond pulse generation

This chapter describes basic principles of mode-locking. Different mode-locking regimes and mechanisms are reviewed with a focus on passive mode-locking using saturable absorbers. Dispersion management and wavelength tuning methods for ultrafast fiber lasers are also considered.

4.1 Basic principles of mode-locking

In general, mode-locking is a method for providing ultrashort pulses with durations typically in the range from picoseconds to femtoseconds from laser cavities. Assuming a single circulating pulse in the cavity, the repetition rate of the laser pulses is determined by the length of the laser cavity and is typically in the range of several tens of megahertz for fiber lasers. The mode-locked pulses can be generated by active or passive means, analogous to Q-switching. Compared to Q-switching, however, a nearly one order of magnitude faster response of the electrical modulator or saturable absorber is required in order to obtain mode-locking.

4.1.1 Active mode-locking

Active mode-locking is implemented using an external signal, typically an electro- or acousto-optic modulator that provides amplitude or phase modulation. The modulator is driven with a modulation frequency ω_m that equals or is very close to the value of the cavity round-trip frequency ω_q, i.e. the axial mode-spacing. The pulse is passed through the modulator only at the transmission maximum of the modulation signal. In a frequency domain approach, the axial cavity modes at the frequency ω_q acquire modulation sidebands at frequencies $\omega_q \pm n \cdot \omega_m$ (the modulator is typically driven with the modulation frequency ω_m or one of its integer multiples). The axial modes interact with the sidebands and therefore become in phase with the modulator. The axial modes couple together, i.e. mode-lock to one or more neighboring modes, which actually leads to the term mode-locking [114]. Fig. 4.1 illustrates the basic principles of active mode-locking in time and frequency domains.

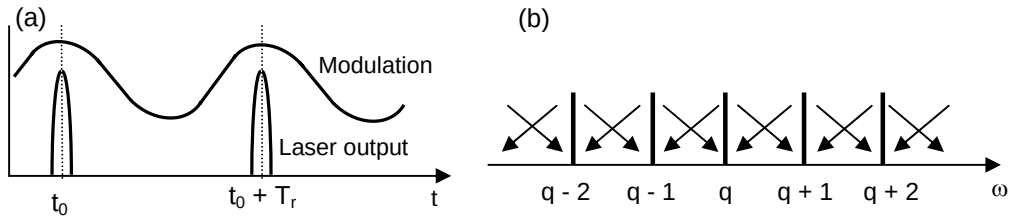

Fig. 4.1. (a) Principle of active mode-locking (time domain). (b) Coupling of the axial modes (frequency domain).

The limiting factor for actively mode-locked lasers is often the speed of the modulation electronics, which typically restricts the attainable pulse widths to picosecond levels. The achievable pulse width also depends on the modulation and on the gain bandwidth of the laser medium. In the simplest case, the pulse width can be calculated by using so called Kuizenga-Siegman theory [135]:

$$\tau = \sqrt[4]{\frac{2g}{M\omega_m^2\omega_g^2}}, \tag{4.1}$$

where g is the gain, ω_g the gain bandwidth, M the modulation strength, and ω_m the modulation frequency. As can be seen, the strength of the modulation tends to shorten the pulse whereas the gain and limited gain bandwidth tends to broaden it. The equation (4.1) does not take into account self phase modulation (SPM) and dispersion and is, therefore, not valid for example for systems with anomalous net cavity dispersion. Using soliton compression effects, sub-picosecond pulses have been reported that are well below the expected duration calculated from equation (4.1) [136,137].

4.1.2 Passive mode-locking

In a passively mode-locked laser, a nonlinear element in the cavity initiates short-pulse operation without an external signal. The nonlinear element provides attenuation for the wings of the pulse with low light intensity and minimum losses for the central part of the pulse with high intensity. This kind of component with an intensity dependent loss-characteristic is called a saturable absorber and it gives rise to a strong pulse shaping mechanism. The pulse shortens with every pass through the saturable absorber, whereas the propagation in the rest of the cavity tends to broaden it. Therefore, the mode-locking is self-sustainable.

The nonlinear element initiating the mode-locking can be a real saturable absorber made of various semiconductor materials or carbon nanotubes [138,139], or an artificial saturable absorber, such as nonlinear polarization rotation (NLPR) [140,141], nonlinear loop mirror [94,142], or Kerr element [143]. Among the different approaches, semiconductor saturable absorbers and nonlinear polarization rotation are the most widely employed methods in fiber lasers. In this thesis, I will mainly concentrate on semiconductor saturable absorber and carbon nanotube mode-lockers. NLPR and nonlinear loop mirror methods are only briefly introduced.

Nonlinear polarization rotation

NLPR mode-locking is based on the nonlinear change of light polarization arising due to the combined effect of self phase modulation (SPM), cross phase modulation (XPM), and birefringence in an optical fiber [144]. A typical cavity configuration employs a polarizer and a polarization tuning element, such as a wave plate or fiber polarization controller. In the NLPR mode-locked cavity, changes in the polarization of the light in the fiber depend on the optical intensity. This leads to a situation where different pulse components experience intensity dependent transmission in the polarizer; pulse components with high intensity experience minimal losses and the wings of the pulse higher losses. Mode-locking using NLPR benefits from its quick response, i.e. the artificial absorber is very

fast. Ultrashort sub-100 fs pulses can be achieved using NLPR mode-locking, especially in stretched pulse regime fiber lasers [145]. In addition, NLPR enables truly all-fiber configurations, as polarizing fiber isolators and fiber polarization controllers are widely available. However, severe stability problems due to drifting of the polarization, for example because of temperature changes, and the consequent need for tuning of the polarization may limit the practical applications of the method. Moreover, a significant length of fiber is required in the cavity.

Nonlinear amplifying loop mirror

Another fiber-based mode-locking method includes light propagation in a nonlinearly amplifying fiber loop mirror (NALM). A NALM is formed by splicing a doped-fiber amplifier onto one end of a loop within a standard fused fiber loop mirror with a reflectivity of ~100% (made from a 50-50 tap coupler). The light entering the loop splits into two counter-propagating beams. At low intensities the loop acts as a linear element, reflecting the signal back to its launching port. On the other hand, high light intensity leads to a change in the optical path lengths for the clockwise and counterclockwise propagating beams around the loop, due to the fiber amplifier located non-symmetrically at one end of the loop [146,147]. This consequently leads to phase changes between the two beams. As a practical mode-locking element, the NALM is often used in so-called figure-of-eight laser configurations [94,142]. This configuration includes two different loops; the NALM as a one cavity end mirror, and a standard loop mirror including an optical isolator that ensures unidirectional propagation as another end mirror. The output can be taken via a tap in the normal loop mirror end of the cavity. Similar to NLPR, the response time of NALM is fast. Using the figure-of-eight fiber laser configuration, ultrashort pulses with durations below 100 fs can be achieved when operated in soliton pulse or stretched pulse regimes [148-150].

Frequency shifted feedback mode-locking

Another mode-locking-like method that is considered passive is frequency shifted feedback (FSF) [151,152]. This method is based on a frequency shift of spectral components achieved by using an AOM in combination with an intra-cavity spectral filtering effect. The AOM or acousto-optic tunable filter (AOTF) is used to displace the spectrum of the intracavity field in the same direction for each cavity round trip. The intra-cavity frequency shift prevents the evolution of the typical standing wave in the cavity but rather generates regenerative amplification. The pulse generation in FSF fiber lasers is enabled by the balance between frequency shifting, spectral broadening through nonlinear effects (Kerr effect), and subsequent spectrum trapping by the spectral filter. The basis of FSF mode-locking is the Kerr-type nonlinearity.

Using the FSF-method in fiber lasers, short pulses in the few picosecond range have been reported [153-155]. Typically, sub-picosecond pulses have remained unfeasible due to the required spectral filtering. However, using external compression, pulses down to ~70 fs have been reported for an Yb-doped fiber laser [156]. In addition to FSF pulse generation, AOTFs can be used for fast wavelength tuning by changing the carrier frequency of the radio frequency (RF) signal [157,158].

Semiconductor saturable absorbers

The fast progress of practical ultrafast laser systems has been enabled by the development of sophisticated semiconductor technology, particularly the development of SESAMs [159,160]. SESAM mode-lockers benefit from the diversity and freedom in the absorber structure and laser cavity design. Semiconductor saturable absorbers can be engineered independently from the laser design, therefore allowing the optimization of the laser cavity and the mode-locker separately. By using different materials, different operation wavelength regimes can be easily attained. In addition, carefully optimized SESAMs provide very stable pulses with an important self-starting property, which is often laborious to achieve with fiber-based mode-locking methods.

Semiconductor saturable absorbers are typically operated in reflection, though transmission-type absorbers have also been demonstrated [161-163]. A SESAM consist of a bottom distributed Bragg mirror (DBR) grown on top of a substrate and an absorbing region. The absorbing region contains one or often multiple quantum wells (QW) that provide the saturable absorption. The wavelength of the absorption can be controlled precisely by adjusting the depth and width of the QWs. The absorbing region is often capped with a top DBR mirror or with an antireflection dielectric coating. The top DBR enhances the nonlinearity in the Fabry-Perot cavity and is used in so-called resonant-type absorbers (see Fig. 3.9). Compared to broadband anti-resonant absorbers, the resonant absorbers provide a higher nonlinearity (larger modulation depth), a narrower operation range, and a smaller saturation fluence, which are often beneficial for self-starting mode-locking of fiber lasers. Resonant structures have been shown to help prevent harmful Q-switch mode-locking [164]. On the other hand, unsaturable losses are often higher for the resonant-structures.

A typical nonlinear reflectivity characteristic of a SESAM including the main parameters is shown in Fig. 4.2. As can be seen, the reflectivity increases with the incoming light fluence, therefore providing strong pulse shaping. The maximum change in the reflectivity is the modulation depth (ΔR). The saturation fluence (F_{sat}) is the fluence of an incident short pulse which is required to cause a 1/e change in reflectivity compared to the fully saturated reflectivity. The nonsaturable losses (α_0) are the remaining excess losses in a fully saturated absorber. These losses are typically harmful and are minimized if possible during the structure design and fabrication process. The modulation depth can be affected by the amount of QWs and the top mirror used. By increasing the amount of QWs the modulation depth increases. However, at the same time the saturation energy might also get slightly increased due to the reduced material quality, which might lead to difficulties in self-starting. Therefore, often a better way to increase the modulation depth is to use a resonant Fabry-Perot SESAM with a top DBR and maintained low saturation energy.

Another important parameter for a saturable absorber is the absorption recovery time (τ). In SESAMs the saturable absorption is related to carrier interband transitions between conduction and valence bands. For high quality material (low amount of defects) the time required for absorption recovery is mainly determined by the radiative carrier recombination, which typically lasts from several hundreds of picoseconds to a few nanoseconds. For ultrafast laser operation it is often necessary to reduce the absorption

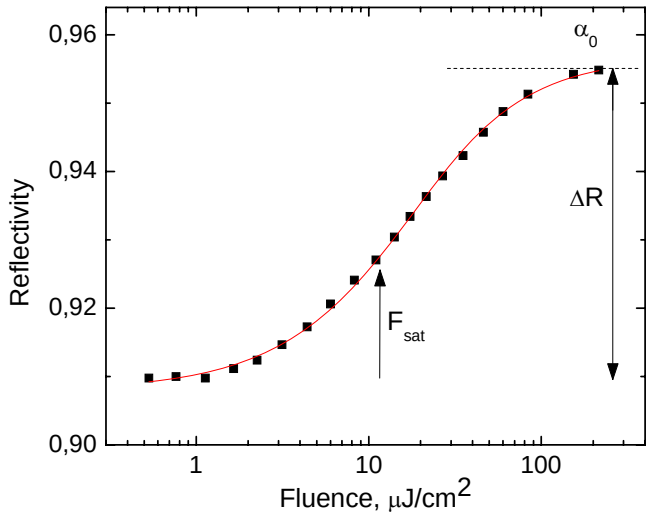

Fig. 4.2. Typical nonlinear reflectivity characteristics of a SESAM.

recovery time down to the level of a few picoseconds or less [160,165]. This can be done by generating more defects in the semiconductor by creating fast non-radiative recombination centers which are responsible for short recovery times. The most commonly used methods include post-growth heavy-ion irradiation of the quantum wells [166,167], low temperature growth [168], and metamorphic growth [169,170]. The absorption recovery time of dilute nitride-based (InGaAsN) SESAMs can also be decreased using in-situ N_2-bombardment of individual quantum wells during the epitaxial growth [171,P8].

The absorber is considered to be fast when the absorber recovery time is much shorter than the pulse width. When the recovery time is in the same range or even longer than the pulse width, the SESAM is considered to be slow. Typically fast absorbers are beneficial for mode-locking, however, slow absorbers can also reliably be used to mode-lock lasers [172]. In slow absorbers the leading edge of the pulse is attenuated more than the trailing edge. This leads to shifting of the pulse center backwards in each cavity round-trip. The cavity has a large amount of net round-trip gain behind the pulse that allows the spontaneous emission to be amplified. However, the pulse moves continuously backwards due to the slow absorber interaction and this causes the amplified noise to be suppressed. Therefore, it is possible to obtain stable mode-locking also with slow absorbers. This phenomenon is especially emphasized in soliton lasers where the cavity dispersion strongly shapes the pulse in combination with the saturable absorber [173,174]. However, the use of slow absorbers often leads to mode-locking stability problems and slightly longer pulse durations compared to fast absorbers. The use of too slow absorbers (τ is larger than $\sim 30 \cdot \tau_{pulse}$) causes so called continuum breakthrough, where the spontaneous noise behind the pulse increases for too large values and distorts the stability and mode-locking [172-174]. Slow absorber recovery in combination with a fiber laser having a long gain fiber, low gain, and small pulse energy might lead to generation of unstable multiple pulsing and large autocorrelation pedestals [P8]. However, with careful absorber and laser cavity design the pedestals can be avoided.

Carbon nanotube saturable absorbers

Quite recently, in 2003 and 2004, novel saturable absorbers for mode-locking of ultrafast fiber lasers were demonstrated using single-walled carbon nanotubes (SWCNTs) [139,175,176]. Since then various reports of SWCNT-based saturable absorbers used both in reflection and transmission configurations in fiber and solid state lasers have followed [177-195]. Typically, the CNT-absorbers have been manufactured by embedding them into a polymer [175-195]. The combination of the SWCNTs and the polymer has then been transferred to the top of a highly reflecting mirror or silica glass substrate. In addition, the SWCNT-films can be transferred on to fiber connectors to be conveniently used in ring cavity all-fiber lasers [184-187]. Mode-locking using SWCNTs and evanescent field interaction in tapered [188,189] and D-shaped fibers have also been demonstrated [190,191]. Very recently, SWCNT-doped plastic optical fiber was shown to initiate mode-locked operation [192]. In general, SWCNT-technology offers substantial flexibility.

Compared to well-developed traditional semiconductor technology, SWCNT-based absorbers have certain advantages. SWCNT-technology benefits from the relatively simple and cost-efficient absorber fabrication. Moreover, SWCNT-absorbers are 'as grown' fast, with sub-picosecond measured absorption recovery times [183,196,197]. SWCNTs are also applicable to a broad spectral range between 1 μm and 2 μm. The band gap of SWCNTs can be varied by using nanotubes with different diameters and structures that determine the operation range and absorption characteristics of the absorber. The nanotube diameters, which in a typical saturable absorber are around 1-2 nm, can be well-controlled during the nanotube fabrication [198]. Mode-locked fiber and solid state lasers operating at 1 μm [183,193], 1.2 μm [194], 1.56 μm [175,180] and 2 μm [186,195] employing SWCNT-absorbers have been demonstrated, with the research directed towards 1.56 μm Er-doped fiber lasers. The amount of absorption in SWCNT-absorbers can be easily controlled by increasing or decreasing the film thickness. However, the increase in the nonlinear absorption typically also results in an increase in the nonsaturable losses. SWCNT-based saturable absorbers are considered to be "non-resonant" by nature and cannot be easily coated due to the porous network of CNTs. Therefore the achievable modulation depths are typically in the sub-20% range with current technologies. However, the ratio of the modulation depth to the non-saturable losses of a CNT-film is significantly increased at wavelengths close to absorption maxima. Therefore, it is very beneficial to employ CNT-films with a strong absorption peak that corresponds either to the E_{22} or E_{11} electronic transition of CNTs at the target operation wavelength.

Figure 4.3(a) shows the linear absorption characteristics of four different pure SWCNT-films fabricated with different aerosol CNT-reactor conditions resulting in different tube diameters. As can be seen, the tube diameters and the corresponding absorption characteristics can be well-controlled. The increased absorption of all the films towards short wavelengths is mainly attributed to increased scattering due to non-ordered CNT-networks, residual aggregates, and catalyst particles in as-grown CNT-films. The scattering could in principle be reduced by aligning the nanotubes better and using CNT-polymer solutions.

As can be seen, film #2 has a clear absorption peak at a wavelength of ~1.56 μm, wheras film #3 does not have a clear absorption maximum at this wavelength but rather a peak at ~1.9-2 μm. In order to find out the nonlinear parameters of each film, nonlinear reflectivity measurements were performed at 1.56 μm. The films were first stamped onto a highly reflecting silver mirror in order to create a saturable absorber mirror (see Fig. 4.3(b)). Figure 4.4 shows the nonlinear reflectivity characteristics measured for film #2. The modulation depth, non-saturable losses, and saturation fluence were determined to be 2.6%, 6.5% and 200 μJ/cm^2, respectively. The measurement data for all the films is summarized in table 4.1. As can be seen, the modulation depth has increased significantly for film #2, but the nonsaturable losses have still remained at a relatively low level. To experimentally test the performance of the CNT-films, each of them was used as a saturable absorber in fiber lasers operating at wavelengths of 1.56 μm (Er-laser) and 1.97 μm (Tm-Ho-laser). At the wavelength of 1.56 μm, film #2 clearly showed the best performance, offering very easy self-starting and stable mode-locking with low threshold. In contrast, film #3 caused only CW- and Q-switched operation. Films #1 and #4 initiated mode-locking. However, the threshold and stability were worse than with absorber #2. Moreover, a CW-component often disturbed the mode-locked operation with films #1 and #4.

On the other hand, at the wavelength of 1.97 μm, film #3 offered the best performance amongst the four films. Film #4, with an obvious absorption peak at ~2.1 μm, also operated well in the Tm-Ho-doped fiber laser. The best film at the wavelength of 1.56 μm, film #2, did not initiate mode-locking at 1.97 μm, however. This clearly indicates the importance of the CNT-film absorption maximum for mode-locking. Outside the local absorption maxima, the modulation depth of the CNT-film is often too small, and the non-saturable losses too high to initiate stable mode-locking.

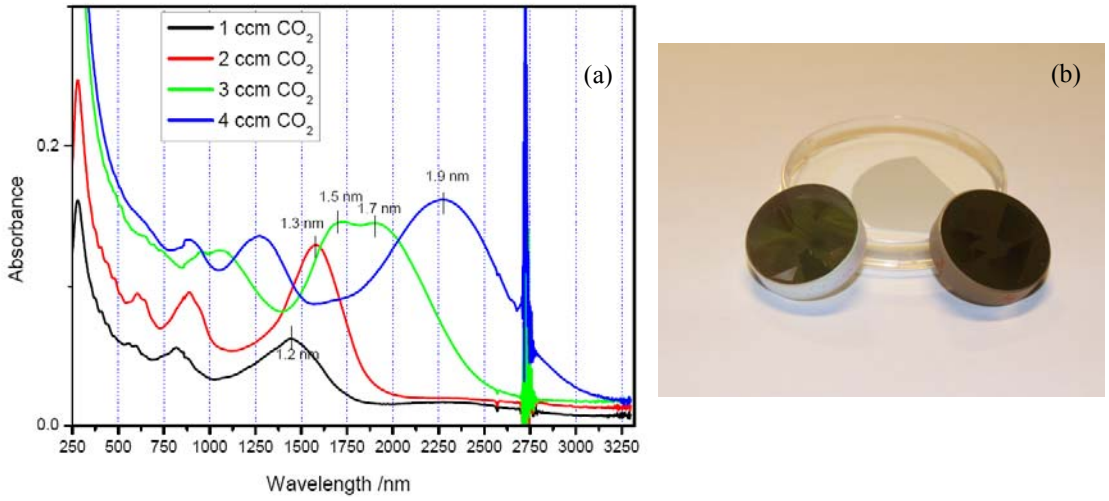

Fig. 4.3. (a) Measured absorptions for four different CNT-films with different nanotube diameters. (b) Photograph of saturable absorber mirrors made using SWCNTs.

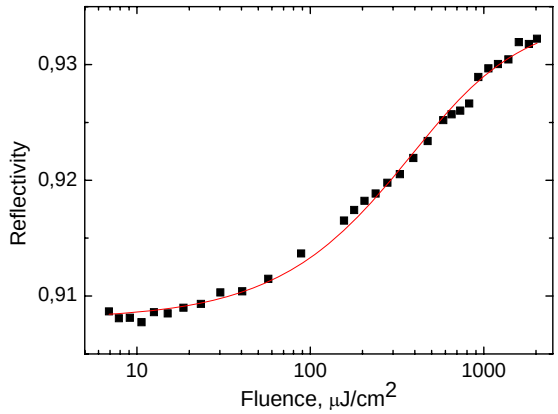

Fig. 4.4. Measured nonlinear reflectivity for the SWCNT-based saturable absorber made from film #2.

Table 4.1. Measured nonlinear parameters for the four different SWCNT-films.

Film	Wavelength, nm	Nonsaturable loss,%	Modulation depth,%	Saturation fluence, μJ/cm^2
#1	1561	2	0.5	~300
#2	1561	6.5	2.6	~200
#3	1561	7	1.5	~200
#4	1561	4	1.0	~130

4.2 Pulse dynamics of ultrafast mode-locked fiber lasers

In general, the pulse dynamics of a fiber laser can be described using the nonlinear Schrödinger equation (NSE) [199]:

$$\frac{\partial A}{\partial z} = -\frac{i\beta_2}{2}\frac{\partial^2 A}{\partial T^2} + \frac{\beta_3}{6}\frac{\partial^3 A}{\partial T^3} + i\gamma|A|^2 A - i\gamma T_R A\frac{\partial|A|^2}{\partial T} - \frac{\gamma}{\omega_0}\frac{\partial}{\partial T}(|A|^2 A) \ , \qquad (4.2)$$

where A is the pulse envelope, z is the distance along the fiber, T is the pulse local time, β_2 is the second order dispersion, β_3 is the third order dispersion, γ is the nonlinear parameter, ω_0 is the carrier frequency, and T_r is a parameter related to the Raman effect. This expression includes various effects such as pulse broadening due to dispersion, spectral broadening due to SPM, self-steepening due to intensity dependence of group velocity, and Raman response. The response of each term strongly depends on the laser cavity and the elements inside it. However, second order dispersion (GVD) has a very dominant effect. It often determines the achievable pulse duration in a mode-locked fiber cavity. In picosecond and several hundred femtosecond lasers the third order dispersion (TOD) term often has only a small effect and is, therefore, negligible. However, too-large uncompensated TOD might limit the shortest achievable pulse duration in lasers with sub-100 fs pulse duration when the GVD is close to zero [200,201]. The Raman scattering response is also small in standard single mode fibers and therefore often neglected. Indeed, when operating in the anomalous dispersion regime with short, intense pulses, the Raman response may occur and generate new wavelength components (Raman shifting) and additional spectral broadening [P9]. The nonlinearity causes

spectral broadening and in very highly nonlinear fibers might lead, in combination with other effects, to supercontinuum generation [S2,P4]. By solving equation (4.2) using the split-step Fourier-transform method and mathematically describing the SESAM with a two-level system rate equation, the pulse evolution in an ultrafast mode-locked fiber laser can be simulated [202-204].

As earlier discussed, saturable absorbers typically initiate the mode-locking and provide some pulse shaping, however, the net cavity dispersion often has a strong role in the pulse shaping within a fiber laser cavity. According to the fiber laser cavity dispersion, the laser operation regimes can be divided into three categories; soliton pulse regime, stretched pulse regime, and all-normal dispersion regime.

In the soliton pulse regime, the anomalous GVD compensates the effect of SPM and allows pulse propagation over long distances without significant changes. In mode-locked fiber lasers the soliton regime characteristically allows high-quality, unchirped (or nearly unchirped) bandwidth-limited pulses. The pulse duration of a soliton laser is usually nearly independent of the absorber recovery time [205]. However, a too long recovery time might lead to difficulties with pulse quality and stability, as will be shown in [P8].

Fiber lasers operating in the soliton pulse regime deliver typically sub-picosecond pulses with pulse durations dependent on the net cavity dispersion. However, very short, few hundred femtoseconds or less, pulse durations are not easily achievable as the intra-cavity dispersion should attain values close to zero. A typical characteristic of a mode-locked soliton fiber laser are the distinct sidebands in the pulse spectrum [206]. These so-called Kelly or soliton sidebands can be conveniently used to estimate the intra-cavity dispersion of the laser [207]. The Kelly sidebands arise due to the interplay of the soliton wave and a non-solitonic dispersive wave. The co-propagating dispersive wave arises from the soliton wave due to periodical loss-induced perturbations in the cavity. At certain frequencies the soliton wave and the dispersive wave are in phase and generate the narrow spikes in the spectrum. The pulse energies of soliton lasers are typically relatively low, in the range of tens of picojoules, and are limited by the soliton area theorem [208]. Higher pump powers lead to wave-breaking due to nonlinear effects [209] and splitting of the solitons, i.e. multiple pulsing, according to energy quantization [210]. The multiple soliton pulses can be randomly ordered, tightly bunched, or stably organized with equal temporal spacing [211]. The latter case is called harmonic mode-locking and can be used to increase the repetition rate of the laser as done in [P7]. Repetition rates up to GHz levels have been generated using harmonically mode-locked fiber lasers [212,213]. The generation and stability of harmonic mode-locking is very dependent on the intra-cavity polarization state and pump power of a fiber laser [211,214].

Another regime with net anomalous cavity dispersion is called the dispersion-managed soliton regime. In this regime the fiber laser cavity comprises segments of anomalous and normal GVD. The generated pulses can be described as average solitons. The mode-locked Yb- and Bi-doped fiber lasers demonstrated in this thesis were operated in this regime. Pulse propagation simulation results of dispersion-managed laser cavities will be presented in the later sections of this thesis.

The shortest pulses from fiber lasers can be generated in so-called stretched pulse lasers. A fiber laser operating in the stretched pulse regime contains elements of anomalous and normal dispersion, causing the sign of the chirp to change within one

cavity round-trip. The overall cavity GVD, which is close to zero, can be either anomalous or normal. It is notable that the border between anomalous stretched pulse regime and dispersion managed soliton pulse regime is wavering. In the stretched pulse regime, the pulse propagating in the cavity encounters strong temporal and spectral changes, i.e. the pulse is 'breathing'. Therefore, special attention should be paid to the pulse evolution and output coupler positioning [P8,204]. Stretched-pulse fiber lasers can typically deliver higher pulse energies and shorter pulses than lasers operating in the pure soliton pulse regime [215-219]. The higher energy can be understood as a decrease in the average peak power inside the cavity due to strong pulse stretching (chirping). The shortest and highest energy pulses have been reported for lasers operating with slightly net normal GVD [96]. However, these lasers suffer from difficulties associated with self-starting and stability of mode-locking.

Another pulse regime that allows generation of very high energy pulses is the all-normal dispersion regime, also sometimes called dispersion compensation-free regime. Lasers operating in this regime consist of segments with only normal dispersion. Pulse energies above 20 nJ have been generated in all-normal dispersion regime Yb-doped fiber lasers [220]. Short externally compressed pulses with nJ energies and pulse durations in the 100-300 fs range have been reported for mode-locked Yb-doped fiber lasers with different configurations [220-224]. Typically, spectral filtering is required for pulse shaping and stabilization. The spectral filtering can be done, for example, using wavelength division multiplexing couplers [222,223], interference filters [220,224], or highly resonant SESAMs [164]. Lasers operating in the all-normal dispersion regime often suffer from issues related to self-starting, but on the other hand benefit from the lack of any additional dispersion compensating elements.

In a broader approach, all-normal dispersion lasers can be considered to operate in a self-similar regime. In this regime the evolution of the pulses is distinct from the evolution of pulses in soliton and stretched-pulse lasers. In the self-similar pulse regime, sometimes also called wave-breaking free regime, the pulses are always positively chirped inside the laser [225]. In contrast to pure soliton or dispersion managed soliton solutions in soliton and stretched pulse regimes, the pulses in the self-similar regime are asymptotic solutions of the NSE. The pulses have parabolic shapes that are a result of the net normal cavity dispersion and parabolic gain profile [226]. The spectral width inside a laser cavity operated in the self-similar regime changes significantly. The spectral width increases strongly in the active fiber section with amplification, and then drastically decreases due to the required spectral filtering in the cavity. This behavior makes high energy pulses attainable [225]. However, at the output pulses attain large linear chirps and need to be externally compressed in order to achieve short sub-200 fs pulse durations.

4.3 Methods for intra-cavity dispersion management

As mentioned in the previous section, the shortest optical pulses are obtained when the fiber cavity net dispersion attains values close to zero. Additionally, it is often very beneficial to operate a fiber laser in the anomalous dispersion regime with improved self-starting capability and pulse stability. The material dispersion of a standard silica optical fiber is normal below the wavelength of 1.3 μm, therefore forcing Yb- and Bi-doped fiber

lasers typically emitting at 1 μm and at 1.2 μm, respectively, to operate at net normal cavity dispersion. Therefore, a special need for additional dispersion compensating elements exists. This section briefly describes the most common methods used for dispersion compensation in ultrafast mode-locked fiber lasers with the main emphasis on the highly reflective chirped fiber Bragg grating (CFBG) dispersion compensators developed in this work.

4.3.1 Dispersion compensation using bulk elements

The most conventional normal GVD compensation methods at wavelengths below ~1.3 μm are a sequence of prisms and a pair of diffraction gratings [227-229]. The use of prisms is mainly limited by their tedious alignment and the relatively large prism separation required for sufficient dispersion. The gratings, on the other hand, are able to provide relatively high second order dispersion but suffer from losses due to limited diffraction efficiency. Additionally, the third order dispersion (TOD) provided by the grating pair has the same sign as the fiber TOD at wavelengths below ~1.3 μm, therefore limiting the shortest attainable pulse width when cavity GVD is close to zero.

In addition to normal GVD compensation, grating pairs can be used in a so-called telescope (sometimes also called grating stretcher) configuration to provide normal dispersion, which is beneficial in mode-locked fiber lasers operating beyond 1.3 μm [230]. The method was recently applied for anomalous GVD cancellation in mode-locked Tm-doped fiber lasers at ~2 μm where conventional fibers with normal GVD are not available [231,232]. The grating telescope configuration can also be used to compensate the third order fiber dispersion [233].

Special devices with a grating structure on a prism surface can also be fabricated to optimize the strength of the second and third order dispersions. These devices are called grisms and are used for generation of femtosecond pulses [234-236]. In addition to grating and prism-based dispersion compensators, other non-fiber based methods have also been employed for dispersion compensation in mode-locked lasers. These include Gires–Tournois interferometers (GTIs) [237,238], Fabry-Perot etalons [239], dielectric chirped mirrors [240], and resonant SESAMs [241]. Though some of the methods have been applied for fiber lasers, they are mainly restricted to solid state lasers with only exiguous net cavity dispersion. In general, the ‘bulk’ elements typically introduce additional losses and break the all-fiber configuration of the fiber laser, which is not practical and desirable. Therefore, fiber-based dispersion compensation methods have been intensively studied and developed.

4.3.2 All-fiber dispersion compensators

In order to make ultrashort pulse fiber laser cavities compact while preserving an all-fiber configuration, fiber-based dispersion compensators are required. At wavelengths above 1.3 μm, standard single mode fibers provide anomalous dispersion. In order to compensate for this dispersion it is necessary to have fibers with opposite signs of dispersion. This can be achieved by tailoring the fiber properties, such as the core diameter and the index difference between the fiber core and the cladding. For example, at the wavelengths of Er-doped fiber lasers around 1.55 μm, both passive and active

single mode fibers with normal and anomalous dispersion are available, allowing the building of mode-locked sources with low net cavity dispersion and sub-200 fs pulse durations [242]. In general, fibers with normal dispersion at 1.55 μm are called *dispersion compensating fibers* (DCF) and are extensively used in optical communications. The zero-dispersion wavelength of an optical fiber can also be shifted to either longer or shorter wavelengths, typically around 1.55 μm. These fibers are called *dispersion-shifted fibers* (DSF). Most of DCFs and DSFs have been tailored for operation near 1.55 μm. Such fibers would also be very beneficial for dispersion management of novel mode-locked Tm-doped fiber lasers operating around 2 μm.

At wavelengths below 1.3 μm, the normal fiber dispersion needs to be compensated with anomalous dispersion. This can be achieved using specialized *higher order mode (HOM) fibers* [243,244], *tapered fibers* [S3], or *microstructured fibers* [245-247]. The dispersion of a HOM fiber is modified at certain wavelengths due to light coupling to higher order modes inside the fiber. These fibers are able to provide relatively large dispersions, but are typically somewhat tricky to use in combination with standard single mode fibers. Standard single mode fibers can also provide anomalous dispersion at wavelengths below 1.3 μm when they are tapered down to a diameter of 2 μm or less [S3]. The amount of dispersion at a certain wavelength is determined by the taper waist diameter, which can be tailored by varying the fabrication process parameters. The tapered fibers are easily spliceable but typically fairly fragile and relatively short, in the range of 10-20 cm, due to technical reasons related to the fabrication, and therefore can provide only reasonably small amounts of dispersion.

Microstructured fibers with cobweb-like structure of air holes and solid silica can be divided into *index guiding photonic crystal fibers* (PCF) and *photonic bandgap fibers* (PBGF). Index guiding PCFs typically have a solid silica core surrounded by a periodic structure of air holes in solid glass (see Fig. 4.5). The first PCFs were manufactured in 1996 [248]. Since then, they have attracted significant attention in the fields of dispersion compensation and nonlinear optics [249]. The fiber dispersion characteristics of a PCF can be controlled by varying the core diameter, and the cladding air-filling fraction. The amount of dispersion and the zero-dispersion wavelength are mainly determined by the core diameter, as with the tapered fibers. Actually, when the air-filling fraction of a PCF is large, the fiber resembles a tapered fiber with a similar core diameter. Compared to tapered fibers, PCFs offer more rugged setups but are, on the other hand, still tricky to splice to standard single mode fibers despite extensive efforts [250]. Various ultrashort pulse mode-locked Yb-doped fiber lasers have been reported employing index-guiding PCFs [246,P3]. In addition, PCFs are also often used in nonlinear fiber optics to generate ultrabroadband supercontinuum radiation under short and intense optical pulses [251,S2].

In PBGFs, light guiding is not based on total internal reflection but on the photonic bandgap effect. The light remains confined in the core for wavelengths around a minimum-loss wavelength due to this effect. Therefore, PBGFs can be designed to have either a solid or a hollow core. Figure 4.6 shows a SEM image of a typical hollow core PBGF. The dispersion properties of PBGFs can be tailored to meet the requirements of the application. Both hollow and solid core PBGFs have been successfully used in

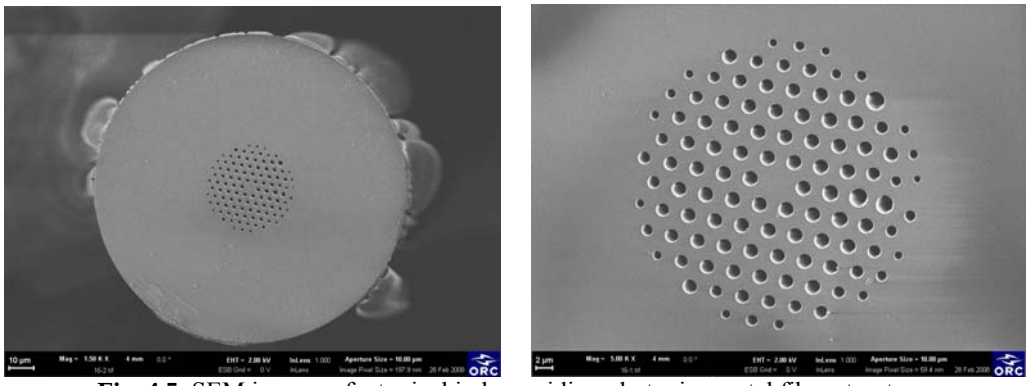

Fig. 4.5. SEM images of a typical index-guiding photonic crystal fiber structure.

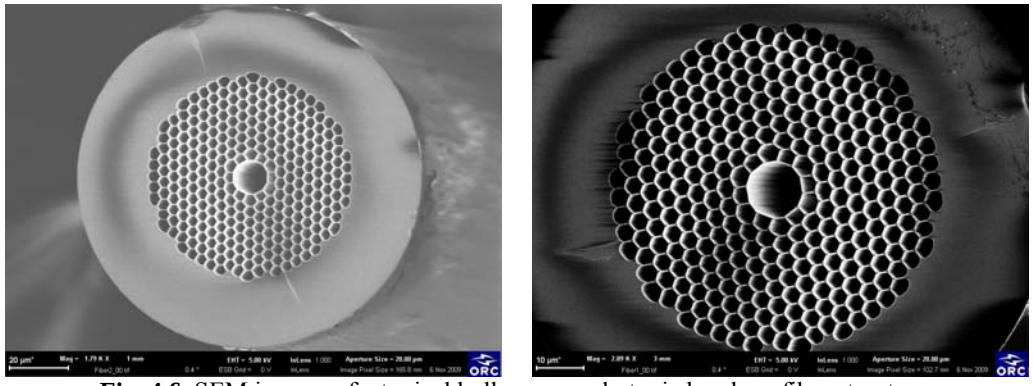

Fig. 4.6. SEM images of a typical hollow-core photonic bandgap fiber structure.

ultrashort pulse mode-locked fiber lasers for dispersion compensation [245,247]. Additionally, in solid core PBGFs the core can be doped with rare-earth elements and be used conveniently both as a fiber laser gain medium and as a dispersion compensating element [252]. PBGFs can be designed to have low nonlinearity, which makes them very suitable for high peak power operation. However, highly nonlinear PBGFs can also be designed and fabricated. The major limitations of PBGFs are related to the restricted operation bandwidth, significant variation of the dispersion within the operation bandwidth, high TOD, and difficulties in splicing. Moreover, the calculation of dispersion and manufacturing of the PBGFs are by no means straightforward.

4.3.3. Environmentally stable 200 fs Yb-doped fiber laser with dispersion compensated by a photonic crystal fiber

Environmental stability with turn-key operation is required in various practical applications of ultrafast mode-locked fiber lasers. This is often difficult to achieve in fiber lasers due to the birefringence of optical fibers and the change of polarization in the cavity. In [P3] we used an index guiding photonic crystal fiber and Faraday rotator mirror for the compensation of fiber dispersion and fiber cavity birefringence, respectively. The robust, mode-locked Yb-doped fiber laser demonstrated operated in the net anomalous dispersion regime and was insensitive to environmental disturbances.

The experimental fiber laser configuration used in this study is shown in Fig. 4.7. The active material was an 80-cm long Yb-doped fiber pumped by a 300 mW diode laser. The light was coupled out via a 25 % tap coupler. The length of passive HI-1060 fiber in the cavity was 120 cm. The self-starting passive mode-locking was initiated by a quantum well resonant-type InGaAs SESAM. The PCF with a core diameter of 2.9 μm and measured zero dispersion wavelength of 874 nm was fabricated from preform by mechanical drilling. The air filling factor for the first ring of holes was $k_1=d/\Lambda=0.75$, and for the second ring of holes $k_2=0.79$. The propagation loss at the wavelength of 1060 nm was measured to be ~7 dB/km. The effective mode area A_{eff} and the nonlinear coefficient γ were calculated to be 4.86 μm², 26 $W^{-1}km^{-1}$, respectively. Fig. 4.8 shows the cross-sectional image and the calculated dispersion of the PCF. The birefringence of the cavity was compensated for by a Faraday rotator mirror acting as the cavity end reflector.

The PCF with a length of 3.4 m and total dispersion of -0.09 ps² was spliced to a single mode fiber using a standard fusion splicer. Reflections from the PCF to silica fiber interface and losses due to the mode field mismatch were minimized using repeated arc discharges. This allowed for smooth collapse of the holes and caused an adiabatic mode field transformation in the PCF, resulting in optimized mode matching [253]. The splice loss was measured to be ~1.5 dB. The net cavity dispersion of the fiber laser was calculated to be -0.04 ps² assuming a dispersion of 25 ps²/km for the ytterbium and the HI 1060 fiber.

The PCF dispersion compensation resulted in soliton operation with transform-limited pulses. Figure 4.9 shows the optical spectrum and the corresponding autocorrelation of the mode-locked laser. The pulse duration of 199 fs was derived using a Gaussian fit resulting in a time-bandwidth product of 0.42. The pulse energy was 460 pJ at a fundamental repetition rate of 18 MHz. A remarkable feature of the laser performance was the obvious tendency to operate with a single pulse in the cavity. There was no evidence of multiple pulse mode-locking at the available pumping power. Without the use of the Faraday rotator the pulse operation start-up and mode-locking performance

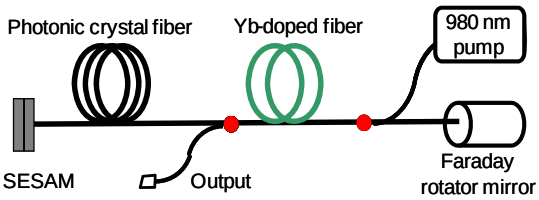

Fig. 4.7. Schematic of the mode-locked laser cavity.

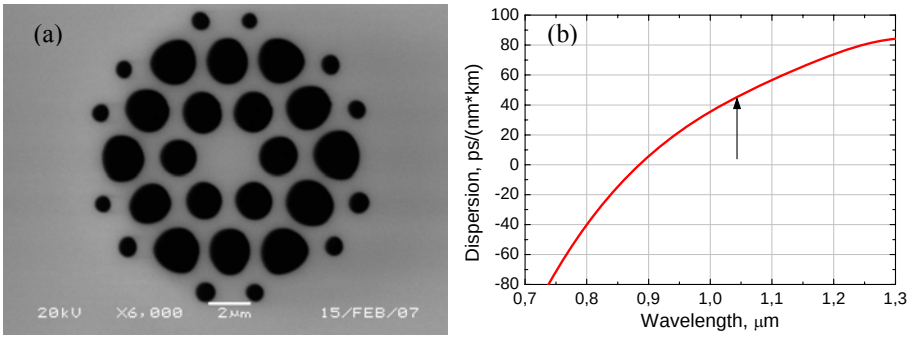

Fig. 4.8. (a) The cross-section image, and (b) the calculated group-velocity dispersion of the PCF. The arrow shows the operation wavelength of the laser.

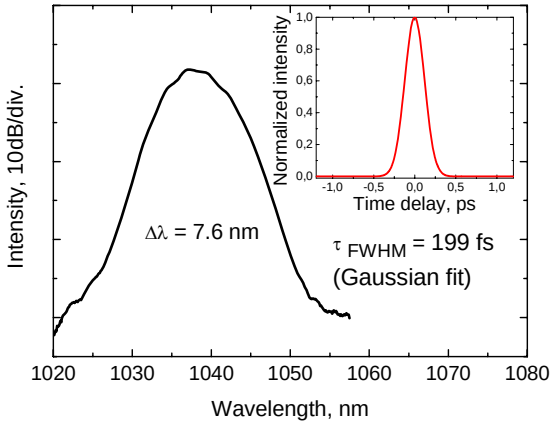

Fig. 4.9. Optical spectrum and autocorrelation (inset) of the mode-locked pulse.

were very sensitive to changes in the polarization state. A polarization controller was then needed to optimize the pulse duration and quality. Due to environmental changes the polarization controller had to be frequently realigned to maintain the operation state. In contrast, with the Faraday rotator, the self-starting and the steady-state operation was independent of fiber bending up to a few centimeters bending radius. Stable mode-locking was observed for several hours without the need for any readjustment and there was no need for readjustment when restarting the laser after a few days.

4.3.4. Dispersion compensation based on chirped fiber Bragg grating technology

Another very fascinating all-fiber dispersion compensation method in mode-locked fiber lasers and in optical fiber communication links is the use of chirped fiber Bragg gratings (CFBGs). In general, a FBG is a periodic or nonperiodic modulation of the fiber core refractive index which forms a mirror for a narrow range of wavelengths satisfying the Bragg condition. This typically periodic refractive index change over a length of several millimeters can be formed using coherent nanosecond UV-light pulses from Excimer lasers usually operating at 248 nm (KrF) or 193 nm (ArF) and employing an interferometric inscription method [254], point-by point inscription [255], or phase mask technique [256]. In general, fs-laser pulses from infrared laser sources can also be used for fabrication of FBGs [257].

In the interferometric inscription method, the refractive index perturbation in the fiber core is created by the interference pattern of two precisely controlled incoming UV-light beams. The interferometer is typically formed by splitting the incoming UV-light beam into two using a beam splitter and then recombining the beams with two rotating mirrors. In this method, the Bragg wavelength can be chosen independently of the UV-laser wavelength. The period of the modulation, i.e. the Bragg wavelength, can be controlled by adjusting the angle of the two interfering light beams.

In the point by point inscription method, a typically single tightly focused UV-laser pulse creates a step in the refractive index profile. The grating is then formed using multiples of single steps, i.e. the grating is fabricated step by step. This manufacturing

method is time-consuming and requires a costly translational stage with extremely high resolution and tight control. On the other hand, the method offers substantial flexibility for creating complex gratings with different spectral shapes and dispersion characteristics.

The simplest and most widely used method employs a diffraction grating, a phase mask, to create the interference pattern of UV-light in the fiber core. The UV-light, which is incident normal to the phase mask, passes through it and is diffracted by the periodic corrugations of the phase mask (see Fig. 4.10). The two first order (+1 and -1 order) diffracted beams interfere and produce the periodic pattern that photoimprints the grating into the fiber close to the phase mask. The phase masks are designed to produce the highest possible visibility, i.e. so that the intensity in the first order diffracted beams is maximized and the intensity in the zero order diffracted beam is minimized. This can be achieved by precisely controlling the depth of the corrugations in the phase mask grating. The phase masks are typically fabricated on a silica substrate holographically or by using electron-beam lithography. Electron-beam lithography allows fabrication of complicated phase masks, but on the other hand suffers from possible stitching errors. Holographically fabricated phase masks do not have stitching errors, but for instance very large chirp rates and complicated grating structures are not possible to achieve.

One of the main advantages in the phase mask technique is the small degree of coherence required from the UV-laser source to create the interference pattern. Moreover, the phase mask method offers very good repeatability in the alignment of the system which allows effective volume production of gratings. On the other hand, for different FBG wavelengths and dispersion, a new phase mask is required.

The phenomenon behind the UV-induced permanent change of refractive index in the fiber core relies on the photosensitivity of the fiber. The effect of visible light exposure on the refractive index of a Ge-doped fiber core was discovered as early as 1978 [258]. At the beginning, the investigations were focused on laser wavelengths of an Argon ion laser around 488 nm. However, quite soon it was observed that large index changes could also be achieved using UV laser light at ~240-250 nm [254]. It was also observed that the largest photosensitivities were recorded for fibers with Ge-doped cores [254].

Although considerable effort has been put into solving the physical mechanism behind the photosensitivity, its origin has not yet been unambiguously identified. However, it seems that the photosensitivity in germanosilicate optical fibers originates mainly from defects (color centers) associated with oxygen deficiencies in the chemical structure of

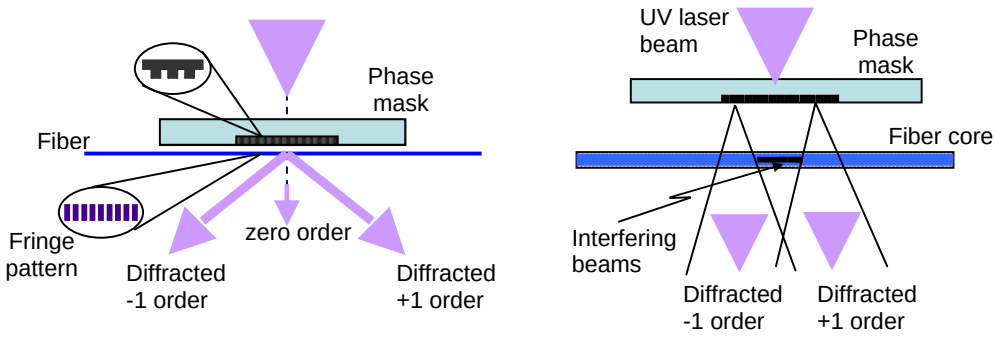

Fig. 4.10. Schematics of the phase-mask technique and geometry used for inscription of FBGs in photosensitive optical fibers.

the fiber. These color centers create absorption bands at UV wavelengths. Other models such as the stress-relaxation model, dipole model, and compaction model have also been proposed to explain the origin of photosensitivity [259]. Actually, photosensitivity is not only a feature of Ge-doped fibers. Fibers doped with boron [260], europium [261], cerium [262], and erbium:germanium [263] have also been reported to be photosensitive under UV-light exposure.

The photosensitivity and the attainable index change under UV-light exposure can be increased by various different methods including high Ge-doping, boron codoping, and hydrogenation using a pressure chamber or a hydrogen-oxygen traveling flame burner [264-266]. The most common and efficient method to diffuse hydrogen into the fiber core is the use of a temperature-controlled high-pressure chamber filled with hydrogen gas [266]. It has been shown that the hydrogen molecules react with the glass and form OH absorbing species and UV bleachable germanium oxygen deficiency centers, which are responsible for the enhanced photosensitivity [259]. By using hydrogen loading, index changes as high as 0.02 have been obtained [267]. The increased index change allows fabrication of gratings with increased reflectivity and reduced inscription time. The high index change is especially important in CFBGs which have wide spectral bandwidths and require smooth reflectivity responses. The quality of FBGs inscribed into LMA fibers, with typically larger claddings and core diameters compared to standard telecom single mode fibers, also benefit greatly from the enhanced photosensitivity. After the FBG inscription, the fiber containing a large amount of hydrogen needs to be annealed for a certain length of time in order to remove the hydrogen. The hydrogen in the fiber causes excess losses for light propagation and failures in splicing with other fibers.

In the CFBG, the period of the grating changes over the grating length either linearly or nonlinearly. In mode-locked laser and optical communication applications it is often beneficial to have a linear predictable chirp, and therefore linear dispersion characteristics. A simplified schematic diagram of the grating period change in a CFBG is shown in Fig. 4.11. In a CFBG that provides anomalous GVD, the longer wavelength components attain a certain delay compared to shorter wavelengths, which depends on the chirp of the grating. In a CFBG that provides normal GVD, the short wavelengths are delayed compared to the long ones. Actually, the same CFBG can be used to provide both anomalous and normal dispersion, depending on the light launching direction.

Theoretically the CFBG dispersion can be estimated by:

$$D = \frac{1}{L}\frac{\Delta\tau}{\Delta\lambda} \approx \frac{2n_{eff}L}{c\Delta\lambda}, \tag{4.3}$$

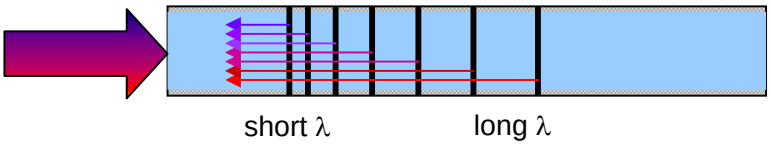

Fig. 4.11. Schematic diagram of the period change in a CFBG. The light is launched from the short wavelength side, i.e. the shorter wavelengths (blue) reflect at the beginning of the grating and the longer ones (red) are delayed and reflected at the end of the structure. The light is launched such that the CFBG provides anomalous dispersion.

where $\Delta\tau$ is the total variation of the group delay due to the CFBG, $\Delta\lambda$ is the FWHM spectral width of the CFBG, L is the length of the CFBG, n_{eff} is the effective refractive index of the fiber core, and c is the speed of light. If the phase mask technique is employed for CFBG manufacturing, the grating spectral width can be expressed using the chirp rate (C_R) of the used phase mask:

$$\Delta\lambda \approx n_{eff} C_R L . \tag{4.4}$$

Actually, the CFBG dispersion therefore theoretically depends only on the chirp rate of the phase mask:

$$D = \frac{2}{cC_R} . \tag{4.5}$$

In practice, group delay ripple resulting from ripple and modulation in the CFBG reflectivity spectrum affects the dispersion characteristics of a CFBG. Moreover, the dispersion values measured from opposite directions of the grating, without taking into account the sign of the dispersion, might attain slightly different values [268]. These differences in the spectrum and dispersion arise due to additional cladding mode losses when the light is launched from the long wavelength side of the CFBG. This is common especially with high reflection gratings that typically initiate cladding modes at the short wavelength side of the grating [269].

The benefits of CFBG-dispersion compensators are their simple integrability into all-fiber configurations. Moreover, CFBGs can conveniently be used simultaneously as dispersion compensators and as output couplers. CFBGs are also free from nonlinearities, and by applying nonlinear stress or by using a temperature gradient across the grating area, the dispersion of a CFBG can be tuned. On the other hand, applications typically require a smooth and flat reflectivity response without ripple, which is usually tricky to achieve with highly chirped gratings. Indeed, the spectral ripple can be reduced by using beam scanning techniques or different apodizations [270,271]. Different amounts of dispersion can also be generated by inscribing a uniform FBG into the transition area of a tapered fiber [272-274]. Recently, dispersion compensation of a mode-locked Yb-doped fiber laser was demonstrated using a tapered-FBG with dispersion set by the slope of the tapered fiber [S4].

In this thesis, I have employed the phase mask technique and a KrF excimer laser operating at 248 nm. Figure 4.12 shows a 3D-image of the used workstation. The focus in this work has been on the inscription of highly chirped gratings with extremely broad and flat reflectivity responses to be used in mode-locked fiber lasers for dispersion compensation. Mode-locked Yb- and Bi-doped fiber lasers have been demonstrated employing CFBGs [P4,P7]. Figure 4.13 shows a typical reflectivity spectrum of a highly chirped FBG. This grating with a spectral width of ~24 nm and dispersion of ~4.4 ps/nm was used for dispersion compensation in the mode-locked Yb-doped fiber laser at 1050 nm. The smooth reflectivity response was achieved by optimizing UV-laser parameters such as the beam profile, pulse energy, pulse repetition rate, and inscription time. In addition, a beam scanning technique with an optimized very low scanning velocity (~0.002 mm/s) was used. The results of the mode-locked laser are described in detail in the next section [P4].

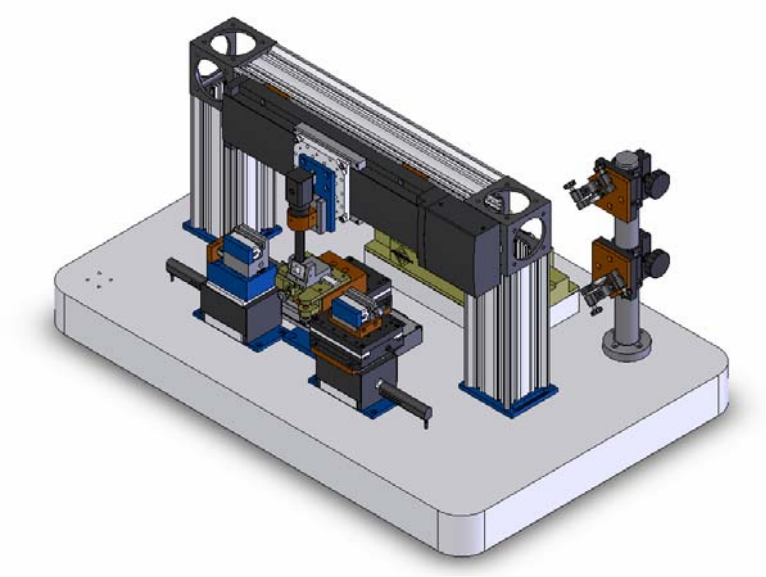

Fig. 4.12. 3D-view of the FBG manufacturing workstation.

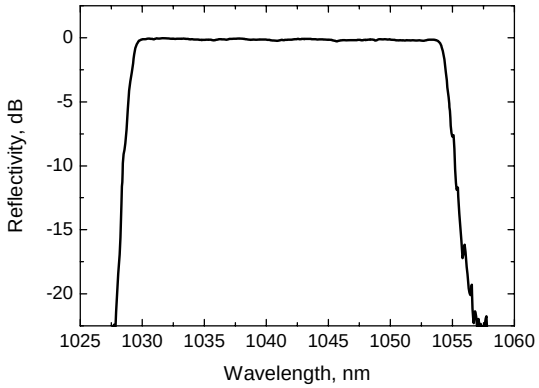

Fig. 4.13. Reflectivity of the chirped fiber Bragg grating with spectral width of 24 nm.

4.3.5 All-fiber supercontinuum generation using a mode-locked Yb-doped laser system with dispersion compensation by a linearly chirped fiber Bragg grating

The CFBG shown in Fig. 4.13 was used for dispersion compensation in a mode-locked Yb-laser shown schematically in Fig. 4.14 [P4]. The linear laser cavity (the master oscillator) comprised ~70 cm of Yb-doped fiber with 500 dB/m absorption at 980 nm pumped with a 980-nm single mode laser diode through a dichroic fiber coupler. A butt-coupled semiconductor saturable absorber mirror (SAM) acting as a cavity end reflector ensured reliable self-starting of the passive mode-locking. The used SAM contained 4 InGaAsN quantum wells and a 26 pair GaAs-AlAs bottom-DBR. The modulation depth, saturation fluence and non-bleachable losses of the absorber were measured to be ~17%, ~50 μJ/cm^2, and ~12%, respectively. The other end of the cavity was terminated by the CFBG. The reflectivity of the CFBG with a center wavelength of 1042 nm was measured

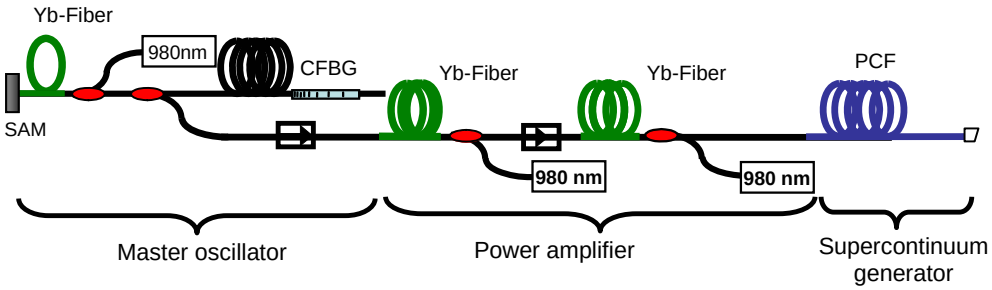

Fig. 4.14. All-fiber supercontinuum source setup. CFBG: Chirped fiber Bragg grating, PCF: Photonic crystal fiber, SAM: Semiconductor saturable absorber mirror.

to be >97% over the bandwidth from 1030 nm to 1054 nm, as seen from Fig. 4.13. The dispersion of the grating at the wavelength around 1 μm could compensate for the normal dispersion of the standard single-mode fiber with a length of over 50 meters.

The mode-locked laser was first operated with a cavity length corresponding to a repetition rate of 47 MHz. The measured pulse spectrum and autocorrelation trace are shown in Fig. 4.15. The laser emitted pulses with a duration of 1.95 ps (FWHM) with clearly visible spectral Kelly sidebands, typical characteristics for a soliton pulse laser. To decrease the pulse repetition rate and to maximize the pulse energy after amplification, a piece of single-mode fiber was added to the cavity. The effect of the cavity length on the pulse width and time-bandwidth product was then investigated both experimentally and numerically. The experimental results are summarized in Fig. 4.16. As can be seen, the pulse width ranged from 2 ps to 1.6 ps and the time-bandwidth product from 0.42 to 0.49 when the length of the fiber cavity was varied from 2.5 m to 37 m. The variation of the time-bandwidth product and the pulse width with the length of fiber inserted into the cavity were due to strong temporal and spectral evolution in the long dispersion managed fiber cavity, as confirmed by the numerical simulations presented below.

The pulse generation and propagation in a fiber laser was described by the nonlinear Schrödinger equation (4.2) including the effects of dispersion, loss, parabolic gain-bandwidth profile, and the SESAM considered as a two-level system. The simulations were started from noise and ran for a sufficient number of consecutive round trips through the cavity elements until a steady-state was reached. The results of the laser

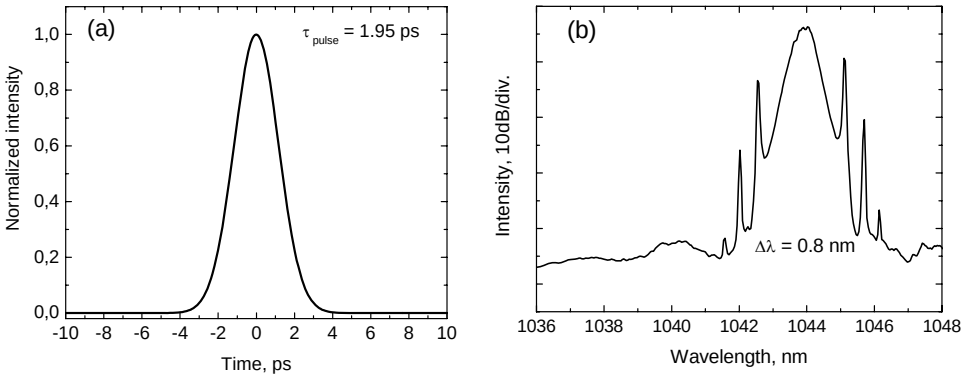

Fig. 4.15. (a) Autocorrelation and (b) spectrum of the pulses with a repetition rate of 47 MHz generated by the fiber oscillator with a chirped fiber Bragg grating as a dispersion compensator.

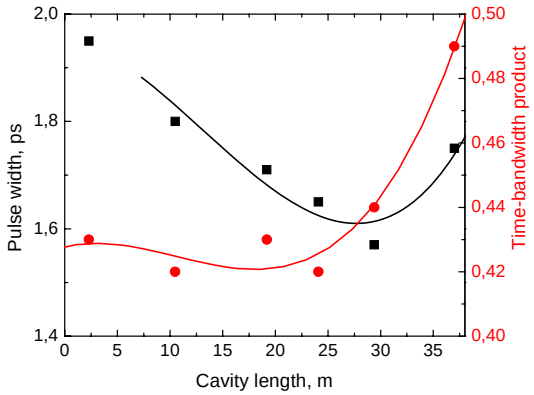

Fig. 4.16. Measured pulse width (squares) and time-bandwidth product (dots) for different cavity lengths/cavity anomalous dispersion of the laser. The lines are the corresponding fittings.

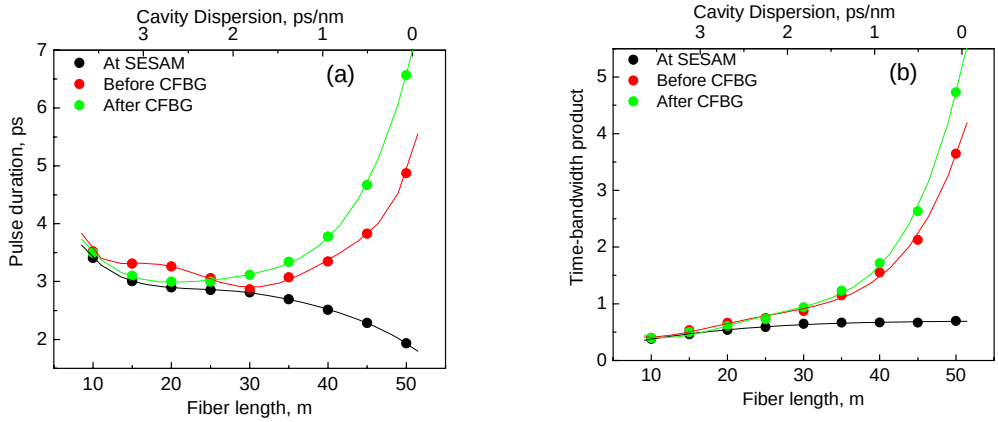

Fig 4.17. (a) Simulated pulse width and (b) time-bandwidth product for different fiber lengths and locations in the laser cavity.

simulation presented in Fig. 4.17 validate that pulse duration and time-bandwidth product exhibit strong variations in dispersion-managed soliton fiber lasers when the value of fiber dispersion becomes close to the value of the dispersion of the CFBG with opposite sign, i.e. the total cavity dispersion approaches zero value. In particular, the pulses are slightly down-chirped at the SAM position, strongly up-chirped before the CFBG, and strongly down-chirped after the CFBG. While the pulse duration continues to decrease gradually with increasing fiber length close to the SAM, it starts to increase at locations near the CFBG. The simulation thus described the observed increase of time-bandwidth product and pulse duration for fiber lengths longer than ~20 m, since the laser output was set at a substantial distance from SAM, as seen from Fig. 4.14.

Supercontinuum generation in a PCF

To boost the pulse energy and output power of the laser, a two-stage ytterbium fiber amplifier core-pumped with fiber-coupled 300-mW pump diodes was built (see Fig. 4.14). After the amplification the average output power was measured to be ~78 mW in

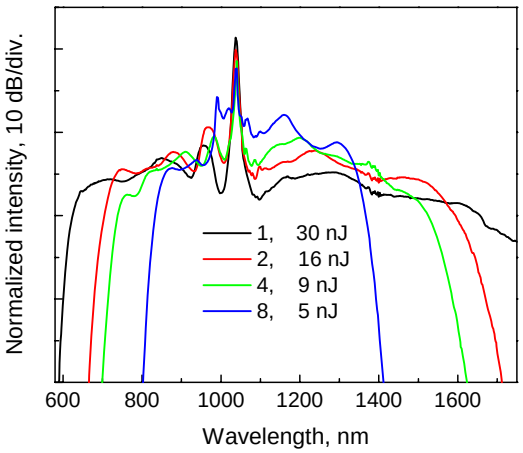

Fig. 4.18. Supercontinuum spectra for single, 2, 4 and 8 pulses circulating in the master laser cavity. Pulse energy ranges from 5 to 30 nJ, as indicated in the Figure.

the single pulse regime of the master oscillator. In order to demonstrate a practical application of this compact low-cost core-pumped all-fiber system, the amplifier output was spliced to a 15-m long photonic crystal fiber with a zero dispersion wavelength at 1065 nm and a nonlinear coefficient of 11 $(W \cdot km)^{-1}$. The aim was to study supercontinuum generation, interesting for example in biomedical applications and metrology, using a low power but high pulse energy low-cost all-fiber source.

The spectra at the output of the PCF presented in Fig. 4.18 corresponded to states with different numbers of pulses circulating in the master oscillator cavity and, consequently, with different pulse energies. Since excessive pump power resulted in multiple pulsing, the amplifier was found to produce the highest pulse energy when the average output power was limited to 78 mW. In the single pulse regime, the supercontinuum spectrum extended from 615 nm to 1700 nm (measured at 10-dB level).

In conclusion, we demonstrated a practical all-fiber supercontinuum source generating an octave-spanning spectrum. Both the soliton pulse regime and low fundamental repetition rate of ~3 MHz in the passively mode-locked ytterbium fiber laser were achieved using a high-performance chirped fiber Bragg grating for dispersion control.

4.4 Wavelength tuning of fiber lasers

Wavelength tunable ultrafast lasers are needed in various applications including spectroscopy, LIDAR, metrology, and optical communications. This chapter introduces a few of the basic tuning methods for fiber lasers.

4.4.1 Methods for wavelength tuning

Diffraction gratings

A very simple wavelength tuning method is to use a diffraction grating in the Littrow configuration as a second cavity end mirror (see Fig. 4.19) or a diffraction grating pair for dispersion compensation. In both approaches the laser wavelength can be tuned by

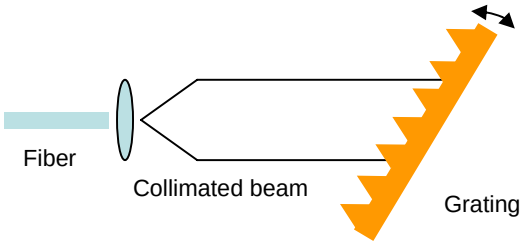

Fig. 4.19. Wavelength tuning using diffraction grating in the Littrow configuration.

varying the angle between the grating and the incoming light beam. Basically, using this method, the wavelength of the laser can be tuned through the fiber gain spectrum. However, the amount of intracavity losses increases due to the limited diffraction efficiency of the available bulk diffraction gratings. Similar wavelength tuning can also be implemented with prisms.

Intracavity filters

Another traditional method is to use a tunable filter which has a loss minimum at some adjustable wavelength inside a cavity. The loss window allows lasing only at this minimum loss region which can be tuned by rotating the filter. Typically the intracavity filter is a thin Fabry-Perot etalon made, for example, from fused silica (see Fig. 4.20) or a birefringent filter such as Lyot filter. The free-spectral range and selectivity of an etalon can be adjusted by modifying the reflectivity of the material surfaces or by increasing or decreasing its thickness. A drawback for the use of intracavity filters in fiber lasers is the intra-cavity free-space beam required. This usually violates the all-fiber configuration of a fiber laser. Moreover, when the filters are used in ultrafast mode-locked systems, special attention should be paid to the filter bandwidth, so that the filter does not limit the laser spectral width and therefore the pulse duration.

Soliton self-frequency shift in optical fibers

A very convenient wavelength tuning method for ultrafast sub-picosecond fiber lasers is the so-called soliton self-frequency shift (SSFS). The SSFS origins from stimulated Raman scattering and is, therefore, often also called Raman shifting. Due to the Raman gain in an optical fiber with anomalous dispersion, the blue portion (high frequency components) of a pulse spectrum pumps the red portion (low frequency components) of the spectrum. This leads to a self-induced continuous red-shift in the spectrum. The effect

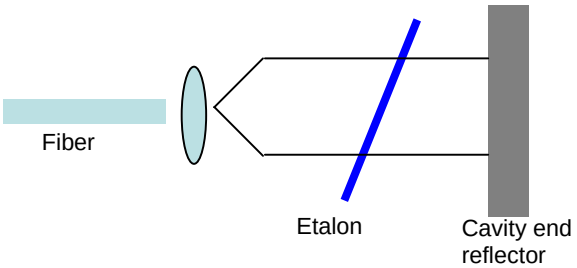

Fig. 4.20. Wavelength tuning using a tunable etalon inside a fiber laser cavity.

of SSFS can take place with short pulses with high enough peak power during propagation in standard or specifically designed optical fibers with anomalous GVD. Using SSFS, exceptionally wide tuning ranges can be achieved and wavelengths that are otherwise unreachable with doped-fiber lasers can be covered. The main parameters of the pulse source affecting the strength of SSFS are the pulse width and the peak power. The fundamental parameters in the Raman fiber affecting SSFS are the dispersion, length and nonlinearity. In general, the shorter the pulse and the higher the launched power in the Raman fiber, the stronger the Raman effect.

SSFS was discovered for the first time in 1986 by Mitschke *et al.* in polarization maintaining single mode fibers [275]. After the discovery, large pump power-dependent Raman wavelength shifts have been demonstrated in standard telecommunication fibers [276,277], fiber amplifiers [278,P9], tapered microstructured fibers [279], high-index core PCFs [280,281], hollow-core PBGFs [282], and in solid HOM fibers [283]. SSFS in standard silica-based step index single mode fibers is restricted to wavelengths above ~1.3 μm due to the normal GVD at shorter wavelengths. Employing dispersion-tailored microstructured or HOM fibers, SSFS can additionally be generated at wavelengths below 1.3 μm, for example at 1 μm employing Yb-doped fiber lasers. The largest wavelength shifts, in the range of hundreds of nanometers, have been generated in photonic crystal fibers. Chan *et al.* recently demonstrated a 1.2- to 2.2-μm tunable Raman soliton source based on a Cr:forsterite laser and a PCF [284]. Using a Yb-doped mode-locked fiber system and PCF, a tuning range from 1 μm up to 1.7 μm has been demonstrated [285]. Er-doped fiber lasers have also been used as a seed source for SSFS to generate a 2 μm pulsed source with high peak power [286,287].

The achievable wavelength shift in the ideal case with a certain Raman fiber length and pulse duration depends only on the available pump power. However, Raman shifting typically stops at a certain wavelength due to fiber dispersion properties, increased fiber loss, or self-steepening [287,288]. Due to these effects the pulse energy in the first order soliton starts to decrease and the increase in the pump power leads only to generation of cascaded higher order solitons rather than further shifting of the first order soliton. With further increases in the pump power, the wavelength gaps between different solitons might gradually start to be filled, leading to a supercontinuum [287,P9]. In addition to wavelength shifting, a nonlinear fiber that generates SSFS can be designed so that it allows spectral broadening or compression [289,290]. Pulse compression or broadening in fibers is mainly determined by the balance between the dispersion and nonlinearity. If these fiber properties are in good balance with the input pulse, significant pulse compression can be achieved [290,291,P9].

A typical wavelength tuning configuration employing SSFS is shown schematically in Fig. 4.21. Ultrashort pulses from a mode-locked system are launched into a nonlinear fiber that generates the SSFS. The insets in Fig. 4.21 show the input and output pulse spectra. As can be seen, the output also contains some unconverted residual pump light, common for SSFS. The Raman conversion efficiency depends on the fiber nonlinearity, GVD, and parameters of the seed pulse, being typically in the range of ~40 to ~80%. Figure 4.22 shows simulation results for a 10 m long Tm-Ho-doped fiber amplifier (15 dB/m gain) seeded by a 600 fs Tm-Ho-doped fiber seed laser operating at 2 μm, described in detail in [P9]. As can be seen, significant power-dependent Raman shifting

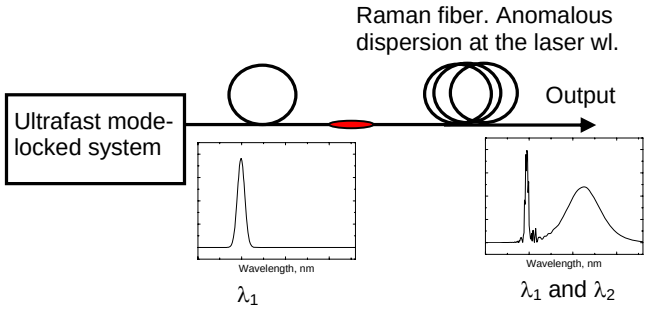

Fig. 4.21. Schematic of a typical Raman soliton source.

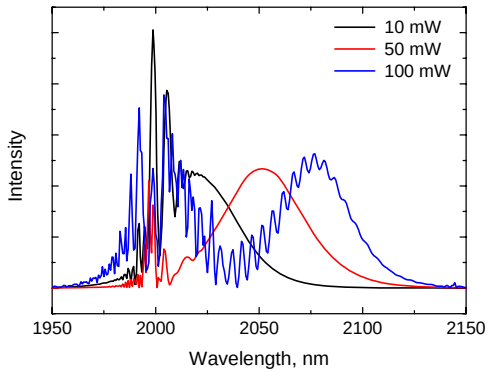

Fig. 4.22. Simulated SSFS in a Tm-Ho-doped fiber amplifier with different power levels. The input pulse duration is 600 fs.

already occurs with relatively small powers. The simulation predicts the tunability of the Raman soliton with pump power well. Simultaneously with the wavelength shifting, the 600 fs pulse is compressed to ~150 fs. With larger powers the Tm-Ho-doped fiber amplifier starts to generate a second order soliton (blue trace). The related experimental work is described later in chapter 5.2.1 [P9].

Electronic tuning using acousto-optic filters

Another very fascinating wavelength tuning method is to employ an acousto-optic tunable filter (AOTF), which is a tunable bandpass filter that uses an acousto-optic interaction inside an anisotropic medium. A computer-controlled RF-signal applied to the AOTF transducer is typically used to control the transmitted and diffracted wavelengths. The main advantage of this wavelength tuning technique is the absence of any moving parts which leads to stable and fast wavelength tuning. Nowadays commercially available AOTFs allow fast tuning with response times in the range of tens of nanoseconds to a few microseconds.

4.4.2 Electronically tunable mode-locked Yb-doped fiber laser

In [P5], we demonstrated and studied an electronically tunable mode-locked Yb-doped fiber laser delivering ~1 ps pulses with fast, ~15 μs, tuning time. Such a pulse source,

having the capacity for accurate and fast wavelength tuning could be used in spectroscopic measurements, biophotonic imaging or optical coherence tomography. Most tunable fiber lasers operating at 1 μm reported to date use mechanical wavelength tuning by rotating intracavity gratings or mirrors. Our approach offered a way to avoid mechanical tuning. We also studied tunable laser mode-locking using a SESAM, FSF, and a combination of SESAM and FSF.

The soliton fiber laser comprised ~1 m of Yb-doped fiber with ~400 dB/m absorption at 980 nm pumped with a 980-nm laser diode through a dichroic fiber coupler, a highly-reflective (HR) mirror, a SESAM, and a transmission grating pair (see Fig. 4.23). The electronic tuning was implemented using an AOTF driven with an RF-signal having a computer controlled frequency. The experimental details can be found in [P5].

Without the AOTF in the cavity, the mode-locked laser operated at a fixed wavelength of 1046 nm and delivered 300 fs pulses. With the AOTF in the cavity and the SESAM initiating mode-locking, the laser was continuously tunable in the range from 1030 nm to 1060 nm. The pulse duration increased slightly to a value of ~1 ps due to spectral filtering of the AOTF (3 nm bandwidth). The build-up time for steady state mode-locking and, consequently, the actual tuning speed of the laser, was measured to be 10-25 μs (400-1000 cavity round trips) depending on the pump power and the wavelength. The tuning time was not limited by the AOTF rise time, which was < 5 μs. The mode-locked operation was also studied in the frequency-shifted feedback regime with the SESAM replaced by a HR-mirror. Self-starting mode-locking with 4-5 ps pulses over the tuning range of 1029 nm - 1072 nm was observed.

Finally, the mechanism of pulse shaping using a SESAM and AOTF was further investigated using numerical simulations. The simulations revealed that the laser mode-locked by the saturable absorber without spectral filtering produces 250 fs pulses with 4.5 nm spectral width. When replacing the SESAM by the AOTF, the pulse duration increases up to 3.7 ps with a corresponding spectral width of 0.35 nm. The pulse shaping by AOTF is, therefore not strong enough to provide shorter pulses with broader spectral width. On the contrary, the spectral broadening up to 1.4 nm achieved with the combination of SESAM+AOTF scheme results in a pulse compression down to 1.1 ps. The simulations also predicted that 360-fs pulses could be generated with the bandwidth of the filter increased from 3 nm to 10 nm. Figure 4.24 shows the simulated pulse traces for the laser mode-locked by the SESAM, SESAM + AOTF, and the AOTF. The experimental results of the work are summarized in Fig. 4.25. The experimental results and the numerical simulations are in very good agreement.

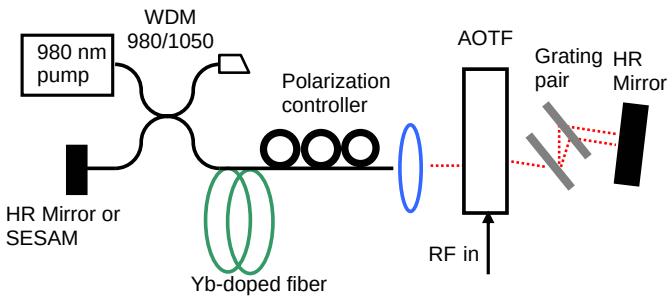

Fig. 4.23. Experimental configuration of the Yb-doped fiber laser electronically tunable with AOTF.

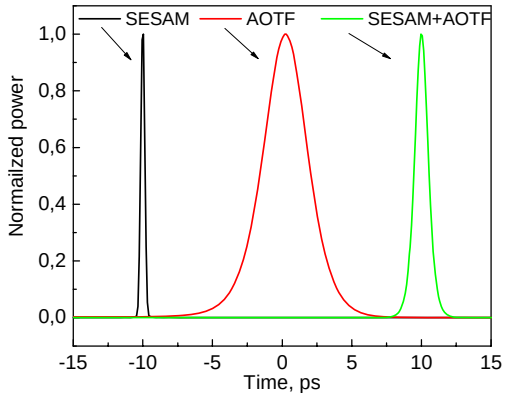

Fig. 4.24. Simulated pulse shapes for the mode-locked fiber laser for SESAM, AOTF, and SESAM+AOTF cavity configurations.

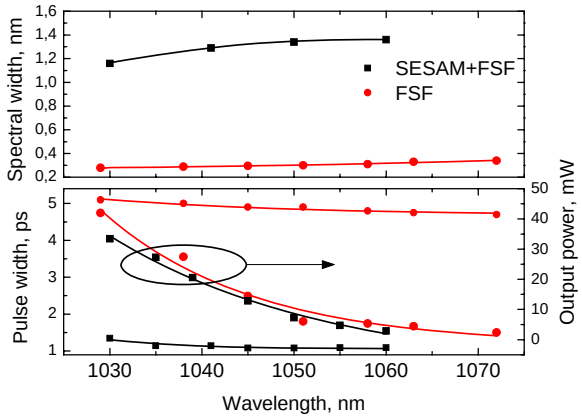

Fig. 4.25. Measured spectral width, pulse width, and output power vs. wavelength for the FSF-laser and for the laser mode-locked by the SESAM (SESAM+FSF). Pump power is 210 mW. Solid lines are the fittings for the experimental data.

5. Ultrashort pulse mode-locked lasers based on novel fibers and saturable absorbers

This chapter is devoted to novel passively mode-locked fiber lasers; the main achievements of this thesis. The first section of the chapter describes the development of ultrafast mode-locked Bi-doped fiber lasers operating both in soliton and normal dispersion regimes. The pulse generation and dynamics of Bi-doped fiber lasers, which actually differ from the pulse dynamics of other fiber lasers based on more conventional active fibers, are described in detail. The demonstrated mode-locked soliton Bi-lasers are the first in the world.

The second section focuses on a mode-locked Tm-Ho-doped fiber laser system. A GaSb-based SESAM has been used for mode-locking, and SSFS for wide wavelength tuning and pulse compression. The third section includes the study and development of ultra-broadband, polymer-free carbon nanotube saturable absorbers for mode-locking of various fiber lasers operating at different wavelength regimes. The widest operation bandwidth for a CNT-based saturable absorber is demonstrated. The Tm-Ho doped fiber laser used also operates at the longest wavelength, 2 μm, reported for any CNT-based saturable absorber.

5.1 Mode-locked bismuth-doped fiber lasers

Recently developed Bi-doped fibers have the ability to provide gain within the 1100-1550 nm wavelength range [76] and thus leverage the well known advantages of fiber lasers and fiber amplifiers to new applications, especially in the field of optical communications. Continuous wave (cw) Bi-doped fiber lasers with cavity lengths in the range of several tens of meters have already been reported to deliver output powers up to several watts [66,15]. The necessity to use a long length of Bi-doped fiber, imposed by the relatively low values of of pump absorption and gain coefficients, is an undesirable feature in mode-locked systems, which would favor a short fiber cavity. Therefore, the mode-locked regime has remained inaccessible to Bi-lasers. The first Bi-fiber laser mode-locked by a semiconductor saturable absorber mirror (SESAM) exhibited relatively long, ~50 ps, pulses with a large pulse pedestal [292]. This was attributed to the combined effects of the narrow bandwidth of the fiber Bragg grating reflector, the large normal dispersion of the long-length cavity and the non-optimized SESAM with slow recovery time. In order to generate subpicosecond high-quality pulses from Bi-fiber lasers, dispersion compensation and a SESAM with picosecond or subpicosecond recovery time is required. Additionally, the relatively low gain of Bi-fibers sets strict limitations on the cavity design and the amount of acceptable losses. Special attention should also be paid to pulse generation and evolution within the long fiber cavity.

5.1.1 Tunable mode-locked bismuth-doped soliton fiber laser

In the [P6], we reported the first mode-locked Bi-doped fiber laser operating in the soliton regime and delivering sub-picosecond pulses. The linear fiber cavity, which was designed to have minimal losses, is described in detail in [P6]. The Bi-doped aluminosilicate fiber with a length of ~12 m had an absorption of ~1.2 dB/m at the pump wavelength of 1060 nm. The Bi-fiber core diameter, core/cladding refractive index difference, and the cutoff wavelength were 8.4 μm, $\Delta n = 5.5 \cdot 10^{-3}$, and ~1100 nm, respectively. The fiber manufacturing and characterization process have been described in detail in [68]. The dispersion of the fiber at the laser wavelength of 1165 nm was calculated to be ~ -0.013 ps/(nm·m). The splice loss between the gain and a standard single mode fiber was ~0.3 dB. The normal dispersion of the fiber cavity was compensated for by a transmission grating pair with 1250 lines/mm and a grating separation of ~19 mm. The net cavity dispersion was estimated to be ~-0.4 ps^2.

The SESAM consisted of 4 InGaAsN quantum wells with widths of 6 nm grown on top of a 24.5 pair GaAs/AlAs DBR. The DBR stopband had a center wavelength of ~1140 nm with an approximately 150-nm bandwidth. The absorption recovery time was tailored to be ~2 ps using in-situ N-irradiation during the MBE-growth [171].

The SESAM ensured self-starting mode-locking at the repetition rate of 7.5 MHz. The wavelength of the laser could be tuned from 1153 nm to 1170 nm using the transmission grating pair. Figures 5.1(a) and (b) show the recorded autocorrelation trace and the tunable pulse spectra. The pulse width, the spectral width and the time-bandwidth product were 0.94 ps ($Sech^2$-fitting), 2.0 nm, 0.4, respectively. The inset to Fig. 5.1(b) shows an image of the pulse train on the oscilloscope screen.

This was an important demonstration towards practical sub-picosecond mode-locked Bi-doped fiber lasers operating in the 1150–1480 nm range.

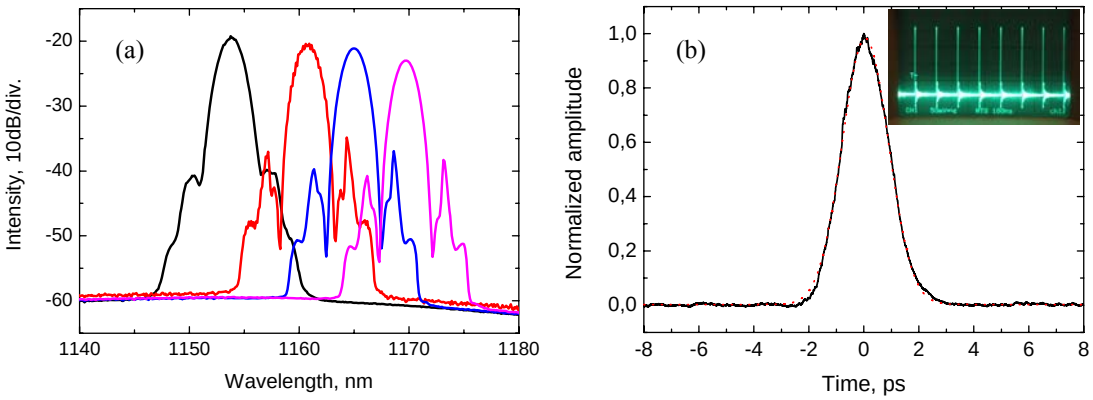

Fig. 5.1. (a) Tunable optical spectra of the mode-locked Bi-doped fiber laser. The spectral width is 2 nm. (b) Measured autocorrelation trace. The dashed line is the $Sech^2$-fitting. The inset shows an image of the 7.5 MHz pulse train on an oscilloscope screen.

5.1.2 All-fiber bismuth laser with dispersion compensation by a chirped fiber Bragg grating

In this work [P7], we demonstrated a mode-locked all-fiber Bi-doped laser. A linearly chirped fiber Bragg grating was used for the dispersion compensation. A schematic of the robust linear all-fiber cavity is shown in Fig. 5.2. The mode-locking was initiated by the dilute nitride SESAM described in the previous section. An additional 5% tap coupler was spliced to the cavity for monitoring purposes. The Bi-doped fiber was the same as that described in section 5.1.1. The length of the Bi-doped fiber was varied within the range of 12-19 m during the measurements. The CFBG was inscribed using the phase mask technique, as described in section 4.3.4. The reflectivity of the CFBG ensuring optimal feedback to the cavity and adequate output coupling was found to be ~90 %. The bandwidth of the grating ranged from 1155 nm to 1186 nm. The dispersion of the CFBG was ~3.0 ps/nm.

Mode-locking experiments were performed with different doped fiber lengths of 12 m, 14.5 m and 19 m, corresponding to overall cavity lengths of 14 m, 16.5 m and 21 m, respectively. The maximum average output power was found to increase from 4 mW to 6 mW for 850 mW of launched pump power when the doped fiber length was increased from 12 to 19 m. Due to the increase in the overall gain with increasing doped-fiber length, the threshold power decreased from ~400 mW (12 m long Bi-fiber) to 300 mW (19 m long Bi-fiber). The effect of the cavity length on the pulse duration and spectral width at the outputs 1 and 2 was studied (see Fig. 5.3.). As can be seen the pulse duration decreased gradually with an increase in the fiber length at the SESAM end (Output 1), but started to increase for cavity lengths over ~18-20 m at locations near the CFBG (Output 2). The changes in the pulse width were expected, due to the strong temporal and spectral pulse re-shaping which occur in a long dispersion managed fiber laser cavity. The time-bandwidth product at Output 2 ranged from 0.5-0.6 depending on the cavity length.

A typical optical spectrum and autocorrelation trace for a cavity length of 21 m are shown in Fig. 5.4. The laser generated low-noise pulses of ~1.9 ps duration (FWHM) with Kelly spectral sidebands, indicating operation in the soliton regime. The spectral width and the calculated time-bandwidth product of the pulses at the output 1 were 0.95 nm and 0.40, respectively. The dashed line in Fig. 5.4 is the spectrum corresponding to the laser operation in the normal dispersion regime without the CFBG dispersion

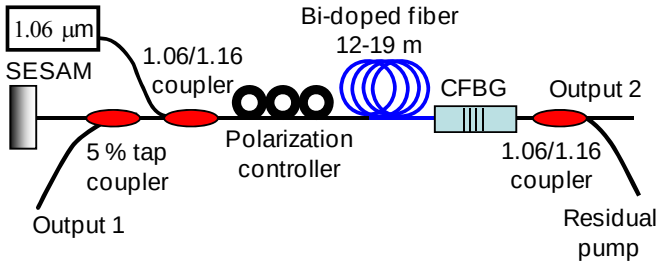

Fig. 5.2. Bi-doped all-fiber laser setup. The self-starting mode-locked operation was initiated by an InGaAsN-based SESAM. The soliton regime was provided by a CFBG.

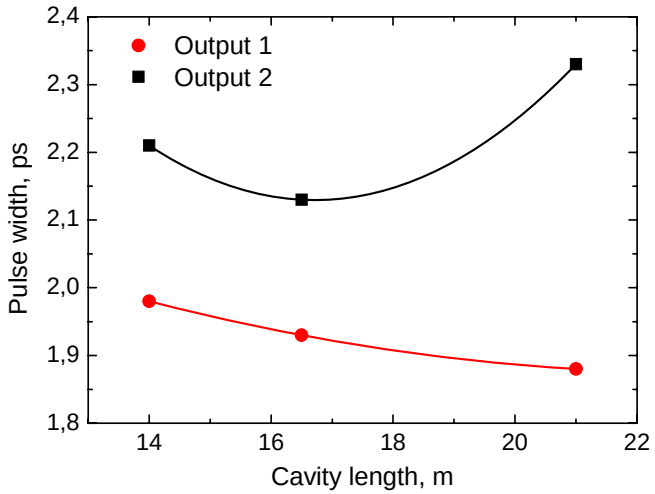

Fig. 5.3. Measured pulse width for different cavity lengths at different cavity outputs. The solid lines are the fittings.

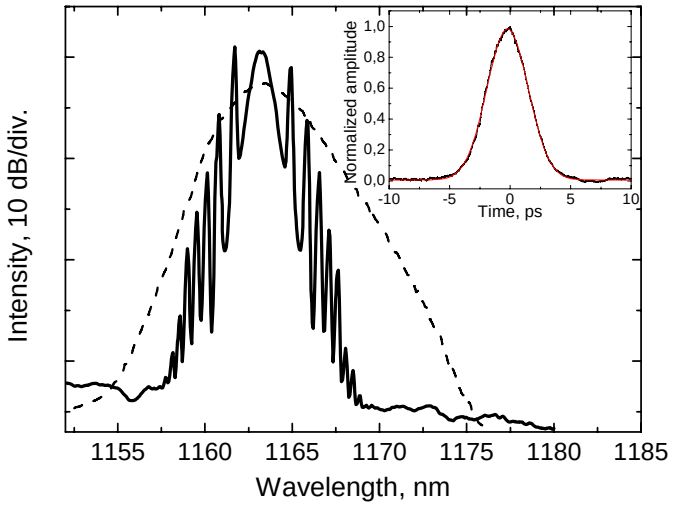

Fig. 5.4. Spectrum and autocorrelation (inset) of the pulses generated by the fiber oscillator with the CFBG as a dispersion compensator. The red line in the inset is the $Sech^2$-fitting giving the pulse width of ~1.9 ps. The total cavity length was ~21 m. Optical spectrum of the laser without dispersion compensation is shown by the dashed line.

compensator. The autocorrelation trace in the normal dispersion regime showed a large pulse pedestal that exceeded the autocorrelator scanning range of 210 ps.

The large net anomalous cavity dispersion provided by the CFBG promoted soliton breakup and allowed multiple soliton pulses to form. For certain positions of the polarization controller, the Bi-fiber laser operated with multiple soliton pulses having equal temporal spacing, i.e. highly-ordered harmonic mode-locking. As a consequence, the pulse repetition rate could be tuned from the fundamental repetition rate of 6.3 MHz up to 100.6 MHz (corresponding to the 16th harmonic of the cavity frequency) by varying the pump power. Adjacent modes were suppressed by more than 45 dB, which indicates a strong soliton pulse self-ordering effect in the cavity. The 100.6 MHz

repetition rate obtained is one order of magnitude higher than previously reported repetition rates of Bi-doped fiber lasers. It is notable that this high value cannot be achieved with Bi-lasers operating at the fundamental pulse frequency, due to their moderate gain and the long length of active fiber consequently required.

5.1.3 Pulse dynamics of passively mode-locked Bi-doped fiber lasers

In this work [P8], pulse generation and evolution in passively mode-locked Bi-lasers with relatively long gain fiber were studied in detail via experiments and numerical simulations. Laser performance was studied using saturable absorbers with different absorption recovery times. The influence of the average cavity dispersion on the pulse generation and quality was also investigated. A behaviour slightly different to other mode-locked lasers based on more traditional active fibers was observed.

The linear cavity of the mode-locked Bi-laser is described in [P8]. The Bi-fiber was the same as that in [P6] and [P7] and had a length of ~12 m. The dispersion compensation was provided by a transmission grating pair. The amount of cavity dispersion was varied during the measurements by changing the grating separation. The fiber cavity was formed between a 97% reflecting fiber loop mirror and a dilute nitride SESAM. An additional 5% tap coupler was spliced close to the SESAM and the dispersion compensator end of the cavity for monitoring purposes. Three different absorbers labeled Absorber #1, Absorber #2 and Absorber #3, having different absorption recovery times of 680 ps, 4 ps, and 2 ps, respectively, were employed. Absorbers #2 and #3 exhibited a double exponential decay of the absorber recovery, with slow components of ~40 ps and ~20 ps, respectively. In general, the slow component of the absorption recovery is useful for ensuring self-starting mode-locking, while the fast component is beneficial for pulse shaping. The Absorber #1 was not irradiated with N-ions during the growth, whereas the quantum wells of Absorbers #2 and #3 were individually exposed to a flux of N for 2 and 3 minutes, respectively, in order to decrease their absorption recovery times [171].

Each of the absorbers enabled self-starting mode-locking. The pulse repetition rate was 7.3 MHz. Figure 5.5 shows the recorded autocorrelation traces and pulse spectra for the mode-locked laser with three different SESAMs. As can be seen, Absorber #1, with an absorption recovery time of ~680 ps, supports a pulse with a large pedestal (black trace) that exceeds the ~210-ps scanning range of the autocorrelator. For Absorber #2 with a recovery time of 4 ps, the pulse pedestal is significantly suppressed (red trace). Using the absorber with a recovery time of 2 ps, the pulse pedestal is completely avoided, providing clean and stable soliton pulses. Fig. 5.5(b) displays the optical spectra illustrating that the spectral width increases with a decrease of the absorption recovery time.

The soliton sidebands seen in the spectra become more pronounced with reduced recovery time, indicating stable soliton operation of the laser with the fastest SESAM. A similar tendency was observed in the pulse train monitored at the oscilloscope. In contrast to the slow absorbers, mode-locking with the fast Absorber #3 resulted in a temporally stable pulse train even for long-span measurements. The average cavity dispersion in these measurements was estimated to be ~-0.4 ps^2.

It was also observed that cavity dispersion plays a role in pulse shaping. When the

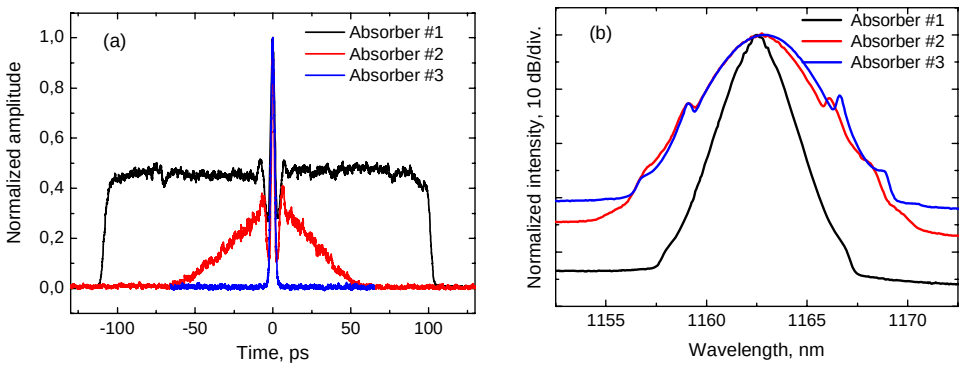

Fig. 5.5. (a) Measured autocorrelations for the three different absorbers and (b) the corresponding optical spectra. The intra-cavity cavity GVD is ~ -0.4 ps^2. The autocorrelator scanning range is ~210 ps.

average cavity dispersion was increased to ~-0.65 ps^2 by lengthening the grating pair separation, the use of Absorber #2 resulted in nearly pedestal-free pulses with a pulse duration of ~1.3 ps. On the other hand, when the laser was operated with an average cavity dispersion lower than ~-0.3 ps^2, even the use of Absorber #3 resulted in a small pedestal in output pulses. The pumping power was also observed to make a contribution to the pulse pedestals. When operated close to the laser threshold, the pulse pedestals were slightly weaker compared to higher pumping powers.

In order to understand pulse generation in Bi-doped fiber lasers, numerical simulations were performed (for details see [P8]). The results of the simulation with a cavity dispersion of -0.4 ps^2 are shown in Fig. 5.6. The simulated autocorrelations and spectra are in very good agreement with the corresponding measurements shown in Fig. 5.5. The simulation predicts the pedestal formation observed in the experiments. The simulations also show that the pumping rate has an influence on the size of the pulse pedestal. When the gain of the Bi-doped fiber is increased from 0.35 dB/m to 0.45 dB/m, the size of the pulse pedestal increases significantly, as can be seen in Fig. 5.6(a) for Absorbers #1 and #2. The inset to Fig. 5.6(a) shows an irregular pulse bunching at a large temporal span for Absorber #1. This indicates that the effective pulse pedestal seen in the autocorrelation trace appears as a result of strong multiple pulsing In conclusion, the laser with the slow absorber actually provides pulse bunches at a repetition rate of 7.3 MHz.

Simulations also predicted the decrease in the autocorrelation pedestals with larger anomalous dispersion, as was noticed in the experiments. The drop in the pedestals could be understood as stronger soliton formation and pulse shaping with higher anomalous dispersion. However, the effect of the cavity dispersion on the pulse pedestal is not as strong as the effect of the absorber recovery time or the fiber pumping level.

The observed pulse pedestals in mode-locked Bi-lasers are, therefore, likely to be due to relatively long absorber recovery times together with the long active fiber. After multiple passes of the pulse, the absorber is saturated, however, the pulse sees net gain for a relatively long time window (~20-1000 ps depending on the absorber) [172]. Within this time interval, the spontaneous noise can be amplified, disturbing the pulse quality or preventing mode-locked operation completely. The autocorrelation pedestals in the mode-locked Bi-laser experiments correspond to multiple pulses propagating in the cavity together with the stronger fundamental pulse.

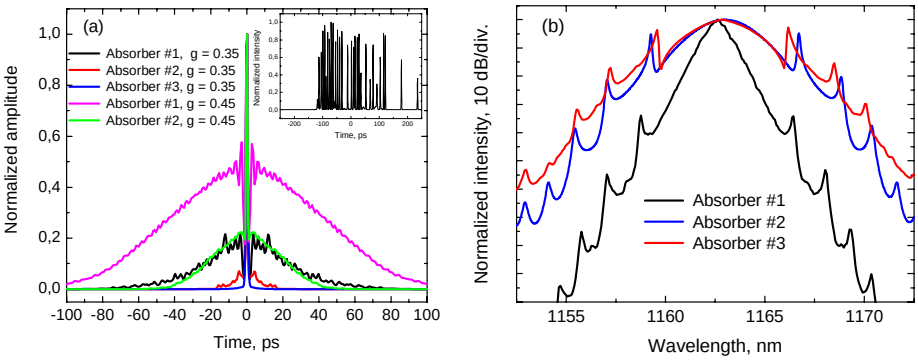

Fig. 5.6. (a) Simulated autocorrelation traces for each absorber and the (b) corresponding pulse spectra. The spectral widths are 0.9 nm, 2.6 nm, 2.6 nm, respectively. The inset shows a simulated time domain pulse shape generated using Absorber #1 with a fiber gain value of 0.45 dB/m.

Additionally, the saturation fluence of the absorber also plays a role in pulse generation. The low saturation fluence of Absorber #1 supports the self-starting operation of the laser, but on the other hand, also promotes generation of multiple noise-like pulses in combination with the long absorber recovery time [203]. In contrast, the higher saturation fluences of Absorbers #2 and #3 promote single or few-pulse operation.

Another important pulse shaping mechanism in mode-locked Bi-lasers is soliton pulse shaping. In the soliton regime, the laser is able to sustain a larger amount of noise arising behind the pulse [172]. However, if the dispersion is reduced to a less anomalous value (in this study ~ -0.3 ps^2), even the strong soliton shaping mechanism cannot prevent the formation of a pulse pedestal when slow absorbers are used. Actually, the soliton-area theorem determines the pulse energy for a cavity with a certain dispersion and nonlinearity for a certain pulse duration. When the minimum pulse duration supported by the system increases, the pulse energy has to decrease proportionally. Therefore, single pulse operation is favored in a soliton laser with a fast absorber because it favors shorter and therefore higher energy pulses compared to a soliton laser with a slow absorber.

In conclusion, it was observed that the mode-locked Bi-doped fiber laser with exceptionally long gain fiber behaves differently than other more traditional fiber lasers. Difficulties with the mode-locked Bi-fiber laser arise due to the long gain fiber required, which easily amplifies noise-like pulses and supports multiple pulsing with low pulse energy. In order to avoid the problems related to pulse bunching, fast saturable absorbers with precisely engineered nonlinear parameters should be used in combination with anomalous average cavity dispersion and careful cavity design. The amount of pulse bunching can also be decreased by using moderate pump powers with values only slightly over the threshold.

Pulse evolution in a mode-locked Bi-doped fiber laser

The Bi-fiber laser was then studied with the fastest absorber initiating mode-locked operation (cavity dispersion was set to ~-0.4 ps^2). The aim was to analyze the pulse evolution within the laser cavity and optimize the position of the output in order to obtain the shortest attainable pulses from this laser configuration. Figures 5.7(a) and (b) show the simulated frequency domain amplitude evolution and time-bandwidth product during

a one cavity round-trip, starting from the location of the SESAM (0 mm) and then mapped according to the laser schematic shown in [P8]. As can be seen from the simulation, the pulses at output 3 (loop mirror) have only a small chirp with a time-bandwidth product of ~0.64 and a 3-dB spectral width of 2.0 nm.

However, the pulses have a significantly broader spectrum close to the dispersion compensation end of the cavity (output 1 and 2) and the pulses undergo a strong temporal chirp. In particular, the pulses at output 2 are strongly negatively chirped with a simulated spectral width of 2.7 nm and time-bandwidth product of 1.02. The pulses with a negative chirp can be compressed in a standard single mode optical fiber with normal dispersion at the laser wavelength of ~1165 nm.

According to the simulations, an additional 5% tap coupler was spliced close to the grating pair dispersion compensator. Optical spectra and the corresponding autocorrelations at the three different outputs were recorded (see Fig. 5.8). As can be seen from Fig. 5.7(b) (circles and squares) the pulses at output 3 are nearly transform-limited with a time-bandwidth product of 0.46. Close to the dispersion compensation end of the

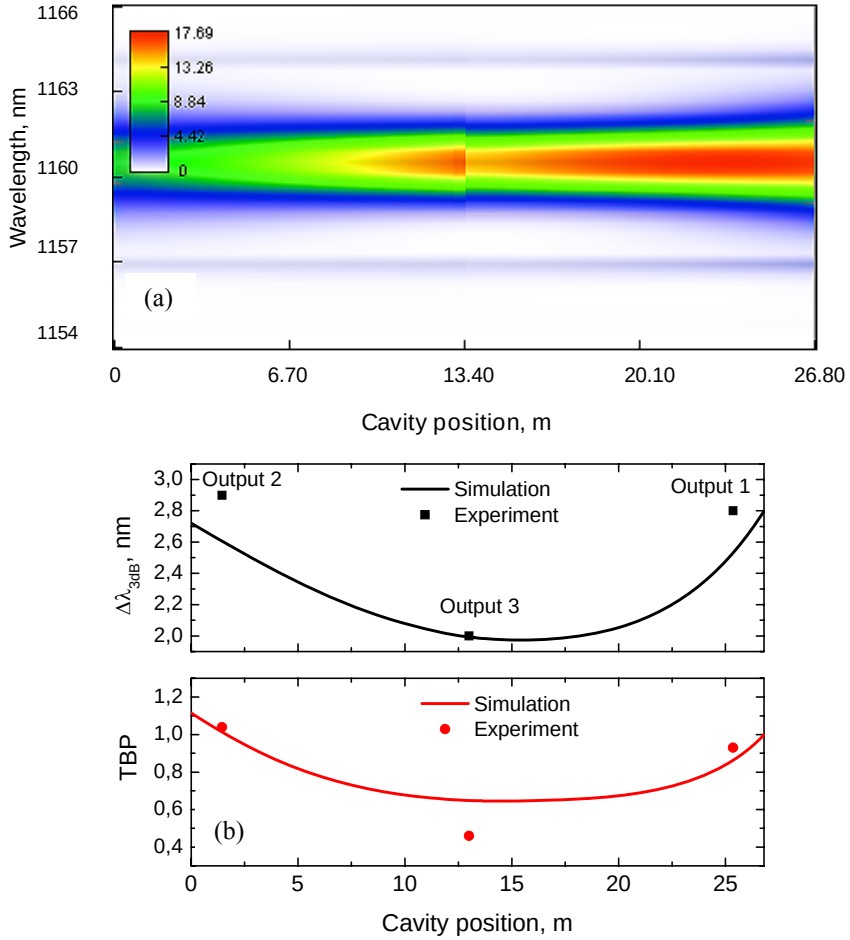

Fig. 5.7. (a). Simulated frequency domain amplitude evolution. (b) Simulated spectral width ($\Delta\lambda_{3dB}$) and time-bandwidth product (TBP) at different locations of the fiber cavity. The points are the experimental measurements.

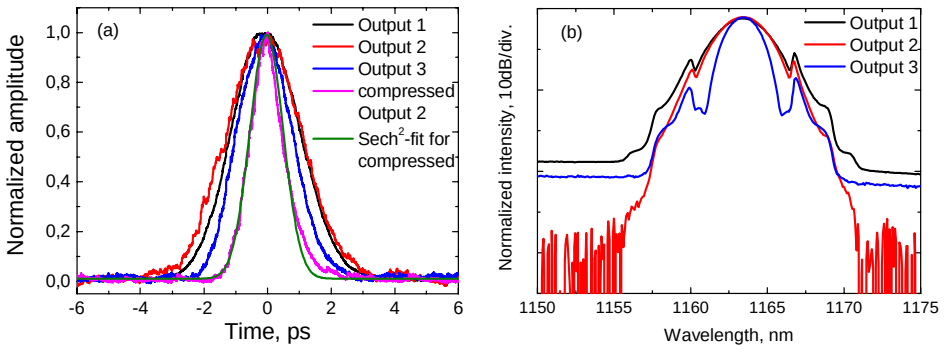

Fig. 5.8. (a) Measured autocorrelations at different positions of the cavity for the fastest SESAM. Pulse widths according to sech^2-fitting are 1.45 ps, 1.67 ps, 1.05 ps, and 0.70 ps for the output 1, 2, 3, and externally compressed 2, respectively. (b) Optical spectra corresponding to the autocorrelations. The spectral widths for the different outputs are 2.9 nm, 2.8 nm, 2.0 nm, respectively.

cavity at the outputs 1 and 2, the pulses are chirped and have a significantly broader spectrum, as also expected from the simulation. The pulses at output 2 have a spectral width of 2.8 nm and time-bandwidth product of 1.04, which is in very good agreement with the simulation. By splicing ~13 m of SMF at this output, the pulses with duration of 1.67 ps were compressed down to 0.7 ps (see Fig. 5.8). It is notable that these pulses are shorter than the pulses recorded at output 3, with a pulse width of 1.05 ps and spectral width of 2.0 nm. This is the shortest pulse duration reported for a mode-locked Bi-doped fiber laser.

5.1.4. Mode-locked Bi-doped fiber laser operating at the wavelength of 1.33 μm

Wavelengths around 1.3 μm are important for fiber optic communications due to the relatively low losses and zero-dispersion for standard single mode optical fibers around this wavelength. However, these wavelengths have so far remained relatively unexplored for mode-locked lasers due to the lack of proper gain material and saturable absorbers. Mode-locked and CW praseodymium (Pr)-doped fluoride fiber lasers operating at 1.3 μm have been reported [293-295]. However, fluoride fibers are not directly spliceable to standard fused silica fibers due to the different melting points of the materials, therefore limiting the practical use of Pr-doped fibers. Moreover, the gain of Pr-fibers is typically relatively weak. Therefore, fiber lasers operating at 1.3 μm based on novel fiber materials are fascinating, and worth investigating. In this work, we report a mode-locked Bi-doped fiber laser operating at 1.33 μm.

The laser system is shown schematically in Fig. 5.9. The all-fiber cavity was optimized to have minimal losses to compensate for the relatively weak gain of ~0.1dB/m of the Bi-fiber. The Bi-doped phosphogermanosilicate fiber, described in detail in [76], with a length of 30 m was pumped by a Raman laser system operating at 1.23 μm and delivering ~800-mW maximum output power. The pump laser system was comprised of a Yb-doped pump laser operating at 1.058 μm and a Raman fiber with two FBGs at 1.23

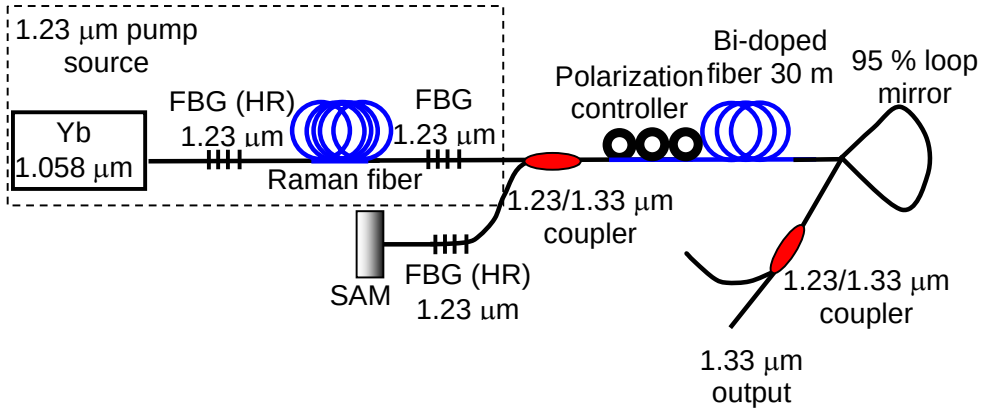

Fig. 5.9. Schematic of the mode-locked Bi-laser operating at 1.33 μm.

μm. The pump light was coupled to the Bi-doped fiber with a core diameter of 6.5 μm through a 1.23/1.33 μm dichroic fiber coupler. The output of the Bi-laser was coupled out via a loop mirror that reflected ~95% of the laser light back to the cavity. The other end of the cavity was formed by a SESAM. An additional FBG at a wavelength of 1.23 μm was used to filter the pump going towards the saturable absorber. An additional pump-separating dichroic coupler was used at the output to separate the residual pump and the signal. A polarization controller was used to optimize the laser operation.

The SESAM used to initiate the mode-locking was grown metamorphically. The structure comprised a 27 pair AlAs/GaAs DBR and 10 AlGaInAs quantum wells. The stopband of the DBR had a center wavelength of ~1300 nm and width of ~130 nm. The resonant wavelength of the SESAM was ~1340 nm.

The mode-locking was self-starting and had a very low threshold of ~15 mW. The laser operated in the normal dispersion regime due to the -10 ps/(nm·km) dispersion of the Bi-doped fiber at 1.33 μm. A typical optical spectrum and autocorrelation trace are shown in Fig. 5.10. The nearly square-shaped spectrum that is typical for a mode-locked laser operating in the normal dispersion regime had a spectral width of 2.3 nm. The autocorrelation shows a large pulse pedestal that can be explained by various unstably moving multiple pulses (a pulse bunch) in the close vicinity of the fundamental pulse within the exceptionally long fiber cavity [P8]. The slow speed autocorrelator then shows an average trace. Due to the various slightly unstable distinct pulses, which can also be seen in Fig. 5.10(a), the autocorrelation trace looks noisy. The Bi-laser delivers pulse bunches at a repetition rate of 3.05 MHz. The pulse width of a single pulse was very roughly estimated to be ~2.2 ps (Gaussian fitting) using the central pulse seen in the autocorrelation (see inset to Fig. 5.10(a)). The time-bandwidth product was calculated to be ~0.85. A typical, very stable pulse train captured on an oscilloscope screen is shown in Fig. 5.11(a), whereas Fig. 5.11(b) shows an RF-spectrum of the laser. The RF-spectrum confirms the mode-locked operation. The relatively slow oscilloscope (200 MHz) cannot detect the moving distinct pulses, and therefore shows a stable image of the whole pulse bunch, as seen in Fig. 5.11(a).

As shown in [P8], the pump power had a strong influence on the pulse bunching. Figure 5.12 shows the dependence of the pulse bunch width on the pump power, measured using a fast 8 GHz detector and a 2.5 GHz real time oscilloscope. With the lowest pump power of ~15 mW the width of the pulse bunch on the oscilloscope was

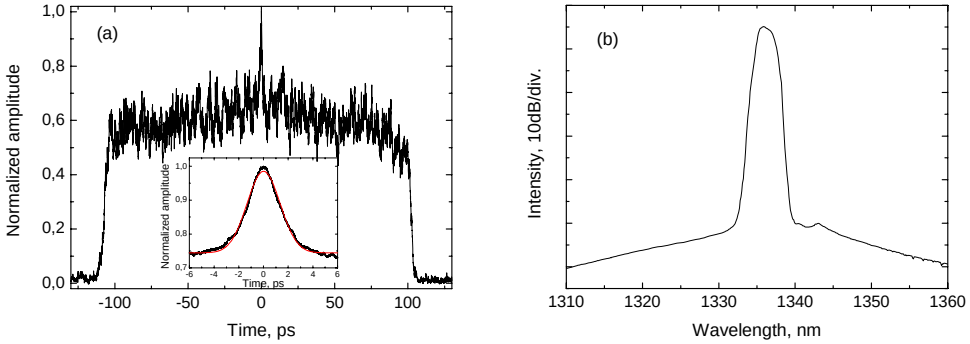

Fig. 5.10. (a) Autocorrelation trace with clearly visible distinct multiple pulses, and (b) the corresponding optical spectrum. The inset to (a) shows the central pulse in detail with Gaussian fitting (the red line).

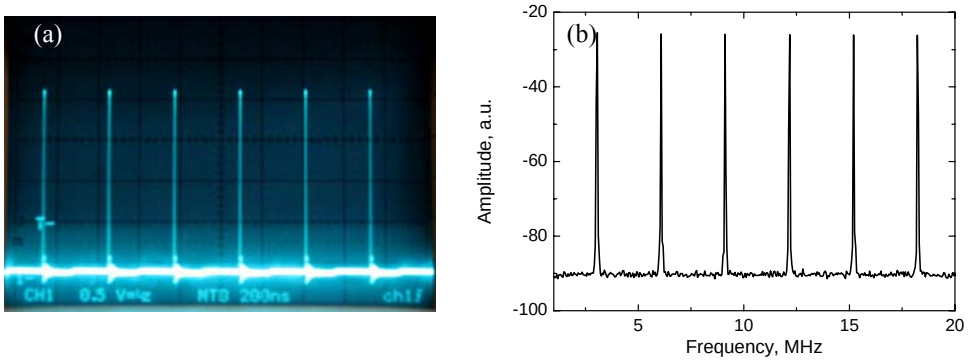

Fig. 5.11. (a) Oscilloscope image of the pulse train with a repetition rate of 3.05 MHz. (b) RF-spectrum of the laser.

~220 ps, but with a pump power of ~140 mW the width was already increased to a value of 3.6 ns. The measured autocorrelation traces did not show remarkable differences between different pump power levels due to the limited autocorrelator scanning rate of ~210 ps. The maximum average output power of the mode-locked laser was ~18 mW.

In order to understand the effect of the absorber recovery time on the pulse bunching in the normal dispersion regime, a SWCNT-based saturable absorber mirror with a fast absorption recovery time (~1 ps) was employed. Mode-locked operation was observed with a slightly increased threshold power of ~40 mW and minor difficulties related to the self-starting and stability. These difficulties can be attributed to the non-optimized SWCNT-absorber with increased non-saturable losses and a significantly shorter absorber recovery time compared to the SESAM. Despite the reduced recovery time, the autocorrelation trace showed a pulse pedestal similar to that observed during operation with the SESAM. The dependence of the pulse bunch width on the pump power was also in qualitative concordance with the operation employing the SESAM. This confirms that the absorption recovery time did not play a significant role in the pulse shaping of the mode-locked Bi-laser operating in the normal dispersion regime. The role of the saturable absorber is only to initiate the mode-locking, but the pulse shaping is mainly a result of the cavity dispersion and the active fiber properties. By operating the mode-locked Bi-laser in the soliton regime, multiple pulse bunching should be reduced and clean, single pulse operation should be achievable with a fast saturable absorber [P8]. This would

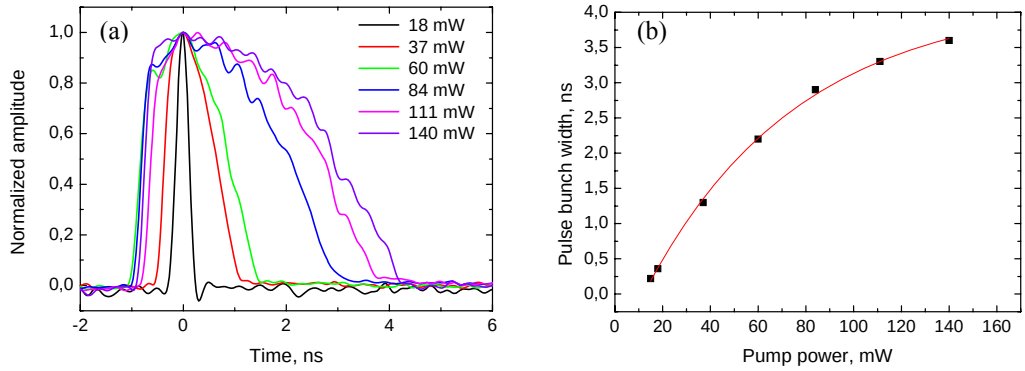

Fig. 5.12. (a). Pulse bunches with different pump powers measured using a 8 GHz detector and a 2.5 GHz oscilloscope. (b) Dependence of the pulse bunch width on the pump power. The red line is a fitting.

require fabrication of a Bi-fiber with anomalous dispersion at 1.33 μm, or intra-cavity dispersion compensation using, for example, a highly chirped FBG.

In conclusion, we demonstrated, for the first time, a mode-locked Bi-doped silica fiber laser operating at the important wavelength of 1.33 μm.

5.2 Mode-locked Tm-Ho-doped fiber lasers

Interest in ultrafast mode-locked laser systems operating at wavelengths around 2 μm has recently increased significantly due to various important applications especially in molecular spectroscopy, LIDAR, defense, and biomedicine. Tm- and Tm-Ho-doped fibers provide broad amplification bandwidths between 1.7 μm and 2.15 μm and are therefore suitable for femtosecond pulse generation and wide wavelength tuning. Semiconductor saturable absorber mirrors, reflective and transmissive SWCNT-based saturable absorbers, and nonlinear polarization rotation have been used to initiate mode-locking of fiber lasers operating in the 1.9-2.0 μm range [186,189,296,297]. Femtosecond pulse generation has, however, been reported in only few publications. The first demonstrated mode-locked Tm-doped fiber laser was based on additive pulse mode-locking and delivered ~500 fs pulses tunable in the 1.8-1.9 μm range [296]. In 1996, Sharp et al. demonstrated 1.9 μm Tm-fiber laser passively mode-locked by an InGaAs-saturable absorber delivering 190 fs pulses with an output power of ~1 mW [297]. Recently, ~200 fs pulses were generated from a stretched pulse Tm-doped fiber laser operating at 1970 nm [232]. Additionally, ~750 fs pulses were obtained from a Tm-doped fiber laser mode-locked by the evanescent field of a thin fiber taper embedded in a SWCNT-polymer composite [189].

5.2.1 Tunable soliton source using a Tm-Ho-doped fiber laser system with a GaSb-based semiconductor saturable absorber

In this work [P9], we demonstrated a GaSb-SESAM mode-locked Tm-Ho-doped master oscillator-power amplifier system that employs SSFS for wide wavelength tuning beyond

2 μm. The master oscillator was mode-locked by a SESAM comprising 15 GaInSb quantum-wells grown on the top of an 18-pairs AlAsSb/GaSb Bragg reflector. The absorber recovery time, saturation fluence, and modulation depth were measured to be ~1 ps, ~47 μJ/cm^2, 10%, respectively. The laser cavity was formed between the SESAM and a fiber loop mirror with a reflectivity of ~85% at the laser wavelength of ~1970 nm. The pump light was launched into the Tm-Ho-doped silica fiber with a core diameter of 7 μm and absorption of ~20 dB/m at 1564 nm through a dichroic 1.56/1.98 μm fused fiber coupler. All the required fused fiber components were made in-house using SMF-28. Wavelength tuning of the laser was accomplished using a thin fused silica free-space etalon. More details of the experimental setup can be found in [P9]. The self-starting Tm-Ho master oscillator was tunable in the range of 1912-1972 nm and delivered ~750 fs (Sech^2-fit) transform-limited pulses (see Fig. 5.13). The maximum average output power of the master oscillator was ~20 mW.

The 4.5 m long Raman shifter/power amplifier was made of Tm/Ho-doped fiber similar to the gain fiber used in the master laser. By increasing the amplifier pump power, the generated Raman soliton was gradually shifted from 1.97 μm up to 2.15 μm, as shown in Fig. 5.14. The largest wavelength shift obtained at a pump power of 2.4 W was 180 nm, corresponding to 230 mW of average power of the Raman soliton. The spectral width of the pulses increased with Raman shifting from 5.5 nm to 32 nm. The shortest pulse width after Raman shifting and compression was ~150 fs.

The efficiency of the Raman conversion, determined as the ratio of the shifted soliton energy to the overall energy including the un-converted seed and amplified spontaneous emission, was 62% at 2 μm and 47% at 2.15 μm. The decrease in the conversion efficiency and the long-wavelength limit of the tuning range was observed to be due to an abrupt increase of silica fiber absorption beyond 2.15 μm, as shown in Fig. 5.15. A further increase in the amplifier pump power resulted first in multiple soliton generation and eventually in a flat Raman-continuum spanning from 1.95 μm to 2.25 μm with an average output power of ~1 W, as shown in Fig. 5.15.

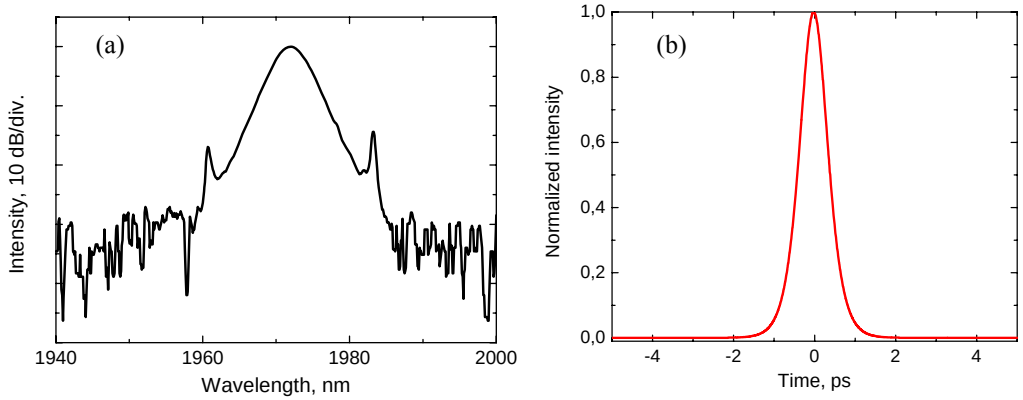

Fig. 5.13. (a) Spectrum of the mode-locked Tm-Ho-doped fiber laser and (b) the corresponding autocorrelation trace.

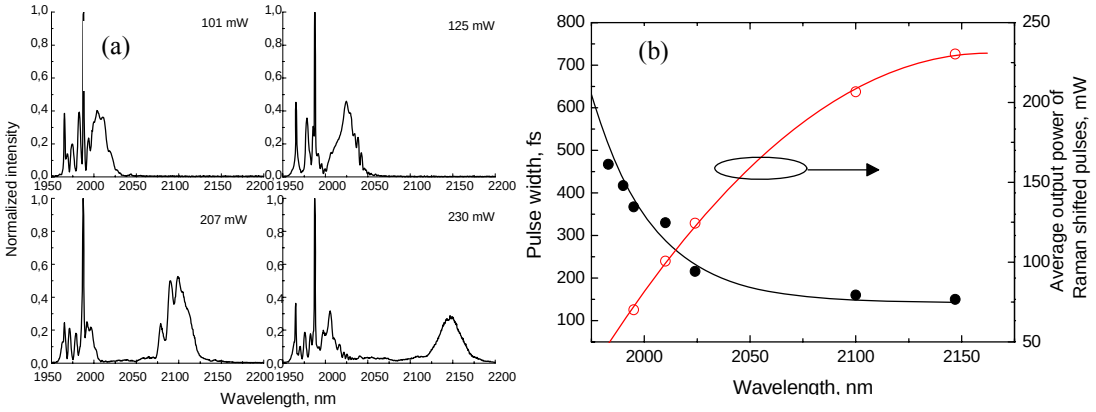

Fig. 5.14. (a) Output spectra for different average powers of the Raman shifted soliton. (b) Pulse width and average output power of Raman shifted solitons as a function of their center wavelength. The master oscillator wavelength was set to 1972 nm

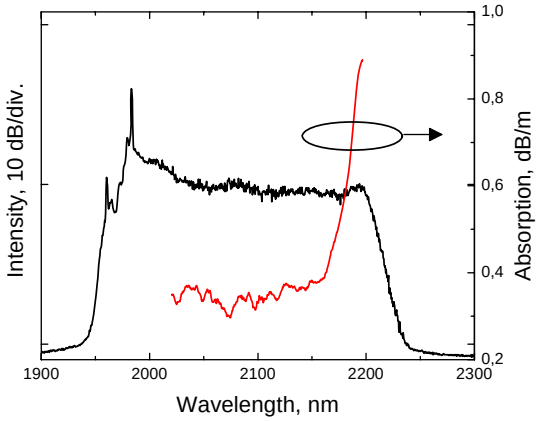

Fig. 5.15. Output spectrum for an average output power of 1 W and measured fiber absorption. The amplifier pump power was 5.3 W.

In conclusion, we demonstrated a compact 2 μm fiber source based on Tm/Ho-doped silica fiber. Using a tunable mode-locked oscillator and Raman shifter/power amplifier made of Tm-Ho-doped fiber, we generated soliton pulses tunable from 1.97 μm to 2.15 μm with an average output power and peak power up to 230 mW and 27 kW, respectively. The spectral shift achieved by varying the amplifier pump power was accompanied by spectral broadening and pulse compression down to a ~150 fs pulse width at 2.15 μm.

5.3 Carbon nanotube saturable absorber with ultrabroadband operation range

In this work [P10], we demonstrated a saturable absorber based on SWCNT-film with a very broad absorption spectrum and wide operation range on top of a silver mirror. Sub-picosecond mode-locked operation of Yb-, Er-, and Tm-Ho-doped fiber lasers was demonstrated using the same polymer-free saturable absorber. We utilized the SWCNT-film as-deposited and no purification or dispersion steps were required. When compared to standard wet deposition methods which may require several time-consuming stages, such as purification, dispersion and filtering, the approach of the SWCNT-film preparation demonstrated here is simple and easily scalable [298].

The SWCNTs used in this work were synthesized by thermal decomposition of ferrocene vapor in a carbon monoxide atmosphere, described in detail in [299]. The SWCNTs fabricated in the reactor are collected by filtering the flow of the chamber through a nitrocellulose membrane filter. The thickness and absorption characteristics of the SWCNT-films can be precisely controlled by varying the collection time and reactor CO_2-conditions. The saturable absorber can then be easily fabricated by stamping the SWCNT-films on the membrane filter on top of a highly reflective mirror. A photo of a SWCNT-based saturable absorber mirror was shown in Fig. 4.3(b).

A scanning electron microscope (SEM) image of the SWCNT-film is seen in Fig. 5.16. SEM-imaging reveals up to 20 nm-wide bundles and iron nanoparticles which give large back-scattered electron yield and high contrast in the images. A high resolution transmission electron microscopy (TEM)-image, shown as an inset to Fig. 5.16(a), reveals that the tube diameter ranges from 1.2 nm to 1.8 nm. The broad range of the tube diameters is essential for broadband operation of the saturable absorber, as the absorption characteristics of the SWCNT-film are mainly determined by the tube diameters and chirality. Figure 5.16(b) shows the linear low-intensity absorption of the SWCNT-film. The nonlinear reflectivity measurements were performed for the fabricated SWCNT-based saturable absorber at the wavelengths of 1.56 μm and 1.05 μm. Nonsaturable loss, modulation depth, and saturation fluence were determined to be 3.96%, 0.94% and ~320 μJ/cm^2 at 1.56 μm, respectively. At the wavelength of 1.05 μm the corresponding parameters were measured to be 18.3%, 1.86% and ~1000 μJ/cm^2. These parameters can be further optimized if the absorber is to be used only at a certain smaller wavelength range, for example at around 1.56 μm.

Mode-locking experiments

The same SWCNT-absorber mirror was used as a mode-locking element in three lasers using Yb, Er and Tm-Ho-doped gain fibers with lengths of 1 m, 2 m, 1.5 m and operation wavelengths of 1 μm, 1.56 μm and 2 μm, respectively. The lasers had a linear fiber cavity. The normal GVD of the Yb-doped fiber laser operating at ~1 μm was compensated by an intra-cavity grating pair. More experimental details can be found in [P10].

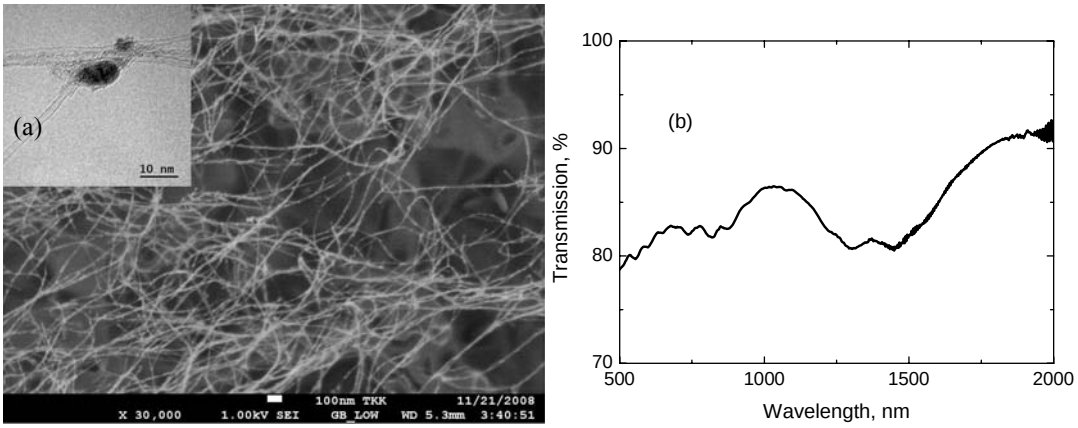

Fig. 5.16. (a) SEM micrograph of the SWCNT-film. The inset shows a high-resolution TEM-image of the sample. The tube diameter ranges from 1.2 nm to 1.8 nm. (b) Optical transmission spectrum of the SWCNT-film. Ripples in absorption near 2000 nm wavelengths are caused by strong absorption of the PET-substrate.

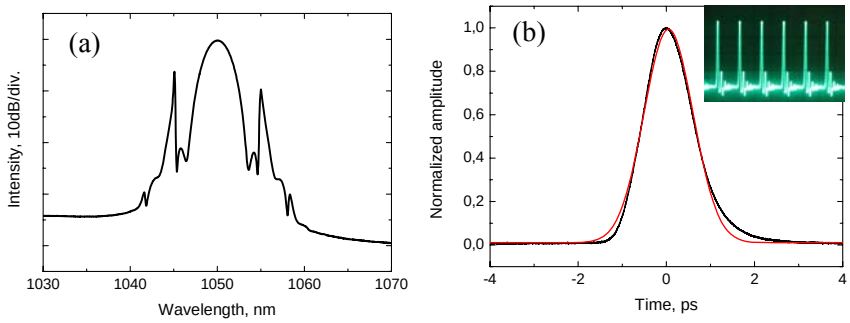

Fig. 5.17. (a) Pulse spectrum of the Yb-fiber laser. (b) Autocorrelation trace and $sech^2$-fit giving a pulse width of ~0.7 ps. The inset shows a typical oscilloscope picture of the generated pulse train.

The mode-locked Yb-fiber laser operated at the central wavelength of 1050 nm with a spectral width of 2.7 nm, as seen in Fig. 5.17(a). Figure 5.17(b) shows the recorded autocorrelation trace with $sech^2$-fitting revealing a pulse duration of 0.67 ps. A photograph of a typical oscilloscope trace of the mode-locked pulse train is shown as an inset to Fig. 5.17(b). The laser output characteristics are summarized in Table 5.1.

The Erbium-doped all-fiber laser produced 0.44 ps pulses at a wavelength of 1563 nm, as seen in Fig. 5.18(a). The spectral width was measured to be 6.0 nm. The same SWCNT-absorber was also capable of initiating mode-locking in the thulium-holmium co-doped fiber laser. The polymer-free CNT-layer on a highly reflective Ag-mirror enabled the building of a robust and compact linear cavity laser with significantly improved output characteristics compared to the recently reported ring-cavity Tm-laser, which had obvious limitations in output power, stability and absorber damage threshold [186]. The all-fiber laser delivered ~1.0 ps pulses with a central wavelength of 1991 nm, as shown in Fig. 5.18(b). To the best of our knowledge, this is the longest operation wavelength for a fiber laser mode-locked by a CNT-absorber. The extension in operation wavelength from ~1.9 μm [186] to ~2 μm is attributed to the use of a Tm-Ho co-doped fiber, instead of a Tm-doped fiber with gain typically peaking at ~1.9 μm.

All the laser output characteristics are summarized in Table 5.1. The relatively high threshold powers for the Yb- and Tm-Ho-doped fiber lasers can be partly explained by

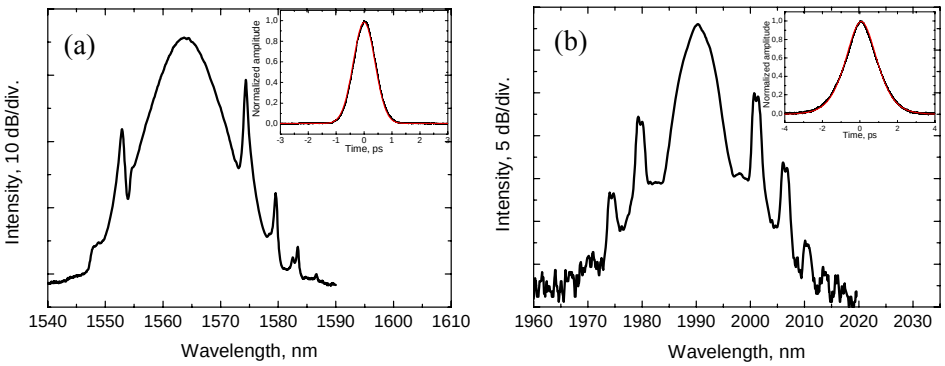

Fig. 5.18. Optical spectra of the Er- (a) and Tm-Ho-doped (b) fiber lasers. The corresponding autocorrelation traces with $Sech^2$-fittings are shown as insets. The pulse widths for the Er- and Tm-Ho-doped fiber lasers are 0.44 ps and 1.0 ps, respectively. The 3-dB spectral widths are 6.0 and 5.0 nm.

the larger nonsaturable losses of the saturable absorber at the wavelengths of 1 μm and 2 μm. The mode-locked operation of the Er-doped laser with a low threshold power could actually be predicted from the linear absorption spectrum shown in Fig. 5.16(b) which has a clear absorption peak at the spectral range of ~1.5 μm. The obtained pulse widths were mainly determined by the average cavity dispersions of the lasers rather than the SWCNT-parameters. The role of the saturable absorber was to initiate the mode-locking.

Table 5.1. Summary of the laser output characteristics.

	Threshold pump power, mW	Repetition rate, MHz	Pulse width, ps	Time-bandwidth product	Average output power, mW
Yb	150	40	0.67	0.48	10
Er	30	15	0.44	0.32	10
Tm-Ho	150	41	1.0	0.37	15

In conclusion, we demonstrated mode-locked operation of Yb-, Er-, and Tm-Ho-doped fiber lasers operating at 1 μm, 1.56 μm, and 2 μm, respectively, using the same saturable absorber based on SWCNTs. To the best of our knowledge, this is the broadest operation range for a SWCNT-based saturable absorber. Our saturable absorber fabrication technique avoids the use of disadvantageous polymers and significantly reduces the required fabrication processing steps. The use of the novel SWCNT-mirror technology offers an attractive opportunity for self-starting passive mode-locking of fiber lasers operating over a very broad spectral range, with potential for further scaling to the mid-infrared spectral region and higher powers.

6. Conclusions

This thesis concerned the design and development of passively mode-locked and Q-switched fiber lasers using novel fibers. The primary focus was on the development of lasers operating at wavelengths of ~1.2 μm and 2 μm, based on Bi- and Tm-Ho-doped fibers. Novel broadband SWCNT-based saturable absorbers, and tunable and dispersion compensated advanced ultrafast fiber lasers delivering fs and ps-pulses have been studied. The main achievements of this thesis are as follows:

Investigations of passively Q-switched Tm-Ho-doped fiber lasers led to a new observation - dynamic gain induced pulse shortening, which significantly affects the characteristics of passively Q-switched fiber lasers. It was shown that dynamic gain induced pulse shortening may occur under strong pumping in fiber lasers with large gain volume. By employing this new effect in combination with a highly resonant SESAM and a short-length fiber cavity incorporating a highly doped Tm-Ho-fiber, energetic 20 ns Q-switched pulses with a repetition rate of 57 kHz at 2 μm was obtained.

Environmentally stable mode-locked Yb-doped fiber laser with dispersion compensation by an index-guiding PCF delivering 200 fs pulses was developed.

Broadband chirped fiber Bragg gratings with flat reflectivity response were fabricated and used for dispersion compensation of mode-locked Yb- and Bi-doped fiber lasers. The output of Yb-doped laser boosted in a power amplifier allowed for an octave-spanning supercontinuum generation in a photonic crystal fiber.

Electronically tunable Yb-doped mode-locked fiber laser employing a computer controlled AOTF was designed. The laser delivering 1-ps pulses could be continuously tuned within a 1030-1060 nm range. The mode-locked operation was studied with a SESAM, FSF, and a combination of FSF and SESAM initiating the mode-locked operation.

Mode-locked Bi-doped fiber lasers operating at a wavelength of ~1.2 μm and delivering sub-picosecond pulses were designed and developed. Pulse evolution and generation within a Bi-fiber cavity were studied in detail. It was observed that the mode-locked Bi-fiber lasers with long-length cavity have a strong tendency to generate pulse bunches. It was shown that the multiple pulsing can be avoided by careful laser cavity and saturable absorber design.

A GaSb-SESAM mode-locked Tm-Ho-doped master oscillator-power amplifier system tunable in the 1.97-2.15 μm range was demonstrated. The pulses of the master oscillator were compressed down to ~150 fs and amplified up to 27 kW

peak power in a Tm-Ho-doped power amplifier/Raman shifter fiber. The wavelength of the laser system could be tuned by employing the soliton self-frequency shift by increasing the pump power of the fiber amplifier.

Mode-locked sub-picosecond Yb-, Er-, and Tm-Ho-doped fiber lasers were demonstrated employing extremely broadband SWCNT-based saturable absorber. The broadband polymer-free saturable absorber was fabricated by stamping SWCNT-film having nanotubes with wide-range diameter distribution on top of a highly reflective mirror.

References

[1] X. Liu, D. Du, and G. Mourou, "Laser Ablation and Micromachining with Ultrashort Laser Pulses," IEEE J. Quantum Electron. 33, pp. 1706-1715, 1997.

[2] F. Korte, S. Nolte, B.N. Chichkov, T. Bauer, G. Kamlage, T.Wagner, C. Fallnich, and H. Welling, "Far-field and near-field material processing with femtosecond laser pulses," Appl. Phys. A 69, pp. S7–S11, 1999.

[3] J. Gabzdyl, "Materials processing: Fibre lasers make their mark," Nature Photonics 2, pp. 21-23, 2008.

[4] B.N. Chichkov, C. Momma, S. Nolte, F. von Alvensleben, and A. Tünnermann, "Femtosecond, picosecond and nanosecond laser ablation of solids," Appl. Phys. A 63, pp. 109-115, 1996.

[5] http://www.rofin.com/en/applications/, referenced 3.2.2010.

[6] T. Juhasz, F. H. Loesel, R. M. Kurtz, C. Horvath, J. F. Bille, and G. Mourou, "Corneal Refractive Surgery with Femtosecond Lasers," IEEE J. Quantum Electron. 5, pp. 902-910, 1999.

[7] S. O. Konorov, V. P. Mitrokhin, A. B. Fedotov, D. A. Sidorov-Biryukov, V. I. Beloglazov, N. B. Skibina, A. V. Shcherbakov, E. Wintner, M. Scalora, and A. M. Zheltikov, "Laser ablation of dental tissues with picosecond pulses of 1.06-μm radiation transmitted through a hollow-core photonic-crystal fiber," Appl. Opt. 43, pp. 2251-2256, 2004.

[8] K. Kim, Z. Guo, J. Li, and S. Kumar, "Radiation heat transfer in tissue welding and soldering with ultrafast lasers," in Proc. 29th Annual IEEE Bioengineering Conf., 2003, pp. 185-186.

[9] J. M. Schmitt, "Optical Coherence Tomography (OCT): A Review," IEEE J. Quantum Electron. 6, pp. 1205-1215, 1999.

[10] B. E. Bouma, L. E. Nelson, G. J. Tearney, D. J. Jones, M. E. Brezinski, and J. G. Fujimoto, "Optical Coherence Tomographic Imaging of Human Tissue at 1.55 μm and 1.81 μm Using Er- and Tm-Doped Fiber Sources," J. Biomed. Opt. 3, pp. 76-79, 1998

[11] http://www.nufern.com/nutx.php, referenced 3.2.2010.

[12] G. N. Pearson, P. J. Roberts, J. R. Eacock, and M. Harris, "Analysis of the performance of a coherent pulsed fiber lidar for aerosol backscatter applications," Appl. Opt. 41, pp. 6442-6450, 2002.

[13] S. W. Henderson, P. J. M. Suni, C. P. Hale, S. M. Hannon, J. R. Magee, D. L. Bruns, and E. H. Yuen, "Coherent Laser Radar at 2 μm Using Solid-state Lasers," IEEE Transact. Geoscience and remote sensing 31, pp. 4-15, 1993.

[14] N. S. Sadick and R. Weiss, "The utilization of a new yellow light laser (578 nm) for the treatment of class I red telangiectasia of the lower extremities," J. Dermatol. Surg. 28, pp. 21–23, 2002.

[15] E. M. Dianov, A. V. Shubin, M. A. Melkumov, O. I. Medvedkov, and I. A. Bufetov, "High-power CW bismuth fiber laser," J. Opt. Soc. Am. B 24, pp. 1749-1755, 2007.

[16] G. Frith, T. McComb, B. Samson, W. Torruellas, A. Carter, J. Farroni, K. Farley, and K. Tankala, "Latest developments in 790 nm-pumped Tm-doped fibre laser systems for DIRCM applications," Proc. SPIE, Technologies for Optical Countermeasures V, pp. 711507-711507-7, 2008.

[17] D. Theisen-Kunde, S. Tedsen, V. Danicke, R. Keller, and R. Brinkmann, "Laser-Scalpel for Kidney Resection Based on 1.94 μm Fibre Laser System," Adv. in Med. Engin. 114, pp. 431-434, 2007.

[18] R. Brinkmann, A. Knipper, G. Droege, F. Schroer, B. Gromoll, and R. Birngruber, "Fundamental studies of fiber-guided soft tissue cutting by means of pulsed mid-infrared lasers and its application in ureterotomy," J. Biomed. Opt. 3, pp. 85-95, 1998.
[19] A. Godard, "Infrared (2–12 μm) solid-state laser sources: a review," C. R. Physique 8, pp. 1100-1128, 2007.
[20] Z. Wu, Z. Chen, X. Du, J. M. Logan, J. Sippel, M. Nikolou, K. Kamaras, J. R. Reynolds, D. B. Tanner, A. F. Hebard, and A. G. Rinzler, "Transparent, Conductive Carbon Nanotube Films," Science 305, pp. 1273 – 1276, 2004.
[21] H. W. C. Postma, T. Teepen, Z. Yao, M. Grifoni, and C. Dekkerdagger, "Carbon Nanotube Single-Electron Transistors at Room Temperature," Science 293, pp. 76-79, 2001.
[22] H. Kataura, Y. Kumazawa, Y. Maniwa, I. Umezu, S. Suzuki, Y. Ohtsuka, and Y. Achiba, "Optical Properties of Single-Wall Carbon Nanotubes," Synthetic Metals 103, pp. 2555-2558, 1999.
[23] O. Zhou, H. Shimoda, B. Gao, S. Oh, L. Fleming, and G. Yue, "Materials Science of Carbon Nanotubes: Fabrication, Integration, and Properties of Macroscopic Structures of Carbon Nanotubes," Acc. Chem. Res. 35, pp. 1045-1053, 2002.
[24] R. Paschotta, J. Nilsson, A. C. Tropper, and D. C. Hanna, "Ytterbium-Doped Fiber Amplifiers," IEEE J. Quantum. Electron. 33, pp. 1049-1056, 1997.
[25] H. W. Etzel, H. W. Gandy, and R. J. Ginther, "Stimulated Emission of Infrared Radiation from Ytterbium Activated Silicate Glass," Appl. Opt. 1, pp. 534-536, 1962.
[26] D. C. Hanna, R. M. Percival, I. R. Perry, R. G. Smart, P. J. Suni, J. E. Townsend, and A. C. Tropper, "Continuous-wave oscillation of a monomode ytterbium-doped fibre laser," Electron. Lett. 21, pp. 1111-1113, 1988.
[27] L. Quintino, A. Costa, R. Miranda, D. Yapp, V. Kumar, and C.J. Kong, "Welding with high power fiber lasers – A preliminary study," Materials and design 28, pp. 1231-1237, 2007.
[28] R. L Harzic, C. Wüllner, D. Bruneel, C. Donitzky, and K. König, "Femtosecond refractive eye surgery: study of laser parameters for even more efficiency and safety," SPIE/OSA 6632, pp. 663217, 2007.
[29] L. Orsila and O. G. Okhotnikov, "Three- and four-level transition dynamics in Yb-fiber laser," Opt. Express 13, pp. 3218-3223, 2005.
[30] J. Swiderski, A. Zajac, M. Skorczakowski, Z. Jankiewicz, and P. Konieczny, "Rare-earth-doped high-power fiber lasers generating in near infrared range," Opto-Electronic Review 12, pp. 169-173, 2004.
[31] J. J. Koponen, M. J. Söderlund, H. J. Hoffman, and S. K. T. Tammela, "Measuring photodarkening from single-mode ytterbium doped silica fibers," Opt. Express 14, pp. 11539-11544, 2006.
[32] I. Manek-Hönninger, J. Boullet, T. Cardinal, F. Guillen, S. Ermeneux, M. Podgorski, R. Bello Doua, and F. Salin, "Photodarkening and photobleaching of an ytterbium-doped silica double-clad LMA fiber," Opt. Express 15, pp. 1606-1611, 2007.
[33] M. J. Söderlund, J. J. Montiel i Ponsoda, J. P. Koplow, and S. Honkanen, "Heat-induced darkening and spectral broadening in photodarkened ytterbium-doped fiber under thermal cycling," Opt. Express 17, pp. 9940-9946, 2009.
[34] M. J. Söderlund, J. J. Montiel i Ponsoda, J. P. Koplow, and S. Honkanen, "Thermal bleaching of photodarkening-induced loss in ytterbium-doped fibers," Opt. Lett. 34, pp. 2637-2639, 2009.
[35] S. B. Poole, D. N. Payne, and M. E. Fermann, "Fabrication of low-loss optical fibres containing rare-earth ions," Electron Lett. 21, pp. 737-738, 1985.
[36] R. J. Mears, L. Reekie, I. M. Jauncey, and D. N Payne, "Low-noise erbium-doped fibre amplifier operating at 1.54 μm," Electron. Lett. 23, pp. 1026-1028, 1987.

[37] R. J. Mears, L. Reekie, I. M. Jauncey, and D. N Payne, "Diode-laser-pumped operation of an Er^{3+}-doped single-mode fibre laser," Electron. Lett. 23, pp. 1076-1078, 1987.
[38] O. G. Okhotnikov, V. V. Kuzmin, and J. R. Salcedo, "General Intracavity Method for Laser Transition Characterization by Relaxation Oscillations Spectral Analysis," IEEE Photon. Technol. Lett. 6, pp. 362-264, 1994.
[39] S. Honkanen, T. Ohtsuki, S. Jiang, S. I. Najafi, and N. Peyghambarian, "High Er concentration phosphate glasses for planar waveguide amplifiers," Proc. SPIE 2996, pp. 32-40, 1997.
[40] D. C. Hanna, I. M. Jauncey, R. M. Percival, I. R. Perry, R. G. Smart, P. J. Suni, J. E. Townsend, and A. C. Tropper, "Continuous-wave oscillation of a monomode thulium-doped fibre laser," Electron. Lett. 24, pp. 1222-1223, 1988.
[41] B. Richards, Y. Tsang, D. Binks, J. Lousteau, and A. Jha, "Efficient ~2 μm Tm^{3+}-doped tellurite fiber laser," Opt. Lett. 33, pp. 402-404, 2008.
[42] A. F. El-Sherif and T A. King, "Analysis and Optimization of Q-Switched Operation of a Tm^{3+}-Doped Silica Fiber Laser Operating at 2 μm," IEEE J. Quantum Electron. 39, pp. 759-765, 2003.
[43] M. Engelbrecht, F. Haxsen, D. Wandt, and D. Kracht, "Wavelength resolved intracavity measurement of the cross sections of a Tm-doped fiber," Opt. Express 16, pp. 1610-1615, 2008.
[44] R. Paschotta, N. Moore, W. A. Clarkson, A. C. Tropper, D. C. Hanna, and G. Maz´e, "230 mW of Blue Light From a Thulium-Doped Upconversion Fiber Laser," IEEE J. Quantum Electron. 3, pp. 1100-1102, 1997.
[45] R. Paschotta, P. R. Barber, A. C. Tropper, and D. C. Hanna, "Characterization and modeling of thulium:ZBLAN blue upconversion fiber lasers," J. Opt. Soc. Am. B, 15, pp. 1213-1218, 1997.
[46] S. Sanders, R. G. Waarts, D. G. Mehuys, and D. F. Welch, "Laser diode pumped 106 mW blue upconversion fiber laser," Appl. Phys. Lett. 67, pp. 1815-1817, 1995.
[47] D. C. Hanna, R. M. Percival, I. R. Perry, R. G. Smart, J. E. Townsend, and A. C. Tropper, "Frequency upconversion in Tm- and Yb:Tm-doped silica fibers," Opt. Commun. 78, pp. 187-194, 1990.
[48] S. D. Jackson, "Cross relaxation and energy transfer upconversion processes relevant to the functioning of 2 μm Tm^{3+}-doped silica fibre lasers," Opt. Commun. 230, pp. 197–203, 2004.
[49] S. D. Jackson, F. Bugge, and G. Erbert, "High-power and highly efficient Tm^{3+}-doped silica fiber lasers pumped with diode lasers operating at 1150 nm," Opt. Lett. 32, pp. 2873-2875, 2007.
[50] S. D. Agger and J. H. Povlsen, "Emission and absorption cross section of thulium doped silica fibers," Opt. Express 14, pp. 50-57, 2006.
[51] S. D. Jackson and S. Mossman, "High-power diode-cladding-pumped Tm,Ho -doped silica fibre laser," Appl. Phys. B 77, pp. 489–491, 2003.
[52] S. D. Jackson, "The Effects of Energy Transfer Upconversion on the Performance of Tm^{3+}, Ho^{3+}-Doped Silica Fiber Lasers," Photon. Tech. Lett. 18, pp. 1885-1887, 2006.
[53] L. Orsila, S. Kivistö, R. Herda, and O. G. Okhotnikov, "Spectroscopy of the relaxation dynamics in Tm-Ho-fiber lasers," in Proc. of CLEO Europe 2007, Münich, Germany pp. CE-24-TUE, 2007.
[54] S. D. Jackson, "2.7-W Ho^{3+}-doped silica fibre laser pumped at 1100 nm and operating at 2.1 μm," Appl. Phys. B 76, pp. 793–795, 2003.
[55] S. D. Jackson, F. Bugge, and G. Erbert, "Directly diode-pumped holmium fiber lasers," Opt. Lett. 32, pp. 2496-2498, 2007.
[56] S. D. Jackson, F. Bugge, and G. Erbert, "High-power and highly efficient diode-cladding pumped Ho^{3+}-doped silica fiber lasers," Opt. Lett. 32, pp. 3349-3351, 2007.

[57] A.S. Kurkov, E.M. Dianov, O.I. Medvedkov, G.A. Ivanov, V.A. Aksenov, V.M. Paramonov, S.A. Vasiliev, and E.V. Pershina, "Efficient silica-based Ho^{3+} fibre laser for 2 μm spectral region pumped at 1.15 μm," Electron. Lett. 36, pp. 1015-1016, 2000.
[58] L. Wetenkamp, "Efficient CW-operation of a 2.9 μm Ho^{3+}-doped fluorozirconate fibre laser pumped at 640 nm," Electron. Lett. 26, pp. 883-884, 1990.
[59] S. D. Jackson, "High-power and highly efficient diode-cladding pumped holmium-doped fluoride fiber laser operating at 2.94 μm," Opt. Lett. 34, pp. 2327-2329, 2009.
[60] T. Haruna, M. Kakui, T. Taru, S. Ishikawa, and M. Onishi, "Silica-based bismuth-doped fiber for ultra broadband light-source and optical amplification around 1.1 μm," in Proc. Optical Amplifiers and their Applications Topical Meeting, Budapest, August 7-10, paper MC3, 2005.
[61] V. Dvoyrin, V. Mashinsky, E. Dianov, A. Umnikov, M. Yashkov, and A. Guryanov, "Absorption, fluorescent and optical amplification in MCVD Bismuth-doped silica glass optical fibers," in Proc. of 31 ECOC (Glasgow, 2005), 4, pp. 949-950, 2005.
[62] I. Bufetov, S. Firstov, V. Khopin, O. Medvedkov, A. Guryanov, and E. Dianov, "Bi-doped fiber lasers and amplifiers for a spectral region of 1300–1470 nm," Opt. Lett. 33, pp. 2227–2229, 2008.
[63] V. V. Dvoyrin, O. I. Medvedkov, V. M. Mashinsky, A. A. Umnikov, A. N. Guryanov, and E. M. Dianov, "Optical amplification in 1430-1495 nm range and laser action in Bi-doped fibers," Opt. Express 16, pp. 16971-16976, 2008.
[64] E. M. Dianov, V. V. Dvoyrin, V. M. Mashinsky, A. A. Umnikov, M. V. Yashkov, and A. N. Guryanov, "CW bismuth fiber laser," Quant. Electron. 35, pp. 1083-1084, 2005.
[65] I. Razdobreev, L. Bigot, V. Pureur, A. Favre, G. Bouwmans, and M. Douay, "Efficient all-fiber bismuth-doped laser," Appl. Phys. Lett. 90, 031103-1–031103-3, 2007.
[66] A. B. Rulkov, A. A. Ferin, S. V. Popov, J. R. Taylor, I. Razdobreev, L. Bigot, and G. Bouwmans, "Narrow-line, 1178nm CW bismuth-doped fiber laser with 6.4 W output for direct frequency doubling," Opt. Express 15, pp. 5473-5476, 2007.
[67] Y. Fujimoto and M. Nakatsuka, "Infrared Luminescence from Bismuth-Doped Silica Glass," Jpn. J. Appl. Phys. 40, pp. L279-L281, 2001.
[68] I. A. Bufetov, K. M. Golant, S. V. Firstov, A. V. Kholodkov, A. V. Shubin, and E. M. Dianov, "Bismuth activated alumosilicate optical fibers fabricated by surface-plasma chemical vapor deposition technology," Apl. Opt. 47, pp. 4940-4944, 2008.
[69] X. Meng J. Qiu, M. Peng, D. Chen Q. Zhao, X. Jiang, and C. Zhu, "Near infrared broadband emission of bismuth-doped aluminophosphate glass," Opt. Exp. 13, pp. 1628-1634, 2005.
[70] J. Ren, L. Yang, J. Qiuc, D. Chen, X. Jiang, and C. Zhu, "Effect of various alkaline-earth metal oxides on the broadband infrared luminescence from bismuth-doped silicate glasses," Solid State Nucl. Magn. Reson. 141, pp. 59-562, 2007.
[71] M. Peng, J. Qiu, D. Chen, X. Meng, and C. Zhu, "Superbroadband 1310 nm emission from bismuth and tantalum codoped germanium oxide glasses," Opt. Lett. 30, pp. 2433-2435, 2005.
[72] V. O. Sokolov, V. G. Plotnichenko, and E. M. Dianov, "Origin of broadband near-infrared luminescence in bismuth-doped glasses," Opt. Lett. 33, pp. 1488-1490, 2008.
[73] V. V. Dvoyrin, V. M. Mashinsky, L. I. Bulatov, I. A. Bufetov, A. V. Shubin, M. A. Melkumov, E. F. Kustov, and E. M. Dianov, "Bismuth-doped-glass optical fibers - a new active medium for lasers and amplifiers," Opt. Lett. 31, pp. 2966-2968, 2006.
[74] M. Peng, J. Qiu, D. Chen, X. Meng, I. Yang, X. Jiang, and C. Zhu, "Bismuth- and aluminum-codoped germanium oxide glasses for super-broadband optical amplification," Opt. Lett. 29, pp. 1998-2000, 2004.
[75] Y. Arai, T. Suzuki, Y. Ohishi, S. Morimoto, and S. Khonthon, "Ultrabroadband near-infrared emission from a colorless bismuth-doped glass," Appl. Phys. Lett. 90, pp. 261110, 2007.

[76] I. A. Bufetov and E. M. Dianov, "Bi-doped fiber lasers," Laser Phys. Lett. 6, pp. 487-504, 2009.
[77] E. M. Dianov, S. V. Firstov, O. I. Medvedkov, I. A. Bufetov, V. F. Khopin, and A. N. Guryanov, "Luminescence and laser generation in Bi-doped fibers in a spectral region of 1300-1520 nm," in Proc. Of OFC'2009, paper OWT3, 2009.
[78] M. Kalita, S. Yoo, R. Quimby, and J. Sahu, "Pump wavelength dependence of bismuth doped fibre laser," proc. of Photonics 2008, New Delhi, India, 2008.
[79] M. Kalita, S. Yoo, and J. Sahu, "Bismuth doped fiber laser and study of unsaturable loss and pump induced absorption in laser performance," Opt. Express 16, pp. 21032-21038, 2008.
[80] S. Yoo, M. Kalita, J. Nilsson, and J. Sahu, "Excited state absorption measurement in the 900–1250 nm wavelength range for bismuth-doped silicate fibers," Opt. Lett. 34, pp. 530-532, 2009.
[81] M. Kalita, S. Yoo, and J. Sahu, "Bismuth doped fiber laser performance on effective fiber cooling," on Proc. of CLEO Europe 2009.
[82] E. Snitzer, "Optical maser action of Nd^{3+} in a Barium crown glass," Phys. Rev. Lett. 7, pp. 444-446, 1961.
[83] C. J. Koester and E. Snitzer, "Amplification in a fiber laser," Appl. Opt. 3, pp. 1182-1186, 1964.
[84] J. Stone and C.A Burrus, "Neodymium-doped silica lasers in end-pumped fiber geometry," Appl. Phys. Lett. 23, pp. 388-389, 1973.
[85] J. Stone, C. A. Burrus, A. G. Dentai, and B. I. Miller, "Nd:YAG single-crystal fiber laser: Room-temperature cw operation using a single LED as an end pump," Appl. Phys. Lett. 29, pp. 37-39, 1976.
[86] J. Stone and C. A. Burrus, "Nd:Y_2O_3 single crystal fiber laser: Room-temperature cw operation at 1.07- and 1.35-μm wavelength," J. Appl. Phys. 49, pp. 2281-2287, 1978.
[87] R. J. Mears, L. Reekie, S. B. Poole, and D. N. Payne, "Neodymium-doped silica single-mode fibre lasers," Electron. Lett. 21, pp. 738-740, 1985.
[88] S. B. Poole, D. N. Payne, R. J. Mears, M. E. Fermann, and R. I. Laming, "Fabrication and characterization of low-loss optical fibers containing rare-earth ions," IEEE J. Lightwave Tech. 4, pp. 870-876, 1986.
[89] I. P. Alcock, A. C. Tropper, A. I. Ferguson, and D. C. Hanna, "Q-switched operation of a neodymium-doped monomode fibre laser," Electron. Lett. 22, pp. 84-84, 1986.
[90] I. P. Alcock, A. I. Ferguson, D. C. Hanna, and A. C. Tropper, "Mode-locking of a neodymium-doped monomode fibre laser," Electron. Lett. 22, pp. 268-269, 1986.
[91] J. D. Kafka, T. Baer, and D. W. Hall, "Mode-locked erbium-doped fiber laser with soliton pulse shaping," Opt. Lett. 14, pp. 1269-1271, 1989.
[92] M. E. Fermann, M. Hofer, F. Haberl, and S. P. Craig-Ryan, "Femtosecond fibre laser," Electron. Lett. 26, pp. 1737-1738, 1990.
[93] M. E. Fermann, M. Hofer, F. Haberl, A. J. Schmidt, and L. Turi, "Additive-pulse-compression mode locking of a neodymium fiber laser," Opt. Lett. 16, pp. 244-246, 1991.
[94] I. N. Duling III, "All-fiber ring soliton laser mode locked with a nonlinear mirror," Opt. Lett. 16, pp. 539-541, 1991.
[95] I. N. Duling III, "Sub-picosecond all-fibre erbium laser," Electron. Lett. 27, pp. 544-545, 1991.
[96] F. Ö. Ilday, J. R. Buckley, H. Lim, F. W. Wise, and W. G. Clark, "Generation of 50-fs, 5-nJ pulses at 1.03 μm from a wave-breaking-free fiber laser," Opt. Lett. 28, pp. 1365-1367, 2003.
[97] M. E. Fermann and I. Hartl, "Ultrafast fiber laser technology", IEEE J. Quantum. Electron. 15, pp. 191-206, 2009.

[98] X. Zhou, Y. Dai Yoshitomi, S. Tani, H. Yokoi, and K. Torizuka, "Generation of sub-30 fs pulses from a mode-locked ytterbium fiber laser oscillator with phase compensation," in Proc. of CLEO, pp. 1–2, 2008.
[99] D. Strickland and G. Mourou, "Compression of amplified chirped optical pulses," Opt. Commun. 55, pp. 447-449, 1985.
[100] A. Galvanauskas, "Mode-scalable fiber-based chirped pulse amplification systems", IEEE J. Sel. Top. Quantum Electron. 7, pp. 504-517, 2001.
[101] R. Paschotta, R. Häring, E. Gini, H. Melchior, U. Keller, H. L. Offerhaus, and D. J. Richardson, "Passively Q-switched 0.1-mJ fiber laser system at 1.53 μm," Opt. Lett. 24, pp. 388-390, 1999.
[102] J. A. Alvarez-Chavez, H. L. Offerhaus, J. Nilsson, P. W. Turner, W. A. Clarkson, and D. J. Richardson, "High-energy, high-power ytterbium-doped Q-switched fiber laser," Opt. Lett. 25, pp. 37-39, 2000.
[103] O. Schmidt, J. Rothhardt, F. Röser, S. Linke, T. Schreiber, K. Rademaker, J. Limpert, S. Ermeneux, P. Yvernault, F. Salin, and A. Tünnermann, "Millijoule pulse energy Q-switched short-length fiber laser," Opt. Lett. 32, pp. 1551-1553, 2007.
[104] M. Eichhorn and S. D. Jackson, "High-pulse-energy actively Q-switched Tm^{3+} doped silica 2 μm fiber laser pumped at 792 nm," Opt. Lett. 32, pp. 2780-2782, 2007.
[105] T. Hakulinen and O. G. Okhotnikov, "8 ns fiber laser Q-switched by the resonant saturable absorber mirror," Opt. Lett. 32, pp. 2677-2679, 2007.
[106] S. V. Chernikov, Y. Zhu, J. R. Taylor, and V. P. Gapontsev, "Supercontinuum self-Q-switched ytterbium fiber laser," Opt Lett 22, pp. 298–300, 1997.
[107] A. A. Fotiadi, P. Mégret, and M. Blondel, "Dynamics of a self-Q-switched fiber laser with a Rayleigh–stimulated Brillouin scattering ring mirror," Opt. Lett. 29, pp. 1078-1080, 2004.
[108] M. Laroche, H. Gilles, S. Girard, N. Passilly, and K. Aït-Ameur, "Nanosecond Pulse Generation in a Passively Q-Switched Yb-Doped Fiber Laser by Cr^{4+}:YAG Saturable Absorber, IEEE Photon. Technol. Lett. 18, pp. 764-766, 2006.
[109] E. Snitzer, H. Po, F. Hakimi, R. Tuminelli, and B. C. McCollum, "Double clad, offset core Nd fiber laser," in Optical Fiber Sensors, 2, paper PD5–1, pp. 533–537, 1989.
[110] M. E. Fermann, "Single-mode excitation of multimode fibers with ultrashort pulses," Opt. Lett. 23, pp. 52-54, 1998.
[111] J. Limpert, A. Liem, H. Zellmer, and A. Tünnermann, "A 500 W continuous-wave fibre laser with excellent beam quality," Electron. Lett. 39, pp. 645-647, 2003.
[112] Y. Jeong, J. K. Sahu, D. N. Payne, and J. Nilsson, "Ytterbium-doped large-core fibre laser with 1 kW of continuous-wave output power," Electron. Lett. 40, pp. 470-471, 2004.
[113] IPG Photonics, "IPG Photonics successfully tests wordl's first 10 kW single mode production laser," http://www.ipgphotonics.com/Collateral/Documents/EnglishUS/PR_Final_10kW_SM_laser.pdf, referenced 16.09.2009
[114] A. E. Siegman, Lasers. (Univ. Science Books, 1986).
[115] J. J. Zayhowski and C. Dill III, "Diode-pumped microchip lasers electro-optically Q-switched at high pulse repetition rates," Opt. Lett. 17, pp. 1201-1203, 1992.
[116] B. Hansson and M. Arvidsson, "Q-switched microchip laser with 65 ps timing jitter," Electron. Lett. 36, pp. 1123-1124, 2000.
[117] J. J. Zayhowski and P. L. Kelley, "Optimization of Q-Switched Lasers," IEEE J. Quantum Electron. 27, pp. 2220-2225, 1991.
[118] Y. Shimony, Z. Burshtein, and Y. Kalinsky, "Cr^{4+}:YAG as passive Q-switch and brewster plate in a pulsed Nd:YAG laser," IEEE J. Quantum Electron. 31, pp. 1738– 1741, 1995.

[119] A. Agnesi, S. Morello, C. Piccinno, G. Reali, and G. Sun, "Diode-pumped Neodymium lasers repetitively Q-switched by Cr^{4+}:YAG solid-state saturable absorbers," IEEE J. Sel. Top. Quantum Electron. 3, pp. 45–52, 1997.
[120] X. Zhang, S. Zhao, Q. Wang, Q. Zhang, L. Sun, and S. Zhang, "Optimization of Cr^{4+}-doped saturable absorber Q-switched lasers," IEEE J. Quantum Electron. 33, pp. 2286-2294, 1997.
[121] V. N. Philippov, A. V. Kir'yanov, and S. Unger, "Advanced configuration of erbium fiber passively Q-switched laser with Co^{2+}:ZnSe crystal as saturable absorber," IEEE Photon. Technol. Lett. 16, pp. 57–59, 2004.
[122] M. Laroche, A. M. Chardon, J. Nilsson, D. P. Shepherd, W. A. Clarkson, S. Girard, and R. Moncorgé, "Compact diode-pumped passively Q-switched tunable Er-Yb double clad fiber laser," Opt. Lett. 27, pp. 1980–1982, 2002.
[123] V. Philippov, J. Nilsson, W. A. Clarkson, A. Abdolvand, V. E. Kisel, V. G. Shcherbitsky, N. V. Kuleshov, V. I. Konstantinov, and V. I. Levchenko, "Passively Q- switched Er-Yb double clad fiber laser with Cr^{2+}:ZnSe and Co^{2+}:$MgAl_2O_4$ as a saturable absorber," Proc. SPIE 5335, pp. 8-15, 2004.
[124] S. D. Jackson, "Passively Q-switched Tm^{3+}-doped silica fiber lasers," Appl. Opt. 46, pp. 3311-3317, 2007.
[125] A. S. Kurkov, E. M. Sholokhov, and O. I. Medvedkov, "All fiber Yb-Ho pulsed laser," Laser Phys. Lett. 6, pp. 135-138, 2008.
[126] T. Hakulinen, R. Koskinen, and O. G. Okhotnikov, "Low jitter Q-switched fiber laser using optically driven surface-normal saturable absorber modulator," Opt. Express 16, pp. 8720-8726, 2008.
[127] J. B. Khurgin, F. Jin, G. Solyar, C. Wang, and S. Trivedi, "Cost-effective low timing jitter passively Q-switched diode-pumped solid-state laser with composite pumping pulses," Appl. Opt. 41, pp. 1095-1097, 2002.
[128] B. Cole, L. Goldberg, C. W. Trussell, A. Hays, B. W. Schilling, and C. McIntosh, "Reduction of timing jitter in a Q-Switched Nd:YAG laser by direct bleaching of a Cr^{4+}:YAG saturable absorber," Opt. Express 17, pp. 1766-1771, 2009.
[129] Y. Wang, X. Ma, J. Peng, H. Tan, and L. Qian, "High-repetition rate Q-switched Nd:YVO_4 laser with a composite semiconductor absorber," Appl. Opt. 45, pp. 6616-6619, 2006.
[130] G. J. Spühler, R. Paschotta, R. Fluck, B. Braun, M. Moser, G. Zhang, E. Gini, and U. Keller, "Experimentally confirmed design guidelines for passively Q-switched microchip lasers using semiconductor saturable absorbers," J. Opt. Soc. Am. B 16, pp. 376-388, 1999.
[131] J. J. Zayhowski and C. Dill III, "Diode-pumped passively Q-switched picosecond microchip lasers," Opt. Lett. 19, pp. 1427-1427, 1994.
[132] B. Braun, F. X. Kärtner, G. Zhang, M. Moser, and U. Keller, "56-ps passively Q-switched diode-pumped microchip laser," Opt. Lett. 22, pp. 381-383, 1997.
[133] Y. Tsang, B. Richards, D. Binks, J. Lousteau, and A. Jha, "Tm^{3+}/Ho^{3+} co-doped tellurite fiber laser," Opt. Lett. 33, pp. 1282-1284, 2008.
[134] M. Eichorn, and S. D. Jackson, "High-pulse-energy, actively Q-switched Tm^{3+},Ho^{3+}-codoped silica 2 μm fiber laser," Opt. Lett. 33, 1044-1046 (2008).
[135] D. Kuizenga and A. Siegmann, "FM and AM Mode Locking of the Homogeneous laser - part I: Theory," IEEE J. Quantum Electron. 6, pp. 694-708, 1970.
[136] F. X. Kärtner, D. Kopf, and U. Keller, "Solitary-pulse stabilization and shortening in actively mode-locked lasers," J. Opt. Soc. Am. B 12, pp. 486-489, 1995.
[137] D. J. Jones, H. A. Haus, and E. P. Ippen, "Subpicosecond solitons in an actively mode-locked fiber laser," Opt. Lett. 21, pp. 1818-1820, 1996.
[138] U. Keller, K. J. Weingarten, F. X. Kärtner, D. Kopf, B. Braun, I. D. Jung, R. Fluck, C. Hönninger, N. Matuschek, and J. Aus der Au, "Semiconductor Saturable Absorber Mirrors

(SESAM's) for Femtosecond to Nanosecond Pulse Generation in Solid-State Lasers," IEEE J. Quantum Electron. 2, pp. 435-453, 1996.
[139] S. Y. Set, H. Yaguchi, Y. Tanaka, M. Jablonski, Y. Sakakibara, A. Rozhin, M. Tokumoto, H. Kataura, Y. Achiba, and K. Kikuchi, "Modelocked fiber lasers based on a saturable absorber incorporating carbon nanotubes," in OFC'03, paper PD44, 2003.
[140] V. Matsas, T. Newson, D. Richardson, and D. Payne, "Self-starting passively mode-locked fibre ring soliton laser exploiting nonlinear polarization rotation," Electron. Lett. 28, pp. 1391-1393, 1992.
[141] M. E. Fermann, M. J. Andrejco, Y. Silberberg, and M. L. Stock, "Passive mode locking by using nonlinear polarization evolution in a polarization-maintaining erbium-doped fiber," Opt. Lett. 18, pp. 894-896, 1993.
[142] C. J. Chen, P. K. A. Wai, and C. R. Menyuk, "Soliton fiber ring laser," Opt. Lett. 17, pp. 417-419, 1992.
[143] T. Brabec, C. Spielmann, P. F. Curley, and F. Krausz, "Kerr lens mode locking," Opt. Lett. 17, pp. 1292-1294, 1992.
[144] M. Hofer, M. E. Fermann, F. Haberl, M. H. Ober, and A. J. Schmidt, "Mode locking with cross-phase and self-phase modulation," Opt. Lett. 16, pp. 502-504, 1991.
[145] K. Tamura, E. P. Ippen, H. A. Haus, and L. E. Nelson, "77-fs pulse generation from a stretched-pulse mode-locked all-fiber ring laser," Opt. Lett. 18, pp. 1080-1082, 1993.
[146] A. G. Bulushev, E. M. Dianov, and O. G. Okhotnikov, "Passive mode locking of a laser with a nonlinear fiber reflector," Opt. Lett. 15, pp. 968-970, 1990.
[147] M. E. Fermann, F. Haberl, M. Hofer, and H. Hochreiter, "Nonlinear amplifying loop mirror," Opt. Lett. 15, pp. 752-754, 1990.
[148] M. J. Guy, D. U. Noske, and J. R. Taylor, "Generation of femtosecond soliton pulses by passive mode locking of an ytterbium-erbium figure-of-eight fiber laser," Opt. Lett. 18, pp. 1447-1449, 1993.
[149] F. Ö. Ilday, F. W. Wise, and T. Sosnowski, "High-energy femtosecond stretched-pulse fiber laser with a nonlinear optical loop mirror," Opt. Lett. 27, pp. 1531-1533, 2002.
[150] W. Zhao, H. Ma, W. Zhang, C. Liu, G. Chen, and K. Lu, "Environmentally stable ytterbium figure-of-eight fiber laser producing 177-fs pulses," Opt. Commun. 273, pp. 242-245, 2007.
[151] F. V. Kowalski, S. J. Shattil, and P. D. Hale, "Optical pulse generation with a frequency shifted feedback laser," Appl. Phys. Lett. 53, pp. 734-736, 1988.
[152] H. Sabert and E. Brinkmeyer, "Pulse Generation in Fiber Lasers with Frequency Shifted Feedback," J. Lightwave Tech. 12, pp. 1360-1368, 1994.
[153] J. Porta, A. B. Grudinin, Z. J. Chen, J. D. Minelly, and N. J. Traynor, "Environmentally stable picosecond ytterbium fiber laser with a broad tuning range," Opt. Lett. 23, pp. 615-617, 1998.
[154] J. M. Sousa, and O. G. Okhotnikov, "Short pulse generation and control in Er-doped frequency-shifted-feedback fibre lasers," Opt. Commun. 183, pp. 227-241, 2000.
[155] A. M. Heidt, J. P. Burger, J. N. Maran, and N. Traynor, "High power and high energy ultrashort pulse generation with a frequency shifted feedback fiber laser," Opt. Express 15, pp. 15892-15897, 2007.
[156] L. Lefort, A. Albert, V. Couderc, and A. Barthélémy, "Highly Stable 68-fs Pulse Generation From a Stretched-Pulse Yb^{3+}-Doped Fiber Laser With Frequency Shifted Feedback," IEEE Photon. Technol. Lett. 14, pp. 1674-1676, 2002.
[157] M. Y. Jeon, H. K. Lee, J. T. Ahn, D. S. Lim, D. I. Chang, K. H. Kim, and S. B. Kang, "Wideband wavelength tunable modelocked fibre laser over 1557 - 1607 nm," Electron. Lett. 36, pp. 300-302, 2000.
[158] S. U. Alam and A. B. Grudinin, "Tunable Picosecond Frequency-Shifted Feedback Fiber Laser at 1550 nm," IEEE Photon. Technol. Lett. 16, pp. 2012-2014, 2004.

[159] U. Keller, "Recent developments in compact ultrafast lasers," Nature 424, pp. 831-838, 2004.
[160] O. Okhotnikov, A. Grudinin, and M. Pessa, "Ultra-fast fibre laser systems based on SESAM technology: new horizons and applications," New J. of Physics 6, 177, 2004.
[161] A. Isomäki, M. Guina, P. Tuomisto, and O. Okhotnikov, "Fiber Laser Mode-Locked With a Semiconductor Saturable Absorber Etalon Operating in Transmission," IEEE Photon. Technol. Lett. 18, pp. 2150-2152, 2006.
[162] Y. Deng, M. W. Koch, F. Lu, G. W. Wicks, and W. H. Knox, "Colliding-pulse passive harmonic mode-locking in a femtosecond Yb-doped fiber laser with a semiconductor saturable absorber," Opt. Express 12, pp. 3872-3877, 2004.
[163] M. Zirngibl, L. W. Stulz, J. Stone, J. Hugi, D. DiGiovanni, and P. B. Hansen, "1.2 ps pulses from passively mode-locked laser diode pumped Er-doped fibre ring laser," Electron. Lett. 27, pp. 1634-1735, 1991.
[164] R. Herda and O. G. Okhotnikov, "Dispersion compensation-free fiber laser mode-locked and stabilized by high-contrast saturable absorber mirror," IEEE J. Quantum Electron. 40, pp. 893-899, 2004.
[165] M. J. Lederera, B. Luther-Davies, H. H. Tan, C. Jagadish, M. Haiml, U. Siegner, and U. Keller, "Nonlinear optical absorption and temporal response of arsenic and oxygen-implanted GaAs," Appl. Phys. Lett. 74, pp. 1993-1995, 1999.
[166] M. J. Lederera, B. Luther-Davies, H. H. Tan, and C. Jagadish, "GaAs based anti-resonant Fabry–Perot saturable absorber fabricated by metal organic vapor phase epitaxy and ion implantation," Appl. Phys. Lett. 70, pp. 3428-3430, 1997.
[167] E.L. Delpon, J.L. Oudar, N. Bouché, R. Raj, A. Shen, N. Stelmakh, and J.M. Lourtioz, "Ultrafast excitonic saturable absorption in ion-implanted InGaAs/InAlAs multiple quantum wells," Appl. Phys. Lett. 72, pp. 759–761, 1998.
[168] S. Gupta, J.F. Whitaker, and G.A. Mourou, "Ultrafast carrier dynamics in III-V semiconductors grown by molecular-beam epitaxy at very low substrate temperatures," IEEE J. Quantum Electron. 28, pp. 2464–2472, 1992.
[169] S. Suomalainen, A. Vainionpää, O. Tengvall, T. Hakulinen, S. Karirinne, M. Guina, O. G. Okhotnikov, T. G. Euser, and W. L. Vos, "Long-wavelength fast semiconductor saturable absorber mirrors using metamorphic growth on GaAs substrates," Appl. Phys. Lett. 87, pp. 121106-1-121106-3, 2005.
[170] S. Suomalainen, M. Guina, T. Hakulinen, O. G. Okhotnikov, T. G. Euser, and S. Marcinkevicius, "1 μm saturable absorber with recovry time reduced by lattice mismatch," Appl. Phys. Lett. 89, pp. 071112-1-071113-3, 2006.
[171] M. Guina, P. Tuomisto, O. G. Okhotnikov, S. Marcinkeviciusc, K. Mizohatad, and J. Keinonen, "Semiconductor saturable absorbers with recovery time controlled through growth conditions," SPIE Proc. 6451, pp. 645113-1 - 645113-7, 2007.
[172] R. Paschotta and U. Keller, "Passive mode locking with slow saturable absorbers," Appl. Phys. B 73, pp. 653-662, 2001.
[173] F. X. Kärtner, I. D. Jung, and U. Keller, "Soliton Mode-Locking with Saturable Absorbers," IEEE J. Quantum Electron. 2, pp. 540-556, 1996.
[174] F. X. Kärtner, J. Aus der Au, and U. Keller, "Mode-Locking with Slow and Fast Saturable Absorbers—What's the Difference?," IEEE J. Quantum Electron. 4, pp. 159-168, 1998.
[175] S. Y. Set, H. Yaguchi, Y. Tanaka, and M. Jablonski, "Ultrafast Fiber Pulsed Lasers Incorporating Carbon Nanotubes," IEEE J. Sel. Top. Quantum Electron. 10, pp. 137-146, 2004.
[176] S. Y. Set, H. Yaguchi, Y. Tanaka, and M. Jablonski, "Laser Mode Locking Using a Saturable Absorber Incorporating Carbon Nanotubes," J. Lightwave Tech. 22, pp. 51-56, 2004.
[177] M. Nakazawa, S. Nakahara, T. Hirooka, M. Yoshida, T. Kaino, and K. Komatsu, "Polymer saturable absorber materials in the 1.5 μm band using poly-methyl methacrylate and polystyrene

with single-wall carbon nanotubes and their application to a femtosecond laser," Opt. Lett. 31, pp. 915-917, 2006.
[178] F. Shohda, T. Shirato, M. Nakazawa, K. Komatsu, and T. Kaino, "A passively mode-locked femtosecond soliton fiber laser at 1.5 μm with a CNT-doped polycarbonate saturable absorber," Opt. Express 16, pp. 21191-21198, 2008.
[179] A. Schmidt, S. Rivier, G. Steinmeyer, J. H. Yim, W. B. Cho, S. Lee, F. Rotermund, M. C. Pujol, X. Mateos, M. Aguiló, F. Díaz, V. Petrov, and U. Griebner, "Passive mode locking of Yb:KLuW using a single-walled carbon nanotube saturable absorber," Opt. Lett. 33, pp. 729-731, 2008.
[180] T. R. Schibli, K. Minoshima, H. Kataura, E. Itoga, N. Minami, S. Kazaoui, K. Miyashita, M. Tokumoto, and Y. Sakakibara, "Ultrashort pulse-generation by saturable absorber mirrors based on polymer-embedded carbon nanotubes," Opt. Express 13, pp. 8025-8031, 2005.
[181] K. H. Fong, K. Kikuchi, C. S. Goh, S. Y. Set, R. Grange, M. Haiml, A. Schlatter, and U. Keller, "Solid-state Er:Yb:glass laser mode-locked by using single-wall carbon nanotube thin film," Opt. Lett. 32, pp. 38-40, 2007.
[182] V. Scardacia, A.G. Rozhina, F. Hennrichb, W.I. Milnea, and A.C. Ferrari, "Carbon nanotube–polymer composites for photonic devices," Physica E 37, pp. 115-117, 2007.
[183] A. Schmidt, S. Rivier, W. B. Cho, J. H. Yim, S. Y. Choi, S. Lee, F. Rotermund, D. Rytz, G. Steinmeyer, V. Petrov, and U. Griebner, "Sub-100 fs single-walled carbon nanotube saturable absorber mode-locked Yb-laser operation near 1 μm," Opt. Express 17, pp. 20109-20116, 2009.
[184] J. W. Nicholson, R. S. Windeler, and D. J. DiGiovanni, "Optically driven deposition of single-walled carbon-nanotube saturable absorbers on optical fiber end-faces," Opt. Express 15, pp. 9176-9183, 2007.
[185] A. G. Rozhin, Y. Sakakibara, S. Namiki, M. Tokumoto, H. Kataura, and Y. Achiba "Sub-200-fs pulsed erbium-doped fiber laser using a carbon nanotube-polyvinylalcohol mode locker," Appl. Phys. Lett. pp. 05118-1–05118-3, 2006.
[186] M. A. Solodyankin, E. D. Obraztsova, A. S. Lobach, A. I. Chernov, A. V. Tausenev, V. I. Konov, and E. M. Dianov, "Mode-locked 1.93 μm thulium fiber laser with a carbon nanotube absorber," Opt. Lett. 33, pp. 1336-1338, 2008.
[187] F. Shohda, T. Shirato, M. Nakazawa, J. Mata, and J. Tsukamoto, "147 fs, 51 MHz soliton fiber laser at 1.56 μm with a fiber-connector-type SWNT/P3HT saturable absorber," Opt. Express 16, pp. 20943-20948, 2008.
[188] K. Kieu and M. Mansuripur, "Femtosecond laser pulse generation with a fiber taper embedded in carbon nanotube/polymer composite," Opt. Lett. 32, pp. 2242-2244, 2007.
[189] K. Kieu, and F. W. Wise, "Soliton Thulium-Doped Fiber Laser With Carbon Nanotube Saturable Absorber," IEEE Photon. Technol. Lett. 21, pp. 128 – 130, 2009.
[190] Y. W. Song, S. Yamashita C. S. Goh, and S. Y. Set, "Carbon nanotube mode lockers with enhanced nonlinearity via evanescent field interaction in D-shaped fibers," Opt. Lett. 32, pp. 148-150, 2007.
[191] Y. W. Song, S. Yamashita, E. Einarsson, and S. Maruyama, "All-fiber pulsed lasers passively mode locked by transferable vertically aligned carbon nanotube film," Opt. Lett. 32, pp. 1399-1401, 2007.
[192] S. Uchida, A. Martinez, Y. W. Song, T. Ishigure, and S. Yamashita, "Carbon Nanotube-Doped Polymer Optical Fiber," Opt. Lett. 34, pp. 3077-3079, 2009.
[193] C. S. Goh, K. Kikuchi, S. Y. Set, D. Tanaka, T. Kotake, M. Jablonski, S. Yamashita, and T. Kobayashi, "Femtosecond mode-locking of an ytterbium-doped fiber laser using a carbon-nanotube-based mode-locker with ultra-wide absorption band," in Conference on Lasers and Electro-Optics, paper CThG2, 2005.

[194] W. B. Cho, J. H. Yim, S. Y. Choi, S. Lee, U. Griebner, V. Petrov, and F. Rotermund, "Mode-locked self-starting Cr:forsterite laser using a single-walled carbon nanotube saturable absorber," Opt. Lett. 33, pp. 2449-2551, 2008.
[195] W. B. Cho, A. Schmidt, J. H. Yim, S. Y. Choi, S. Lee, F. Rotermund, U. Griebner, G. Steinmeyer, V. Petrov, X. Mateos, M. C. Pujol, J. J. Carvajal, M. Aguiló, and F. Díaz, "Passive mode-locking of a Tm-doped bulk laser near 2 μm using a carbon nanotube saturable absorber," Opt. Express 17, pp. 11007-11012, 2009.
[196] Y. C. Chen, N. R. Raravikar, L. S. Schadler, P. M. Ajayan, Y. P. Zhao, T. M. Lu, G. C. Wang, and X. C. Zhang, "Ultrafast optical switching properties of single-wall carbon nanotube polymer composites at 1.55 μm," Appl. Phys. Lett. 81, pp. 975-977, 2002.
[197] J. H. Yim, W. B. Cho, S. Lee, Y. H. Ahn, K. Kim, H. Lim, G. Steinmeyer, V. Petrov, U. Griebner, and F. Rotermund, "Fabrication and characterization of ultrafast carbon nanotube saturable absorbers for solid state laser mode-locking near 1 μm," Appl. Phys. Lett. 93, pp. 161106-1 – 161106-3, 2008.
[198] H. Kataura, Y. Kumazawa, Y. Maniwa, Y. Ohtsuka, R. Sen, S. Suzuki, and Y. Achiba, "Diameter control of single-walled carbon nanotubes," Carbon 38, pp. 1691-1697, 2000.
[199] G. Agrawal, Nonlinear Fiber Optics, Academic Press 2001.
[200] M. Schultz, O. Prochnow, A Ruehl, D. Wandt, D. Kracht, S. Ramachandran, and S. Ghalmi, "Sub-60-fs ytterbium-doped fiber laser with a fiber based dispersion compensation," Opt. Lett. 32, pp. 2372-2374, 2007.
[201] R. L. Fork, C. H. Brito Cruz, P. C. Becker, and C. V. Shank, "Compression of optical pulses to six femtoseconds by using cubic phase compensation," 12, pp. 483-485, 1987.
[202] T. Schreiber, B. Ortaç, J. Limpert, and A. Tünnermann, "On the study of pulse evolution in ultra-short pulse mode-locked fiber lasers by numerical simulations," Opt. Express15, pp. 8252-8262, 2007.
[203] O. Shtyrina, M. Fedoruk, S. Turitsyn, R. Herda, and O. Okhotnikov, "Evolution and stability of pulse regimes in SESAM-mode-locked femtosecond fiber lasers," J. Opt. Soc. Am. B 26, pp. 346-352, 2009.
[204] R. Herda and O. G. Okhotnikov, "Mode-locked Yb-doped fiber laser with external compression to 89 fs in normal dispersion fiber," Appl. Opt. 47, pp. 1182-1186, 2008.
[205] F. X. Kärtner and U. Keller, "Stabilization of solitonlike pulses with a slow saturable absorber," Opt. Lett. 20, pp. 16-18, 1995.
[206] S. M. Kelly, "Characteristic sideband instability of periodically amplified average soliton," Electron Lett. 28, pp. 806-807, 1992.
[207] M. L. Dennis and I. N. Duling III, "Experimental Study of Sideband Generation in Femtosecond Fiber Lasers," IEEE J. Quantum Electron. 30, pp. 1469-1477, 1994.
[208] K. Tamura, L. E. Nelson, H. A. Haus, and E. P. Ippen, "Soliton versus nonsoliton operation of fiber ring lasers," Appl. Phys. Lett. 64, 149 (1994).
[209] D. Anderson, M. Desaix, M. Lisak, and M. L. Quiroga-Teixeiro, "Wave breaking in nonlinear-optical fibers," J. Opt. Soc. Am. B 9, pp. 1358-1361, 1994.
[210] A. B. Grudinin, D. J. Richardson, and D. N. Payne, "Energy quantisation in figure eight fibre laser," Electron. Lett. 28, pp. 67–68, 1992.
[211] A. B. Grudinin and S. Gray, "Passive harmonic mode locking in soliton fiber lasers," J. Opt. Soc. Am. B 14, pp. 144-154, 1997.
[212] S. Zhou, D. G. Ouzounov, and F. W. Wise, "Passive harmonic mode-locking of a soliton Yb fiber laser at repetition rates to 1.5 GHz," Opt. Lett. 31, pp. 1041-1043, 2006.
[213] G. Lin, Y. Chang, and J. Wu, "Rational Harmonic Mode-Locking of Erbium-Doped Fiber Laser at 40 GHz Using a Loss-Modulated Fabry–Pérot Laser Diode," IEEE Photon. Technol. Lett. 16, pp. 1810-1812, 2004.

[214] S. Gray and A. B. Grudinin, "Soliton fiber laser with a hybrid saturable absorber," Opt. Lett. 21, pp. 207-209, 1996.
[215] V. Cautaerts, D. J. Richardson, R. Paschotta, and D. C. Hanna, "Stretched pulse Yb^{3+} silica fiber laser," Opt. Lett. 22, pp. 316-318, 1997.
[216] K. Tamura, E. P. Ippen, and H. A. Haus, "Pulse dynamics in stretched-pulse fiber lasers," Appl. Phys. Lett. 67, pp. 158-160, 1995.
[217] H. Lim, F. Ö. Ilday, and F. W. Wise, "Generation of 2-nJ pulses from a femtosecond ytterbium fiber laser," Opt. Lett. 28, pp. 660-662, 2003.
[218] B. Ortaç, A. Hideur, T. Chartier, M. Brunel, C. Özkul, and F. Sanchez, "90 fs generation from a stretched pulse ytterbium doped fiber laser," Opt. Lett. 28, pp. 1305-1307, 2003.
[219] B. Ortaç, J. Limpert, and A. Tünnermann, "High-energy femtosecond Yb-doped fiber laser operating in the anomalous dispersion regime," Opt. Lett. 32, pp. 2149-2151, 2007.
[220] A. Chong, W. H. Renninger, and F. W. Wise, "All-normal-dispersion femtosecond fiber laser with pulse energy above 20 nJ," Opt. Lett. 32, pp. 2408-2410, 2007.
[221] A. Chong, J. Buckley, W. Renninger, and F. Wise, "All-normal-dispersion femtosecond fiber laser," Opt. Express 14, pp. 10095-10100, 2006.
[222] K. Kieu and F. W. Wise, "All-fiber normal-dispersion femtosecond laser," Opt. Express 16, pp. 11453-11458, 2008.
[223] M. Schultz, H. Karow, O. Prochnow, D. Wandt, U. Morgner, and D. Kracht, "All-fiber ytterbium femtosecond laser without dispersion compensation," Opt. Express 16, pp. 19562-19566, 2008.
[224] M. Schultz, H. Karow, D. Wandt, U. Morgner, and D. Kracht, "Ytterbium femtosecond fiber laser without dispersion compensation tunable from 1015 nm to 1050 nm," Opt. Commun. 282, pp. 2567–2570, 2009.
[225] J. R. Buckley, F. W. Wise, F. Ö. Ilday, and T. Sosnowski, "Femtosecond fiber lasers with pulse energies above 10 nJ," Opt. Lett. 30, pp. 1888-1890, 2005.
[226] F. Ö. Ilday, J. R. Buckley, W.G. Clark, and F.W.Wise, "Self-Similar Evolution of Parabolic Pulses in a Laser," Phys. Rev. Lett. 92, pp. 213902-1–213902-4, 2004.
[227] R. L. Fork, O. E. Martinez, and J. P. Gordon, "Negative dispersion using pairs of prisms," Opt. Lett. 9, pp. 150-152, 1984.
[228] J. D. Kafka, and T. Baer, "Prism-pair dispersive delay lines in optical pulse compression," Opt. Lett. 12, pp. 401-403, 1987.
[229] E. B. Treacy, "Optical Pulse Compression With Diffraction Gratings," IEEE J. Quantum Electron. 5, pp. 54-458, 1969.
[230] A. Frenkel, J. P. Heritage, and M. Stern, "Compensation of Dispersion in Optical Fibers for the 1.3-1.6 μm Region with a Grating and Telescope," IEEE J. Quantum Electron. 25, pp. 1981-1984, 1989.
[231] M. Engelbrecht, F. Haxsen, A. Ruehl, D. Wandt, and D. Kracht, "Ultrafast thulium-doped fiber-oscillator with pulse energy of 4.3 nJ," Opt. Lett. 33, pp. 690-692, 2008.
[232] F. Haxsen, A. Ruehl, M. Engelbrecht, D. Wandt, U. Morgner, and D. Kracht, "Stretched-pulse operation of a thulium-doped fiber laser," Opt. Express 16, pp. 20471-20476, 2008.
[233] M. Stern, J. P. Heritage, and E. W. Chase, "Grating Compensation of Third-Order Fiber Dispersion," IEEE J. Quantum Electron. 28, pp. 2742-2748, 1992.
[234] S. Kane and J. Squier, "Grating Compensation of Third-Order Material Dispersion in the Normal Dispersion Regime: Sub-100-fs Chirped-Pulse Amplification Using a Fiber Stretcher and Grating-Pair Compressor," IEEE J. Quantum Electron. 31, pp. 2052-2057, 1995.
[235] S. Kane, and J. Squier, "Grism-pair stretcher–compressor system for simultaneous second- and third-order dispersion compensation in chirped-pulse amplification," J. Opt. Soc. Am. B 14, pp. 661-665, 1997.

[236] J. R. Buckley, S. W. Clark, and F. W. Wise, "Generation of ten-cycle pulses from an ytterbium fiber laser with cubic phase compensation," Opt. Lett. 31, pp. 1340-1342, 2006.
[237] L. Orsila, L. A. Gomes, N. Xiang, T. Jouhti, and O. G. Okhotnikov, "Mode-locked ytterbium fiber lasers," Appl. Opt. 43, pp. 1902-1906, 2004.
[238] J. Kuhl and J. Heppner, "Compression of femtosecond optical pulses with dielectric multilayer interferometers," IEEE J. Quantum Electron. 22, pp. 182-185, 1986.
[239] L. Orsila, R. Herda, T. Hakulinen, and O. G. Okhotnikov, "Thin-Film Fapry-Pérot Dispersion Compensator for Mode-Locked Fiber Lasers," IEEE Photon. Technol. Lett. 19, pp. 6-8, 2007.
[240] R. Szipöcs, K. Ferencz, C. Spielmann, and F. Krausz, "Chirped multilayer coatings for broadband dispersion control in femtosecond lasers," Opt. Lett. 19, pp. 201-203, 1994.
[241] D. Kopf, G. Zhang, R. Fluck, M. Moser, and U. Keller, "All-in-one dispersion-compensating saturable absorber mirror for compact femtosecond laser sources," Opt. Lett. 21, pp. 486-488, 1996.
[242] H. A. Haus, K. Tamura, L. E. Nelson, and E. P. Ippen, "Stretched-Pulse Additive Pulse Mode-Locking in Fiber Stretched-pulse Ring Lasers: Theory and Experiment," IEEE J. Quantum Electron. 31, pp. 591-598, 1995.
[243] S. Ramachandran, S. Ghalmi, J. W. Nicholson, M. F. Yan, P. Wisk, E. Monberg, and F. V. Dimarcello, "Anomalous dispersion in a solid, silica-based fiber," Opt. Lett. 31, pp. 2532-2534, 2006.
[244] M. Schultz, O. Prochnow, A. Ruehl, D. Wandt, D. Kracht, S. Ramachandran, and S. Ghalmi, "Sub-60-fs ytterbium-doped fiber laser with a fiberbased dispersion compensation," Opt. Lett. 32, pp. 2372-2374, 2007.
[245] A. Isomäki and O. G. Okhotnikov, "All-fiber ytterbium soliton mode-locked laser with dispersion control by solid-core photonic bandgap fiber," Opt. Express 14, pp. 4368-4370, 2006.
[246] H. Lim, F. Ö. Ilday, and F. W. Wise, "Femtosecond ytterbium fiber laser with photonic crystal fiber for dispersion control," Opt. Express 10, pp. 1497-1502, 2002.
[247] H. Lim and F. W. Wise, "Control of dispersion in a femtosecond ytterbium laser by use of hollow-core photonic bandgap fiber," Opt. Express 12, pp. 2231-2235, 2004.
[248] J. C. Knight, T. A. Birks, P. St. J. Russell, and D. M. Atkin, "All-silica single-mode optical fiber with photonic crystal cladding," Opt. Lett. 21, pp. 1547-1549, 1996.
[249] P. St. J. Russell, "Photonic-Crystal Fibers," J. Lightwave Tech. 24, pp. 4729-4749, 2006.
[250] Y. Wang, H. Bartelt, S. Brueckner, J. Kobelke, M. Rothhardt, K. Mörl, W. Ecke, and R. Willsch, "Splicing Ge-doped photonic crystal fibers using commercial fusion splicer with default discharge parameters," Opt. Express 16, pp. 7258-7263, 2008.
[251] G. Genty, S. Coen, and J. M. Dudley, "Fiber supercontinuum sources," J. Opt. Soc. Am. B 24, pp. 1771-1785, 2007.
[252] A. Isomäki and Oleg G. Okhotnikov, "Femtosecond soliton mode-locked laser based on ytterbium-doped photonic bandgap fiber," Opt. Express 20, pp. 9238-9243, 2006.
[253] L. Xiao, W. Jin, and M. S. Demokan, "Fusion splicing small-core photonic crystal fibers and single-mode fibers by repeated arc discharges," Opt. Lett. 32, pp. 115-117, 2007.
[254] G. Meltz, W. W. Morey, and W. H. Glenn, "Formation of Bragg gratings in optical fibers by a transverse holographic method," Opt. Lett. 14, pp. 823-825, 1989.
[255] B. Malo, K. O. Hill, F. Bilodeau, D. C. Johnson, and J. Albert, "Point-by-point fabrication of micro-Bragg gratings in photosensitive fibre using single excimer pulse refractive index modification techniques," Electron. Lett. 29, pp. 1668-1669, 1993.
[256] K. O. Hill, B. Malo, F. Bilodeau, D. C. Johnson, and J. Albert, "Bragg gratings fabricated in monomode photosensitive optical fiber by UV exposure through a phase mask," Appl. Phys. Lett. 62, pp. 1035-1037, 1993.

[257] S. J. Mihailov, C. W. Smelser, P. Lu, R. B. Walker, D. Grobnic, H. Ding, G. Henderson, and J. Unruh, "Fiber Bragg gratings made with a phase mask and 800-nm femtosecond radiation," Opt. Lett. 28, pp. 995-997, 2003.
[258] K. O. Hill, Y. Fujii, D. C. Johnson, and B. S. Kawasaki, "Photosensitivity in optical fiber waveguides: Application to reflection filter fabrication," Appl. Phys. Lett. 32, pp. 647-649, 1978.
[259] A. Othonos, "Fiber Bragg gratings," Rev. Sci. Instrum. 68, pp. 4309-4341, 1997.
[260] D. L. Williams, B. J. Ainslie, J. R. Armitage, R. Kashyap, and R. Campbell, "Enhanced UV photosensitivity in boroncodoped germanosilicate fibers," Electron. Lett. 29, pp. 45–47, 1993.
[261] K. O. Hill, B. Malo, F. Bilodeau, D. C. Johnson, T. F. Morse, A. Kilian, L. Reinhart, and O. Kyunghwan, "Photosensitivity in Eu^{2+}:Al_2O_3-Doped-Core Fiber: Preliminary Results and Application to Mode Converters," Proc. of OFC'91, 14, PD3-1, 1991.
[262] M. Broer, C. L. Cone, and J. R. Simpson, "Ultraviolet-induced distributed-feedback gratings in Ce^{3+}-doped silica optical fibers," Opt. Lett. 16, pp. 1391-1393, 1991.
[263] F. Bilodeau, D. C. Johnson, B. Malo, K. A. Vineberg, and K. O. Hill, "Ultraviolet-light photosensitivity in Er^{3+}-Ge-doped optical fiber," Opt. Lett. 15, pp. 1138-1140, 1990.
[264] F. Bilodeau, B. Malo, J. Albert, D. C. Johnson, K. O. Hill, Y. Hibino, M. Abe, and M. Kawachi, "Photosensitization of optical fiber and silica-on-silicon/silica waveguides," Opt. Lett. 18, pp. 953-955, 1993.
[265] M. Konstantaki, G. Tamiolakis, A. Argyris, A. Othonos, and A. Ikiades, "Effects of Ge-concentration, boron codoping, and hydrogenation on fiber Bragg grating characteristics," Microwave and Optical Technol. Lett. 44, pp. 148-152, 2005.
[266] P. J. Lemaire, R. M. Atkins, V. Mizrahi, and W. A. Reed, "High-pressure H_2-loading as a technique for achieving ultrahigh UV photosensitivity and thermal sensitivity in GeO_2-doped optical fibers," Electron. Lett. 29, pp. 1191–1193, 1993.
[267] K. O. Hill and G Meltz, "Fiber Bragg Grating Technology Fundamentals and Overview," J. Lightwave Tech. 15, pp. 1263-1276, 1993.
[268] D. J. Kitcher, A. Nand, S. A. Wade, R. Jones, G. W. Baxter, and S. F. Collins, "Directional dependence of spectra of fiber Bragg gratings due to excess loss," Opt. Soc. Am. A 23, pp. 2906-2911, 2006
[269] V. Mizrahi and J. E. Sipe, "Optical Properties of Photosensitive Fiber Phase Gratings," J. Lightwave Tech. 11, pp. 1513-1517, 1993.
[270] J. Martin and F. Ouellette, "Novel writing technique of long and highly reflective in-fibre gratings," Electron Lett. 30, pp. 811-812, 1994.
[271] K. Ennser, M. N. Zervas, and R. I. Laming, "Optimization of Apodized Linearly Chirped Fiber Gratings for Optical Communications," IEEE J. Quantum Electron. 34, pp. 770-778, 1998.
[272] K. C. Byron, K. Sugden, T. Bricheno, and I. Bennion. "Fabrication of chirped Bragg gratings in photosensitive fibre," Electron. Lett. 29, pp. 1659-1660, 1993.
[273] J. Mora, A. Diez, M. V. Andres, P. Y. Fonjallaz, and M. Popov, "Tunable dispersion compensator based on a fiber Bragg grating written in a tapered fiber," IEEE Photonics Technol. Lett. 16, pp. 2631-2633, 2004.
[274] J. Mora, J. Villatoro, A. Dìez, J. L. Cruz, and M. V. Andrés, "Tunable chirp in Bragg gratings written in tapered core fibers," Opt. Commun. 210, pp. 51–55, 2002.
[275] F. M. Mitschke and L. F. Mollenauer, "Discovery of the soliton self-frequency shift," Opt. Lett. 11, pp. 659-661, 1986.
[276] J. K. Lucek and K. J. Blow, "Soliton self-frequency shift in telecommunications fibers," Phys. Rev. A 45, pp. 6666-6674, 1992.
[277] D. P. Wei, T.V. Galstian, A. Zohrabyan, and L. Mouradian, "Tunable femtosecond soliton generation in Ge-doped fibre," Electron. Lett. 40, pp. 1329-1330, 2004.
[278] X. Zhu and W. Sibbett, "Propagation Characteristics of Femtosecond Pulses in Erbium-Doped Monomode Optical Fibers," IEEE J. Quantum Electron. 27, pp. 101-113, 1991.

[279] X. Liu, C. Xu, W. H. Knox, J. K. Chandalia, B. J. Eggleton, S. G. Kosinski, and R. S. Windeler, "Soliton self-frequency shift in a short tapered air–silica microstructure fiber," Opt. Lett. 26, pp. 358-360, 2001.
[280] B. R. Washburn, S. E. Ralph, P. A. Lacourt, J. M. Dudley, W. T. Rhodes, R. S. Windeler, and S. Coen, "Tunable near-infrared femtosecond soliton generation in photonic crystal fibres," Electron. Lett. 37, pp. 1510–1512, 2001.
[281] I. G. Cormack, D. T. Reid, W. J. Wadsworth, J. C. Knight, and P. S. J. Russell, "Observation of soliton self-frequency shift in photonic crystal fibre," Electron. Lett. 38, pp. 167–169, 2002.
[282] D. G. Ouzounov, F. R. Ahmad, D. Muller, N. Venkataraman, M. T. allagher, M. G. Thomas, J. Silcox, K. W. Koch, and A. L. Gaeta, "Generation of megawatt optical solitons in hollow-core photonic band-gap fibers," Science 301, pp. 1702–1704, 2003.
[283] J. van Howe, J. H. Lee, S. Zhou, F. Wise, C. Xu, S. Ramachandran, S. Ghalmi, and M. F. Yan, "Demonstration of soliton self-frequency shift below 1300 nm in higher-order mode, solid silica-based fiber," Opt. Lett. 32, pp. 340–342, 2007.
[284] M. Chan, S. Chia, T. Liu, T. Tsai, M. Ho, A. Ivanov, A. Zheltikov, J. Liu, H. Liu, and C. Sun, "1.2- to 2.2-μm Tunable Raman Soliton Source Based on a Cr : Forsterite Laser and a Photonic-Crystal Fiber," IEEE Photon. Technol. Lett. 20, pp. 900-902, 2008.
[285] J. Takayanagi, T. Sugiura, M. Yoshida, and N. Nishizawa, "1.0–1.7-μm Wavelength-Tunable Ultrashort-Pulse Generation Using Femtosecond Yb-Doped Fiber Laser and Photonic Crystal Fiber," IEEE Photon. Technol. Lett. 18, pp. 2284-2286, 2006.
[286] G. Imeshev and M. E. Fermann, "230-kW peak power femtosecond pulses from a high power tunable source based on amplification in Tm-doped fiber," Opt. Express 13, pp. 7424-7431, 2005.
[287] N. Nishizawa and T. Goto, "Widely Wavelength-Tunable Ultrashort Pulse Generation Using Polarization Maintaining Optical Fibers," IEEE J. Sel. Top. Quantum Electron. 7, pp. 518-524, 2001.
[288] A. A. Voronin and A. M. Zheltikov, "Soliton self-frequency shift decelerated by self-steepening," Opt. Lett. 33, pp. 1723-1725, 2008.
[289] A. B. Fedotov, A. A. Voronin, I. V. Fedotov, A. A. Ivanov, and A. M. Zheltikov, "Spectral compression of frequency-shifting solitons in a photonic-crystal fiber," Opt. Lett. 34, pp. 662-664, 2009.
[290] F. Druon, N. Sanner, G. Lucas-Leclin, P. Georges, K. P. Hansen, and A. Petersson, "Self-compression and Raman soliton generation in a photonic crystal fiber of 100-fs pulses produced by a diode-pumped Yb-doped oscillator," Appl. Opt. 42, pp. 6768-6770, 2003.
[291] R. Herda and O. G. Okhotnikov, "All-fiber soliton source tunable over 500 nm," in Proc. of CLEO Europe 2005, paper JWB39, 2005.
[292] E. M. Dianov, A. A. Krylov, V. V. Dvoyrin, V. M. Mashinsky, P. G. Kryukov, O. G. Okhotnikov, and M. Guina, "Mode-locked Bi-doped fiber laser," J. Opt. Soc. Am. B 27, pp. 1807-1808, 2007.
[293] Y. Durteste, M. Monerie, J. Y. Allain, and H. Poignant "Amplification and lasing at 1.3 μm in praseodymium-doped fluorozirconate fibres," Electron. Lett. 27, pp. 628-629, 1991.
[294] T. Sugawa, E. Yoshida, Y. Miyajima, and M. Nakazawa, "1.6 ps pulse generation from a 1.3 μm Pr^{3+}-doped fluoride fibre laser," Electron. Lett. 29, pp. 902-903, 1993.
[295] M. J. Guy, D. U. Noske, A. Boskovic, and J. R. Taylor, "Femtosecond soliton generation in a praseodymium fluoride fiber laser," Opt. Lett. 19, pp. 828-830, 1994.
[296] L. E. Nelson, E. P. Ippen, and H. A. Haus, "Broadly tunable sub-500 fs pulses from an additive-pulse mode-locked thulium-doped fiber ring laser," Appl. Phys. Lett. 67, pp. 19–21, 1995.

[297] R. C. Sharp, D. E. Spock, N. Pan, and J. Elliot, "190-fs passively mode-locked thulium fiber laser with a low threshold," Opt. Lett. 21, pp. 881–883, 1996.
[298] A. G. Nasibulin, A. Ollikainen, A. S. Anisimov, D. P. Brown, P. V. Pikhitsa, S. Holopainen, J. S. Penttilä, P. Helistö, J. Ruokolainen, M. Choi, and E. I. Kauppinen, "Integration of single-walled carbon nanotubes into polymer films by thermo-compression," Chem. Eng. J. 136, pp. 409-413, 2008.
[299] A. Moisala, A. G. Nasibulin, D. P. Brown, H. Jiang, L. Khriachtchev, and E. I. Kauppinen, "Single-walled carbon nanotube synthesis using ferrocene and iron pentacarbonyl in a laminar flow reactor," Chem. Eng. Sci. 61, pp. 4393-4402, 2006.

Appendix 1

Publication 1

R. Herda, S. Kivistö, and O. G. Okhotnikov, "Dynamic gain induced pulse shortening in Q-switched lasers," *Optics Letters*, Vol. 33, No. 9, pp. 1011-1013, 2008.

Dynamic gain induced pulse shortening in *Q*-switched lasers

Robert Herda,[1,2,*] Samuli Kivistö,[1] and Oleg G. Okhotnikov[1]

[1]*Optoelectronics Research Centre, Tampere University of Technology, P.O. Box 692, Tampere 33101, Finland*
[2]*Current address: TOPTICA Photonics AG, Lochhamer Schlag 19, 82166 Graefelfing, Germany*
[*]*Corresponding author: robert.herda@toptica.com*

Received January 15, 2008; revised March 28, 2008; accepted March 28, 2008;
posted April 1, 2008 (Doc. ID 91779); published April 30, 2008

We describe a novel mechanism of pulse shortening in a *Q*-switched laser induced by the gain compression effect under strong pumping conditions. The pulse shortening requires a large variation of the gain excursion during the saturation process and benefits from the large volume of the gain medium. The effect has been experimentally demonstrated using a passive *Q*-switched Tm/Ho-doped fiber laser that shows gain-induced pulse compression from 800 ns down to 160 ns when the pump threshold is exceeded by 15 times.

OCIS codes: 060.3510, 140.3540.

The *Q*-switching technique, which has been known and intensively studied for decades, is now a classical and compulsory subject of university laser courses [1]. The physics of this regime, though well investigated, is still fascinating. The remarkable features that distinguish *Q*-switching from continuous wave and mode locking are the extremely high levels of population inversion stored in the cavity and the specific build-up mechanism whereby laser oscillation starts up from noise again and again for every consecutive pulse. Therefore, the term steady-state may not be quite suitable for *Q*-switching. *Q*-switched lasers can produce extremely high-energy "giant" pulses and are used in a wide variety of applications. These lasers are currently enjoying a renaissance, mainly owing to impressive achievements in high-energy picosecond pulse generation demonstrated by diode-pumped solid-state microchip *Q*-switched lasers [2]. The motivation that triggered this study was an unexpected performance observed in a passively *Q*-switched fiber laser that produced pulses with durations much shorter than expected from the well-established theory of *Q*-switching.

It is known that the duration of the pulses passively *Q*-switched using saturable absorbers critically depends on the cavity round-trip time, modulation depth of the absorber, and the output coupler reflectivity [2–7]. As the pulse width has been shown to be directly proportional to the cavity round-trip time and inversely proportional to the modulation depth of the saturable absorber, short-pulse operation is typically demonstrated using short-length cavity and/or high-modulation depth absorbers. In [8] the influence of the excited-state absorption on the pulse duration was investigated; however, in our absorbers we did not observe an excited-state absorption [9].

In fiber lasers the pulse width is usually set by the cavity length, which cannot be made as short as the value achievable, for example, in microchip lasers. In addition to these design guidelines, the output coupler reflectivity can also be instrumental in *Q*-switched laser optimization.

Using the above-mentioned guiding principles, we have built the thulium-holmium fiber laser *Q*-switched with an Sb-semiconductor saturable absorber mirror (SAM) described in detail in [10]. The linear cavity is terminated by a SAM and a narrow bandwidth fiber Bragg grating (FBG) also serving as an output coupler. The Tm/Ho-doped (16:1 doping ratio) fiber with a cutoff wavelength of 1550 nm, a core diameter of 7 μm, and absorption of ~30 dB/m at the wavelength of 1564 nm was core pumped by an erbium-doped fiber laser.

The oscilloscope trace reveals the Gaussian shape of the pulse shown in the inset in Fig. 1. The maximum average output power of 750 mW corresponding to a repetition rate of 420 kHz and pulse energy of ~1.8 μJ has been achieved for an absorbed pump power of 2.6 W. The optical-to-optical efficiency and the laser threshold were 29% and ~150 mW, respectively. The operation wavelength of the laser was 1970 nm.

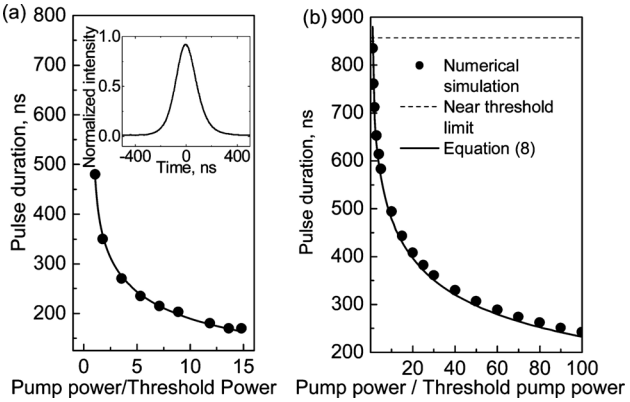

Fig. 1. (a) Measured *Q*-switched pulse durations for different pump powers fitted according to Eq. (8) and oscilloscope trace of a ~170 ns *Q*-switched pulse for the laser highly pumped above the threshold, $15\times P_{\mathrm{threshold}}$ (inset), (b) *Q*-switched pulse width obtained from numerical simulation using the rate Eqs. (1) and (3) (scatter plot) in the near threshold limit (dashed curve) assuming $\Delta g = 2q_0$ and estimated with Eq. (8) (solid curve). The value of the pulse duration near the laser threshold without gain compression effect is shown by the dashed curve.

As seen in Fig. 1(a), which shows the effect of pump power on the Q-switching performance, the pulse width essentially depends on the pump power. Close inspection of the experimental results revealed that the values of pulse duration achieved here cannot be experimentally understood from the analysis reported in [2,3]. In particular, the shortest pulse width that can be obtained from a Q-switched laser with the cavity parameters listed above is 800 ns according to the classical model, e.g., [2], expression (2), which is well above the value of 160 ns experimentally observed. In attempts to resolve this discrepancy, we apply the rate-equation analysis [3], taking into account an accurate description of the gain recovery process for the Q-switched laser studied here.

The saturation of the gain g in a Q-switched laser can be described by the rate equation

$$\frac{dg(t)}{dt} = -\frac{g(t)-g_0}{\tau_g} - \frac{gP(t)}{E_{\mathrm{sat},g}}, \tag{1}$$

and the saturable absorption q can be found from a similar equation:

$$\frac{dq(t)}{dt} = -\frac{q(t)-q_0}{\tau_a} - \frac{qP(t)}{E_{\mathrm{sat},a}}, \tag{2}$$

where q_0 is the saturable absorber loss and g_0 is the small signal gain. $E_{\mathrm{sat},g}$ and $E_{\mathrm{sat},a}$ are the saturation energies and τ_g and τ_a the recovery times for the saturable gain and loss, respectively. The temporal evolution of the intracavity power P is described by

$$\frac{dP}{dt} = (g-l-q)\frac{P}{T_r}, \tag{3}$$

where l is the cavity loss and T_r is the round-trip time. The simulation results of the pulse dynamics in a Q-switched laser based on these rate equations are presented in Fig. 2 (the parameters used are $E_{\mathrm{sat},g}=10\ \mu$J, $E_{\mathrm{sat},a}=10$ pJ, $\tau_g=1$ ms, $\tau_a=1$ ns, $q_0=0.083$, $l=0.693$, $T_r=20$ ns, and $P_0=1$ nW). Numerical simulation shows that the absorber recovery time has little effect on the pulse duration as long as the gain recovery time is short enough to recover between the pulses and sufficienctly long to enable a proper saturation of the absorber by the Q-switched pulse. The lowest level of the power in the cavity was set to P_0 to account for the noise in the cavity. Figure 2(a) corresponds to operation close to the lasing threshold [$g_0=1.1\ (q_0+l)$], while Fig. 2(b) shows the operation far above threshold [$g_0=25\ (q_0+l)$]. It can be seen that for strong pumping, the gain recovers to a value far above the level q_0+l and drops to a value much lower than $l-q_0$, in contrast to the assumption that gain variation ranges from q_0+l to $l-q_0$, typically used in Q-switched laser calculations [2–4]. The increased range of gain variation under strong pumping found above is an observation that provides a basis for explaining the pulse narrowing mechanism.

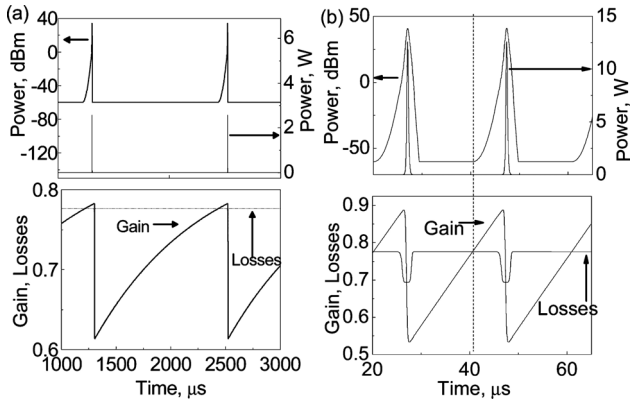

Fig. 2. Simulation of Q-switching illustrated with temporal evolution of cavity gain/loss and output power during Q-switched pulse formation. Pumping condition corresponds to operation (a) close to lasing threshold $g_0=1.1\ (q_0+l)$ and (b) far above the lasing threshold $g_0=25\ (q_0+l)$. The intracavity power is shown both in linear and dBm scale.

It can also be seen from Fig. 2(b) that during the gain recovery stage, occurring between consecutive pulses far in advance of sizeable pulse development, the intracavity power is too small to cause any gain saturation. In this phase of gain and pulse buildup, the gain recovery can be calculated by solving Eq. (1) with $P(t)\approx 0$. The solution yields

$$g(t) = [l+q_0-g_0]\exp(-t/\tau_g) + g_0, \tag{4}$$

assuming an unbleached saturable absorber. Here the gain reaches the level of the losses $l+q_0$ at the time $t=0$. At the time $t=0$ the pulse power starts to develop from the noise level $P(t=0)=P_0$. The value at which the gain is saturated can be calculated from Eq. (1) by setting $dg/dt=0$. Assuming the pumping level to be far above the threshold, the gain increases until the power level reaches the value of $g_0E_{\mathrm{sat},g}/\tau_g$. When the gain parameter g_0 is close to the threshold gain, the gain recovers to a value close to the threshold value $g=l+q_0$. In contrast, when the gain is much higher than the threshold gain, the gain recovers to a much higher value. For times well before the gain recovery time, $t \ll \tau_g$, the temporal gain evolution can be approximated by a linear time dependence $g(t)=l+q_0+t(g_0-l-q_0)/\tau_g$. Setting this equation into the rate Eq. (3) and assuming $q=q_0$, the intracavity power during the gain recovery can be expressed in the form $P(t)=P_0\exp[0.5t^2\ (g_0-l-q_0)/(t_gT_r)]$. Then we immediately get an expression for the time needed for the gain to be recovered from the threshold value to the onset of the gain saturation when $P(t)=g_0E_{\mathrm{sat},g}/\tau_g$:

$$t = \sqrt{\frac{2\tau_g T_r}{g_0-l-q_0}\log\left(\frac{g_0E_{\mathrm{sat},g}}{\tau_g P_0}\right)}. \tag{5}$$

At this point the gain has recovered to the value

$$g_i = l+q_0+\sqrt{2}\sqrt{\frac{T_r}{\tau_g}}\sqrt{g_0-l-q_0}\sqrt{\log\left(\frac{g_0E_{\mathrm{sat},g}}{\tau_g P_0}\right)}. \tag{6}$$

The gain reduction/compression during the Q-switching process can be expressed as [3] Δg

$+l\log(1-\Delta g/g_i)=0$. Using this equation and Eq. (6) with the approximations $\log(1-\Delta g/g_i) \approx -\Delta g/g_i - 1/2(\Delta g/g_i)^2$, $\Delta g \ll l$, and $\log(E_{\mathrm{sat},g}/\tau_g P_0) \gg \log(g_0)$, it follows that the magnitude of the total gain variation during the Q-switching process is

$$\Delta g = 2q_0 + 2\sqrt{2}\sqrt{\frac{T_r}{\tau_g}}\sqrt{g_0 - l - q_0}\sqrt{\log\left(\frac{E_{\mathrm{sat},g}}{\tau_g P_0}\right)} = 2(q_0 + A\sqrt{P/P_{\mathrm{threshold}-1}}) \quad (7)$$

with

$$A = \sqrt{2}\sqrt{\frac{T_r}{\tau_g}}\sqrt{\log\left(\frac{E_{\mathrm{sat},g}}{\tau_g P_0}\right)}\sqrt{l+q_0}, \qquad \frac{P}{P_{\mathrm{threshold}}} = \frac{g_0}{l+q_0}.$$

In the limit of a large outcoupling ratio, $l \gg q_0$, the pulse duration can be estimated from

$$\tau = 7.04T_r/\Delta g = \frac{3.52T_r}{q_0 + A\sqrt{P/P_{\mathrm{threshold}-1}}}. \quad (8)$$

This expression for the pulse duration converts to the expression now widely used for Q-switched pulse width estimation in the limit of a low, near threshold, pumping rate [2]. The solid curve in Fig. 1(b) calculated with Eq. (8) is in good agreement with the numerical simulations. Deviations below 5% are caused by the limited validity of the $\Delta g \ll l$ approximation. Figure 1(a) shows the experimental data fitted to Eq. (8). The best fit corresponds to values $q_0=0.12$ and $A=0.08$.

It is possible to summarize and derive some general conclusions resulting from the analysis presented herein that are capable of explaining the experimental observations. The strong pumping and corresponding enhanced rate of gain recovery (the temporal slope dg/dt in Fig. 2 increases with the pumping) allows an unsaturated gain value substantially exceeding the cavity loss to be obtained. In turn, this feature also leads to the significantly lower value of the saturable gain depleted by the Q-switched pulse. Together, these factors significantly increase the magnitude of gain excursion $\Delta g = g_{\mathrm{unsat}}^{\mathrm{max}} - g_{\mathrm{sat}}^{\mathrm{min}}$ that occurs during pulse buildup. Since the value Δg eventually sets the limit for the shortest pulse width according to expression (8), it is then explicable why the Q-switched pulse duration observed in a laser pumped well above the threshold is much shorter as compared to the estimation made using an analysis assuming operation close to the laser threshold [2–5].

It is now relevant to speculate why this effect, clearly seen in the Tm/Ho fiber laser described here, has not been reported in other Q-switched lasers (to our knowledge). The primary characteristic of the laser studied here that allows the gain-induced pulse shortening to be observed is the large gain volume of the Tm/Ho fiber. This feature is typically in conflict with design guidelines of Q-switched lasers that target short-pulse operation that requires a short-length cavity with a low round-trip time.

In conclusion, we have described a novel mechanism for pulse shortening in a Q-switched laser induced by the gain compression effect under strong pumping conditions. The pulse shortening requires a large variation of the gain excursion during the saturation process and benefits from a large-gain medium volume. The effect has been experimentally demonstrated using passively Q-switched Tm/Ho-doped fiber laser. The all-fiber core-pumped laser shows gain-induced pulse compression from 800 ns down to 160 ns when the pump power was 15 times the threshold pump power.

The authors acknowledge K. Rößner and A. Forchel from the University of Würzburg (Germany) for providing the Sb-SAM.

References

1. A. E. Siegman, *Lasers* (University Science, 1986).
2. J. J. Zayhowski and C. Dill III, Opt. Lett. **19**, 1427 (1994).
3. G. J. Spühler, R. Paschotta, R. Fluck, B. Braun, M. Moser, G. Zhang, E. Gini, and U. Keller, J. Opt. Soc. Am. B **16**, 376 (1999).
4. J. J. Zayhowski and P. L. Kelley, IEEE J. Quantum Electron. **27**, 2220 (1991).
5. J. J. Zayhowski and P. L. Kelley, IEEE J. Quantum Electron. **29**, 1239 (1993).
6. J. J. Degnan, IEEE J. Quantum Electron. **31**, 1890 (1995).
7. T. Hakulinen and O. G. Okhotnikov, Opt. Lett. **32**, 2677 (2007).
8. G. Xiao and M. Bass, IEEE J. Quantum Electron. **33**, 41 (1997).
9. T. Hakulinen, R. Herda, and O. G. Okhotnikov, IEEE Photon. Technol. Lett. **19**, 333 (2007).
10. S. Kivistö, T. Hakulinen, M. Guina, and O. G. Okhotnikov, IEEE Photon. Technol. Lett. **19**, 934 (2007).

Appendix 2

Publication 2

S. Kivistö, R. Koskinen, J. Paajaste, S. D. Jackson, M. Guina, and O. G. Okhotnikov, "Passively Q-switched Tm^{3+}, Ho^{3+}-doped silica fiber laser using a highly nonlinear saturable absorber and dynamic gain pulse compression," *Optics Express*, Vol. 16, No. 26 pp. 22058–22063, 2008.

Passively Q-switched Tm^{3+}, Ho^{3+}-doped silica fiber laser using a highly nonlinear saturable absorber and dynamic gain pulse compression

Samuli Kivistö,[1,*] Riku Koskinen,[1] Jonna Paajaste,[1] Stuart D. Jackson,[2] Mircea Guina,[1] and Oleg G. Okhotnikov[1]

[1]*Optoelectronics Research Centre, Tampere University of Technology, P.O. Box 692, FIN-33101 Tampere, Finland*
[2]*Optical Fibre Technology Centre, University of Sydney, 206 National Innovation Centre, Australian Technology Park, Eveleigh, 1430 Australia*
**Corresponding author: samuli.kivisto@tut.fi*

Abstract: We demonstrate a compact core-pumped 2 μm Tm^{3+}, Ho^{3+}-doped all-fiber laser passively Q-switched with an antimony-based saturable absorber. The 20 ns pulses are the shortest Q-switched pulses from a fiber laser operating beyond 1850 nm and were produced at a repetition rate of 57 kHz and pulse energy of 15 μJ using a short-length (4 ns) cavity. The large absorber modulation depth of ~70% together with transient gain compression is shown to provide an efficient mechanism for Q-switched pulse shortening.

OCIS codes: (060.3510) Lasers, fiber; (140.3540) Lasers, Q-switched

References and links

1. R. A. Hayward, W. A. Clarkson, P. W. Turner, J. Nilsson, A. B. Grudinin, and D. C. Hanna, "Efficient cladding-pumped Tm-doped silica fibre laser with high power single mode output at 2 μm," Electron. Lett. **36**, 711–712 (2000).
2. S. D. Jackson, F. Bugge, and G. Erbert, "High power and highly efficient diode-cladding-pumped Ho^{3+}-doped silica fiber lasers," Opt. Lett. **32**, 3349-3351 (2007).
3. Y. Tsang, B. Richards, D. Binks, J. Lousteau, and A. Jha, "Tm^{3+}/Ho^{3+} co-doped tellurite fiber laser," Opt. Lett. **33**, 1282-1284 (2008).
4. S. D. Jackson, F. Bugge, and G. Erbert, "High power and highly efficient Tm^{3+}-doped silica fiber lasers pumped with diode lasers operating at 1150 nm," Opt. Lett. **32**, 2873-2875 (2007).
5. S. D. Jackson, "Passively Q-switched Tm^{3+}-doped silica fiber lasers," Appl. Opt. **46**, 3311-3317 (2007).
6. M. Eichorn, S. D. Jackson, "High-pulse-energy actively Q-switched Tm^{3+}-doped silica 2 μm fiber laser pumped at 792 nm," Opt. Lett. **32**, 2780-2782 (2007).
7. M. Eichorn, S. D. Jackson, "High-pulse-energy, actively Q-switched Tm^{3+},Ho^{3+}-codoped silica 2 μm fiber laser," Opt. Lett. **33**, 1044-1046 (2008).
8. J. J. Zayhowski and C. Dill III, "Diode-pumped passively Q-switched picosecond microchip lasers," Opt. Lett. **19**, 1427–1429 (1994).
9. G. J. Spühler, R. Paschotta, R. Fluck, B. Braun, M. Moser, G. Zhang, E. Gini, and U. Keller, "Experimentally confirmed design guidelines for passively Q-switched microchip lasers using semiconductor saturable absorbers," J. Opt. Soc. Am. B **16**, 376-388 (1999).
10. T. Hakulinen, and O. G. Okhotnikov, "8 ns fiber laser Q-switched by the resonant saturable asbsorber," Opt. Lett. **32**, 2677–2679 (2007).
11. R. Herda, S. Kivistö, and O. G. Okhotnikov, "Dynamic gain induced pulse shortening in Q-switched lasers," Opt. Lett. **33**, 1011-1013 (2008).
12. A. A. Fotiadi, P. Mégret, and M. Blondel, "Dynamics of a self-Q-switched fiber laser with a Rayleigh–stimulated Brillouin scattering ring mirror," Opt. Lett. **29**, 1078-1080 (2004).
13. M. Laroche, A. M. Chardon, J. Nilsson, D. P. Shepherd, W. A. Clarkson, S. Girard and R. Moncorgé, "Compact diode-pumped passively Q-switched tunable Er–Yb double-clad fiber laser," Opt. Lett. **27**, 1980-1982 (2002).
14. M. Salhi, A. Hideur, T. Chartier, M. Brunel, G. Martel, C. Ozkul, and F. Sanchez, "Evidence of Brillouin scattering in an ytterbium-doped double-clad fiber laser," Opt. Lett. **27**, 1294-1296 (2002).
15. A. E. Siegman, Lasers. (Univ. Science Books, 1986).

#102588 - $15.00 USD Received 10 Oct 2008; revised 16 Dec 2008; accepted 17 Dec 2008; published 19 Dec 2008

16. J. B. Khurgin, F. Jin, G. Solyar, C. Wang, and S. Trivedi, "Cost-effective low timing jitter passively Q-switched diode-pumped solid-state laser with composite pumping pulses," Appl. Opt. **41**, 1095–1097 (2002).

1. Introduction

Thulium- (Tm^{3+}), holmium- (Ho^{3+}), and Tm^{3+}, Ho^{3+}-co-doped fibers have been shown to be efficient gain media for lasers operating near 2 μm [1-3] with several options available for diode pumping particularly at 0.8 μm [1] and 1.15 μm [4]. The pump wavelength of 1.56 μm from Er^{3+}-doped fiber lasers, however, allows for core pumping with significantly reduced quantum defect [3]. The fiber lasers operating around 2 μm have become an important tool for many applications, especially those requiring narrow-line pulsed operation and high power.

Passively and actively Q-switched Tm^{3+}-based fiber lasers have been recently demonstrated exhibiting pulse durations in the range from ~40 ns to 1 μs [3,5-7]. Among them, the most advanced 2 μm Q-switched fiber laser sources demonstrated to date rely on active switching techniques delivering, however, rather unstable pulses with fairly broad spectra [6,7]. Compared to active Q-switching, passive switching offers a more compact geometry but the pulse duration depends critically on the modulation depth of the saturable absorber and the cavity round-trip time [8,9]. Since the pulse width is directly proportional to the cavity round-trip time and inversely proportional to the modulation depth of the saturable absorber, the shortest pulse width achievable from fiber lasers is typically set by the cavity length, which can not be made as short as the value used in, for example, microchip lasers [10].

We have shown recently that under strong pumping conditions, the Q-switch pulses can be significantly compressed in lasers with a large volume of the gain medium due to strong dynamic gain deviations [11]. In this paper we demonstrate a compact passively Q-switched 2 μm fiber laser that delivers nearly Gaussian-shaped 20 ns pulses with narrow spectrum and a repetition rate of 57 kHz. The highly doped $Tm^{3+,}$ Ho^{3+}-doped aluminosilicate fiber that was core-pumped with 1.56 μm erbium fiber laser enables the use of exceptionally short-length cavity and hence shorter pulse operation. Q-switched operation is initiated by a resonant antimonide-based semiconductor saturable absorber mirror with a modulation depth of 70% at 1970 nm. The large dynamic gain excursion provides an additional but important impact on Q-switched pulse characteristics.

2. Experiment

The all-fiber laser is shown schematically in Fig. 1. The oscillator comprised of a short piece of highly doped Tm^{3+} (2.5 wt.%), Ho^{3+} (0.25 wt.%)-doped aluminosilicate fiber, a dichroic pump coupler, a narrow bandwidth fiber Bragg grating (FBG) and InGaSb-based semiconductor saturable absorber mirror (SAM). The fiber core diameter was 10 μm and the numerical aperture was 0.2. The splice loss with standard single mode fiber (SMF-28) was ~0.5 dB. The resonant SAM was manufactured using solid source molecular beam epitaxy

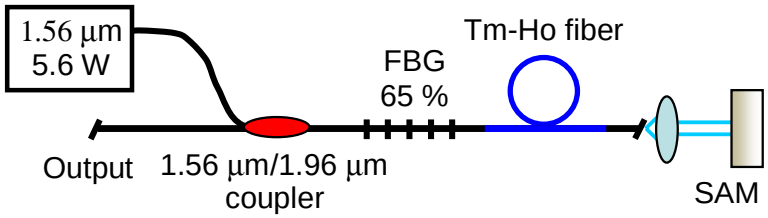

Fig. 1. Schematic of the passively Q-switched Tm^{3+}, Ho^{3+}-doped aluminosilicate fiber laser.

and comprised 20 InGaSb quantum-wells placed within a GaSb cavity with a Fabry-Pérot resonance at 1970 nm, and 18 AlAsSb/GaSb pairs for the distributed Bragg reflector (DBR). To enhance the cavity induced effect and to increase the nonlinear response, the structure was

#102588 - $15.00 USD Received 10 Oct 2008; revised 16 Dec 2008; accepted 17 Dec 2008; published 19 Dec 2008

capped with a 4-pair AlAsSb/GaSb DBR which increases the finesse of the Fabry-Pérot structure. The low intensity reflectivity of the SAM is shown in Fig. 2. At the resonant wavelength of 1970 nm, the modulation depth of the absorber approached ~70%. A ~300 μm-diameter collimated beam was directed onto the SAM; the fluence at the resonant wavelength was ~70 mJ/cm^2 which corresponded to fully bleached absorption. Continuous wave (CW) operation was studied by replacing the SAM with a highly reflective (HR) dielectric mirror. A 5.6 W, 1.56 μm single-mode Er^{3+}-doped fiber laser was used as the pump source. Core-pumping combined with high Tm^{3+} doping allowed a short (22 cm) optimal cavity length. The operating wavelength of the Tm^{3+}, Ho^{3+}-doped fiber laser was set with a FBG output coupler with a reflectivity of ~65%. To study the effect of the absorber modulation depth on the Q-switching performance near the resonant wavelength of the SAM, four FBGs with center wavelengths of 1942 nm, 1948 nm, 1957 nm, and 1970 nm were manufactured and used.

Figures 3(a) and (b) show the average output power for operation in both CW and Q-switched modes at 1948 nm (off-resonance) and 1970 nm (resonant). As expected, the nonsaturable losses at the resonant wavelength reduced the average power ratio for Q-switched and CW regimes from 95% to 78% as the modulation depth (ΔR_{SAM}) was increased from 17% to 70%, respectively. The overall cavity losses associated with the resonant SAM also increased the laser threshold from 900 mW to 1350 mW. The maximum average output power at 1970 nm was 800 mW.

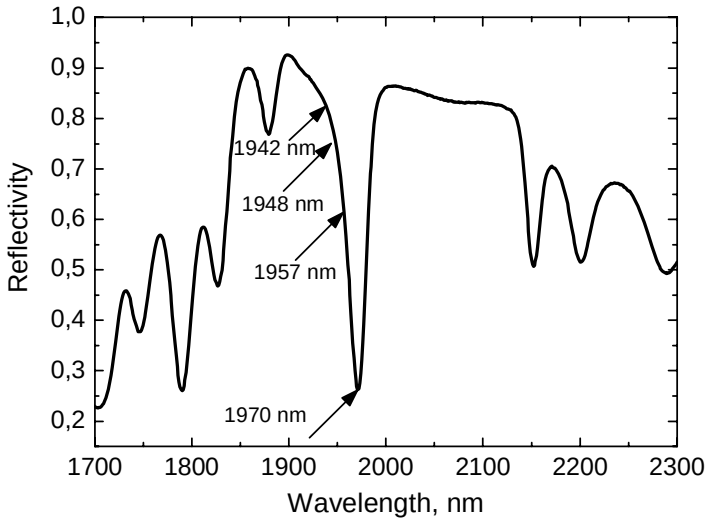

Fig. 2. Low intensity reflectivity of the SAM. The arrows show the operation wavelengths of the laser. The resonant wavelength is 1970 nm.

Figure 4(a) shows the effect of the modulation depth on the pulse width; at the highest absorbed pump power of 5 W, the pulse width decreased from 67 ns to 19.6 ns for ΔR_{SAM} = 10% and 70%, respectively. When the SAM was operated off-resonance at 1942 nm, 1948 nm or 1957 nm, the laser produced a pump dependent pulse width which approached, at high pump powers, values that are shorter than those expected from classical passive Q-switching theory [see dashed lines in Fig. 4(a)] [8,9]. This pulse shortening mechanism has been observed recently in another Tm^{3+}, Ho^{3+}-doped fiber laser and was found to originate from gain-induced pulse compression under strong pumping conditions [11]. The pulse width reduction in the current investigation was due to the large difference between the unsaturated

#102588 - $15.00 USD Received 10 Oct 2008; revised 16 Dec 2008; accepted 17 Dec 2008; published 19 Dec 2008

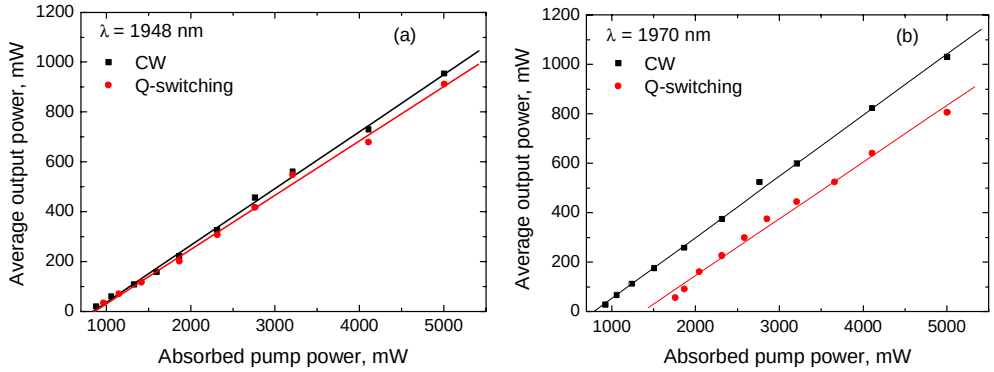

Fig. 3. Average output power in CW operation with HR mirror and Q-switched operation with SAM at the wavelengths of (a) 1948 nm corresponding to the absorber modulation depth of ΔR_{SAM} = 17%, and (b) 1970 nm corresponding to ΔR_{SAM} = 70%.

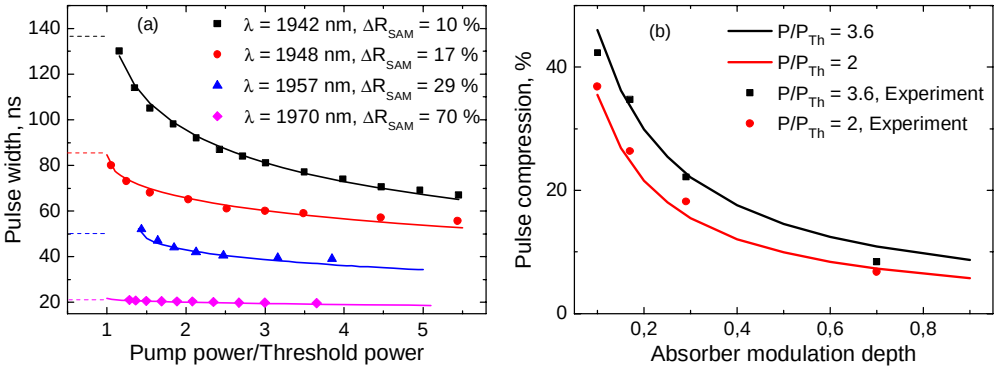

Fig. 4.(a) The effect of the pump power and operation wavelength (hence ΔR_{SAM}) on the pulse width. Dashed lines show the pulse width calculated from theory without taking into account the gain induced pulse compression. (b) The effect of the modulation depth on pulse compression at different power levels exceeding the threshold power. Solid lines are the fittings according to egn. (8) in [11].

gain before the onset of the Q-switched pulse and the saturated gain from the significantly depleted population inversion after the Q-switched pulse. The passively Q-switched pulse width under strong pumping conditions has been shown to be inversely proportional to this gain difference [11]. We note that dynamical pulse compression resulting in the generation of pulses shorter than the cavity round-trip time has been reported for passively and self-Q-switched fiber lasers employing stimulated Brillouin scattering (SBS) [12-14]. In our study, the effects from SBS were not observed.

As can be seen in Fig. 4(a), for ΔR_{SAM} = 70 % at 1970 nm, the modulation depth of the SAM played a dominant role in setting up the width of the Q-switched pulse producing pulses nearly independent of the pump power with compression from 21.3 ns to 19.6 ns. At a low modulation, however, the pulse compression effect contributed significantly to the shaping of the pulse; see results for ΔR_{SAM} = 10%. Figure 4(b) illustrates further the effect of the modulation depth on pulse compression which we define as $(\tau_{P,threshold}-\tau_P)/\tau_{P,threshold}$, where $\tau_{P,threshold}$ is the pulse width at the lasing threshold and τ_P is the pulse width at a given pump power. The experimental results for pulse compression, shown in Fig. 4(a), are also plotted against SAM modulation depth in Fig. 4(b) for two values of the pump power. As can be seen, the pulse compression at a pump power that is 3.6 times the laser threshold (black scatter) decreased from 43% for ΔR_{SAM} = 10% to 8% for ΔR_{SAM} = 70%. The solid lines represent the numerical results on Eqn. (8) in [11] and are in a good agreement with the experimental data.

#102588 - $15.00 USD Received 10 Oct 2008; revised 16 Dec 2008; accepted 17 Dec 2008; published 19 Dec 2008

Although the repetition rate of the laser, as seen from Fig. 5, increased linearly with pump power at high modulation depth, saturation effects appeared with off-resonance operation. As expected from classical theory, the repetition rate decreased with ΔR_{SAM} as $f_{repetition} \sim (\Delta R_{SAM})^{-1}$. The pulse energy at off-resonance was pump dependent as observed in Fig. 5 for ΔR_{SAM} = 10% at λ = 1942 nm. For resonant operation at 1970 nm with ΔR_{SAM} = 70%, the pulse energy was somewhat independent on the pump power with a mean value of ~15 μJ. The solid lines in Fig. 5 represent numerical simulations based on $E_{released} = E_{sat,g}\Delta g$, where $E_{sat,g}$ is the gain saturation energy, and Δg the gain variation which takes into account pulse compression for operation well above threshold by replacing the value for the gain variation $\Delta g=2q_0$ used in the near-threshold analysis [9] (dashed lines in Fig. 5) by Eqn. (7) from Ref. [11]. The pulse energy is now pump dependent at low modulation depth but differs from the value expected from classical theory in agreement with experimental observations. With large modulation depth, the pulse energy is effectively constant and close to the calculated near-threshold value. The difference in the laser characteristics (i.e. the pulse width, repetition rate, and pulse energy) between the off-resonant and resonant operation of the absorber is therefore due to the pulse compression effect that is strong for small modulation depth but is minimal at resonant operation, where ΔR_{SAM} attains large values.

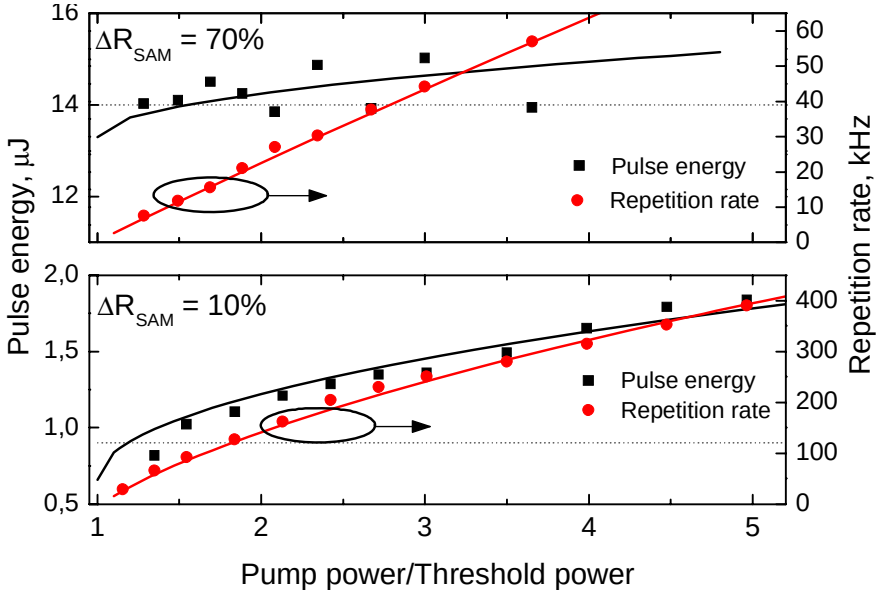

Fig. 5. The effect of the pump power and operation wavelength (hence ΔR_{SAM}) on the Q-switched pulse energy and repetition rate. Solid lines are the numerical fittings, and the dashed lines the near-threshold limit values for the pulse energy.

The corresponding peak power at the resonant wavelength was 0.7 kW and the laser slope efficiency and optical conversion efficiency were 23% and 16%, respectively. A typical oscilloscope trace reveals a nearly Gaussian-shaped pulse without any substructure, as shown in Fig. 6. The small asymmetry in the pulse shape is due to the large initial inversion leading to a fast rise time and a slightly slower decay time of the pulse [15]. Optical spectra at the four operating wavelengths are shown in the inset of Fig. 6. The spectral width was <0.6 nm which was limited by instrument resolution. The pulse jitter ranged from ~20 μs to 5 μs as the repetition rate increased, see inset to Fig. 6. The large jitter, which is typical for passively Q-switched lasers, is caused by amplified spontaneous emission, fluctuations in the pump power,

#102588 - $15.00 USD Received 10 Oct 2008; revised 16 Dec 2008; accepted 17 Dec 2008; published 19 Dec 2008

loss and temperature effects [16]. The pulse stability in amplitude and time (pulse duration) were better than 20% and ~5%, respectively.

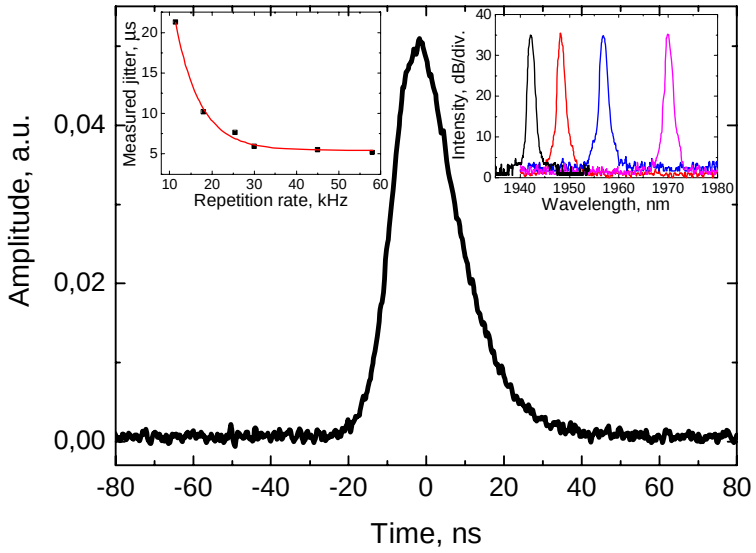

Fig. 6. Oscilloscope trace of a 19.6 ns Q-switched pulse observed at the resonant wavelength of the SAM. The insets show the narrow optical spectra at the four operating wavelengths (right) and the jitter vs. repetition rate of the laser (left).

3. Conclusion

We have studied a passively Q-switched ~2-µm Tm^{3+}, Ho^{3+}-doped fiber laser using a high contrast InGaSb resonant semiconductor saturable absorber mirror. The compact core-pumped all-fiber laser incorporating an optimized absorber mirror and pumping far above the threshold delivered 20 ns pulses with a narrow spectrum, an average output power of 800 mW, and pulse energy of 15 µJ. The absorber modulation depth was shown to have a significant influence on the contribution of dynamic gain induced pulse compression on the Q-switched pulse characteristics.

Acknowledgments

The authors acknowledge the support of the graduate school of Tampere University of Technology, Finnish Foundation for Economic and Technology Sciences, the Jenny and Antti Wihuri Foundation, the Nokia Foundation, the Emil Aaltonen foundation, The Elisa Foundation, and the Australian Research Council. The authors thank Soile Suomalainen for valuable discussions related to the SAM structure and fabrication, and Antti Tukiainen for measuring the low intensity reflectivity of the SAM.

#102588 - $15.00 USD Received 10 Oct 2008; revised 16 Dec 2008; accepted 17 Dec 2008; published 19 Dec 2008

Appendix 3

Publication 3

R. Herda, S. Kivistö, O. G. Okhotnikov, A. F. Kosolapov, A. E. Levchenko, S. L. Semjonov, and E. M. Dianov, "Environmentally Stable Mode-Locked Fiber Laser With Dispersion Compensation by Index-Guided Photonic Crystal Fiber," *IEEE Photonics Technology Letters*, Vol. 20, No. 3, pp. 217-219, 2008.

Environmentally Stable Mode-Locked Fiber Laser With Dispersion Compensation by Index-Guided Photonic Crystal Fiber

Robert Herda, Samuli Kivistö, Oleg G. Okhotnikov, Aleksey F. Kosolapov, Andrei E. Levchenko, Sergei L. Semjonov, and Evgueni M. Dianov

***Abstract*—We exploit the anomalous dispersion generated by an index-guided photonic crystal fiber (PCF) for dispersion compensation in an ytterbium fiber laser passively mode-locked with a semiconductor saturable absorber. A PCF, reasonably compatible with standard fiber, and a Faraday rotator in the cavity allow for robust all-fiber subpicosecond operation at 1 μm, insensitive to environmental disturbance.**

***Index Terms*—Dispersion compensation, Faraday rotator, fiber lasers, mode-locked lasers, photonic crystal fibers.**

I. Introduction

PRACTICAL femtosecond fiber lasers require all-fiber low-loss means for group-velocity dispersion compensation. Among the different types of photonic crystal fibers (PCFs), photonic bandgap (PBG) fibers, both hollow-core and solid-core, can generate a large amount of anomalous dispersion and may have large mode size [1], [2]. Hollow-core PBG fibers with air holes in a glass cladding allow propagation with much smaller nonlinearity and larger damage threshold compared with normal fibers. An all-silica solid-core PBG fiber is typically made of a silica core and an array of higher index Ge-doped strands in the cladding. It has the advantage of good mode matching with standard fibers and is attractive as a low-loss intracavity dispersion compensator for femtosecond fiber lasers [2], [3]. In addition, the solid-core structure exhibits no surface modes, allowing for high anomalous dispersion with low nonlinearity compared with index-guiding PCFs, and can have a core doped with rare-earth ions. Studies have shown, however, that PBG fibers exhibit a large amount of high-order dispersion that has a notable effect on the pulse formation [4]. Another constraint expected with PBG fibers is that the presence of a bandgap structure would eventually limit the shortest pulsewidths achievable with such fibers. With these arguments in mind, an index-guided PCF may provide a competitive alternative to PBG fiber because of the absence of bandgap restrictions and because of low higher order dispersion which is as low as in ordinary fibers.

In this letter, an index-guided PCF to be used for dispersion compensation in a mode-locked fiber laser was developed that generates a sufficient amount of anomalous dispersion around 1 μm with mode-size and nonlinearity close to that of ordinary fiber. An environmentally stable femtosecond fiber laser is demonstrated using a Faraday rotator mirror for compensation of the high birefringence typical for PCF [5], [6]. In contrast to [5], double pulsing is avoided due to the compensation of the birefringence; however, the birefringence of the PCF in combination with the Faraday rotator controls the polarization. The laser incorporates a semiconductor saturable absorber mirror (SESAM), exhibits robust self-starting single-pulse operation, and could be of interest as a practical oscillator with moderate output powers. This approach should allow for a commercially packaged femtosecond laser system without the need for polarization control.

II. Photonic Crystal Fiber

The preform from which the PCF was drawn was fabricated by mechanical drilling. An F-300 glass rod (Heraus) with a diameter of 22 mm and a height of 100 mm was mechanically drilled with a tube instrument with a diamond crown. Note that the fabrication of microstructured preforms by mechanical drilling offers a number of advantages compared to the "stack and draw technique" and extrusion method. In particular, almost all kinds of glasses, except strongly strained, can be drilled. A complicated hole geometry can be produced simply by using mechanical drilling, and in addition this method also substantially reduces the number of technological operations. The drilled preform was etched, resized, and jacked. Thermal processing was performed in the flame of an oxygen–hydrogen burner. This results in the polishing of the internal surface of the holes. During drawing and jacketing, a noble gas at excess pressure was introduced into the internal holes to compensate for surface tension forces tending to collapse the holes.

The cross section and the measured group-velocity dispersion of the PCF are shown in Fig. 1. As can be seen, the air filling factors are different in the first and second ring of holes. The air filling factor for the first ring of holes is $k_1 = d/\Delta = 0.75$, and for the second ring of holes $k_2 = 0.79$. The core diameter of the fiber is 2.9 μm and the measured zero dispersion wavelength is

Manuscript received June 3, 2007; revised September 24, 2007. This work was supported by the EU-FP6 URANUS Project, by the Graduate School of Tampere University of Technology, by the Finnish Foundation for Economic and Technology Sciences, by the Jenny and Antti Wihuri Foundation, and by the Nokia Foundation.

R. Herda, S. Kivistö, and O. G. Okhotnikov are with the Optoelectronics Research Centre, Tampere University of Technology, FIN-333101 Tampere, Finland (e-mail: robert.herda@tut.fi).

A. F. Kosolapov, A. E. Levchenko, S. L. Semjonov, and E. M. Dianov are with the Fiber Optics Research Center, Moscow 119333, Russia.

Digital Object Identifier 10.1109/LPT.2007.913236

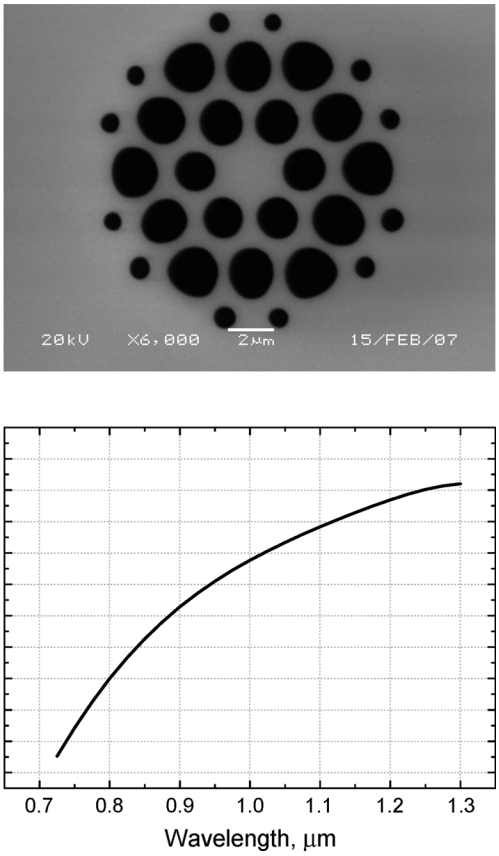

Fig. 1. Actual fiber cross section and measured group-velocity dispersion.

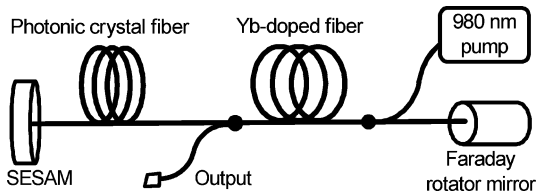

Fig. 2. Schematic of the mode-locked laser cavity.

874 nm. The loss at 1060 nm is 7 dB/km. The calculated effective mode area A_{eff} is 4.86 μm^2, and the calculated nonlinear coefficient γ is 26 W$^{-1}\cdot$km^{-1}.

III. Mode-Locking Experiments

The fiber laser used in this experiment is shown in Fig. 2. The active material is an 80-cm-long ytterbium-doped fiber pumped by a 300-mW diode laser. The light is coupled out via a 25% tap coupler. The length of passive HI-1060 fiber in the cavity is 120 cm.

The birefringence of the cavity is compensated for by a Faraday rotator mirror acting as a cavity end reflector. Another cavity mirror, the high modulation depth SESAM, is capable of starting passive mode-locking both with and without the dispersion compensation by the PCF [7], [8]. The resonant absorber mirror used in this study is similar to the absorber described in [8]. The In–GaAs–GaAs quantum-well absorber has a modulation depth of 10% and a saturation fluence of 7 μJ/cm^2.

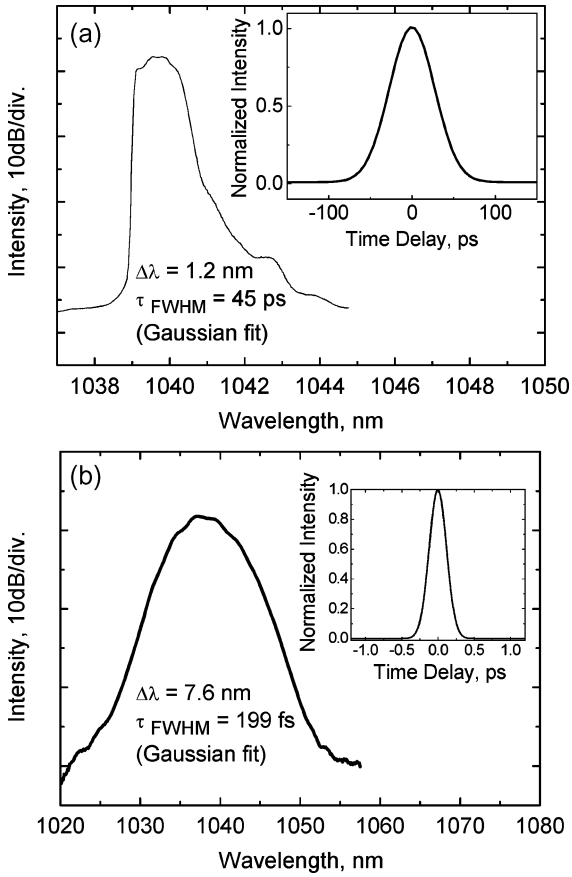

Fig. 3. Optical spectrum and intensity autocorrelation (inset) of the mode-locked pulse (a) without PCF and (b) with PCF.

Fig. 3(a) shows the spectrum and the autocorrelation of the mode-locked laser without dispersion compensation at a pulse energy of 500 pJ. A pulse duration of 45 ps was derived from measurements assuming Gaussian pulse shape corresponding to a time bandwidth product of 16.

The PCF was spliced to single-mode fiber using a standard fusion splicer. Reflections from the PCF to silica fiber interface and losses due to the mode field mismatch were minimized using repeated arc discharges. This allows for smooth collapse of the air holes and causes an adiabatic mode field transformation in the PCF which results in optimized mode matching [9]. Ripples in the spectrum, caused likely by reflections, are smaller than 0.2 dB. The splice loss was measured to be 1.5 dB.

Splicing the PCF of 3.5-m length with a total dispersion of 0.09 ps^2 resulted in a net cavity dispersion of -0.04 ps^2 assuming a dispersion of 25 ps^2/km for the ytterbium and the HI 1060 fiber. Fig. 3(b) shows the optical spectrum and autocorrelation of the mode-locked laser.

The PCF dispersion compensation results in soliton operation with transform-limited pulses. The pulse duration of 199 fs was derived using a Gaussian fit resulting in a time-bandwidth product of 0.42. The pulse energy was 460 pJ at a fundamental repetition rate of 18 MHz. It is important to note from Fig. 3 that the optimized compensator using PCF with reduced nonlinearity does not display noticeable Raman scattering. Another remarkable feature of the laser performance is the obvious ten-

dency to operation with a single pulse in the cavity. There was no evidence of multiple pulse mode-locking at the available pumping power.

Without the use of the Faraday rotator, the pulse operation start-up and mode-locking performance were very sensitive to changes in the polarization state. A polarization controller was then essentially needed to optimize the pulse duration and quality. Due to environmental changes, the polarization controller has to be frequently realigned to maintain operation state.

In contrast, with the Faraday rotator, self-starting and steady-state operation was independent of the fiber bending up to a few centimeters bending radius. Stable mode-locking was observed for several hours without the need for any readjustment and there was no need for readjustment when restarting the laser after a few days.

IV. Conclusion

We have demonstrated an environmentally stable femtosecond ytterbium laser using index-guided PCF for dispersion compensation at 1 μm. The self-starting mode-locked operation of the subpicosecond soliton laser is achieved by the use of a semiconductor saturable absorber. This approach may constitute an important step towards highly practical ultrafast fiber oscillators. Further experiments to increase the pulse energy are in progress.

References

[1] H. Lim, A. Chong, and F. W. Wise, "Environmentally-stable femtosecond ytterbium fiber laser with birefringent photonic bandgap fiber," *Opt. Express*, vol. 13, no. 9, pp. 3460–3464, May 2005 [Online]. Available: http://www.opticsinfobase.org/abstract.cfm?URI=oe-13-9-3460

[2] A. Isomäki and O. G. Okhotnikov, "All-fiber ytterbium soliton mode-locked laser with dispersion control by solid-core photonic bandgap fiber," *Opt. Express*, vol. 14, no. 10, pp. 4368–4373, 2006.

[3] A. Isomäki and O. G. Okhotnikov, "Femtosecond soliton mode-locked laser based on ytterbium-doped photonic bandgap fiber," *Opt. Express*, vol. 14, pp. 9238–9243, 2006.

[4] R. Herda, A. Isomäki, and O. G. Okhotnikov, "Soliton sidebands in photonic bandgap fibre lasers," *Electron. Lett.*, vol. 42, no. 18, pp. 19–20, 2006.

[5] H. Lim, F. Ilday, and F. Wise, "Femtosecond ytterbium fiber laser with photonic crystal fiber for dispersion control," *Opt. Express*, vol. 10, pp. 1497–1502, 2002 [Online]. Available: http://www.opticsinfobase.org/abstract.cfm?URI=oe-10-25-1497

[6] A. Peyrilloux, T. Chartier, A. Hideur, L. Berthelot, G. Mélin, S. Lempereur, D. Pagnoux, and P. Roy, "Theoretical and experimental study of the birefringence of a photonic crystal fiber," *J. Lightw. Technol.*, vol. 21, no. 2, pp. 536–539, Feb. 2003.

[7] R. Herda and O. G. Okhotnikov, "Effect of amplified spontaneous emission and absorber mirror recovery time on the dynamics of mode-locked fiber lasers," *Appl. Phys. Lett.*, vol. 86, no. 1, p. 011113, 2005.

[8] R. Herda and O. G. Okhotnikov, "Dispersion compensation-free fiber laser mode-locked and stabilized by high-contrast saturable absorber mirror," *IEEE J. Quantum Electron.*, vol. 40, no. 7, pp. 893–899, Jul. 2004.

[9] L. Xiao, W. Jin, and M. S. Demokan, "Fusion splicing small-core photonic crystal fibers and single-mode fibers by repeated arc discharges," *Opt. Lett.*, vol. 32, pp. 115–117, 2007.

Appendix 4

Publication 4

S. Kivistö, R. Herda, and O. G. Okhotnikov, "All-fiber supercontinuum source based on a mode-locked ytterbium laser with dispersion compensation by linearly chirped Bragg grating," *Optics Express*, Vol. 16, No. 1, pp. 265-270, 2008.

All-fiber supercontinuum source based on a mode-locked ytterbium laser with dispersion compensation by linearly chirped Bragg grating

S. Kivistö, R. Herda, and O. G. Okhotnikov

Optoelectronics Research Centre, Tampere University of Technology,
P.O. Box 692, FIN-33101 Tampere, Finland
samuli.kivisto@tut.fi

Abstract: We demonstrate an all-fiber picosecond soliton laser with dispersion management performed by a chirped Bragg grating that generates ~1.6 ps pulses representing the shortest pulsewidth reported to date using this technology. The large anomalous dispersion provided by the grating allows building of a long-length cavity laser with an extremely low fundamental repetition rate of 2.6 MHz. This source allows us to use an original approach for producing energetic pulses that after boosting in a medium power core-pumped amplifier produce an octave-spanning supercontinuum radiation in a nonlinear photonic crystal fiber.

OCIS codes: (060.3735) Fiber Bragg gratings; (320.6629) Supercontinuum generation; (140.3510) Lasers, fiber; (140.4050) Mode-locked lasers

References and links

1. J. W. Nicholson, M. F. Yan, P. Wisk, J. Fleming, F. DiMarcello, E. Monberg, A. Yablon, C. Jørgensen, and T. Veng, "All-fiber, octave-spanning supercontinuum," Opt. Lett. **28**, 643-645 (2003).
2. G. Genty, S. Coen, and J. M. Dudley, "Fiber supercontinuum sources," J. Opt. Soc. Am. B **24**, 1771-1785 (2007).
3. J. M. Dudley, L. Provino, N. Grossard, H. Maillotte, R. S. Windeler, B. J. Eggleton, and S. Coen, "Supercontinuum generation in air–silica microstructured fibers with nanosecond and femtosecond pulse pumping," J. Opt. Soc. Am. B **19**, 765-771 (2002).
4. M. Rusu, R. Herda, S. Kivistö, and O. G. Okhotnikov, "Fiber taper for dispersion management in a mode-locked ytterbium fiber laser," Opt Lett. **31**, 2257-2259 (2006).
5. A. Isomäki and O. G. Okhotnikov, "Femtosecond soliton mode-locked laser based on ytterbium-doped photonic bandgap fiber," Opt. Express **14**, 9238-9243 (2006).
6. H. Lim, F. Ö. Ilday, and F. W. Wise, "Femtosecond ytterbium fiber laser with photonic crystal fiber for dispersion control," Opt. Express **10**, 1497-1502 (2006).
7. O. Katz , Y. Sintov, Y. Nafcha, and Y. Glick, "Passively mode-locked ytterbium fiber laser utilizing chirped-fiber-Bragg-gratings for dispersion control," Opt. Commun. **269**, 156-165 (2007).
8. O. G. Okhotnikov, L. Gomes, N. Xiang, T. Jouhti, and A. B. Grudinin, "Mode-locked ytterbium fiber laser tunable in the 980-1070-nm spectral range," Opt Lett. **28**, 1522-1524 (2003).
9. K. O. Hill, Y. Fujii, D. C. Johnson, and B. S. Kawasaki, "Photosensitivity in optical fiber waveguides: Application to reflection filter fabrication," Appl. Phys. Lett. **32**, 647-649 (1978).
10. K. O. Hill, B. Malo, F. Bilodeau, D. C. Johnson, and J. Albert, "Bragg gratings fabricated in monomode photosensitive optical fiber by UV exposure through a phase mask," Appl. Phys. Lett. **62**, 1035-1037 (1993).
11. M. L. Dennis and I. N. Duling III, "Experimental study of sideband generation in femtosecond fiber lasers," IEEE J. Quantum Electron. **30**, 1469-1477 (1994).
12. Y. Chen, F. X. Kärtner, U. Morgner, S. H. Cho, H. A. Haus, E. P. Ippen, and J. G. Fujimoto, "Dispersion-managed mode locking," J. Opt. Soc. Am. B **16**, 1999-2004 (1999).
13. T. Schreiber, B. Ortaç, J. Limpert, and A. Tünnermann, "On the study of pulse evolution in ultra-short pulse mode-locked fiber lasers by numerical simulation," Opt. Express **15**, 8252-8262 (2007).
14. A. B. Grudinin, D. J. Richardson and D. N. Payne, "Energy quantisation in figure eight fibre laser," Electron. Lett. **28**, 67-68, (1992).

1. Introduction

Supercontinuum sources based on the nonlinear broadening of spectrum in microstructured fiber present an attractive alternative to white light sources based on low-power broadband fluorescence, because they can offer radiation with very high spectral brightness and coherence. Many of the supercontinuum sources available today use solid-state femtosecond lasers for pumping the nonlinear media. Supercontinuum sources would benefit greatly if they are based entirely on all-fiber technology [1, 2]. However, fiber sources are either based on 1.55 μm seed lasers and do not extend into the wavelength range below 1 μm, which is required for biological applications, or they rely on environmentally sensitive high-power double clad technology with rather high noise level. Scaling the repetition rate of fiber laser system below 5 MHz would offer a compact and cost-effective core-pumped fiber oscillator with medium average power while with pulse energy sufficient for supercontinuum generation. The repetition rates are still >100 times higher than in Q-switched microchip lasers [3] and are, therefore, suitable for applications in optical coherence tomography.

The large group velocity dispersion of an optical fiber at wavelengths of 1 μm and below needs to be addressed in order to achieve short pulses from fiber lasers. Dispersion compensators based on fiber technology are highly advantageous because they allow for low-loss and compact cavities [4-6]. Among different solutions demonstrated to date, those based on photonic crystal fiber look most promising [5, 6]. Dispersion compensation using chirped fiber Bragg grating (CFBG) is another attractive method that benefits from the flexible and mature technology used for inscription of the gratings in optical fibers [7].

Here we demonstrate a practical all-fiber supercontinuum source using a picosecond soliton fiber laser as a pumping source with a chirped fiber Bragg grating (CFBG) dispersion compensator. The device is based entirely on low-cost core-pumping technology. The soliton seed laser delivers ~1.6 ps pulses which are, by our knowledge, the shortest pulses reported to date from an all-fiber laser using dispersion compensation by CFBG. The chirped grating offers large anomalous dispersion and allows for a robust soliton pulse regime in a long-length cavity, resulting in a low repetition rate. The refined fiber grating technology allows for novel low repetition-rate oscillator with medium average power but with pulse energy sufficient to exploit efficiently the nonlinear effects in photonic crystal fiber (PCF). The developed pulse source with 1.8 ps width and 2.6 MHz repetition rate used instead of high-power double-clad technology demonstrates an octave-spanning supercontinuum.

2. Mode-locked master oscillator using chirped Bragg grating dispersion compensator

The experimental setup of the supercontinuum source is shown in Fig. 1. The linear cavity of the mode-locked fiber laser (master oscillator) comprises 70 cm of Yb-doped fiber with 500 dB/m absorption at 980 nm pumped with a 980-nm single mode laser diode through a dichroic fiber coupler. A butt-coupled semiconductor saturable absorber mirror (SAM) acting as a

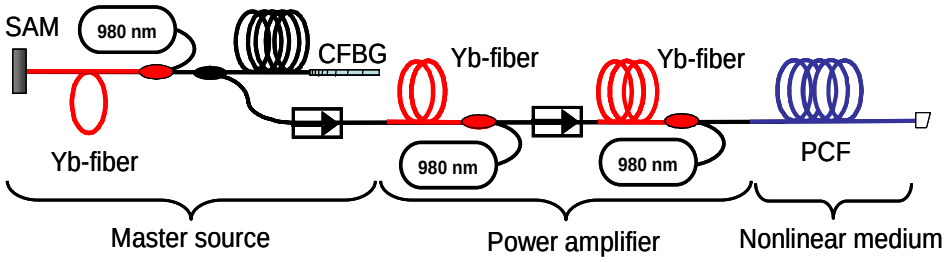

Fig. 1. All-fiber supercontinuum source setup. CFBG: Chirped fiber Bragg grating, PCF: Photonic crystal fiber, SAM: Semiconductor saturable absorber mirror.

cavity end reflector ensured reliable self-starting of the passive mode-locking. The SAM used in this study has been described in detail earlier [8]. The other end of the cavity is terminated by a CFBG.

The CFBG was imprinted into the core of a H_2-loaded single-mode fiber using phase-mask technique [9, 10]. The fiber was exposed to 248 nm ultraviolet light from a KrF excimer laser through the phase mask with a length of 10 mm using a beam scanning technique. Optimization of the scanning and writing parameters allowed to a broadband and exceptionally flat reflection response of the CFBG to be achieved. The reflectivity of the CFBG with the center wavelength of 1042 nm was measured to be >97% over the bandwidth from 1030 nm to 1054 nm, as seen from Fig. 2. The grating dispersion was estimated from the measurements to be 4.5 ps/nm using soliton sideband in the mode-locked pulse spectrum [11]. The dispersion of the grating at the wavelength around 1 μm could compensate for the normal dispersion of the standard single-mode fiber with a length of over 50 meters.

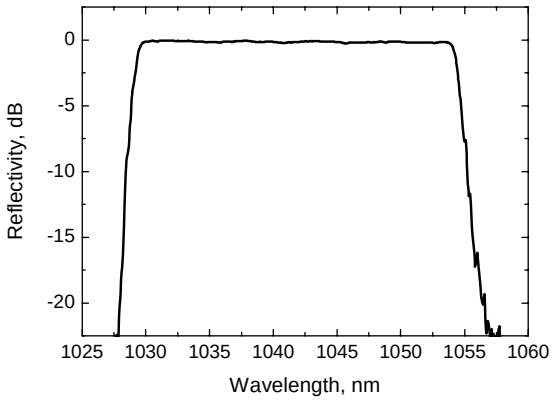

Fig. 2. Reflectivity of the chirped fiber Bragg grating.

The characteristics of the mode-locked pulses generated from the laser with a cavity length corresponding to a repetition rate of 47 MHz are presented in Fig. 3. The laser emits low-noise pulses with duration of 1.95 ps (FWHM) with the spectral resonances, so-called Kelly side-bands that apparently indicates operation in the soliton regime [11].

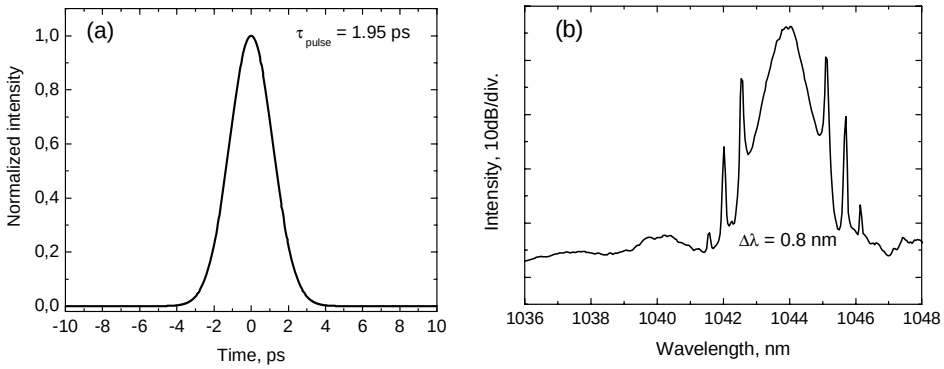

Fig. 3. (a). Autocorrelation and (b) spectrum of the pulses with a repetition rate of 47 MHz generated by the fiber oscillator with a chirped fiber Bragg grating as a dispersion compensator. Mode-locking is initiated by the semiconductor saturable absorber mirror.

To decrease the pulse repetition rate and to maximize the pulse energy after amplification, a piece of single-mode fiber was added to the cavity. The effect of the cavity length on the pulse width and time-bandwidth product was experimentally investigated. The results are summarized in Fig. 4. As can be seen, the pulse width ranges from 2 ps to 1.6 ps and the time-bandwidth product from 0.42 to 0.49 when the length of the fiber cavity varies from 2.5 m to 37 m. 1.6 ps duration pulses has been achieved for a cavity length of 29 m corresponding to a

pulse repetition rate of ~3.5 MHz. These are the shortest pulse reported to date for a fiber laser using a CFBG dispersion compensator.

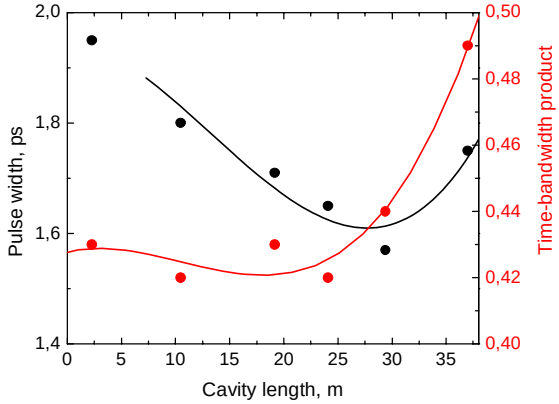

Fig. 4. Measured pulse width and time-bandwidth product for different cavity lengths / cavity anomalous dispersion of the laser.

Some increase of the time-bandwidth product with the length of fiber inserted into the cavity, seen from Fig. 4, is due to strong temporal and spectral evolution in a long cavity, as confirmed by the numerical simulation presented below [12].

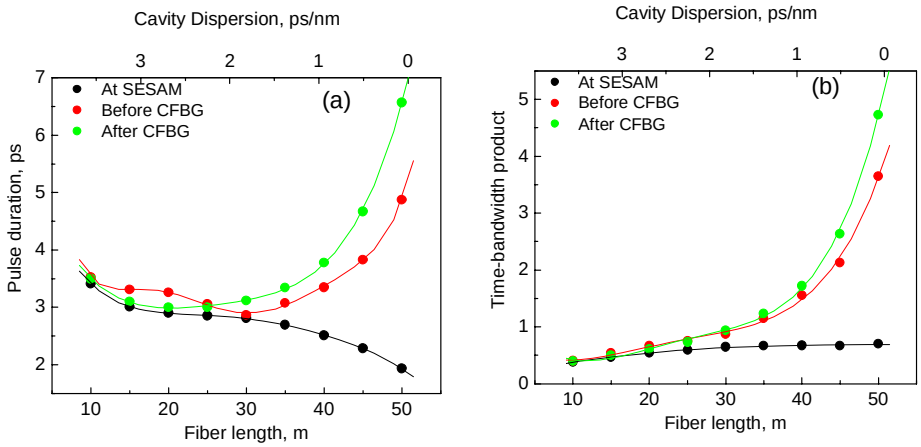

Fig. 5. (a). Simulated pulse width and (b) time-bandwidth product for different fiber lengths and locations in the laser cavity

The results of the laser simulation presented in Fig. 5 validate the increase of the time-bandwidth product observed in the experiments. The pulse generation and propagation in a fiber laser was described by the nonlinear Schrödinger equation including the effects of dispersion, loss, parabolic gain-bandwidth profile, and SESAM considered as a two-level system. The simulations start from noise and run for a sufficient number of consecutive round trips through the cavity elements until a steady-state is reached [13]. These elements include the saturable absorber, active and passive fiber, and the CFBG. The simulation shows that pulse duration and time-bandwidth product exhibit strong variations in dispersion managed soliton fiber lasers when the value of fiber dispersion becomes close to the value of the dispersion of the CFBG with opposite sign, i.e. the total cavity dispersion approaches zero value. Figure 5(a) shows the pulse duration and Fig. 5(b) the time-bandwidth product for different fiber lengths at different cavity locations. In particular, the pulses are slightly down-

chirped at the SAM position, strongly up-chirped before the CFBG, and strongly down-chirped after the CFBG. While the pulse duration continues to decrease gradually with increasing fiber length close to the SAM, it starts to increase at locations near the CFBG. The simulation thus describes the observed increase of time-bandwidth product and pulse duration for fiber lengths longer than ~20 m, since the laser output was set at substantial distance from SAM, as seen from Fig. 1.

With an increase in the length of the fiber in the cavity, the laser tends to oscillate in multiple pulse regime. This behavior is generally expected with soliton pulse laser [14]. For cavity lengths longer than ~37 meters single-pulse operation was not achievable. To achieve pulse energy sufficient for generation octave-spanning spectrum broadening, power scaling of the master oscillator has been performed using a two-stage ytterbium fiber amplifier core-pumped with fiber-coupled 300-mW pump diodes, as shown in Fig. 1. The highly doped ytterbium fibers peak absorption of ~1000 dB/m at 980 nm have lengths of 70 cm and 1.5 m for the 1st and 2nd amplifier stages, respectively. Average output power for a single pulse regime was 1 mW and 78 mW, correspondingly after the first and the second amplifier stages. The changes in the pulse shape and spectrum after the first amplifier stage were found to be negligible owing to long dispersion and nonlinear lengths of 30 m and 400 m, respectively. The efficiency of the second amplifier stage depends on the seed power and was 33% for the strongest seed signal. Parasitic optical back-coupling between the seed laser and the amplifier stages was prevented with the use of fiber-pigtailed optical isolators.

3. Supercontinuum generator

The amplifier output was spliced to the photonic crystal fiber with 0.5-dB excess loss. The 15-m long photonic crystal fiber has a zero dispersion wavelength at 1065 nm and a nonlinear coefficient of 11 $(W\cdot km)^{-1}$. The master oscillator was optimized for the lowest repetition rate that still allows the multiple pulsing regime to be avoided, using the results presented in the previous section. Seed laser pulses with an energy of 0.004 nJ at a repetition rate of 2.6 MHz were extracted from the cavity with a 20% tap coupler. Figure 6 shows the spectrum (a) and the autocorrelation (b) of these pulses at the laser output (black lines). The autocorrelation reveals a pulse duration of ~1.8 ps assuming a Gaussian fit. The pulses from the master laser were then scaled in the two-stage power amplifier up to energy of 30 nJ. The spectrum and autocorrelation of the pulses at the amplifier output are also shown in Figs. 6(a) and 6(b) (red lines). The spectrum bandwidth increased to 30 nm after the amplifier, while the pulse broadened slightly but acquired a complicated shape, as seen from the Fig. 6.

The pulses from the power amplifier were then coupled to the nonlinear fiber. The spectra at the output of the PCF presented in Fig. 7 correspond to states with different numbers of pulses circulating in the cavity and, consequently, with different pulse energies. The central peak in the broadened spectrum corresponds to the unconverted pump radiation and contains about 34 % of the total power. The central peak is believed to be developed largely due to the mismatch between the lasing wavelength and the zero dispersion wavelength of the photonic crystal fiber equal to λ_{ZD}=1065 nm. Tuning the central wavelength of the CFBG reflectivity bandwidth, and consequently, the master oscillator operation wavelength toward λ_{ZD} is expected to improve the conversion efficiency [2].

Since an excessive pump power results in multiple pulsing, the amplifier was found to produce the highest pulse energy when the average output power was limited to 78 mW. With a single pulsed regime, the supercontinuum spectrum extends from 615 nm to 1700 nm (measured at 10-dB level). As seen from Fig. 7, the supercontinuum bandwidth decreases from 1085 nm observed for single-pulse operation to 500 nm for the 8-pulse regime, corresponding to the effective repetition rate of ~20 MHz. Compared to single-pulse

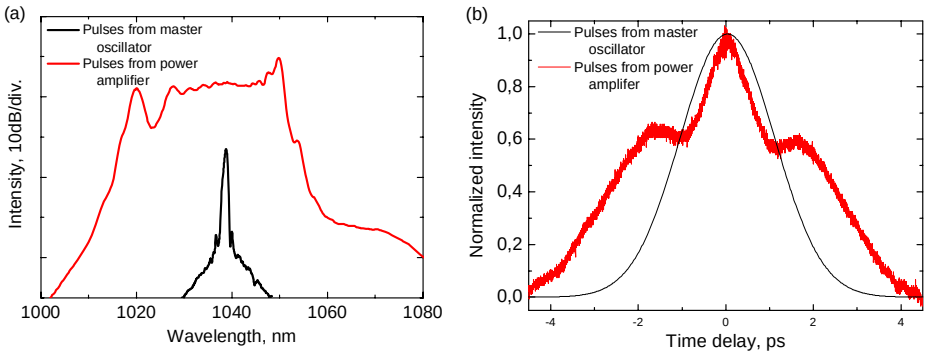

Fig. 6. (a). Spectrum and (b) autocorrelation of the 2.6 MHz repetition rate pulses from the fiber laser (black lines) and at the output of the power amplifier (red lines).

operation, the average power for 8-pulse operation increases slightly to 97 mW corresponding, however, to a substantial reduction in the pulse energy to 4.6 nJ.

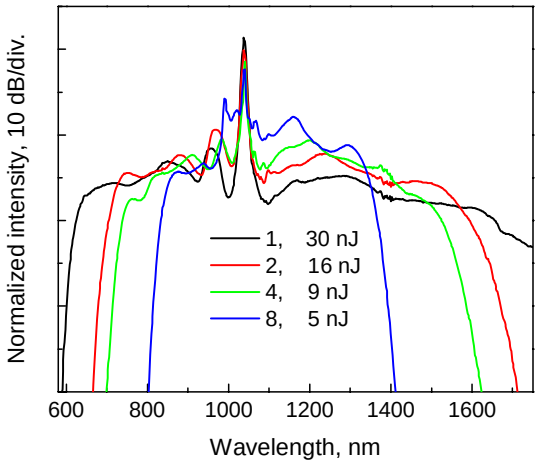

Fig. 7. Supercontinuum spectra for single, 2, 4 and 8 pulses circulating in the master laser cavity. Pulse energy ranges from 5 to 30 nJ, as indicated in the figure.

4. Conclusion

We have demonstrated a practical all-fiber supercontinuum source generating an octave-spanning spectrum. Both the soliton pulse regime and low fundamental repetition rate of ~3 MHz in a passively mode-locked ytterbium fiber laser have been achieved using a high-performance chirped fiber Bragg grating for dispersion control. The ytterbium-doped fiber laser is capable of producing 1.6 ps pulses, which are the shortest pulses reported to date using CFBG as a dispersion compensator in an Yb-doped fiber laser. Energy scaling of the master oscillator up to 30 nJ at 1040 nm was achieved in a core-pumped two-stage fiber amplifier. These pulses were then spectrally broadened in a photonic crystal fiber to form supercontinuum radiation ranging from 615 nm to 1700 nm. The fiber system demonstrated offers an attractive cost-effective solution for medium power broadband sources.

Acknowledgments

The authors acknowledge the support of the graduate school of Tampere University of Technology, the Finnish Foundation for Economic and Technology Sciences, the Ulla Tuominen Foundation, the Jenny and Antti Wihuri Foundation, and the Nokia Foundation.

Appendix 5

Publication 5

S. Kivistö, R Herda, and O. G. Okhotnikov, "Electronically tunable mode-locked Yb-doped fiber laser," *IEEE Photonics Technology Letters*, Vol. 20, No.1, pp. 51-53, 2008.

Electronically Tunable Yb-Doped Mode-Locked Fiber Laser

Samuli Kivistö, Robert Herda, and Oleg G. Okhotnikov

***Abstract*—We report a passively mode-locked picosecond Yb-doped fiber laser that is electronically tunable over 30 nm around 1.04 μm. The fiber laser with a tuning accuracy of better than 0.1 nm and a tuning time of as fast as $\sim$15 μs employs an acoustooptic filter. The semiconductor saturable absorber mirror used in a cavity with a frequency-shifted feedback improves noticeably the mode-locked operation.**

***Index Terms*—Acoustooptic filters, fiber lasers, mode-locked lasers, ytterbium.**

I. Introduction

In various applications accurate and wide wavelength tuning is needed often together with a short pulse regime. Tunable fiber lasers operating at 1 μm reported to date use, however, mechanical wavelength tuning by rotating intracavity gratings or mirrors [1], [2]. Among different technologies, using acoustooptic tunable filters (AOTFs) in conjunction with a semiconductor saturable absorber mirror (SESAM) looks very promising to achieve electronically tunable and ultrashort pulse Yb-doped fiber lasers [3]–[6]. Particularly an AOTF offers an opportunity for both electronic tuning and short-pulse operation through a frequency-shifted feedback (FSF) mechanism [6], [7]. FSF-based lasers reported to date deliver, however, rather long (few-picosecond) pulses without or with mechanical wavelength tuning [7]–[9].

In this letter, we demonstrate an Yb-doped fiber laser that employs an AOTF for the wavelength tuning and a SESAM for short pulse generation. The SESAM as a cavity end mirror provides a strong mode-locking mechanism that tolerates the filtering effects induced by the AOTF and results in enhanced pulse shortening that cannot be achieved with FSF mode alone. We report picosecond pulses continuously tunable over the range of 30 nm without any mechanical alignment of the cavity. Four- to five-picosecond pulses obtained with the frequency-shifted feedback configuration were compressed down to 1-ps transform-limited pulses by placing SESAM into the laser cavity. To our knowledge, this is a first demonstration of an electronically tunable mode-locked Yb-doped fiber laser delivering 1-ps pulses over the whole tuning range.

Manuscript received May 20, 2007; revised August 21, 2007. This work was supported by the Graduate School of Tampere University of Technology, by the Finnish Foundation for Economic and Technology Sciences, by the Ulla Tuominen Foundation, by the Jenny and Antti Wihuri Foundation, and by the Nokia Foundation.

The authors are with the Optoelectronics Research Centre, Tampere University of Technology, FIN-33101 Tampere, Finland (e-mail: samuli.kivisto@tut.fi).

Color versions of one or more of the figures in this letter are available online at http://ieeexplore.ieee.org.

Digital Object Identifier 10.1109/LPT.2007.910093

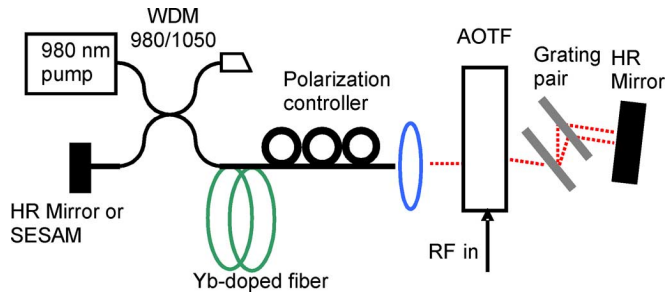

Fig. 1. Experimental configuration of the Yb-doped fiber laser electronically tunable with AOTF.

II. Experimental Details and Results

The experimental setup of the electronically tunable Yb-doped fiber laser is shown in Fig. 1. The linear cavity comprises 1 m of Yb-doped fiber with 400-dB/m absorption at 980 nm pumped with 980-nm laser diode through a dichroic fiber coupler. The cavity is completed by a highly reflective (HR) mirror and a SESAM. The AOTF directs a laser beam to the HR mirror, as shown in Fig. 1. The normal group velocity dispersion of the optical fiber around 1-μm wavelength range is compensated by a transmission grating pair with 1250 lines/mm and separation of 15 mm. A polarization controller is needed to adjust the polarization state in the cavity with birefringence induced by the AOTF and the grating compensator.

The AOTF was driven by the RF signal from a 15-bit direct digital synthesizer (DDS). The signal frequency from the DDS could be set with an accuracy of 15 kHz and a tuning time of $<$5 μs. The corresponding wavelength accuracy was better than 0.1 nm with a 3-dB bandwidth of the AOTF of 3-nm at 1040 nm. The amplitude and the frequency of the RF signal were controlled electronically using a computer. In the experiment performed here, we used frequency up-shifting by 65–70 MHz corresponding to the wavelengths between 1085 and 1015 nm, since the AOTF was optimized to operate in $+1$-diffraction order.

The Yb-doped fiber laser was first operated using a SESAM as a cavity reflector and without the AOTF. The SESAM used in this study was described in detail in [1]. The pulse spectrum, shown in Fig. 2, reveals the transform-limited 300-fs soliton pulses with a central wavelength of 1046 nm. The repetition rate was 40 MHz and the maximum output power $\sim$20 mW.

Then the AOTF was inserted into the cavity. The separation of the transmission gratings and the length of the cavity were kept

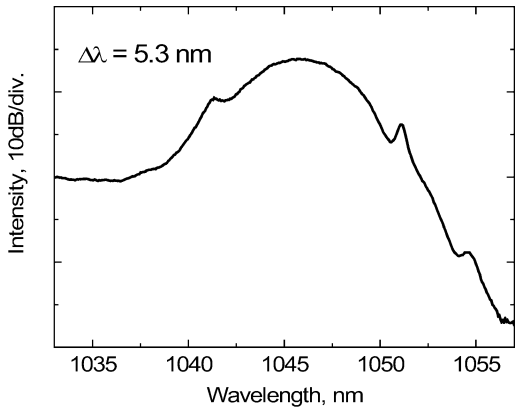

Fig. 2. Spectrum of 300-fs pulses without AOTF in the laser cavity. Transmission grating pair has been used as a dispersion compensator.

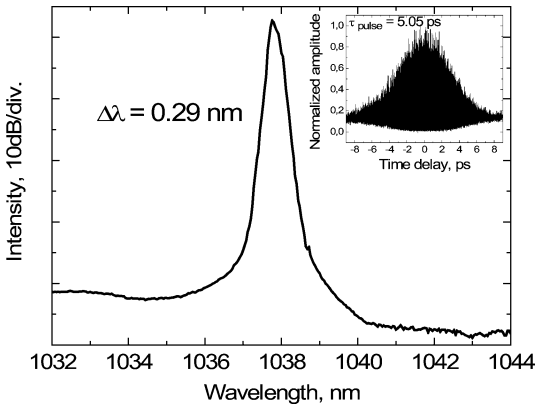

Fig. 3. Spectrum and interferometric autocorrelation of the pulses from the FSF Yb laser. The time-bandwidth product is 0.41 (Gaussian-fit of the pulse).

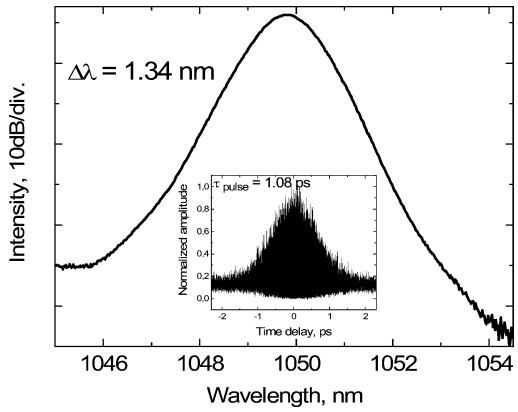

Fig. 4. Spectrum and interferometric autocorrelation of the pulse from the laser mode-locked by the SESAM. The time-bandwidth product is ∼0.40 assuming Gaussian-pulse shape.

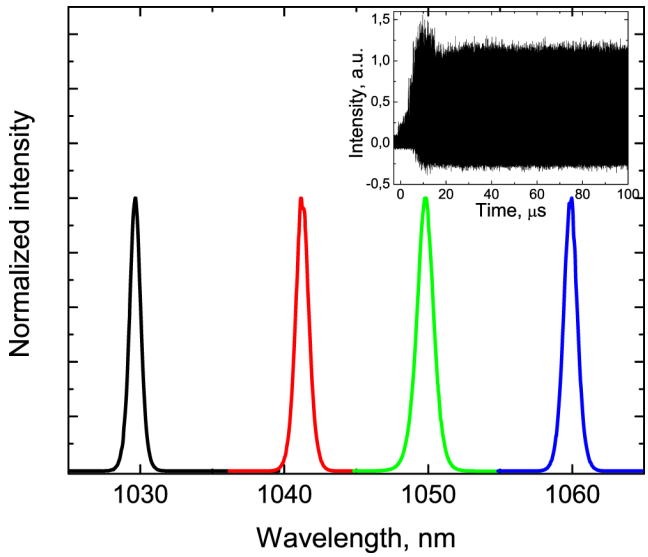

Fig. 5. Electronically tunable spectra with the SESAM as a mode-locking element. Build-up time measurement of the laser is shown as an inset.

unchanged. The fiber laser was primary tested with two HR mirrors terminating the cavity. Self-starting mode-locking with 4- to 5-ps pulses over the tuning range of 1029–1072 nm was observed. Typical interferometric autocorrelation trace and wavelength spectrum of the FSF laser are shown in Fig. 3. The FSF laser demonstrates self-starting pulse operation with the 43-nm tuning range achieved electronically by changing the driving frequency from the DDS without need for cavity or polarization alignment. The laser threshold was ∼40 mW of the pump power.

The mode-locked operation was then examined with the SESAM replacing one of the HR dielectric mirrors. The SESAM-assisted mode-locked operation in the cavity with frequency up-shifting resulted in 1-ps pulses tunable over 30 nm (1030–1060 nm), as seen in Figs. 4 and 5. The bandwidth of the pulse spectrum was ∼1.3 nm (FWHM) determined by the AOTF. The spectral filtering prevents further pulse shortening to 0.3 ps as obtained without the AOTF in the cavity. The laser threshold was between 30 and 60 mW over the tuning range. The maximum average output power of the laser was 47 mW. The build-up time of the steady state mode-locking and, consequently, the actual tuning speed of the laser was measured to be 10–25 μs (400–1000 cavity round-trips) depending on the pump power and the wavelength. The typical oscilloscope trace of the laser start-up after the AOTF switching is shown as an inset of Fig. 5.

The mechanism of pulse shaping using SESAM and AOTF was further investigated using numerical simulations. The pulse generation and propagation in a fiber laser was described by the nonlinear Schrödinger equation including the effects of dispersion, loss, parabolic gain-bandwidth profile, and SESAM considered as a two-level system. The AOTF was simulated by a bandpass filter and a frequency shifter. The pulse shapes and the spectra obtained from the computer simulation are shown in Figs. 6 and 7. The simulation revealed that the laser mode-locked by the saturable absorber without spectral filtering produces 250 fs pulses with 4.5-nm spectral width. When replacing the SESAM by the AOTF, the pulse duration increases up to 3.7 ps with a corresponding spectral width of 0.35 nm. The pulse shortening by AOTF is, therefore, not strong enough to combat its spectral bandwidth. On the contrary, the spectral broadening up to 1.4 nm achieved with the SESAM + AOTF scheme results in a pulse compression down to 1.1 ps. Simulations predict that

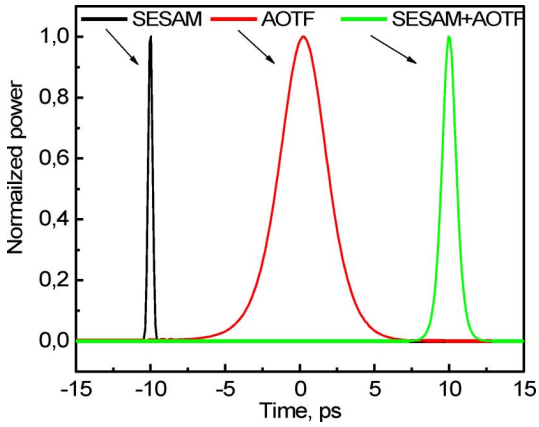

Fig. 6. Simulated pulse shapes for the mode-locked fiber laser for SESAM, AOTF, and SESAM + AOTF cavity configurations.

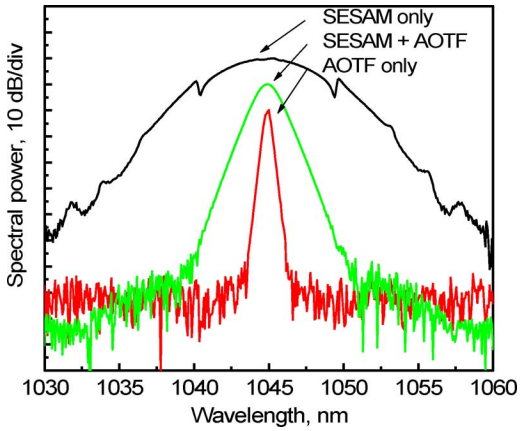

Fig. 7. Simulated pulse spectra corresponded to the simulated pulse shapes shown in Fig. 6.

360-fs pulses could be generated with the bandwidth of the filter increased from 3 to 10 nm.

The tunable performance of the frequency-shifted feedback mode-locked laser was further studied in detail experimentally with and without SESAM assistance. The results are plotted in Fig. 8 where we see the pulsewidth, spectral width, and the output power measured over the tuning range. As can be seen, the laser employing the SESAM delivers ∼4 times shorter pulses with only minor penalty to the output power as compared to the FSF-based laser. This indicates the efficient pulse shortening provided by the SESAM as compared with the FSF mechanism that allows us to cope with spectral filtering induced by the AOTF. The decrease in the pulsewidth seen in Fig. 8 is due to the increase of the AOTF bandwidth towards longer wavelengths which enables broader spectra to be formed.

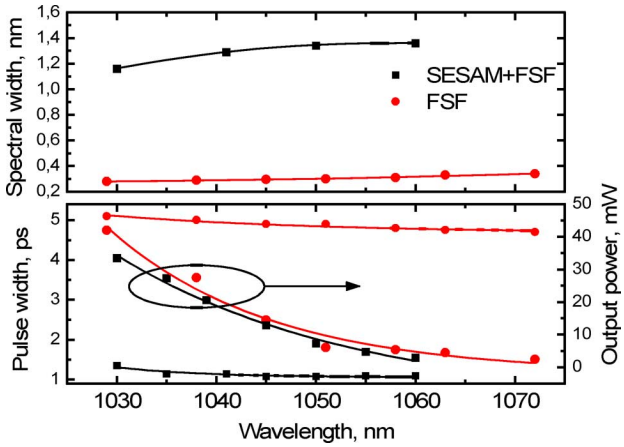

Fig. 8. Measured spectral width, pulsewidth, and output power versus wavelength for the FSF laser and for the laser mode-locked by the SESAM (SESAM + FSF). Pump power is 210 mW. Solid lines are the fittings for the experimental data.

III. Conclusion

We have demonstrated an electronically tunable mode-locked Yb-doped fiber laser using an AOTF and saturable absorber mirror. We show that SESAM improves notably the mode-locking of the frequency-shifted feedback owing to efficient mechanism of pulse shortening. The fast (∼10–25 μs) continuous wavelength tuning of 1-ps pulses was achieved over the wavelength range of 1030–1060 nm.

References

[1] O. G. Okhotnikov, L. Gomes, N. Xiang, T. Jouhti, and A. B. Grudinin, "Mode-locked ytterbium fiber laser tunable in the 980–1070-nm spectral range," *Opt. Lett.*, vol. 28, pp. 1522–1524, 2003.

[2] J. Porta, A. B. Grudinin, Z. J. Chen, J. D. Minelly, and N. J. Traynor, "Environmentally stable picosecond ytterbium fiber laser with a broad tuning range," *Opt. Lett.*, vol. 23, pp. 615–617, 1998.

[3] F. Ö. Ilday, J. R. Buckley, H. Lim, F. W. Wise, and W. G. Clark, "Generation of 50-fs 5-nJ pulses at 1.03 μm from a wave-breaking-free fiber laser," *Opt. Lett.*, vol. 28, pp. 1365–1367, 2003.

[4] A. Isomäki and O. G. Okhotnikov, "Femtosecond soliton mode-locked laser based on ytterbium-doped photonic bandgap fiber," *Opt. Express*, vol. 14, pp. 9238–9243, 2006.

[5] R. Herda and O. G. Okhotnikov, "Effect of amplified spontaneous emission and absorber mirror recovery time on the dynamics of mode-locked fiber lasers," *Appl. Phys. Lett.*, vol. 86, no. 1, p. 011113, 2005.

[6] S. H. Chang, I. K. Hwang, B. Y. Kim, and H. G. Park, "Widely tunable single-frequency Er-doped fiber laser with long linear cavity," *IEEE Photon. Technol. Lett.*, vol. 13, no. 4, pp. 287–289, Apr. 2001.

[7] J. M. Sousa and O. G. Okhotnikov, "Short pulse generation and control in Er-doped frequency-shifted-feedback lasers," *Opt. Commun.*, vol. 183, pp. 227–241, 2000.

[8] L. Lefort, A. Albert, V. Couderc, and A. Barthélémy, "Highly stable 68-fs pulse generation from a stretched-pulse Yb^{3+}-doped fiber laser with frequency shifted feedback," *IEEE Photon. Technol. Lett.*, vol. 14, no. 12, pp. 1674–1676, Dec. 2002.

[9] S. U. Alam and A. B. Grudinin, "Tunable picosecond frequency-shifted feedback fiber laser at 1550 nm," *IEEE Photon. Technol. Lett.*, vol. 16, no. 9, pp. 2012–2014, Sep. 2004.

Appendix 6

Publication 6

S. Kivistö, J. Puustinen, M. Guina, O. G. Okhotnikov, and E. M. Dianov, "Tunable mode-locked bismuth-doped soliton fibre laser," *IEE Electronics Letters*, Vol. 44, No. 25, pp. 1456-1458, 2008.

Tunable modelocked bismuth-doped soliton fibre laser

S. Kivistö, J. Puustinen, M. Guina, O.G. Okhotnikov and E.M. Dianov

A modelocked bismuth-doped soliton fibre laser is reported. A stable passively modelocked operation in an anomalous dispersion regime is achieved using a dilute nitride (GaInNAs)-based semiconductor saturable absorber mirror and a transmission grating pair for dispersion compensation. The laser generated 0.9 ps soliton pulses with a repetition rate of 7.5 MHz and wavelength tunable from 1153–1170 nm. These are the shortest pulses obtained so far from Bi-doped fibre lasers.

Introduction: Ultrafast modelocked fibre lasers based on neodymium, ytterbium, erbium, thulium, and thulium-holmium doped active fibres have been proved to generate high quality short optical pulses in a broad wavelength range [1–5]. However, the development of practical ultrafast fibre lasers in the 1150–1400 nm window has lacked suitable gain fibres. Lasers operating in this wavelength range are needed for various applications in optical communications as well as for generating visible short pulses at yellow–red by frequency doubling [6].

Recently, the first bismuth-doped fibres and fibre laser have been reported to offer optical amplification and broad emission spectra in the range 1100–1300 nm [7–9]. High power continuous wave Bi-doped fibre lasers have been developed by employing active fibres with lengths of a few tens of metres [6, 10]. The requirement for using a long length Bi-doped fibre, determined by the relatively low values of pump absorption and gain coefficients, is an undesirable feature in modelocked systems that would favour a short fibre cavity. Preliminary investigations of short pulse generation in a mode-locked Bi-doped fibre laser employing a dilute nitride semiconductor saturable absorber mirror (SESAM) led to the generation of pulses with duration of ~50 ps [11]. Owing to the large normal dispersion of the long-length cavity, narrowband fibre Bragg grating reflector and non-optimised SESAM in this demonstration, the pulse has a low quality and a narrow spectral bandwidth.

In this Letter, we demonstrate a modelocked soliton Bi-doped fibre laser delivering stable ~0.9 ps pulses with a repetition rate of 7.5 MHz and tunable from 1153–1170 nm. The short pulse operation is initiated by a fast dilute nitride based SESAM. The operation in a soliton regime was achieved using careful dispersion management with a transmission grating pair and an improved Bi-doped fibre allowing for the cavity with a reduced length. To our knowledge, this is the first demonstration of modelocked Bi-doped fibre laser operating in a soliton regime and delivering the shortest pulses.

Experimental: The schematic of the bismuth-doped fibre laser is shown in Fig. 1. The laser cavity comprises 12 m of Bi-doped silicate glass fibre with an absorption of ~1.2 dB/m at the pump wavelength of 1062 nm, a 1062/1165 pump coupler, and a fibre loop output mirror with ~95 % reflectivity at the lasing wavelength. The laser was core-pumped with a 1 W Yb-doped singlemode fibre laser.

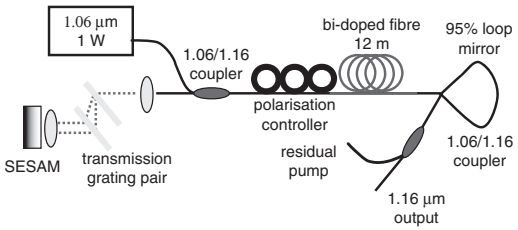

Fig. 1 *Cavity setup of modelocked Bi-doped fibre laser*

The Bi-doped silica fibre was drawn from a preform synthesised by the surface-plasma chemical vapour deposition (SPCVD) method under oxygen deficiency. The core glass was composed of 97 mol:% of SiO_2 and 3 mol:% of Al_2O_3. The bismuth concentration in the core glass was $\sim 3 \times 10^{18}$ cm^{-3}. The glass composition and the bismuth concentration were determined by an X-ray microprobe analysis. The fibre has an outer diameter of 125 μm, a core diameter of 8.4 μm, a core/cladding refractive index difference of $\Delta n = 5.5 \times 10^{-3}$, and a cutoff wavelength of ~1100 nm [12].

The length of the doped fibre was optimised in order to achieve efficient pump absorption and, consequently, sufficient gain, while minimising the length and dispersion of the fibre section of the cavity. The splice loss to a standard singlemode fibre was ~0.3 dB. The overall cavity losses were further minimised using a loop mirror and a pump coupler with high reflectivity and extinction ratio, respectively. An additional dichroic fibre coupler was used at the output of the laser to separate the residual pump and the signal light.

The normal group velocity dispersion (GVD) of the optical fibre at 1.16 μm wavelength range was compensated for by a transmission grating pair with 1250 lines/mm and a grating separation of ~19 mm. A polarisation controller was used to prevent the decrease in the diffraction efficiency of the grating pair. The GaInNAs-based semiconductor saturable absorber mirror grown by solid source molecular beam epitaxy ensured a self-starting passive modelocking [13]. The SESAM consisted of four GaInNAs quantum wells with a width of 6 nm grown on top of 24.5 pair GaAs/AlAs DBR. The DBR stopband had a centre wavelength of ~1140 nm with approximately a 150 nm bandwidth. The absorption recovery time of the SESAM was ~2 ps.

Results: Our cavity design enabled stable short-pulse operation with a repetition rate of 7.5 MHz. A typical pulse train observed with an oscilloscope is shown in Fig. 2. The autocorrelation trace and the corresponding sech^2-fit, shown in Fig. 3, reveal a pulse duration of 0.94 ps. The aperture of the objective, focusing the beam onto SESAM, provides spatial filtering of wavelength components dispersed by the grating pair. A continuous wavelength tuning, in the range 1153–1170 nm, could be achieved by moving the objective in the transverse direction. Fig. 4 presents the tunable spectra with spectral width of ~2.0 nm. The average cavity dispersion was estimated to be ~−0.4 ps^2 [14]; it consists of double-pass fibre dispersion of ~0.3 ps^2 and double-pass grating dispersion of ~− 0.7 ps^2. The typical pulse energy of the laser was ~0.2 nJ. At the loop mirror output the pulses acquire a small chirp resulting in a time–bandwidth product of 0.40. This small chirp could be expected from the cavity dispersion map, which includes pulse propagation over long fibre in the cavity and in an output pigtail that comprises an additional fibre coupler for separation of residual pump light.

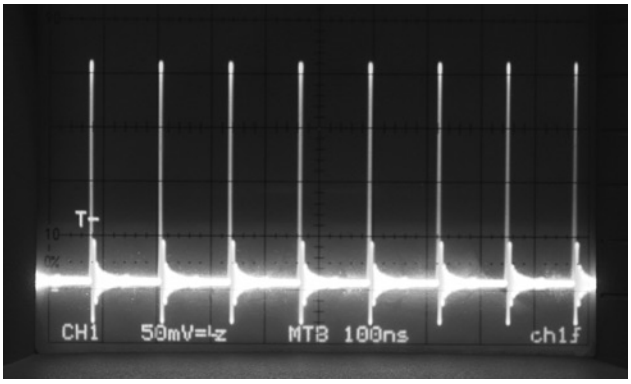

Fig. 2 *Oscilloscope picture of generated pulse train*

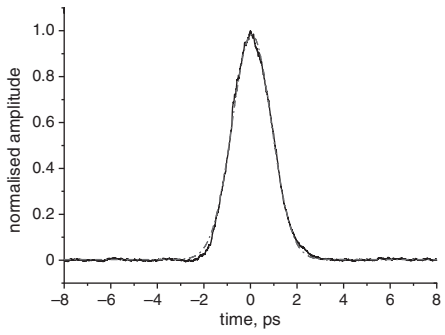

Fig. 3 *Autocorrelation trace (line) fitted with sech^2 function (dashed line)*
Pulse width is 0.94 ps

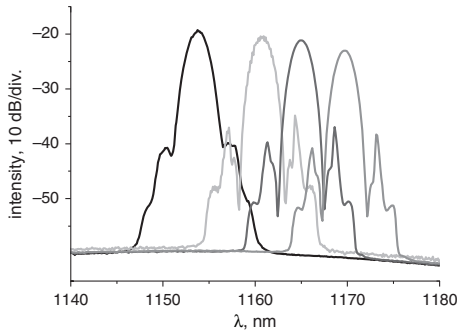

Fig. 4 *Tunable optical spectra*
Spectral width is 2 nm

Conclusion: A modelocked subpicosecond soliton Bi-doped fibre laser is demonstrated. The laser delivers nearly transform-limited ~0.9 ps pulses tunable in the wavelength range 1153–1170 nm. These record short pulses from a Bi-doped fibre laser are achieved with careful cavity design incorporating a fast dilute nitride SESAM and a transmission grating pair. This is an important step towards practical demonstration of pulsed Bi-doped fibre lasers operating in the 1150–1480 nm range.

Acknowledgments: The authors acknowledge the support of the graduate school of Tampere University of Technology, the Finnish Foundation for Economic and Technology Sciences, the Jenny and Antti Wihuri Foundation, the Nokia Foundation, the Emil Aaltonen Foundation, and the Elisa Foundation. The authors thank A. V. Kholodkov and K. M. Golant for fabricating the Bi-doped fibre, C. Thür for manufacturing the fibre couplers and the loop mirror and V. M. Korpijärvi for his help with epitaxial growth.

1 October 2008
Electronics Letters online no: 20089831
doi: 10.1049/el:20089831

S. Kivistö, J. Puustinen, M. Guina and O.G. Okhotnikov (*Optoelectronics Research Centre, Tampere University of Technology, PO Box 692, Tampere FIN-33101, Finland*)

E-mail: samuli.kivisto@tut.fi

E.M. Dianov (*Fiber Optics Research Center, Russian Academy of Sciences, 38 Vavilov Street, Moscow 119333, Russia*)

M. Guina: Also with RefleKron Ltd., Muotialankuja 5 C5, 33800 Tampere, Finland

References

1 Okhotnikov, O.G., Gomes, L., Xiang, N., Jouhti, T., and Grudinin, A.B.: 'Mode-locked ytterbium fibre laser tunable in the 980-1070-nm spectral range', *Opt. Lett.*, 2003, **28**, pp. 1522–1524
2 Okhotnikov, O.G., Jouhti, T., Konttinen, J., Karirinne, S., and Pessa, M.: '1.5-μm monolithic GaInNAs semiconductor saturable-absorber mode locking of an erbium fibre laser', *Opt. Lett.*, 2003, **28**, pp. 364–366
3 Rusu, M., Karirinne, S., Guina, M., Grudinin, A.B., and Okhotnikov, O.G.: 'Femtosecond neodymium-doped fibre laser operating in the 894–909 nm spectral range', *IEEE Photonics. Technol. Lett.*, 2004, **16**, pp. 1029–1031
4 Nelson, L.E., Ippen, E.P., and Haus, H.A.: 'Broadly tunable sub-500 fs pulses from an additive-pulse mode-locked thulium-doped fibre ring laser', *Appl. Phys. Lett.*, 1995, **67**, pp. 19–21
5 Kivistö, S., Hakulinen, T., Guina, M., and Okhotnikov, O.G.: 'Tunable Raman soliton source using mode-locked Tm-Ho fibre laser', *IEEE Photonics. Technol. Lett.*, 2007, **19**, pp. 934–936
6 Dianov, E.M., Shubin, A.V., Melkumov, M.A., Medvedkov, O.I., and Bufetov, I.A.: 'High-power CW bismuth fibre laser', *J. Opt. Soc. Am. B*, 2007, **24**, pp. 1749–1755
7 Dvoyrin, V.V., Mashinsky, V.M., Dianov, E.M., Umnikov, A.A., Yashkov, M.V., and Guryanov, A.N.: 'Absorption, fluorescent and optical amplification in MCVD Bismuth-doped silica glass optical fibres'. Proc. of 31 ECOC, Glasgow, UK, 2005, pp. 949–950
8 Haruna, T., Kakui, M., Taru, T., Ishikawa, S., and Onishi, M.: 'Silica-based bismuth-doped fibre for ultra broadband light-source and optical amplification around 1.1 μm'. Proc. Optical Amplifiers and their Applications Topical Meeting, Budapest, August 2005 (paper MC3)
9 Dianov, E.M., Dvoyrin, V.V., Mashinsky, V.M., Umnikov, A.A., Yashkov, M.V., and Guryanov, A.N.: 'CW bismuth fibre laser', *Quantum Electron.*, 2005, **35**, pp. 1083–1084
10 Razdobreev, I., Bigot, L., Pureur, V., Favre, A., Bouwmans, G., and Douay, M.: 'Efficient all-fibre bismuth-doped laser', *Appl. Phys. Lett.*, 2007, **90**, 031103
11 Dianov, E.M., Krylov, A.A., Dvoyrin, V.V., Mashinsky, V.M., Kryukov, P.G., Okhotnikov, O.G., and Guina, M.: 'Mode-locked Bi-doped fibre laser', *J. Opt. Soc. Am. B*, 2007, **27**, pp. 1807–1808
12 Bufetov, I.A., Golant, K.M., Firstov, S.V., Kholodkov, A.V., Shubin, A.V., and Dianov, E.M.: 'Bismuth activated alumosilicate optical fibres fabricated by surface-plasma chemical vapor deposition technology', *Appl. Opt.*, 2008, **47**, pp. 4940–4944
13 Okhotnikov, O., and Pessa, M.: 'Dilute nitride saturable absorber mirrors for optical pulse generation', *J. Phys. Condens. Matter.*, 2004, **16**, S3107–S3120
14 Dennis, M.L., and Duling, I.N.: 'Experimental study of sideband generation in femtosecond fibre lasers', *IEEE J. Quantum Electron.*, 1994, **30**, pp. 1469–1477

Appendix 7

Publication 7

S. Kivistö, R. Gumenyuk, J. Puustinen, M. Guina, E. M. Dianov, and O. G. Okhotnikov, "Mode-locked Bi-doped all-fiber laser with chirped fiber Bragg grating," *IEEE Photonics Technology Letters*, Vol 21, No. 9, pp. 599-601, 2009.

Mode-Locked Bi-Doped All-Fiber Laser With Chirped Fiber Bragg Grating

Samuli Kivistö, Regina Gumenyuk, Janne Puustinen, Mircea Guina, Evgeny M. Dianov, and Oleg. G. Okhotnikov

***Abstract*—We demonstrate a Bi-doped fiber laser with dispersion compensation provided by a linearly chirped fiber Bragg grating. Reliable self-starting mode-locking was achieved by using an InGaAsN semiconductor saturable absorber mirror. The all-fiber laser generated short optical pulses with a duration of 1.9 ps at ∼1165 nm. The large anomalous dispersion of the fiber grating ensured operation in the soliton pulse regime. This in turn enabled us to increase the repetition rate of the output pulse train up to 100.6 MHz via harmonic mode-locking.**

***Index Terms*—Bismuth, fiber Bragg gratings, fiber lasers, mode-locked lasers.**

I. Introduction

AMONG different techniques for dispersion compensation implemented in ultrashort-pulse fiber lasers, those based on fiber technology are most attractive because they preserve the low-loss and compact characteristics of an all-fiber cavity. However, recently demonstrated dispersion compensators based on photonic crystal and photonic bandgap fiber bring additional losses to the laser cavity due to the distinctive mode mismatch with standard single-mode fibers [1], [2]. Dispersion compensation using chirped fiber Bragg grating (CFBG) is another attractive method that benefits from the flexible and mature technology used for inscription of the gratings in optical fibers. CFBGs have been used to compensate the fiber dispersion or to produce positively chirped pulses in Yb-doped mode-locked fiber lasers at 1 μm [3]–[6].

Recent work in the field of gain fibers has led to the demonstration of active fibers with gain at 1100- to 1400-nm wavelength range by using Bi–ion as dopant [7], [8]. Continuous-wave Bi-doped fiber lasers have been demonstrated to deliver output powers with watt-level [9], [10]. The development of mode-locked Bi-fiber lasers has, however, remained hindered due to the relatively low value of the gain coefficient in the fiber, rendering a long-length cavity to achieve the sufficient gain. Preliminary investigations of pulse generation in a mode-locked Bi-doped fiber laser operating with net normal cavity dispersion regime without dispersion compensation led to the generation of large pedestal pulses with a duration of ∼50 ps [11].

In this letter, we report the first demonstration of a Bi-doped all-fiber laser with dispersion compensation provided by a CFBG. The length of the Bi-doped fibers required to generate sufficient gain was ∼15 m resulting in a large cavity dispersion that was balanced by the CFBG in order to exploit the soliton pulse shaping. The compact and low-loss all-fiber laser demonstrated in this study delivers 1.9-ps pulses at a fundamental repetition rate of ∼6 MHz and a wavelength of ∼1165 nm. We also demonstrate harmonic mode-locking, which enables us to increase the pulse repetition rate. The laser could operate in mode-locking regime with a repetition rate of up to 100.6 MHz corresponding to 16th harmonic of the cavity frequency. This value is one order of magnitude higher than the highest repetition rate reported previously for mode-locked Bi-lasers.

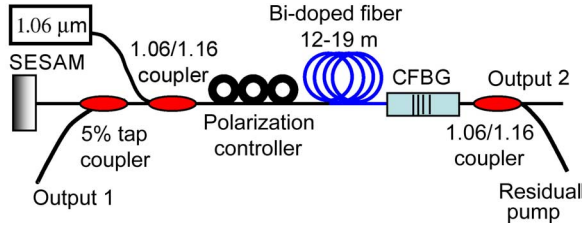

Fig. 1. Bi-doped all-fiber laser setup. The self-starting mode-locked operation was initiated by an InGaAsN-based SESAM. The soliton regime was provided by a CFBG.

II. Experimental Details and Results

The experimental setup of the Bi-doped all-fiber laser is shown in Fig. 1. The linear cavity laser comprised Bi-doped fiber with ∼1.2-dB/m absorption at 1062 nm pumped with a single-mode Yb-fiber system through a 1062/1165-nm dichroic fiber coupler. A butt-coupled semiconductor saturable absorber mirror (SESAM) acting as a cavity end reflector was used for self-starting passive mode-locking. The opposite end of the cavity was terminated by a CFBG, coupling 10% of the signal to the output. A 5% fiber tap splitter was used for characterization purposes. A polarization controller was used to optimize the laser operation. A pump-blocking fiber coupler was spliced to the output of the laser to separate the residual pump and the signal light.

The Bi-doped silica fiber was drawn from a preform synthesized by the surface-plasma chemical vapor deposition method

Manuscript received December 11, 2008; revised January 22, 2009. First published February 24, 2009; current version published April 17, 2009. This work was supported in part by the Graduate school of Tampere University of Technology, in part by the Finnish Foundation for Economic and Technology Sciences, in part by the Jenny and Antti Wihuri Foundation, in part by the Nokia Foundation, in part by the Emil Aaltonen Foundation, and in part by the Elisa Foundation.

S. Kivistö, R. Gumenyuk, J. Puustinen, M. Guina, and O. G. Okhotnikov are with the Optoelectronics Research Centre, Tampere University of Technology, FIN-33101 Tampere, Finland (e-mail: samuli.kivisto@tut.fi; regina.gumenyuk@tut.fi; janne.puustinen@tut.fi; Mircea.Guina@tut.fi; Oleg.Okhotnikov@tut.fi).

E. M. Dianov is with the Fiber Optics Research Center, Russian Academy of Sciences, 119333 Moscow, Russia (e-mail: dianov@fo.gpi.ru).

Color versions of one or more of the figures in this letter are available online at http://ieeexplore.ieee.org.

Digital Object Identifier 10.1109/LPT.2009.2015277

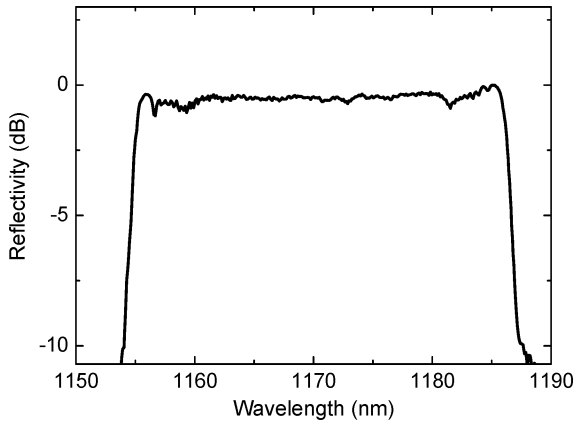

Fig. 2. Reflectivity response of the CFBG. The center wavelength is 1170 nm and the reflectivity is ∼90%.

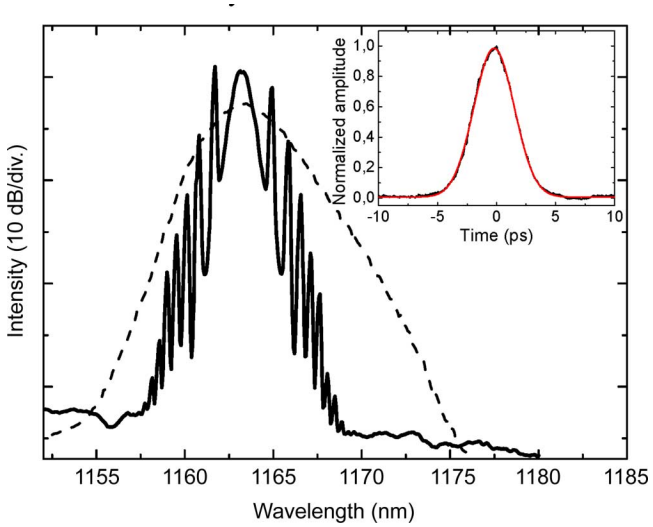

Fig. 3. Spectrum and autocorrelation (inset) of the pulses generated by the fiber oscillator with the CFBG as a dispersion compensator. The red line in the inset is the Sech^2-fitting giving the pulsewidth of ∼1.9 ps. The total cavity length was ∼21 m. Optical spectrum of the laser without dispersion compensation is shown by the dashed line.

under oxygen deficiency. The core glass was composed of 97 mol% of SiO_2 and 3 mol% of Al_2O_3. The Bi concentration in the core glass was $\sim 3 \cdot 10^{18}$ cm^{-3}. The glass composition and the bismuth concentration were determined by means of X-ray microprobe analysis. The fiber had an outer diameter of 125 μm, a core diameter of 8.4 μm, a core/cladding refractive index difference of $\Delta n = 5.5 \cdot 10^{-3}$, and a cutoff wavelength of ∼1100 nm [12]. The dispersion of the fiber at the wavelength of 1165 nm was calculated to be ~ -0.013 ps/(nm · m). The splice loss between the gain and a standard single-mode fiber was ∼0.3 dB.

The InGaAsN-based SESAM was grown by solid-source molecular beam epitaxy. The absorber section consisting of four InGaAsN quantum wells with a width of 6 nm was grown on the top of a 24.5 pair GaAs–AlAs distributed Bragg reflector (DBR). The DBR's stopband had a bandwidth of ∼150 nm and a center wavelength of ∼1140 nm. The absorption recovery time of the SESAM was measured to be ∼2 ps.

The CFBG was imprinted into the core of an H_2-loaded single-mode fiber using a phase-mask technique [13], [14]. The fiber was exposed to 248-nm ultraviolet light from a KrF excimer laser through a phase mask with a length of 10 mm using a beam scanning technique. Optimization of the scanning and writing parameters allowed for a broadband and flat reflection response of the CFBG to be achieved. The reflectivity of the CFBG ensuring the optimal feedback to the cavity and adequate output coupling was found to be ∼90%. The bandwidth of the grating ranged from 1155 to 1186 nm, as seen in Fig. 2. The grating dispersion was estimated to be ∼3.0 ps/nm using the soliton sidebands in the mode-locked pulse spectrum [15].

Mode-locking experiments were performed with different lengths of doped fiber. First a Bi-doped fiber with a length of ∼19 m was used; the overall cavity length was ∼21 m. The corresponding autocorrelation trace and the optical spectrum measured at Output 1 are shown in Fig. 3. The laser generated low-noise pulses of ∼1.9-ps duration (full-width at half-maximum) with Kelly spectral sidebands indicating the operation in the soliton regime. The spectral width and the calculated time-bandwidth product of the pulses were 0.95 nm and 0.40, respectively. The effect of the cavity length on the

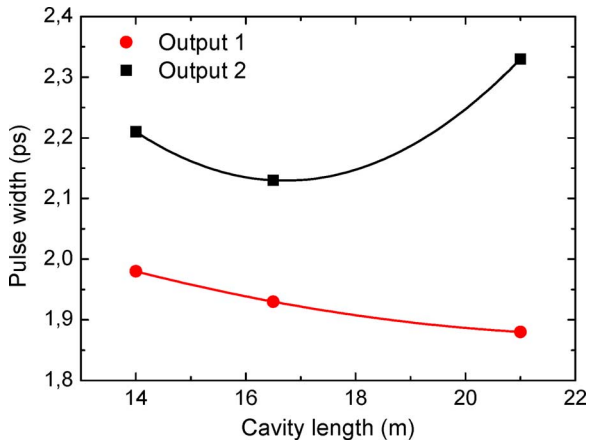

Fig. 4. Measured pulsewidth for different cavity lengths at different cavity outputs. Solid lines are the fittings.

pulse duration at Outputs 1 and 2 is illustrated in Fig. 4. While the pulse duration decreased gradually with an increase in the fiber length at the SESAM end, it started to increase for cavity lengths over ∼18–20 m at locations near the CFBG. The changes in the pulsewidth were expected due to strong temporal and spectral pulse reshaping in a long dispersion-managed fiber laser cavity [5], [16]. Particularly, the pulses were slightly down-chirped at the SESAM position, up-chirped before the CFBG, and down-chirped after reflection from the CFBG, as derived from the pulsewidth and time-bandwidth product observed at different cavity locations. The time-bandwidth product at Output 2 ranged from 0.5 to 0.6 depending on the cavity length. The threshold pump powers for the self-start of the mode-locking were ∼400, ∼350, and ∼300 mW for the cavity lengths of 14, 16.5, and 21 m, respectively. The maximum average output power was found to increase from 4 to 6 mW for 850 mW of launched pump power when the cavity length was increased from 14 to 21 m.

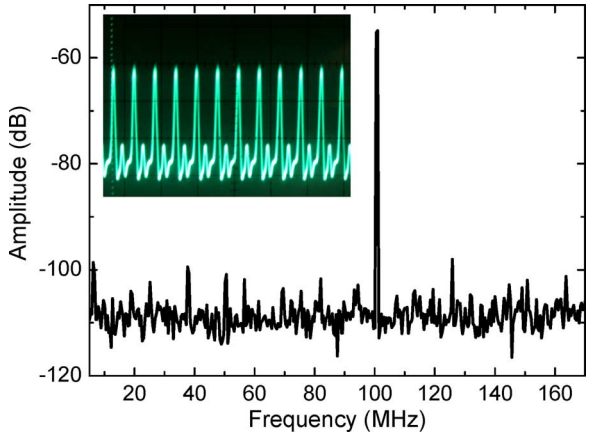

Fig. 5. Radio-frequency spectrum of the 16th harmonic frequency. The inset shows an oscilloscope picture of the pulse train at a repetition rate of 100.6 MHz.

The large net anomalous cavity dispersion promoted soliton breakup and allowed multiple soliton pulses to be formed. For certain positions of the polarization controller, the Bi-fiber laser operated with multiple soliton pulses having equal temporal spacing, i.e., highly ordered harmonic mode-locking [17]. After a build-up of the mode-locking, the soliton pulses, first randomly ordered or bunched, were transformed into a highly uniform periodic pulse train, demonstrating a strong repulsing force in the cavity [17]. The ordered mode-locking with harmonic number determined by the pump power was observed to be an inherent characteristic of the steady-state pulse regime. As a consequence, the repetition rate could be tuned from 6.3 MHz up to 100.6 MHz (corresponding to 16th harmonic of the cavity frequency) by varying the pump power. A radio-frequency spectrum of the 16th harmonic frequency is shown in Fig. 5. As can be seen, the adjacent modes are suppressed by more than 45 dB indicating the strong soliton pulse self-ordering effect in the cavity [17].

Mode-locked operation was also investigated without dispersion compensation by replacing the CFBG with a broadband fiber loop mirror having a ∼90% reflectivity at the laser wavelength. The recorded optical spectrum is shown in Fig. 3 (the dashed line). Without dispersion compensation, the laser operated only with a single pulse in the cavity having a large pulse pedestal that exceeded the autocorrelation scanning range of ∼200 ps.

III. Conclusion

We have reported a mode-locked Bi-doped all-fiber laser delivering 1.9-ps pulses. The dispersion compensation based on high-performance CFBG technology enabled laser operation in the soliton regime with a long-length cavity, typical for Bi-fibers with moderate gain. By taking advantage of harmonic mode-locking and soliton self-ordering mechanism, the repetition rate of the laser could be increased up to 100.6 MHz corresponding to a 16th harmonic fundamental cavity frequency.

Acknowledgment

The authors would like to thank A. V. Kholodkov and K. M. Golant for fabricating the Bi-fiber and S. Marcinkevicius for measuring the absorption recovery time of the SESAM.

References

[1] H. Lim, F. Ö. Ilday, and F. W. Wise, "Femtosecond ytterbium fiber laser with photonic crystal fiber for dispersion control," *Opt. Express*, vol. 10, pp. 1497–1502, 2006.

[2] A. Isomäki and O. G. Okhotnikov, "Femtosecond soliton mode-locked laser based on ytterbium-doped photonic bandgap fiber," *Opt. Express*, vol. 14, pp. 9238–9243, 2006.

[3] I. Hartl, G. Imeshev, L. Dong, G. C. Cho, and M. E. Fermann, "Ultra-compact dispersion compensated femtosecond fiber oscillators and amplifiers," in *Proc. Conf. Lasers & Electro-Optics (CLEO)*, 2005, pp. 1641–1643, Paper CThG1.

[4] O. Katz, Y. Sintov, Y. Nafcha, and Y. Glick, "Passively mode-locked ytterbium fiber laser utilizing chirped-fiber-Bragg-gratings for dispersion control," *Opt. Commun.*, vol. 269, pp. 156–165, 2007.

[5] S. Kivistö, R. Herda, and O. G. Okhotnikov, "All-fiber supercontinuum source based on a mode-locked ytterbium laser with dispersion compensation by linearly chirped Bragg grating," *Opt. Express*, vol. 16, pp. 265–270, 2008.

[6] B. Ortaç, M. Plötner, J. Limpert, and A. Tünnermann, "Self-starting passively mode-locked chirped pulse fiber laser," *Opt. Express*, vol. 15, pp. 16794–16799, 2007.

[7] V. V. Dvoyrin, V. M. Mashinsky, E. M. Dianov, A. A. Umnikov, M. V. Yashkov, and A. N. Guryanov, "Absorption, fluorescent and optical amplification in MCVD Bismuth-doped silica glass optical fibers," in *Proc. 31st ECOC*, Glasgow, 2005, vol. 4, pp. 949–950.

[8] I. Bufetov, S. Firstov, V. Khopin, O. Medvedkov, A. Guryanov, and E. Dianov, "Bi-doped fiber lasers and amplifiers for a spectral region of 1300–1470 nm," *Opt. Lett.*, vol. 33, pp. 2227–2229, 2008.

[9] E. M. Dianov, A. V. Shubin, M. A. Melkumov, O. I. Medvedkov, and I. A. Bufetov, "High-power CW bismuth fiber laser," *J. Opt. Soc. Amer. B*, vol. 24, pp. 1749–1755, 2007.

[10] A. B. Rulkov, A. A. Ferin, S. V. Popov, J. R. Taylor, I. Razdobreev, L. Bigot, and G. Bouwmans, "Narrow-line, 1178 nm CW bismuth-doped fiber laser with 6.4 W output for direct frequency doubling," *Opt. Express*, vol. 15, pp. 5473–5476, 2007.

[11] E. M. Dianov, A. A. Krylov, V. V. Dvoyrin, V. M. Mashinsky, P. G. Kryukov, O. G. Okhotnikov, and M. Guina, "Mode-locked Bi-doped fiber laser," *J. Opt. Soc. Amer. B*, vol. 27, pp. 1807–1808, 2007.

[12] I. A. Bufetov, K. M. Golant, S. V. Firstov, A. V. Kholodkov, A. V. Shubin, and E. M. Dianov, "Bismuth activated alumosilicate optical fibers fabricated by surface-plasma chemical vapor deposition technology," *Appl. Opt.*, vol. 47, pp. 4940–4944, 2008.

[13] K. O. Hill, Y. Fujii, D. C. Johnson, and B. S. Kawasaki, "Photosensitivity in optical fiber waveguides: Application to reflection filter fabrication," *Appl. Phys. Lett.*, vol. 32, pp. 647–649, 1978.

[14] K. O. Hill, B. Malo, F. Bilodeau, D. C. Johnson, and J. Albert, "Bragg gratings fabricated in monomode photosensitive optical fiber by UV exposure through a phase mask," *Appl. Phys. Lett.*, vol. 62, pp. 1035–1037, 1993.

[15] M. L. Dennis and I. N. Duling, III, "Experimental study of sideband generation in femtosecond fiber lasers," *IEEE J. Quantum Electron.*, vol. 30, no. 6, pp. 1469–1477, Jun. 1994.

[16] R. Herda and O. G. Okhotnikov, "Mode-locked Yb-doped fiber laser with external compression to 89 fs in normal dispersion fiber," *Appl. Opt.*, vol. 47, pp. 1182–1186, 2008.

[17] A. B. Grudinin and S. Gray, "Passive harmonic mode locking in soliton fiber lasers," *J. Opt. Soc. Amer. B*, vol. 14, pp. 144–153, 1997.

Appendix 8

Publication 8

S. Kivistö, J. Puustinen, M. Guina, S. Marcinkevicius, E. M. Dianov, and O. G. Okhotnikov, "Pulse dynamics of a passively mode-locked Bi-doped fiber laser," *Optics Express*, Vol. 18, No. 2, pp.1041-1048, 2010.

Pulse dynamics of a passively mode-locked Bi-doped fiber laser

Samuli Kivistö,[1,*] Janne Puustinen,[1] Mircea Guina,[1] Robert Herda,[2] Saulius Marcinkevicius,[3] Evgueny M. Dianov,[4] and Oleg. G. Okhotnikov[1]

[1]*Optoelectronics Research Centre, Tampere University of Technology, P.O. Box 692, FIN-33101 Tampere, Finland*
[2]*TOPTICA Photonics AG, Lochhamer Schlag 19, D-82166 Graefelfing, Germany*
[3]*Royal Institute of Technology, Electrum 229, Kista, 16440, Sweden*
[4]*Fiber Optics Research Center, Russian Academy of Sciences, 38 Vavilov Street, 119333 Moscow, Russia*
**samuli.kivisto@tut.fi*

Abstract: The pulse evolution in Bi-doped soliton fiber laser with slow and fast saturable absorber has been studied both experimentally and numerically. Semiconductor saturable absorbers with balanced slow and fast absorption recovery mechanisms exhibit a bi-temporal recovery dynamics which permits both reliable start-up of passive mode-locking and short pulse generation and stabilization. The pulse dynamics within the Bi fiber laser cavity have been investigated.

OCIS codes: (060.3510) Lasers, fiber; (140.4050) Mode-locked lasers

References and links

1. V.V. Dvoyrin, V.M. Mashinsky, E.M. Dianov, A.A. Umnikov, M.V. Yashkov, A.N. Guryanov, "Absorption, fluorescent and optical amplification in MCVD Bismuth-doped silica glass optical fibers," in Proc. of 31 ECOC (Glasgow, 2005), **4**, 949–950 (2005).
2. I. A. Bufetov, and E. M. Dianov, "Bi-doped fiber lasers," Laser Phys. Lett. **6**(7), 487–504 (2009).
3. E. M. Dianov, A. V. Shubin, M. A. Melkumov, O. I. Medvedkov, and I. A. Bufetov, "High-power CW bismuth fiber laser," J. Opt. Soc. Am. B **24**(8), 1749–1755 (2007).
4. A. B. Rulkov, A. A. Ferin, S. V. Popov, J. R. Taylor, I. Razdobreev, L. Bigot, and G. Bouwmans, "Narrow-line, 1178nm CW bismuth-doped fiber laser with 6.4W output for direct frequency doubling," Opt. Express **15**(9), 5473–5476 (2007).
5. E. M. Dianov, A. A. Krylov, V. V. Dvoyrin, V. M. Mashinsky, P. G. Kryukov, O. G. Okhotnikov, and M. Guina, "Mode-locked Bi-doped fiber laser," J. Opt. Soc. Am. B **24**(8), 1807–1808 (2007).
6. U. Keller, K. Weingarten, F. Kärtner, D. Kopf, B. Braun, I. Jung, R. Fluck, C. Hönninger, N. Matuschek, and J. Aus der Au, "Semiconductor saturable absorber mirrors (SESAM's) for femtosecond to nanosecond pulse generation in solid state lasers," IEEE J. Sel. Top. Quantum Electron. **2**(3), 435–453 (1996).
7. O. G. Okhotnikov, L. A. Gomes, N. Xiang, T. Jouhti, and A. B. Grudinin, "Mode-locked ytterbium fiber laser tunable in the 980-1070-nm spectral range," Opt. Lett. **28**(17), 1522–1524 (2003).
8. S. Kivistö, T. Hakulinen, M. Guina, and O. G. Okhotnikov, "Tunable Raman soliton source using mode-locked Tm-Ho fiber laser," IEEE Photon. Technol. Lett. **19**(12), 934–936 (2007).
9. O. Okhotnikov, and M. Pessa, "Dilute nitride saturable absorber mirrors for optical pulse generation," J. Phys. Condens. Matter **16**(31), S3107–S3120 (2004).
10. M. Guina, P. Tuomisto, O. G. Okhotnikov, S. Marcinkevicius, K. Mizohatad, and J. Keinonen, "Semiconductor saturable absorbers with recovery time controlled through growth conditions," SPIE Proc. 6451, 645113–1 - 645113–7 (2007).
11. S. Kivistö, J. Puustinen, M. Guina, O. G. Okhotnikov, and E. M. Dianov, "Tunable modelocked bismuth-doped soliton fibre laser," Electron. Lett. **44**(25), 1456–1458 (2008).
12. I. A. Bufetov, K. M. Golant, S. V. Firstov, A. V. Kholodkov, A. V. Shubin, and E. M. Dianov, "Bismuth activated alumosilicate optical fibers fabricated by surface-plasma chemical vapor deposition technology," Appl. Opt. **47**(27), 4940–4944 (2008).
13. O. Shtyrina, M. Fedoruk, S. Turitsyn, R. Herda, and O. Okhotnikov, "Evolution and stability of pulse regimes in SESAM-mode-locked femtosecond fiber lasers," J. Opt. Soc. Am. B **26**(2), 346–352 (2009).
14. R. Paschotta, and U. Keller, "Passive mode locking with slow saturable absorbers," Appl. Phys. B **73**(7), 653–662 (2001).
15. H. A. Haus, K. Tamura, L. E. Nelson, and E. P. Ippen, "Stretched-pulse additive pulse mode-locking in fiber ring lasers: theory and experiment," IEEE J. Quantum Electron. **31**(3), 591–598 (1995).
16. R. Herda, and O. G. Okhotnikov, "Mode-locked Yb-doped fiber laser with external compression to 89 fs in normal dispersion fiber," Appl. Opt. **47**(9), 1182–1186 (2008).

1. Introduction

Recently developed Bi-doped fibers have the ability to provide gain within the 1100-1550 nm wavelength range [1,2] and thus leverage the well known advantages of fiber lasers and fiber amplifiers to new applications. Continuous wave (CW) Bi-doped fiber lasers have already been reported to deliver output powers up to several Watts [3,4]. However, there are several challenges in the development of mode-locked Bi-fiber lasers. Due to the relatively low gain coefficient of Bi-doped fiber, the lasers typically have a long cavity length to achieve sufficient gain. The first Bi-fiber lasers mode-locked by semiconductor saturable absorber mirror (SESAM) exhibited relative long ~50 ps pulses with large pulse pedestal [5]. This was attributed to the combined effect of the narrow bandwidth of the fiber Bragg grating reflector, large normal dispersion of the long-length cavity and the non-optimized SESAM. In order to generate subpicosecond high-quality pulses from Bi-fiber lasers, dispersion compensation and a SESAM with picosecond or subpicosecond recovery time is required.

Semiconductor saturable absorber mirrors are widely used to passively mode-lock a large variety of lasers operating in different wavelength regimes [6–8]. Development of high-quality SESAMs operating at 1150-1400 nm requires corresponding absorbing regions grown on top of broadband reflectivity GaAs/AlAs distributed Bragg reflectors (DBR). InGaAsN/GaAs based SESAM used in this study meets these requirements [9]. It was shown that its absorption recovery time can be conveniently controlled by N-ion content generated during the plasma process [10,11].

In this paper, we investigate both experimentally and by numerical simulations the peculiarity of pulse dynamics in a mode-locked Bi-doped soliton fiber laser depending on SESAMs parameters.

2. Experimental

The fiber laser cavity is shown schematically in Fig. 1. The laser cavity comprised ~12 meters of Bi-doped glass fiber, a 1062/1165 pump coupler, and a fiber loop mirror acting as an output coupler with ~97% reflectivity at the lasing wavelength. The fiber was core-pumped with a cw Yb-doped single-mode fiber laser system. A monitoring 5% tap coupler was spliced close to the location of dispersion compensator as seen from Fig. 1. The Bi-doped aluminosilicate fiber with core glass composition of 97 mol:% of SiO_2 and 3 mol:% of Al_2O_3, a core diameter of 8.4 μm, a core/cladding refractive index difference of $\Delta n = 5.5 \cdot 10^{-3}$, and a cutoff wavelength of ~1100 nm has been described in detail in [12]. The length of the doped fiber was optimized in order to achieve efficient pump absorption while minimizing the length and dispersion of the fiber section of the cavity. The splice loss of Bi-fiber to a standard single mode fiber was ~0.3 dB. An additional dichroic fiber coupler was used at the output of the laser to separate the signal light from residual pump. The normal group velocity dispersion

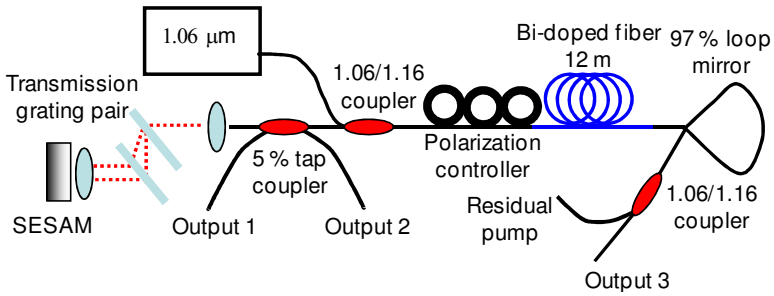

Fig. 1. Schematic of the mode-locked Bi-doped fiber laser operating in soliton regime.

(GVD) of the optical fiber at 1.16 μm wavelength range was compensated by a transmission grating pair with 1250 lines/mm. A polarization controller was used to maintain the optimal functioning of the grating pair.

InGaAsN-based semiconductor saturable absorber mirrors with different absorption recovery times were grown by molecular beam epitaxy to explore the effect of the absorber recovery time on the mode-locking performance. The Absorber #1 comprises 12 InGaAsN quantum wells (QWs) while the Absorbers #2 and #3 used in this study include 4 QWs grown on top of 24.5 pair GaAs/AlAs DBR. The DBR stopband had a center wavelength of ~1140 nm with a 150-nm bandwidth.

In order to decrease the absorber recovery time, the absorbers #2 and #3 were in situ irradiated with N-ions for 2 and 3 minutes, respectively [10]; the quantum wells were individually exposed to a flux of N-ions after they were grown. The absorption recovery time was measured at ~1160 nm by using a degenerate pump-probe measurement set-up. The results shown in Fig. 2(a) and (b) reveal that the absorption recovery time decreases from ~680 ps for the non-irradiated sample down to 4 ps and 2 ps for the samples irradiated for 2 min and 3 min, respectively. It can be observed that absorption recovery has clear two-exponential decay behavior with fast components of 4 and 2 ps and the slow components of ~40 ps and ~20 ps, respectively. We should mention here that a slow component of the absorption recovery is useful for ensuring a self-starting mode-locking, while the fast component performs efficiently the pulse shaping.

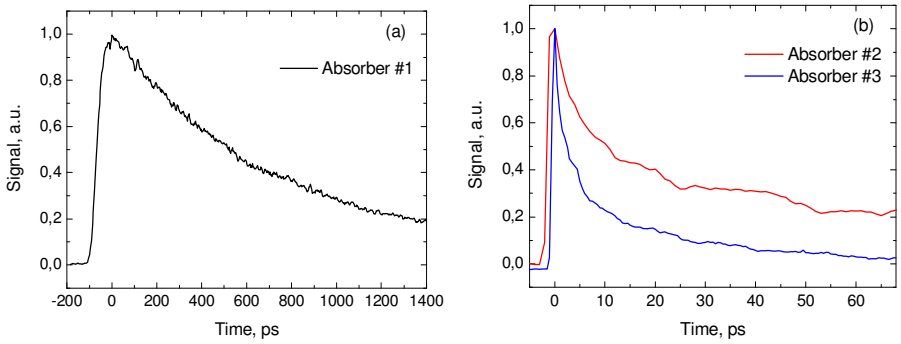

Fig. 2. Temporal response of saturable absorption (a) for the absorber #1, and (b) for the absorbers #2 and #3.

It was found that the laser enabled self-starting mode-locking at a repetition rate of 7.3 MHz for each absorber with steady-state pulses shown in Fig. 3. The threshold pump powers were ~400 mW, ~600 mW, and ~700 mW, respectively, for the laser cavities with absorbers #1, #2, and #3. The pump powers for the autocorrelations and pulse spectra shown in Fig. 3 (a) and (b) were ~1 W. As it can be seen, the absorber #1 with absorption recovery time of

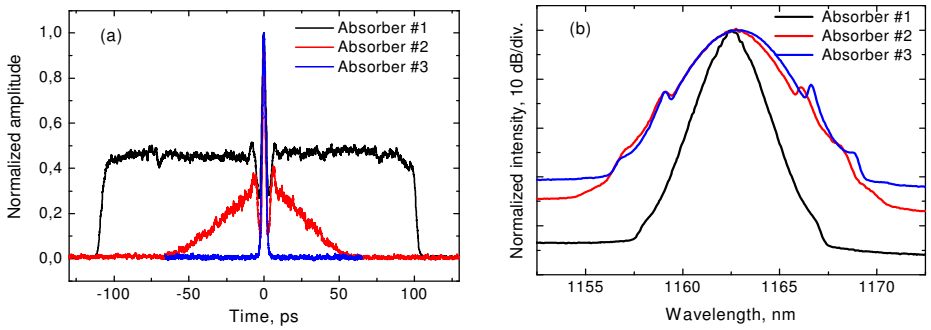

Fig. 3. (a) Measured autocorrelations for the three different absorbers. (b) Corresponding optical spectra. The intra-cavity cavity GVD is ~-0.4 ps^2. The autocorrelator scanning range is ~210 ps.

~680 ps supports a pulse with a large pedestal (black trace) that exceeds the ~210-ps scanning range of the autocorrelator. For the absorber #2 with the recovery time of 4 ps, the pulse pedestal is significantly suppressed (red trace). By using the absorber with recovery time of 2 ps, the pulse pedestal is completely avoided providing clean and stable soliton pulses. Figure 3(b) displays the optical spectra illustrating that the spectral width increases with a decrease of the absorption recovery time.

The soliton sidebands seen in the spectra become more pronounced with reduced recovery time indicating a stable soliton operation of the laser with the fast SESAM. The similar tendency was observed in the pulse train monitored at the oscilloscope. Contrary to the slow absorbers, mode-locking with fast absorber #3 revealed temporally stable pulse train even for long-span measurements. The average cavity dispersion in these measurements was estimated to be ~-0.4 ps^2.

The cavity dispersion also plays a role in the pulse shaping. When the average cavity dispersion was increased to ~-0.65 ps^2 by lengthening the grating pair separation, the use of absorber #2 resulted in nearly pedestal-free pulses with pulse duration of ~1.3 ps. On the other hand, when the laser was operated with average cavity dispersion lower than ~-0.3 ps^2, even the use of absorber #3 resulted in a small pedestal in output pulses. The pumping power was also observed to have a contribution to the pulse pedestals. When operated close to the laser threshold, the pulse pedestals were slightly weaker compared to higher pumping powers.

3. Numerical simulations and discussions

To address the specific features characteristic to mode-locked Bi fiber laser, we assume that

1. the cavity has long length and consequently high tendency to multiple pulsing;
2. the laser generates pulses with low pulse (E), therefore, E_q is very close to E_{q+1}; q – number of pulses circulating in the laser cavity.

The Bi-doped fiber laser was numerically simulated by propagating the pulse through the different cavity elements depending on the speed of absorption recovery consequently. The Schrödinger equation included the dispersion, loss, parabolic gain-bandwidth profile and saturable absorption [13]. The simulation procedure took into account the bi-exponential character of absorber recovery. The total intra-cavity dispersion was varied by changing the separation of the grating pair compensator. The values of the nonlinear parameters and dispersion of the passive and active fibers used in the numerical modeling were $\gamma_1 = 5$ $W^{-1}km^{-1}$ (passive fiber), $\gamma_2 = 10$ $W^{-1}km^{-1}$ (Bi-doped fiber), $\beta_2 = 10$ ps^2/km, and $\beta_3 = 0.026$ ps^3/km. The Bi-doped fiber gain was varied within a range of 0.35 dB/m - 0.45 dB/m corresponding to different pumping rates. The Bi-fiber also had an additional unsaturable absorption of 0.2 dB/m. The parameters for the saturable absorbers used in the model are shown in Table 1.

Figures 4(a) and (b) illustrate the simulated spectra and autocorrelations for different recovery time of saturable absorber and cavity dispersion of -0.4 ps^2. When running the simulations it could be observed that for low dispersion and long recovery time, the temporal pulse shape and spectrum change slightly for each consecutive roundtrip passage through the cavity.

Table 1. SESAM parameters used in numerical simulation

	Absorber #1	**Absorber #2**	**Absorber #3**
Recovery time 1, ps	680 ps	4	2
Recovery time 2, ps	-	40	20
Saturation energy, pJ	2	4	8
Modulation depth, %	5	10	13
Nonsaturable loss, %	1	2	4.5

The autocorrelations and spectra presented here have been averaged over 8000 roundtrips to emulate measured autocorrelation and spectrum. As it can be seen, the simulation predicts

the pedestal formation observed in the experiments. The simulations also show that the pumping rate has an influence on the size of the pulse pedestal. When the gain of the Bi-doped fiber is increased from 0.35 dB/m to 0.45 dB/m, the size of the pulse pedestal increases significantly, as it can be seen in the Fig. 4(a) for the absorbers #1 and #2. The inset to Fig. 4(a) shows an irregular pulse bunching at the large temporal span for Absorber #1. A multiple pulsing appears then as an effective pulse pedestal seen in the autocorrelation trace. The simulation results are in a qualitative agreement with the experimental data shown in Fig. 3(a). Small deviations in the autocorrelations can be explained due to minor variation of pumping levels used in the experiments. The simulated pulse spectra shown in Fig. 4(b) are in very good agreement with the measured spectra given in Fig. 3(b). Difference in the depth of the soliton sidebands might be due to some additional spectral filtering in the experimental fiber cavity. Figure 5 shows simulation results for the laser with total intra-cavity dispersion of $-0.65 ps^2$. The pedestal levels have dropped compared to the case with cavity dispersion of $-0.4 ps^2$, as it was also noticed in the experiments. This can be understood by the stronger soliton formation and pulse shaping with higher anomalous dispersions. However, the effect of the cavity dispersion on the pulse pedestal is not as strong as the effect of the absorber recovery time or the fiber pumping level. The inset to Fig. 5 shows the pulse shape for the laser cavity with the Absorber #2 initiating the mode-locked operation. The smaller satellite pulse results in the observed small pedestal of the autocorrelation.

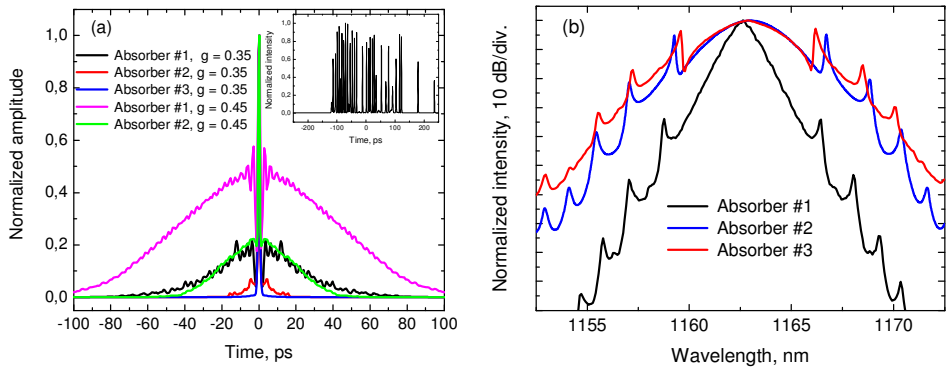

Fig. 4. (a) Simulated autocorrelation traces for each absorber and the (b) corresponding pulse spectra. The spectral widths are 0.9 nm, 2.6 nm, 2.6 nm, respectively. The inset shows a simulated time domain pulse shape generated using the Absorber #1 with fiber gain value of 0.45 dB/m.

The observed pulse pedestals are likely to be due to relatively long absorber recovery times. Indeed, after the multiple passage of the pulse the absorber is saturated, however the pulse sees net gain for relatively long time window (~20-1000 ps depending on the absorber) [14]. Within this time interval, the spontaneous noise can be amplified disturbing the pulse quality or preventing the mode-locked operation completely. The autocorrelation pedestals in the mode-locked Bi-laser experiments are emulated by multiple pulses propagating in the cavity together with the stronger fundamental pulse.

The tendency of the slow absorber for supporting the multiple pulsing operation within its window of low losses can be explained by looking at the absorber saturation in the simulations. As a measure for the SESAM saturation, the simulated losses for a pulse was used, rather than the simple measure of pulse energy divided by saturation energy which is an inaccurate measure for the saturation when the pulse durations are in the same order of magnitude as the recovery time. For the slowest absorber with $-0.40\ ps^2$ of dispersion and 0.45 dB/m of gain, the saturable losses in the absorber are 2% for the entire group of pulses. When isolating the strongest pulse in the group, the saturable losses of 25% would occur if this pulse would be a single pulse. When looking at the simulation of the fastest absorber, the whole group of pulses has losses of 34% whereas the strongest pulse in the group would only

have losses of 26% (the losses are lower for a single pulse than for the group of pulses because the strongest pulse was only looked at). The slow absorber favors lower energy pulses that saturate the absorber much better when they are spaced closely together and therefore favors multiple pulsing. The fast absorber provides as good saturation for a high energy single pulse as for a group of pulses and, therefore, favors single pulse operation more than the slow absorber. The saturation fluencies of the absorber also have a role in the pulse generation. The low saturation fluence of the Absorber #1 supports the self-starting operation of the laser, but on the other hand generation of multiple noise-like pulses together with the long absorber recovery time [13]. Whereas, the higher saturation fluencies of the Absorber #2 and #3 promotes single or few-pulses operation.

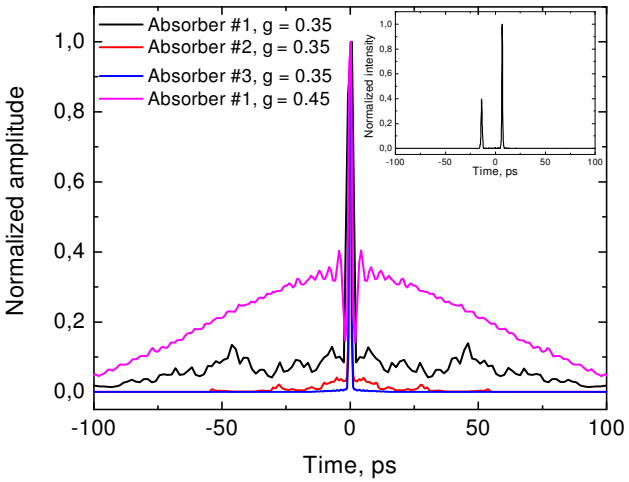

Fig. 5. Simulated autocorrelations for cavity dispersion of –0.65 ps^2. The inset shows a time domain pulse shape generated using the absorber #2 and fiber gain value of 0.35 dB/m.

An important pulse shaping mechanism in this study was also the soliton pulse shaping. The soliton formation allowed self-starting operation with each absorber. In the soliton regime, the laser is able to sustain larger amount of noise arising behind the pulse [14]. However, if the dispersion is reduced to a less anomalous value (in this study ~-0.3 ps^2), even the strong soliton shaping mechanism cannot prevent the formation of the pulse pedestal when slow absorbers are used. Actually, the soliton-area theorem determines the pulse energy for a cavity with a certain dispersion and non-linearity for certain pulse duration. When the minimum pulse duration supported by the system increases, the pulse energy has to decrease proportionally. Therefore single pulse operation is favored in a soliton laser with a fast absorber because it favors shorter and therefore pulses with higher energy compared to a soliton laser with a slow absorber.

To obtain here clean pulses with pulse duration in the range of few hundreds of femtoseconds or less, a SESAM with even faster absorption recovery should be used. In conclusion, a very careful and detailed design of the mode-locked Bi-doped fiber laser system (both the absorber and the fiber cavity) is required for ultra-short and high-quality pulses.

4. Pulse evolution in Bi-doped fiber cavity

The Bi-fiber laser was then studied with the fastest absorber initiating the mode-locked operation (cavity dispersion was set to ~-0.4 ps^2). The aim was to analyze the pulse evolution in the laser cavity, as it has been shown that the pulses propagating inside the dispersion managed fiber laser cavity encounter strong temporal evolution [15,16]. The same numerical simulations were used as described in previous section.

Figure 6 illustrates the evolution of the spectral width and the time-bandwidth product (TBP) during a one cavity round-trip started from the location of the SESAM (0 mm) and then mapped according to the laser schematic shown in Fig. 1. The pulses at the output 3 have only a small chirp with a time-bandwidth product of ~0.64 and spectral width of 2.0 nm. However, the pulses have a significantly broader spectrum close to the dispersion compensation end of the cavity (output 1 and 2) and the pulses undergo a strong temporal chirp. In particular, the pulses at the output 2 are strongly negatively chirped with a simulated spectral width of 2.7 nm and time-bandwidth product of 1.02. The negative chirp can be then compensated by about 10 m of standard single mode optical fiber, with normal dispersion at the laser wavelength, placed at output 2. The estimated pulse width after compression was ~0.6 ps.

According to simulations an additional 5% tap coupler was spliced close to the grating pair dispersion compensator (see Fig. 1) in order to get the broadest temporal bandwidth and negative chirp of the pulses. The pulse evolution was then investigated experimentally by recording the optical spectrum and the corresponding autocorrelation at the three different outputs (see Fig. 7). As it can be seen from Fig. 6 (scatters) the pulses at the output 3 are nearly transform-limited with a time-bandwidth product of 0.46. Close to the dispersion compensation end of the cavity at the output 1 and 2 pulses are chirped and have a significantly broader spectrum, as also expected from the simulation. The pulses at the output 2 have spectral width of 2.8 nm and time-bandwidth product of 1.04, which is in very good agreement with the simulation.

The pulse compression in the fiber output pigtail (output 2) was then experimentally investigated by splicing standard single mode fiber to the output. It was found that the shortest pulses were obtained with the output fiber length of ~13 m. The compression of negatively chirped 1.67-ps pulses resulted in nearly bandwidth limited 0.7-ps pulses, as seen in Fig. 7. We note that these compressed pulses are shorter than the pulses recorded at the output 3 with pulse width of 1.05 ps and spectral width of 2.0 nm. This is the shortest pulse duration reported for a Bi-doped fiber laser.

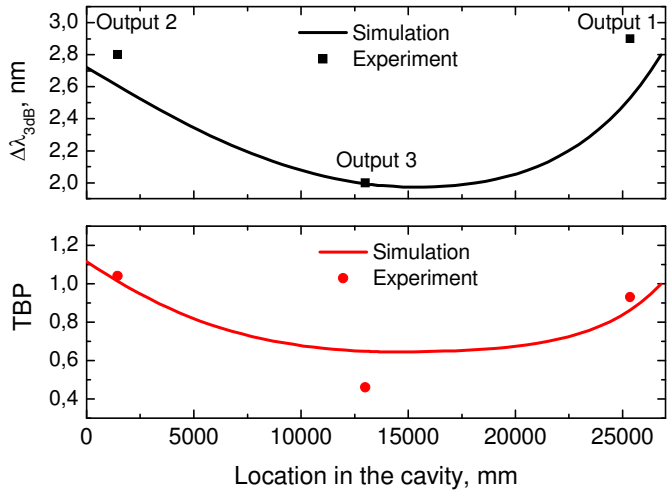

Fig. 6. Numerically simulated spectral width ($\Delta\lambda_{3dB}$) and time-bandwidth product (TBP) at different locations of the fiber cavity. Scatters are the experimental measurements.

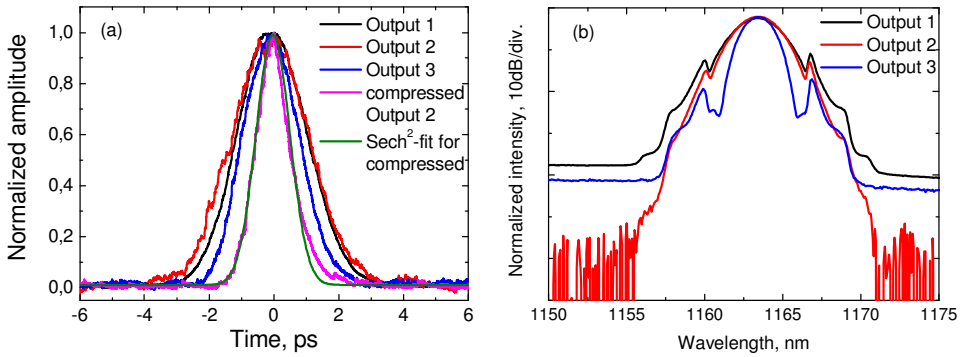

Fig. 7. (a) Measured autocorrelations at different positions of the cavity for the fastest SESAM. Pulse widths according to sech^2-fitting are 1.45 ps, 1.67 ps, 1.05 ps, and 0.70 ps for the output 1, 2, 3, and externally compressed 2, respectively. (b) Optical spectra corresponding to the autocorrelations. The spectral widths for the different outputs are 2.9 nm, 2.8 nm, 2.0 nm, respectively.

5. Conclusions

The pulse dynamics of a mode-locked Bi-doped fiber laser has been studied in detail both numerically and experimentally using semiconductor saturable absorbers with different absorption recovery time. It was shown that the pulse quality was improved significantly when the absorber recovery time was decreased from the initial value of ~680 ps down to 2 ps. The effect of the gain fiber pumping level, absorption saturation, and average cavity dispersion were also shown to have a detrimental effect on the pulse generation and shaping in the Bi-doped fiber laser operating around 1160 nm. In addition, pulse propagation dynamics of the Bi-fiber laser cavity were investigated.

Acknowledgements

The authors acknowledge the support of the graduate school of Tampere University of Technology, the Finnish Foundation for Economic and Technology Sciences, the Jenny and Antti Wihuri Foundation, the Nokia Foundation, the Emil Aaltonen Foundation, and the Elisa Foundation. A. V. Kholodkov and K. M. Golant are acknowledged for fabricating the Bi-doped fiber, and V. M. Korpijärvi for his help with epitaxial growth.

Appendix 9

Publication 9

S. Kivistö, T. Hakulinen, M. Guina, and O. G. Okhotnikov "Tunable Raman Soliton Source Using Mode-Locked Tm-Ho Fiber Laser," *IEEE Photonics Technology Letters*, Vol. 19, No. 12, pp. 934-936, 2007.

Tunable Raman Soliton Source Using Mode-Locked Tm–Ho Fiber Laser

Samuli Kivistö, Tommi Hakulinen, Mircea Guina, and Oleg G. Okhotnikov

***Abstract*—We report a femtosecond pulse source that uses a mode-locked Tm–Ho oscillator and a self-frequency shift of Raman solitons in Tm–Ho power amplifier. The master oscillator mode-locked by an antimonide-based saturable absorber mirror produces 750-fs transform-limited soliton pulses over the tuning range from 1912 to 1972 nm. The soliton self-frequency shift in the amplifier resulted in transform-limited pulses with the wavelength adjusted by varying the amplifier pump power. We obtain ∼150-fs soliton pulses at the wavelength of 2150 nm with average power up to 230 mW corresponding to the peak power of 27 kW. The efficiency of Raman conversion ranges from 47% to 62% over the tuning range.**

***Index Terms*—Lasers and laser optics, optical fibers, short pulse formation, solitons.**

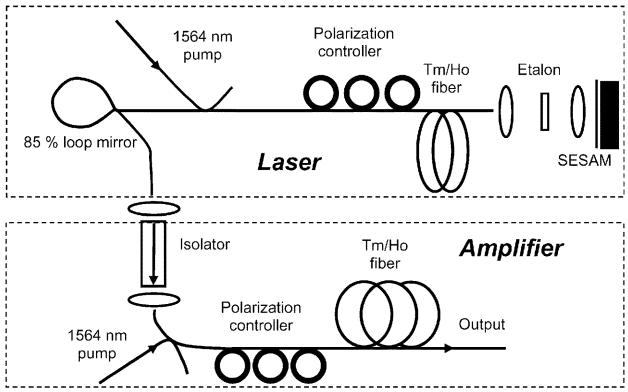

Fig. 1. Schematic of tunable mode-locked Tm–Ho fiber system.

I. Introduction

OVER the past decade, ultrafast fiber laser technology has progressed remarkably and now it starts to actually challenge other laser technologies, particularly based on bulk solid-state lasers. Advantages of compact fiber lasers producing ultrashort pulses using semiconductor saturable absorber mirrors (SESAMs) include excellent beam and pulse quality, high efficiency, and turn-key operation. Pulse generation covering a large wavelength range from 895 to 1560 nm have been reported using neodymium, ytterbium, and erbium mode-locked fiber systems [1]–[3].

In the meanwhile, the interest in the midinfrared (mid-IR) spectral range firmly increases. The mid-IR light sources and detectors operating in the eye-safe range beyond 2 μm find applications in LIDAR, spectroscopy, medicine, and combustion monitoring. Thulium- and thulium–holmium-doped fibers have proven to be efficient gain media for high-power light sources operating around 2 μm [4]–[7]. Thulium fiber has a broad amplification bandwidth between 1.65 and 2.1 μm and is, therefore, suitable for short pulse generation and wide wavelength tuning [8]–[10].

Mode-locked fiber sources based on thulium-doped fibers delivering femtosecond pulses have been reported in just a few publications. A 1.9-μm thulium fiber laser passively mode-locked by InGaAs-saturable absorber has been demonstrated [11]. The system delivered 190-fs pulses with an output power of 1 mW. Nelson *et al.* used additive pulse mode-locking to generate sub-500-fs pulses tunable from 1.8 to 1.9 μm with an average output power of few hundreds of microwatts [10]. The tuning range can be extended remarkably using soliton self-frequency shift in a fiber [12]–[15]. Recently, 108-fs pulses with 230-kW peak power at 1.98 μm and wavelength tuning over the range of 140 nm were reported from cladding-pumped large mode area Tm-doped fiber amplifier seeded by a Raman shifted erbium all-fiber oscillator [16].

In this letter, we demonstrate a mode-locked fiber laser/power-amplifier system based on core-pumped Tm–Ho-doped silica fiber and soliton self-frequency shift. Sb-based saturable absorber mirrors have been used to initiate passive self-starting mode-locking of the Tm–Ho master oscillator. The system delivers femtosecond soliton pulses in a wavelength range from 1.97 to 2.15 μm with an average output power up to 230 mW. The 150-fs pulses at 2.15 μm with a peak power of 27 kW have been achieved.

II. Experimental Details and Results

The experimental setup of the fiber system is shown in Fig. 1. The master oscillator is comprised of 1.2 m of Tm–Ho-doped fiber, pump coupler, a fiber loop mirror with 85% reflectivity at ∼1950 nm, and a saturable absorber mirror. The Tm–Ho-doped fiber has a cutoff wavelength of 1550 nm, a core diameter of 7 μm, and absorption of ∼20 dB/m at 1564 nm. The thulium fiber with estimated dispersion of ~ -70 ps^2/km at 1.9 μm was core-pumped by high-power erbium-doped fiber laser. We note that the erbium fiber laser is nearly an ideal pumping source for Tm–Ho fiber because of the low quantum defect.

The mode-locking was achieved by a Sb-based SESAM with saturation fluence of 47 μJ/cm^2 and modulation depth of 10%. The nonlinear reflectivity response of the SESAM is plotted in Fig. 2. The absorber material consisted of 15 GaInSb quantum-

Manuscript received February 16, 2007; revised March 29, 2007.

S. Kivistö, T. Hakulinen, and O. G. Okhotnikov are with the Optoelectronics Research Centre, Tampere University of Technology, FIN-33101 Tampere, Finland (e-mail: samuli.kivisto@tut.fi).

M. Guina is with the Optoelectronics Research Centre, Tampere University of Technology, FIN-33101 Tampere, Finland, and also with RefleKron Ltd., 33710 Tampere, Finland (e-mail: mircea.guina@reflekron.com).

Digital Object Identifier 10.1109/LPT.2007.898877

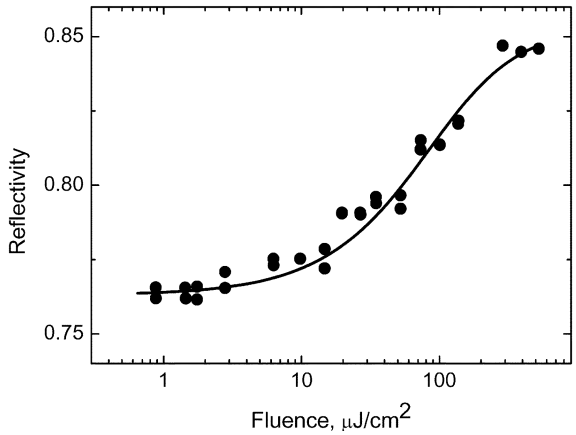

Fig. 2. Nonlinear response of the Sb-based SESAM.

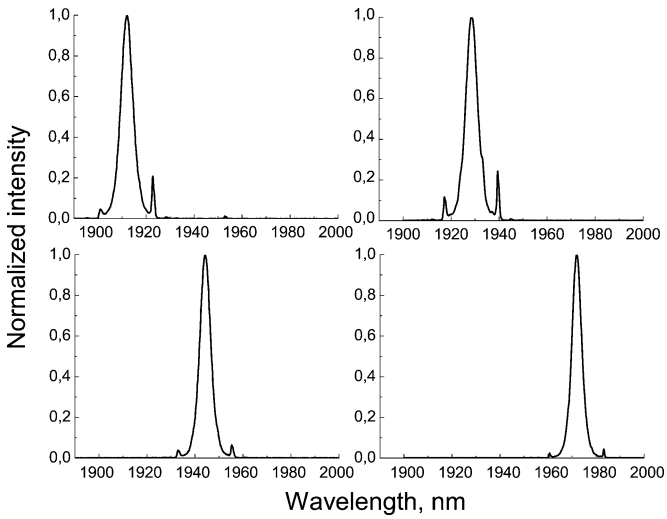

Fig. 3. Tunable spectra of the Tm–Ho master oscillator.

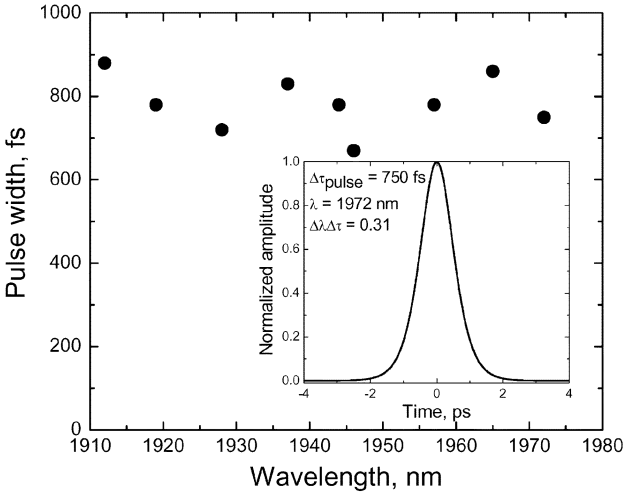

Fig. 4. Pulsewidth versus wavelength of the Tm–Ho master oscillator. Autocorrelation trace at 1972 nm is shown as an inset.

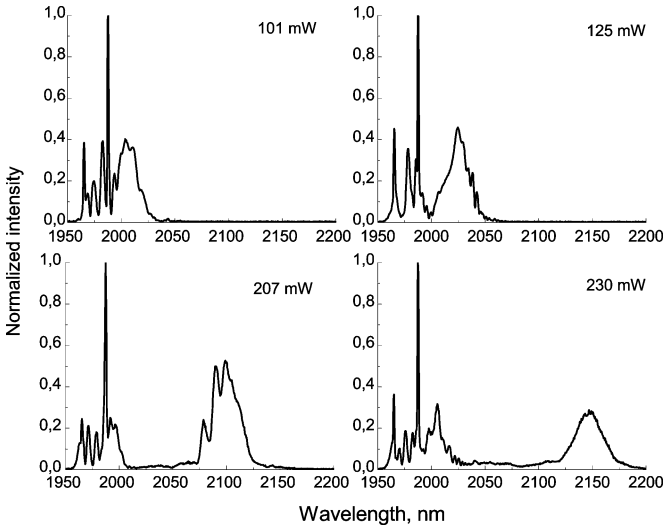

Fig. 5. Output spectra for different average powers of the Raman shifted soliton. Master oscillator wavelength is set to 1972 nm.

wells placed within a $3-\lambda$ GaSb cavity grown on the top of an 18-pair AlAsSb–GaSb Bragg reflector. The room-temperature photoluminescence emission from the quantum wells is peaked at 2035 nm. The distributed Bragg reflector has a reflectance of 99.8% in a wavelength range from 1850 to 2150 nm. The absorption recovery time was decreased to few picoseconds using ion irradiation.

The Tm–Ho-fiber master oscillator generates ~650- to 850-fs transform-limited sech^2-shape pulses with a repetition rate of 50 MHz and average output power of ~20 mW at wavelengths between 1912 and 1972 nm, as shown in Figs. 3 and 4. The wavelength tunability was achieved by using a 25- μm-thick fused silica etalon placed inside the laser cavity.

The 4.5-m-long Raman shifter/amplifier was made of Tm–Ho-doped fiber similar to the gain fiber used in the master laser. A free-space optical isolator optimized for 2 μm was placed at the output of the master oscillator to prevent back reflections from the power amplifier. All the fiber ends were angle cleaved to suppress Fresnel reflections. Polarization controllers were used to optimize the performance since the Raman frequency shift exhibits a strong dependence on the input polarization [17].

By increasing the amplifier pump power, the Raman soliton was gradually shifted from 1.97 up to 2.15 μm, as shown in Fig. 5. The largest wavelength shift obtained at a pump power of 2.4 W was 180 nm corresponding to 230 mW of average power of the Raman soliton. The spectral width of the pulses increases with the Raman shifting from 5.5 to 32 nm. The shortest pulse length after Raman shifting and compression was ~150 fs, as seen from Fig. 6.

The efficiency of the Raman conversion, determined as the ratio of the shifted soliton energy to the overall energy including the unconverted seed and amplified spontaneous emission, was 62% at 2 μm and 47% at 2.15 μm. The decrease in the conversion efficiency, seen from Fig. 7, and the long-wavelength limit of tuning range is due to an abrupt increase of silica fiber absorption beyond 2.1 μm, as shown in Fig. 8. Further increase in the amplifier pump power resulted first in multiple soliton generation and eventually in a flat Raman-continuum spanning from

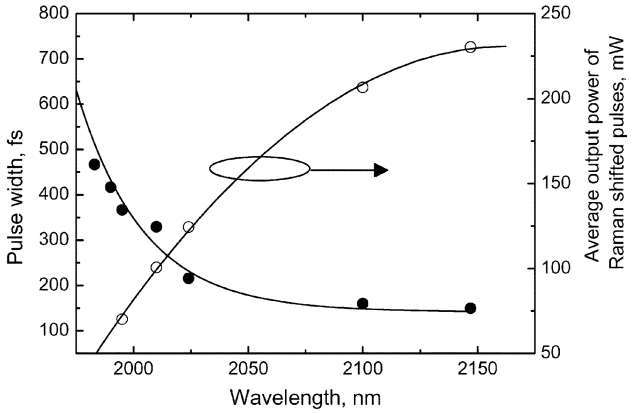

Fig. 6. Pulsewidth and average output power of Raman shifted solitons as a function of their center wavelength.

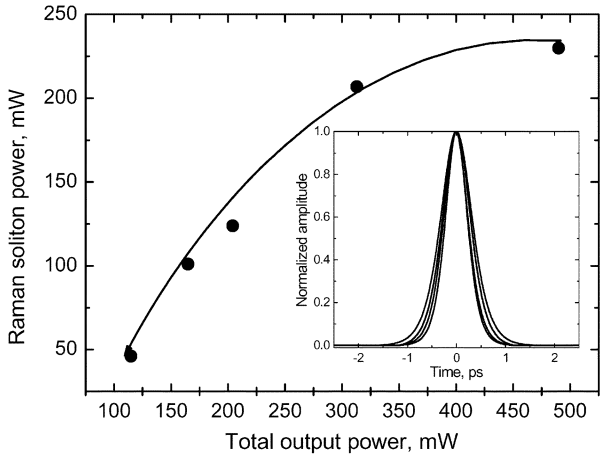

Fig. 7. Average power of the Raman shifted soliton versus total power at the output of the amplifier. Typical autocorrelation traces of Raman solitons are shown as an inset with $\triangle v \triangle \tau$ in a range 0.35–0.38.

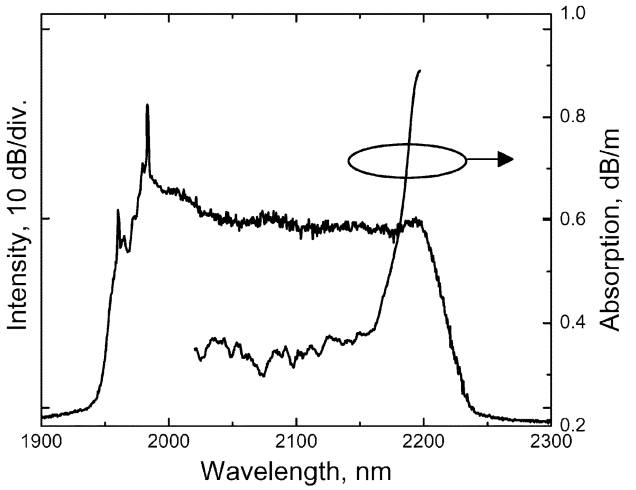

Fig. 8. Output spectrum for average output power of 1 W and measured fiber absorption. Amplifier pump power is 5.3 W.

1.95 to 2.25 μm with average output power of $\sim$1 W, as shown in Fig. 8.

III. Conclusion

We have demonstrated a practical and compact fiber source based on Tm–Ho-doped silica fiber. Using a tunable mode-locked oscillator and Raman shifter/power amplifier both made of Tm–Ho fiber, we have obtained soliton pulses tunable from 1.97 to 2.15 μm with an average output power up to 230 mW. The long-wavelength, self-starting, passive mode-locking was initiated by antimonide-based saturable absorber mirror. The spectral shift achieved by varying the amplifier pump power is accompanied by spectral broadening and pulse compression down to $\sim$150-fs pulsewidth at 2.15 μm with average power of 230 mW corresponding to a peak power of $\sim$27 kW. The conversion efficiency to Raman soliton was 62% at 2 μm and 47% at 2.15 μm. The decreased efficiency is due to absorption increase of silica glass fiber beyond 2.1 μm.

References

[1] O. G. Okhotnikov, L. Gomes, N. Xiang, T. Jouhti, and A. B. Grudinin, "Mode-locked ytterbium fiber laser tunable in the 980–1070-nm spectral range," *Opt. Lett.*, vol. 28, pp. 1522–1524, 2003.

[2] O. G. Okhotnikov, T. Jouhti, J. Konttinen, S. Karirinne, and M. Pessa, "1.5-μm monolithic GaInNAs semiconductor saturable-absorber mode locking of an erbium fiber laser," *Opt. Lett.*, vol. 28, pp. 364–366, 2003.

[3] M. Rusu, S. Karirinne, M. Guina, A. B. Grudinin, and O. G. Okhotnikov, "Femtosecond neodymium-doped fiber laser operating in the 894–909 nm spectral range," *IEEE Photon. Technol. Lett.*, vol. 16, no. 4, pp. 1029–1031, Apr. 2004.

[4] R. A. Hayward, W. A. Clarkson, P. W. Turner, J. Nilsson, A. B. Grudinin, and D. C. Hanna, "Efficient cladding-pumped Tm-doped silica fibre laser with high power single mode output at 2 μm," *Electron. Lett.*, vol. 36, pp. 711–712, 2000.

[5] W. A. Clarkson, N. P. Barnes, P. W. Turner, J. Nilsson, and D. C. Hanna, "High-power cladding-pumped Tm-doped silica fiber laser with wavelength tuning from 1860 to 2090 nm," *Opt. Lett.*, vol. 27, pp. 1989–1991, 2002.

[6] S. D. Jackson and S. Mossman, "Efficiency dependence on the Tm^{3+} and Al^{3+} concentrations for Tm^{3+}-doped silica double-clad Fiber Lasers," *Appl. Opt.*, vol. 42, pp. 2702–2707, 2003.

[7] D. Y. Shen, J. K. Sahu, and W. A. Clarkson, "High-power widely tunable Tm:fibre lasers pumped by an Er,Yb co-doped fibre laser at 1.6 μm," *Opt. Express*, vol. 14, pp. 6084–6090, 2006.

[8] S. D. Agger and J. H. Povlsen, "Emission and absorption cross section of thulium doped silica fibers," *Opt. Express*, vol. 14, pp. 50–57, 2005.

[9] R. L. Shubochkin, V. A. Kozlov, A. L. G. Carter, and T. F. Morse, "Tunable thulium-doped all-fiber laser," *IEEE Photon. Technol. Lett.*, vol. 10, no. 7, pp. 944–945, Jul. 1998.

[10] L. E. Nelson, E. P. Ippen, and H. A. Haus, "Broadly tunable sub-500 fs pulses from an additive-pulse mode-locked thulium-doped fiber ring laser," *Appl. Phys. Lett.*, vol. 67, pp. 19–21, 1995.

[11] R. C. Sharp, D. E. Spock, N. Pan, and J. Elliot, "190-fs passively mode-locked thulium fiber laser with a low threshold," *Opt. Lett.*, vol. 21, pp. 881–883, 1996.

[12] A. A. Gouveia-Neto, A. S. L. Gomes, and J. R. Taylor, "Femtosecond soliton Raman generation," *IEEE. J. Quantum Electron.*, vol. 24, no. 2, pp. 332–340, Feb. 1988.

[13] N. Nishizawa and T. Goto, "Compact system of wavelength-tunable femtosecond soliton pulse generation using optical fibers," *IEEE Photon. Technol. Lett.*, vol. 11, no. 3, pp. 325–327, Mar. 1999.

[14] D.-P. Wei, T. V. Galstian, A. Zohrabyan, and L. Mouradian, "Tunable femtosecond soliton generation in Ge-doped fibre," *Electron. Lett.*, vol. 40, pp. 1329–1330, 2004.

[15] F. Druon, N. Sanner, G. Lucas-Leclin, P. Georges, K. P. Hansen, and A. Petersson, "Self-compression and Raman soliton generation in a photonic crystal fiber of 100-fs pulses produced by a diode-pumped Yb-doped oscillator," *Appl. Opt.*, vol. 42, pp. 6768–6770, 2003.

[16] G. Imeshev and M. E. Fermann, "230-kW peak power femtosecond pulses from a high power tunable source based on amplification in Tm-doped fiber," *Opt. Express*, vol. 13, pp. 7424–7432, 2005.

[17] M. N. Islam, "Raman amplifiers for telecommunication," *IEEE J. Sel. Topics Quantum Electron.*, vol. 8, no. 3, pp. 548–559, May/Jun. 2002.

Appendix 10

Publication 10

[P10] S. Kivistö, T. Hakulinen, B. Aitchison, D. Brown, A. Kaskela, A. Nasibulin, E. Kauppinen, A. Härkönen, and O. G. Okhotnikov, "Carbon nanotube films for ultrafast broadband technology," *Optics Express*, Vol. 17, No. 4, pp. 2358-2363, 2009.

Carbon nanotube films for ultrafast broadband technology

Samuli Kivistö,[1,*] Tommi Hakulinen,[1] Antti Kaskela,[2] Brad Aitchison,[3] David P. Brown,[3] Albert G. Nasibulin,[2] Esko I. Kauppinen,[2] Antti Härkönen,[1] and Oleg G. Okhotnikov[1]

[1]Optoelectronics Research Centre, Tampere University of Technology, P.O. Box 692, FIN-33101 Tampere, Finland
[2]NanoMaterials Group, Department of Applied Physics and Center for New Materials, Helsinki University of Technology, P.O.Box 5100, FIN-02015 TKK, Finland
[3]Canatu Ltd., Tekniikantie 21, FI-02150 Espoo, Finland
[*]Corresponding author: samuli.kivisto@tut.fi

Abstract: Mode-locked sub-picosecond operation of Yb-, Er- and Tm:Ho-doped fiber lasers operating at 1.05 μm, 1.56 μm and 1.99 μm, respectively, is demonstrated using the same sample carbon nanotube-based saturable absorber mirror. A mesh of single-walled carbon nanotubes was deposited on an Ag-mirror using a one-step dry-transfer contact press method to combine broadband saturable absorption and high reflectance properties. The novel fabrication method of the polymer-free absorber and device parameters determined using nonlinear reflectivity measurement are described in detail. To our knowledge the observed operation bandwidth of ~1 μm is the broadest reported to date for a single carbon nanotube-based saturable absorber.

OCIS codes: (060.3510) Lasers, fiber; (140.4050) Mode-locked lasers.

References and links

1. M. E. Fermann, M. J. Andrejco, Y. Silberberg, and M. L. Stock, "Passive mode locking by using nonlinear polarization evolution in a polarization-maintaining erbium-doped fiber," Opt. Lett. **18**, 894-896 (1993).
2. T. Brabec, Ch. Spielmann, P. F. Curley, and F. Krausz, "Kerr lens mode locking," Opt. Lett. **17**, 1292-1294 (1992).
3. U. Keller, K. Weingarten, F. Kärtner, D. Kopf, B. Braun, I. Jung, R. Fluck, C. Hönninger, N. Matuschek, and J. Aus der Au, "Semiconductor saturable absorber mirrors (SESAM's) for femtosecond to nanosecond pulse generation in solid state lasers," IEEE J. Sel. Top. Quantum Electron. **2**, 435-453 (1996).
4. E.P. Ippen, C.V. Shank, and A. Dienes, "Passive mode locking of the cw dye laser," Appl. Phys. Lett. **37**, 267-269 (1980).
5. S. Y. Set, H. Yaguchi, Y. Tanaka, M. Jablonski, Y. Sakakibara, A. Rozhin, M. Tokumoto, H. Kataura, Y. Achiba, and K. Kikuchi, "Modelocked fiber lasers based on a saturable absorber incorporating carbon nanotubes," in OFC'03, paper PD44 (2003).
6. C. S. Goh, K. Kikuchi, S. Y. Set, D. Tanaka, T. Kotake, M. Jablonski, S. Yamashita, and T. Kobayashi, "Femtosecond mode-locking of an ytterbium-doped fiber laser using a carbon-nanotube-based mode-locker with ultra-wide absorption band," in Conference on Lasers and Electro-Optics, paper CThG2 (2005).
7. J. H. Yim, W. B. Cho, S. Lee, Y. H. Ahn, K. Kim, H. Lim, G. Steinmeyer, V. Petrov, U. Griebner, and F. Rotermund, "Fabrication and characterization of ultrafast carbon nanotube saturable absorbers for solid state laser mode-locking near 1 μm," Appl. Phys. Lett. **93**, 161106 (2008).
8. Y.-C. Chen, N. R. Raravikar, L. S. Schadler, P. M. Ajayan, Y.-P. Zhao, T.-M. Lu, G.-C. Wang, and X.-C. Zhang, "Ultrafast optical switching properties of single-wall carbon nanotube polymer composites at 1.55 μm," Appl. Phys. Lett. **81**, 975-977 (2002).
9. M. A. Solodyankin, E. D. Obraztsova, A. S. Lobach, A. I. Chernov, A. V. Tausenev, V. I. Konov, and E. M. Dianov, "Mode-locked 1.93 μm thulium fiber laser with a carbon nanotube absorber," Opt. Lett. **33**, 1336-1338 (2008).
10. H. Kataura, Y. Kumazawa, Y. Maniwa, Y. Ohtsuka, R. Sen, S. Suzuki, and Y. Achiba, "Diameter control of single-walled carbon nanotubes," Carbon **38**, 1691-1697 (2000).
11. S. Y. Set, H. Yaguchi, Y. Tanaka, and M. Jablonski, "Laser Mode Locking Using a Saturable Absorber Incorporating Carbon Nanotubes," J. Lightwave Technol. **22**, 51-56 (2004).
12. F. Wang, A. G. Rozhin, Z. Sun, V. Scardaci, R. V. Penty, I. H. White, and A. C. Ferrari, "Fabrication, characterization and mode locking application of single-walled carbon nanotube/polymer composite saturable absorbers," Int. J. Mater. Form. **1**, 107–112 (2008).

13. S. Yamashita, Y. Inoue, S. Maruyama, Y. Murakami, H. Yaguchi, M. Jablonski, and S. Y. Set, "Saturable absorbers incorporating carbon nanotubes directly synthesized onto substrates and fibers and their application to mode-locked fiber lasers," Opt. Lett. **29**, 1581-1583 (2004).
14. A. G. Nasibulin, A. Ollikainen, A. S. Anisimov, D. P. Brown, P. V. Pikhitsa, S. Holopainen, J. S. Penttilä, P. Helistö, J. Ruokolainen, M. Choi, and E. I. Kauppinen, "Integration of single-walled carbon nanotubes into polymer films by thermo-compression," Chem. Eng. J. **136**, 409-413 (2008).
15. A. Moisala, A. G. Nasibulin, D. P. Brown, H. Jiang, L. Khriachtchev, and E. I. Kauppinen, "Single-walled carbon nanotube synthesis using ferrocene and iron pentacarbonyl in a laminar flow reactor," Chem. Eng. Sci. **61**, 4393-4402 (2006).
16. Y. Zhou, L. Hu, and G. Grüner, "A method of printing carbon nanotube thin films," Appl. Phys. Lett. **88**, 123109 (2006).

1. Introduction

Ultrafast passively mode-locked lasers are of unprecedented interest for a large variety of applications which has led to a recent search for novel, low-cost approaches. Passive mode-locking can be initiated by nonlinear polarization evolution, the Kerr-lens method or saturable absorption [1-3]. Saturable absorption can be generated by e.g. semiconductor saturable absorber mirrors (SESAMs) or various dyes [3,4]. Recently, new types of saturable absorbers based on single-walled carbon nanotubes (SWCNTs) have been used in fiber and solid-state lasers to initiate mode-locking [5-7]. The CNT-based devices benefit from a fairly simple manufacturing process, offer short absorption recovery times (<1 ps) and reasonable modulation depths [7,8]. Different SWCNT-absorbers have been reported to mode-lock lasers at wavelength regimes of 1 μm [6], 1.55 μm [5] and 1.9 μm [9]. However, none of the so far demonstrated absorbers have been shown to operate at all of these wavelengths. The operational parameters of a CNT-absorber can be tailored during the fabrication process since its absorption characteristics are determined by the diameter of the nanotubes and details of the structure [10].

CNT-based absorbers can be fabricated to operate both in transmission or reflection, which allows the use of either ring or linear cavity configuration [11]. Typically, CNTs have been embedded into polymer or liquid [7-9]. The CNTs, together with the polymer-based material, have then been applied on the surface of an optical fiber or a quartz substrate and used in transmission to mode-lock a ring-cavity laser [9,12,13]. Recently, a new method for placing SWCNTs onto a polymer film by a single-step dry-transfer thermo-compression method has been demonstrated, which is more practical compared with the conventional wet deposition methods [14,15]. Polymer is undesirable as an intracavity laser material due to its relatively low damage threshold and high optical absorption. It should be avoided, especially for high power and mid-IR applications. Therefore a new method to create CNT-based absorbers that does not employ polymer is very desirable.

In this paper, we report the use of a novel polymer-free carbon nanotube-based saturable absorber produced using a simple dry-transfer contact press method onto a highly reflective Ag-mirror. The same SWCNT-absorber mirror, used in a compact linear cavity configuration, is shown to provide self-starting sub-picosecond mode-locked operation of Yb-, Er- and Tm:Ho-doped fiber lasers at wavelengths of 1.05 μm, 1.56 μm and 1.99 μm, respectively. To our knowledge, this is the broadest operation bandwidth that has been reported to date for a single carbon nanotube-based saturable absorber.

2. Carbon nanotube production

SWCNTs were synthesized by thermal decomposition of ferrocene vapor in a carbon monoxide atmosphere [15]. Briefly, the Carbon Nanotube Reactor consisted of a saturator, a water-cooled injector probe, and a heated growth chamber. A 300 cm^3/min flow of CO was passed through the saturator filled with a mixture of silicon dioxide and ferrocene powders. This provided the conditions for the CO ferrocene vapor saturation of 0.8 Pa at room temperature. The growth chamber was an alumina tube inserted inside a tube furnace. The flow containing ferrocene vapor was then introduced directly into the high temperature zone of the growth chamber through the water-cooled probe. An additional CO flow (100 cm^3/min)

was introduced outside the injector probe. The Ferrocene thermally decomposed in the high temperature gradient formed between the injector probe and the ambient reactor temperature. The decomposition leads to supersaturation conditions that result in iron nanoparticle formation. Iron nanoparticles are the catalysts from which the CNTs grow.

The reactor temperature was maintained at ~1100 ^{o}C. Catalytic CO disproportionation reactions resulted in the synthesis of single-walled CNTs. The product was collected downstream of the reactor by filtering the flow through a nitrocellulose membrane filter. The thickness and therefore optical transparency of the collected SWCNT-films can be accurately controlled by varying the collection time [14].

3. Absorber design and fabrication

A Saturable Absorber Incorporating NanoTubes (SAINT) was prepared by a room temperature dry-transfer process previously applied to SWCNT-films on polyethylene substrates [14]. A piece of a nitrocellulose membrane filter with a SWCNT-film was placed on a protected Ag-mirror with the SWCNT-film upside down. Then, the mirror and the filter were pressed together at a pressure of 1000 Pa. After the pressing procedure, the membrane filter was peeled off and the SWCNT-film was strongly adhered to the mirror surface. It is worth noting that the SWCNT-film was utilized as-deposited and no purification or dispersion steps were required. When compared to standard wet deposition methods, which may require several time-consuming stages, such as purification, dispersion and filtering, the approach of the SWCNT-film preparation demonstrated here is simple and easily scalable [16].

4. CNT-absorber mirror characterization

The SAINT-film was characterized by scanning and transmission electron microscopy, and optical absorption measurements. SWCNT-network morphology of the SAINT is depicted in the Fig. 1. SEM-imaging reveals up to 20 nm-wide bundles and iron nanoparticles which give large back-scattered electron yield and large contrast in the images. SEM-imaging of the SWCNT-network was performed on the nitrocellulose membrane filter prior to transfer. A

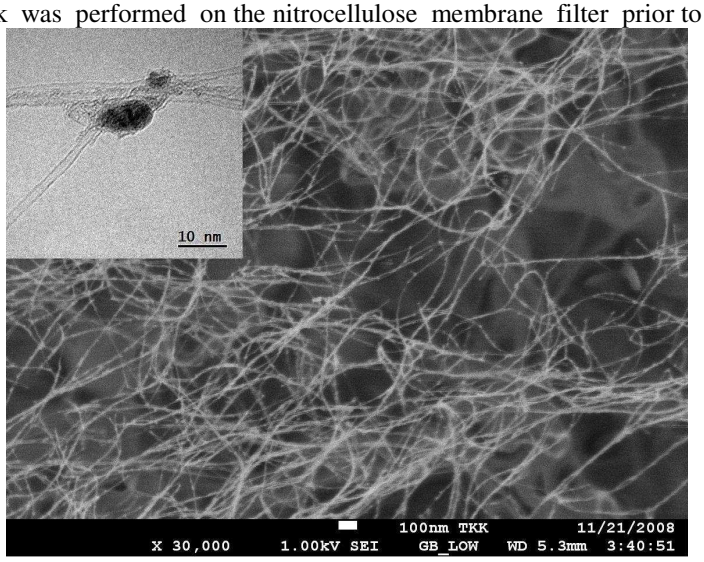

Fig. 1. SEM micrograph of the SWCNT-film. The inset shows high-resolution TEM-image of the sample. The tube diameter ranges from 1.2 nm to 1.8 nm.

sample of SWCNT-film was also transferred to a carbon coated TEM-grid for Carbon Nanotube diameter estimation. A high resolution TEM-image, shown as an inset to Fig. 1, reveals the tube diameter ranging from 1.2 nm to 1.8 nm.

Optical transmission spectroscopy was performed on a test sample using a dual-beam spectrophotometer. The test sample was prepared for this measurement by transferring

another piece of the SWCNT-film to a PET-substrate using a dry-transfer process [15]. A blank PET-substrate was used in the reference beam. Figure 2(a) depicts the optical transmission spectrum of SWCNT-film with a thickness of ~80 nm. As can be seen, the absorption bands extend an ultra-broad wavelength range. The strongest absorption sub-bands of the SWCNT-film are located at 800 nm and 1400 nm. Optical uniformity of the SWCNT-film was estimated by measuring optical transmission over the SWCNT-film on PET-substrate at seven randomly located spots. Spectrophotometer beam diameter was limited to 1 mm. 1% standard deviation of optical transmission was observed at the wavelength of 550 nm, suggesting good optical uniformity of the SWCNT-film. The wavelength of 550 nm is typically used to characterize optical transmission of SWCNT-films [14].

Prior to use in laser experiments, the absorption saturation of the SAINT-mirror was determined from the dependence of the reflectivity on the incident pulse fluence for two wavelengths, 1.05 μm and 1.56 μm. The measurements were carried out using short pulse Yb- and Er-fiber systems. Figure 2(b) shows the nonlinear reflectivity at the wavelength of 1.56 μm. Non-bleachable loss (α_0), modulation depth (ΔR), and saturation fluence (F_{sat}) were determined to be 3.96%, 0.94% and 320 μJ/cm^2, respectively. At the wavelength of 1.05 μm the corresponding parameters were measured to be 18.3%, 1.86% and 1000 μJ/cm^2. We note that the Ag-mirror increases losses of the absorber by an additional 1-2%.

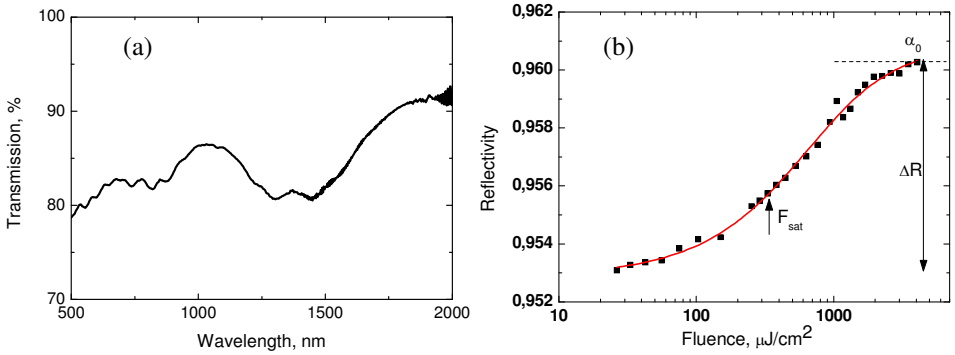

Fig. 2. (a) Optical transmission spectrum of the SWCNT-film. Ripples in absorption near 2000 nm wavelengths are caused by strong absorption of the PET-substrate. (b) Nonlinear reflectivity of the absorber measured at 1560 nm.

5. Mode-locked fiber laser experiments at 1.05 μm, 1.56 μm and 1.99 μm wavelengths

The same SWCNT absorber mirror was used as a mode-locking element in three lasers using Yb, Er and Tm:Ho doped fiber gain media with lengths of 1 m, 2 m, 1.5 m and operation wavelengths of 1 μm, 1.56 μm and 2 μm, respectively. The lasers had a linear cavity (see Fig. 3) that consisted of a pump laser, a wavelength selective fiber pump coupler, an ~10 % fiber output coupler, a highly reflecting dielectric end mirror and the SWCNT absorber mirror. A polarization controller was used in the cavity to optimize the laser performance. The Er- and Tm:Ho-doped fiber lasers operated in the soliton regime without dispersion compensation, while the Yb-doped fiber laser required a grating pair to compensate for the normal dispersion of an optical fiber. The Er- and Yb-lasers were pumped by a fiber-coupled 976-nm laser diode. The Tm:Ho laser was pumped by an Er-fiber laser emitting at 1.56 μm. The CNT absorber mirror, assembled with fiber butt-coupling, was typically oversaturated by the intracavity fluence of the laser.

The mode-locked Yb-fiber laser was operated at the central wavelength of 1050 nm with a

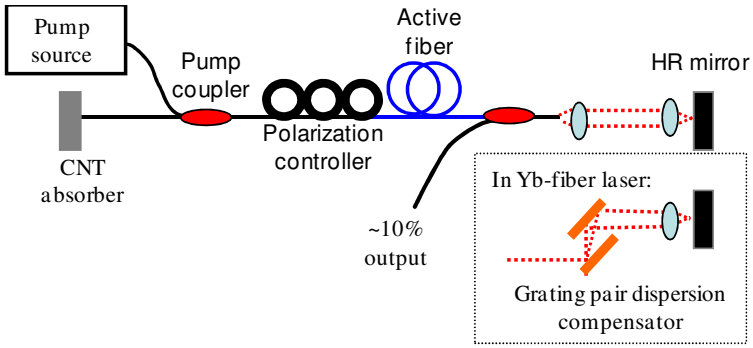

Fig. 3. Schematic of the experimental fiber laser setup used in the study. Active fibers acting as gain medium were doped with Yb, Er or Tm:Ho rare-earth materials. Yb-fiber laser requires the grating pair to achieve the soliton pulse regime.

spectral width of 2.7 nm, as seen in Fig. 4(a). Figure 4(b) shows the recorded autocorrelation trace with a $sech^2$-fitting revealing a pulse duration of 0.67 ps, resulting in a time-bandwidth-product of 0.48. The chirp could be expected from the strong dispersion management within the cavity and some additional chirp acquired in the output pigtail with a length of ~1.5 m. A photograph of a typical oscilloscope trace of the mode-locked pulse train is shown as an inset to Fig. 4(b). The average output power and threshold power were ~10 mW and ~150 mW, respectively. Once the laser operated in the mode-locked regime, the pump power could be reduced down to ~50 mW, revealing the hysteresis behavior typical for the soliton regime. With pump powers exceeding ~170 mW, multiple pulse operation expected for soliton fiber lasers was observed. The laser output characteristics are summarized in Table 1.

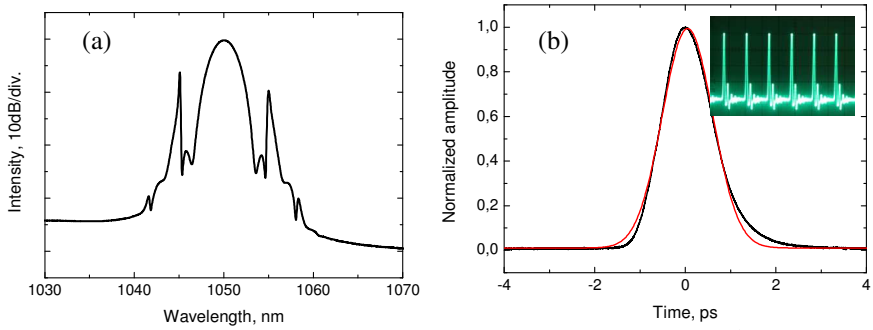

Fig. 4. (a) Pulse spectrum of the Yb-fiber laser. (b) Autocorrelation trace and $sech^2$-fit giving a pulse width of ~0.7 ps. The inset shows a typical oscilloscope picture of the generated pulse train.

The Erbium-doped fiber laser produced 0.44 ps pulses at a wavelength of 1563 nm, as seen in Fig. 5(a). The spectral width was measured to be 6.0 nm, giving a time-bandwidth product of 0.32 that corresponds to transform-limited pulses. The mode-locked operation was environmentally stable and self-starting with a low threshold pump power of ~30 mW.

The same SWCNT-absorber was also capable of initiating mode-locking in the thulium-holmium co-doped fiber laser. The polymer-free CNT-layer on a highly reflective Ag-mirror enabled the building of a robust and compact linear cavity laser with significantly improved output characteristics compared to the recently reported ring-cavity Tm-laser that had obvious limitations in output power, stability and absorber damage threshold [9]. The all-fiber laser delivered ~1.0 ps pulses with a central wavelength of 1991 nm, as shown in Fig. 5(b). The laser output parameters are summarized in Table 1. To our knowledge, this is the longest operation wavelength for a fiber laser mode-locked by a CNT-absorber. The extension in operation wavelength from ~1.9 μm [9] to ~2 μm is attributed to the use of a Tm:Ho co-doped fiber instead of a Tm-doped fiber with gain typically peaking at ~1.9 μm.

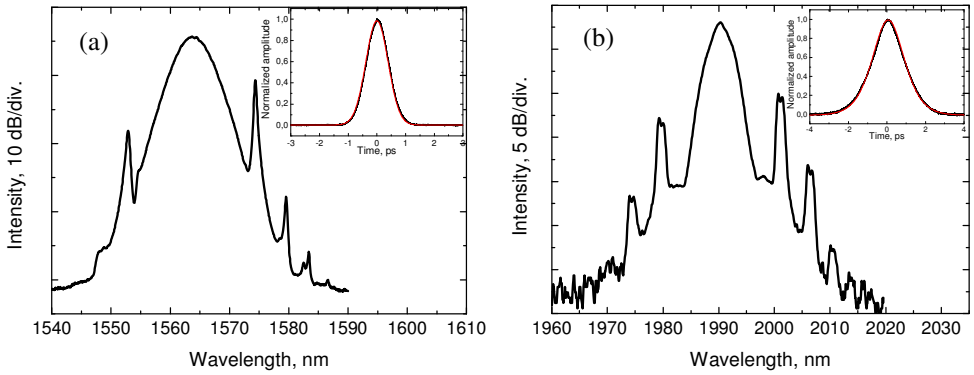

Fig. 5. Optical spectra of the Er- (a) and Tm:Ho-doped (b) fiber lasers. The corresponding autocorrelation traces with $Sech^2$-fittings are shown as insets. The pulse widths for the Er- and Tm:Ho-doped fiber lasers are 0.44 ps and 1.0 ps, respectively. The 3-dB spectral widths are 6.0 and 5.0 nm.

Table 1. Summary of the laser output characteristics.

	Threshold pump power, mW	Repetition rate, Mhz	Pulse width, ps	Time-bandwidth product	Average output power, mW
Yb	150	40	0.67	0.48	10
Er	30	15	0.44	0.32	10
Tm:Ho	150	41	1.0	0.37	15

All the mode-locking measurements were carried out in normal laboratory conditions at room temperature. The lasers were operated continuously for several hours at a time during the characterization. When the lasers were restarted after a few days, the mode-locked pulse train was immediately built up. No aging effects or degradation of the CNT-absorber at the used powers were observed during the measurements.

6. Conclusion

We have fabricated a novel saturable absorber mirror with single-walled carbon nanotubes transferred to an Ag-mirror using a simple contact press method. When compared to standard wet deposition methods, which require several processing stages, the presented approach for the SWCNT-film preparation is simple and scalable. Avoiding polymers as a host material, which could degrade the laser performance and increase absorber loss at wavelengths above 2 μm, allows for higher laser efficiency and power scalability.

Yb-, Er- and Tm:Ho-doped fiber lasers mode-locked using the same SAINT-mirror delivered sub-picosecond pulses at the wavelengths of 1.05 μm, 1.56 μm and 1.99 μm, respectively, thus demonstrating the ultra-broadband performance of the easily produced device. To our knowledge, this is the largest operation range reported to date for a SAINT-mirror. The use of the novel CNT-mirror technology offers an attractive opportunity for self-starting passive mode-locking of fiber lasers operating over a very broad spectral range with potential for further scaling to the mid-infrared spectral region and higher powers.

Acknowledgments

The authors acknowledge the support of the graduate school of Tampere University of Technology, the Finnish Foundation for Economic and Technology Sciences, the Jenny and Antti Wihuri Foundation, the Nokia Foundation, the Emil Aaltonen foundation, the Elisa Foundation, Academy of Finland (Project Nos 128445 and 128495) and TEKES (Project No 2729/31/07)